VNIVERSITAT DE VALÈNCIA

Automatic early detection of decay in citrus fruit using optical technologies and machine learning techniques

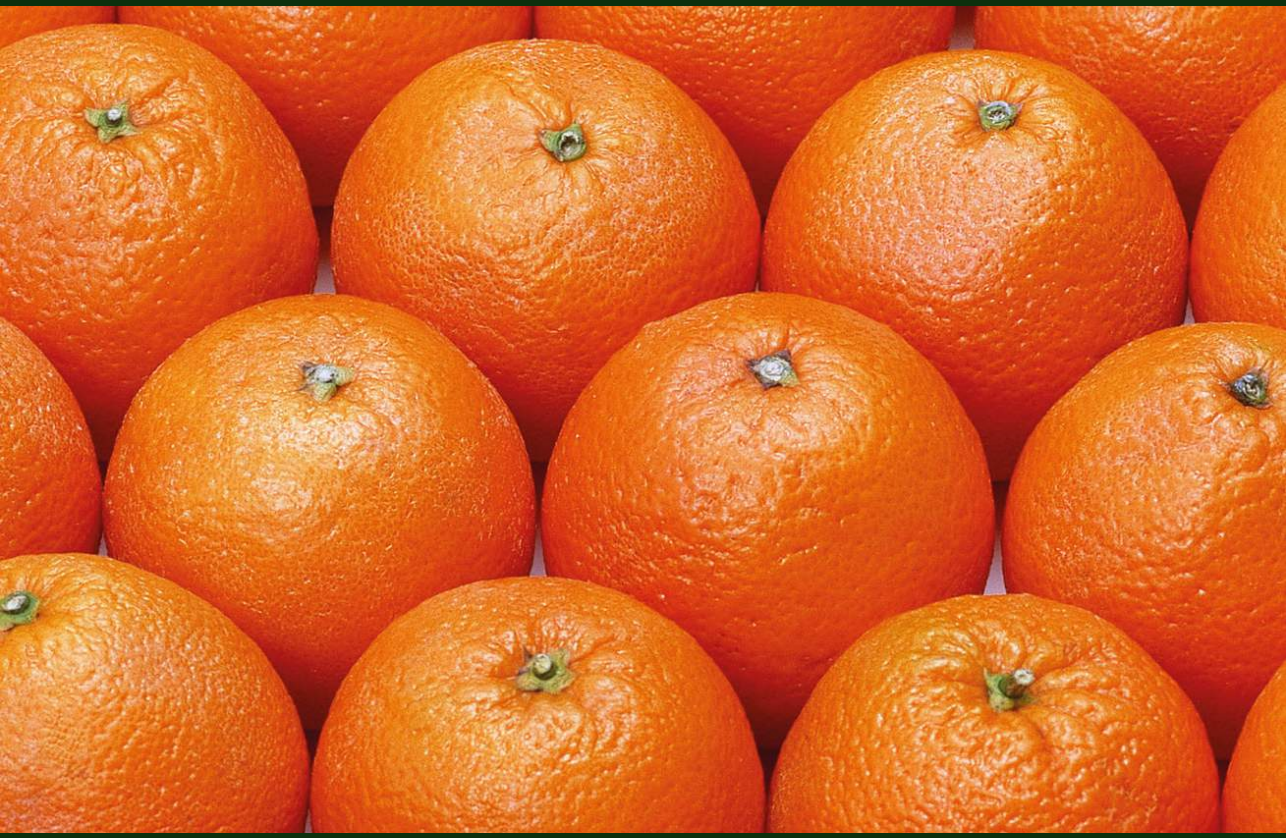

Doctoral thesis

Delia Lorente Garrido

DOCTORAL THESIS

Automatic early detection of decay in citrus fruit using optical technologies and machine learning techniques

Author

Delia Lorente Garrido

Directors

Dr. José Blasco Ivars

Dr. Juan Gómez Sanchis

Electronic Engineering Department

University of Valencia

Valencia – December, 2014

Automatic early detection of decay in citrus fruit using optical technologies and machine learning techniques

Delia Lorente Garrido, December 2014

VNIVERSITAT DE VALÈNCIA Escola Tècnica Superior d'Enginyeria
Departament d´Enginyeria Electrònica

Departamento de Ingeniería Electrónica
Escuela Técnica Superior de Ingeniería

D. JOSÉ BLASCO IVARS, Doctor en Informática por la Universitat Politècnica de València, Director del Centro de Agroingeniería del Instituto Valenciano de Investigaciones Agrarias (IVIA), y

D. JUAN GÓMEZ SANCHIS, Doctor en Ingeniería Electrónica por la Universitat de València, Profesor Ayudante Doctor del Departamento de Ingeniería Electrónica de la Escuela Técnica Superior de Ingeniería de la Universitat de València,

HACEN CONSTAR QUE:

La Ingeniera en Electrónica Dña. Delia Lorente Garrido ha realizado bajo nuestra dirección el trabajo titulado "Automatic early detection of decay in citrus fruit using optical technologies and machine learning techniques", que se presenta en esta memoria para optar al grado de Doctora.

Y para que así conste a los efectos oportunos, firmamos el presente certificado, en Valencia, a _____.

Dr. José Blasco Ivars	Dr. Juan Gómez Sanchis	Dr. Rafael Magdalena Benedito Dir. del Departamento

Tesis Doctoral:	AUTOMATIC EARLY DETECTION OF DECAY IN CITRUS FRUIT USING OPTICAL TECHNOLOGIES AND MACHINE LEARNING TECHNIQUES
Autora:	DELIA LORENTE GARRIDO
Directores:	Dr. JOSÉ BLASCO IVARS Dr. JUAN GÓMEZ SANCHIS

El tribunal nombrado para juzgar la Tesis Doctoral arriba citada, compuesto por los doctores:

Presidente: _____

Vocal: _____

Secretario: _____

Acuerda otorgarle la calificación de _____

Y para que así conste a los efectos oportunos, firmamos el siguiente certificado.

Valencia, a _____.

Agradecimientos

El camino recorrido para desarrollar esta tesis doctoral ha sido enriquecedor, pero también largo y sacrificado, y sin duda no habría sido posible recorrerlo sin todas las personas que han ayudado de una forma u otra a quitar los obstáculos, a guiarme y, sobre todo, a levantarme de las caídas.

En primer lugar, tengo agradecer la financiación recibida por el Ministerio de Ciencia e Innovación de España a través de beca predoctoral FPI-INIA número 42, sin la cual la presente tesis no habría sido posible.

Sin ninguna duda, esta tesis doctoral se ha llevado a cabo gracias a la inestimable ayuda de mis directores, el Dr. José Blasco y el Dr. Juan Gómez. A lo largo de estos cuatro años me han ayudado a recorrer, paso a paso, el camino científico que ha llevado a la realización de esta tesis. En todo momento, me han dado plena libertad para escoger cada uno de mis pasos, pero siempre guiándome y asesorándome con su experiencia cuando lo he necesitado. Han confiado y creído en mí en cada momento, lo cual agradezco profundamente. Con grandes dosis de paciencia y enriquecedores debates, siempre me han hecho aprender algo nuevo, así como también me han ayudado a mejorar y a corregir los errores cometidos a lo largo del tiempo.

Tengo que agradecer especialmente la gran acogida que he tenido por parte de mis compañeros del Centro de Agroingeniería del IVIA, todos los que han pasado a lo largo de estos cuatro años, los cuales han hecho que estos años me haya sentido como en una gran familia. Siempre me han ofrecido su ayuda cuando la he necesitado y, además, puedo afirmar que no sólo he tenido compañeros, sino que ahora muchos de ellos son también amigos.

Debo agradecer, por supuesto, a personas de otros departamentos del IVIA su valiosa ayuda en los experimentos realizados durante la tesis doctoral, tanto en los procesos de inoculación con hongos como en la recolección de cítricos. En especial, agradezco la activa colaboración de Lluís Palou, Clara Montesinos y Alejandro Medina.

No puedo olvidar hacer un especial agradecimiento al *Leibniz-Institut für Agrartechnik* en Potsdam (Alemania), donde he realizado dos estancias de tres meses cada una, bajo la atenta y

amable supervisión de la Dra. Manuela Zude. Estas estancias han sido de gran valor científico para esta tesis doctoral, así como también me han permitido conocer a grandes amigos y conocer de forma más profunda Alemania, un país que me ha conquistado.

Muchas gracias también a los miembros del grupo de investigación IDAL de la Universitat de València por su ayuda y asesoramiento en numerosas partes de la tesis relacionadas con el análisis de datos. Siempre han estado dispuestos a echar una mano cuando ha hecho falta.

También tengo que hacer mención a todos mis amigos, gracias a los cuales esta tesis se ha podido terminar. Sin duda, ellos han sido grandes motores de esta tesis, por su comprensión, por sus constantes ánimos y, por supuesto, por los momentos de desconexión y alegría que me han dado.

Por supuesto, jamás podré dejar de agradecer a mi madre, a mi padre y a mi hermano su gran apoyo, tan incondicional como sincero, en todos los proyectos en los que me he embarcado en esta vida, incluyendo esta tesis doctoral. Siempre han creído en mí y me han animado en los momentos difíciles, así como también han disfrutado conmigo de los buenos. También me han enseñado que hay que luchar por los sueños y por la felicidad y que, a pesar de las dificultades que pueda haber en el camino, siempre hay que continuar intentándolo.

En último lugar, me gustaría agradecer la inmensa ayuda recibida por Pablo. A cualquier hora, en cualquier lugar y bajo cualquier circunstancia, ha estado ahí para apoyarme, aconsejarme y, sobre todo, animarme, tanto en el ámbito científico como en el personal. Cada día me ayuda a entender realmente el significado de la frase "un hecho vale más que mil palabras", porque con cada acto desinteresado y lleno de generosidad me demuestra que existe realmente el amor.

Delia Lorente Garrido
Valencia, diciembre de 2014

A mis padres, a mi hermano y a Pablo,
por apoyarme incondicionalmente

Table of contents

List of figures

List of tables

List of acronyms and abbreviations

ANN	Artificial neural network
AOTF	Acousto-optic tunable filter
ATB	Leibniz-Institute for Agricultural Engineering Potsdam-Bornim
AUC	Area under a ROC curve
BD	Bhattacharyya distance
CA	Correlation analysis
CCD	Charge-coupled device
CCI	Citrus colour index
CD	Correlation dimension estimator
CMOS	Complementary metal-oxide semiconductor
CTP	Centro de Tecnología Poscosecha
EB	Eigenvalue-based estimator
ELM	Extreme learning machine
FA	Factor analysis
FAO	Food and Agriculture Organization of the United Nations
FDA	Fisher's discriminant analysis
FEDER	Fondo Europeo de Desarrollo Regional
GC-MS	Gas chromatography-mass spectrometry
GL	Gaussian-Lorentzian cross product distribution function

GMST	Geodesic minimum spanning tree estimator
GS	Green sound skin
HLBI	Hyperspectral light backscattering imaging
HPLC	High performance liquid chromatography
HSI	Hue-saturation-intensity
IDAL	Intelligent Data Analysis Laboratory
IDM	Integrated disease management
InGaAs	Indium-gallium-arsenide
INIA	Instituto Nacional de Investigación y Tecnologia Agraria y Alimentaria de España
IVACE	Instituto Valenciano de Competitividad Empresarial
IVIA	Instituto Valenciano de Investigaciones Agrarias
JCR	Journal Citation Reports
KLD	Kullback-Leibler divergence
LBI	Light backscattering imaging
LCTF	Liquid crystal tunable filter
LDA	Linear discriminant analysis
LLBI	Laser-light backscattering imaging
MCARI	Modified chlorophyll absorption in reflectance index
MI	Mutual information
MICINN	Ministerio de Ciencia e Innovación de España
ML	Maximum likelihood estimator
MLBI	Multispectral light backscattering imaging
MLP	multilayer perceptron
MRMRd	Minimum redundancy maximum relevance difference criterion
MRMRq	Minimum redundancy maximum relevance quotient criterion

MSC Multiplicative scatter correction

NDVI Normalised difference vegetation index

NIR Near-infrared

OS Orange sound skin

OSAVI Optimised soil-adjusted vegetation index

OVA *One vs. all*

PCA Principal component analysis

PCI Peripheral component interconnect

PD Decay caused by *P. digitatum*

PDA Photodiode array

PDA Potato dextrose agar

PI Decay caused by *P. italicum*

PLS Partial least squares

PRI Photochemical reflectance index

RAM Random access memory

RGB Red-green-blue

RMSE Root mean squared error

ROC Receiver operating characteristic

RVSI Red-edge vegetation stress index

SAVI Soil-adjusted vegetation index

SC Defective skin by scars

SNV Standard normal variate

SSC Soluble solids content

TCARI Transformed chlorophyll absorption in reflectance index

TT T-test

UMH Universidad Miguel Hernández de Elche

UV Ultraviolet

VARI Visible atmospherically resistant index

WBI Water band index

WI Water index

WL Wilks' lambda

Abstract

Citrus fruit is the highest value fruit crop in terms of international trade, with Spain being the first worldwide exporter of citrus fruit for fresh consumption. However, the presence of decay caused by *Penicillium* spp. fungi is among the main problems affecting postharvest and marketing processes of citrus fruit. A small number of decayed fruit can infect a whole consignment, during long-term storage or fruit shipping to export markets, thus involving enormous economic losses and the blackening of the reputation of citrus producers. Therefore, effective early detection of fungal infections and removal of infected fruit are issues of major concern in commercial packinghouses in order to prevent the spread of the infections, thus ensuring an excellent fruit quality and absolute absence of infected fruit. In this respect, this doctoral thesis focuses on addressing such an important challenge for the citrus industry as the automation of the detection of early symptoms of decay, in order to provide alternatives to human inspection under dangerous ultraviolet illumination, thus accomplishing this detection task more efficiently and, consequently, leading to a possible reduction of the use of fungicides. Specifically, this doctoral thesis advances in the field of the automatic detection of decay in citrus fruit using optical systems and machine learning methods. In particular, three different optical techniques operating in the visible and near-infrared spectral regions are investigated, including hyperspectral imaging, light backscattering imaging and spectroscopy. The optical systems used in this thesis are not limited to the visible part of the electromagnetic spectrum, thus presenting capabilities beyond those of the naked human eye and traditional computer vision systems based on colour cameras, this fact being of special interest for detecting hardly-visible damage in citrus fruit, such as decay at early stages. Furthermore, a vast number of machine learning techniques aimed at data dimensionality reduction and classification are explored for dealing with the optical measurements of citrus fruit in order to discriminate fruit with symptoms of decay from sound fruit. The three optical techniques, coupled with suitable machine learning methods, investigated in this doctoral thesis provide good results in the classification of skin of citrus fruit into sound or decaying, with a percentage of well-classified samples above 90% for both classes despite their similarity. In the

light of the results, this doctoral thesis lays the foundation for the future establishment of the explored optical technologies on a commercial fruit sorter aimed at decay detection in citrus fruit.

Resumen

Los cítricos representan el cultivo frutal de mayor valor en términos de comercio internacional, siendo España el primer exportador mundial de cítricos para consumo en fresco. Sin embargo, la presencia de podredumbres causadas por hongos del género *Penicillium* se encuentra entre los principales problemas que afectan la postcosecha y comercialización de cítricos. Un número reducido de frutas infectadas puede contaminar una partida completa de cítricos durante el almacenamiento de la fruta por largos períodos de tiempo o en el transporte al extranjero, lo que conlleva grandes pérdidas económicas y el desprestigio de los productores de cítricos. Por lo tanto, la detección temprana de infecciones por hongos de forma efectiva y la eliminación de la fruta infectada son asuntos de especial interés en los almacenes de confección de fruta para impedir la propagación de las infecciones fúngicas, asegurando de esta forma una excelente calidad de la fruta y la ausencia total de fruta infectada. En este sentido, la presente tesis doctoral se centra en abordar un reto tan importante para la industria citrícola como es la automatización del proceso de detección de podredumbres incipientes, con el fin de proporcionar alternativas a la inspección manual con peligrosa luz ultravioleta que permitan realizar esta detección de forma más eficiente y, en consecuencia, reducir potencialmente el uso de fungicidas. En concreto, esta tesis doctoral avanza en el campo de la detección automática de podredumbres en cítricos mediante sistemas ópticos y técnicas de aprendizaje automático. Específicamente, se investigan tres técnicas ópticas diferentes que operan en las regiones del visible e infrarrojo cercano del espectro electromagnético, incluyendo la técnica de imagen basada en *backscattering*, visión hiperespectral y espectroscopía. Los sistemas ópticos usados en esta tesis no están limitados a la parte visible del espectro, por lo que sus capacidades superan a las del ojo humano y a las de los sistemas de visión convencionales basados en cámaras de color, lo cual resulta de especial interés para detectar daños en cítricos que son difícilmente visibles a simple vista, como las podredumbres en estadios tempranos de infección. Además, se exploran numerosas técnicas de aprendizaje automático de reducción de la dimensionalidad de los datos y clasificación, con la finalidad de usar las medidas ópticas de los cítricos para discriminar la fruta afectada por podredumbre de la fruta sana. Las tres técnicas ópticas, junto con métodos de aprendizaje automático adecuados, proporcionan buenos

resultados en la clasificación de la piel de los frutos cítricos en sana o podrida, consiguiendo un porcentaje de muestras bien clasificadas superior al 90% para ambas clases, a pesar de la gran similitud entre ellas. En vista de los resultados obtenidos, esta tesis doctoral sienta las bases para la futura implementación de las técnicas ópticas estudiadas en un sistema comercial de clasificación automática de fruta destinado a la detección de podredumbres en cítricos.

Part I

Introduction

Chapter 1

Introduction and objectives

This introductory chapter basically sets out the context of the thesis, and provides the background necessary to understand the remainder of the thesis. In particular, this chapter introduces in a general way the problem of the decay detection in citrus fruit, and gives an overview of the different optical techniques analysed in this thesis to automate this detection, with particular attention being paid on technical principles of these technologies and their applications for fruit and vegetable quality assessment. Furthermore, it is included a brief introduction to the use of machine learning techniques for quality assessment of agricultural products from the corresponding optical measurements. In addition, the objectives and the research framework of the doctoral thesis are also presented. At the end of this chapter, the structure of this thesis report is described.

1.1. Introduction

1.1.1. Importance of the citrus industry

Citrus fruit is the highest value fruit crop in terms of international trade. The annual production of all types of citrus fruit was estimated at around 115.5 million tons in the period 2010-2011 (FAO, 2012), thus evidencing the importance of this fruit crop within the world economy. Oranges constitute the bulk of citrus fruit production, accounting for around 61% of global production.

However, significant quantities of mandarins, lemons, limes and grapefruits are also produced. Citrus production is mainly aimed at two differentiated markets, including the processed citrus industry and the citrus market for consumption as fresh produce, with the latter accounting for around 75% of total production.

Spain is one of the leading citrus producers in the world, with a production of around 6.6 million tons in the period 2010-2011, only being surpassed by China, Brazil, India, the United States of America and Mexico. Furthermore, Spain is the first worldwide exporter of citrus fruit for fresh consumption, exporting more than half of total citrus production (around 3.6 million tons). In particular, the Valencian Community is the first Spanish exporter, accounting for around 76% of total national exports of citrus fruit in 2012 (IVACE, 2013). When considering only the most important citrus fruit cultivars, the Valencian Community exported 87% of total Spanish mandarins and 78% of total oranges. In 2012, the biggest importers of Valencian citrus fruit were France, Germany, Netherlands and the United Kingdom, which represented around 61% of total exports. The rest of Valencian citrus fruit was exported to other countries, such as Russia, Italy and the United States of America, where the Valencian exports are increasing in popularity among consumers due to their high quality. However, the intense competition with the rest of Mediterranean countries could jeopardise the dominant position of the Valencian Community in the citrus market. Therefore, the Valencian citrus industry is constantly making enormous efforts to ensure high product quality, especially when the citrus fruits are consumed as fresh fruit.

1.1.2. External quality of citrus fruit

The quality of a piece of fruit or vegetable is defined by several attributes that determine its marketability and shelf life. Quality assessment is therefore one of the most important goals of the highly competitive food industry. Product quality includes external appearance, such as colour, size or the presence of skin diseases or bruises, and internal quality features, such as sugar content, acidity or maturity. These properties cover all the factors that exert considerable influence on consumers regarding the appearance of the product, its nutritional and organoleptic qualities and its suitability for preservation. Nevertheless, the presence of skin defects is one of the most influential factors in the quality and price of fresh fruits and vegetables, since consumers strongly associate product quality with appearance and base their purchasing decisions on the good appearance of the product and the total absence of external defects (Kays, 1999).

In particular, external defects appearing on citrus fruit can be classified into two categories according to their economic consequences: defects that evolve over time after the citrus harvest and defects that do not evolve. Defects that do not evolve, such as scars caused by branch frictions

or chilling injury, affect only the appearance of the fruit, thus reducing the commercial value of the fruit. However, although fruit with cosmetic defects is not exported, it can still be commercialised in the internal market as fresh produce or used in the processed citrus industry, since these defects do not affect the organoleptic properties. On the other hand, evolving defects are more dangerous and it is absolutely necessary to detect them because they affect to the organoleptic quality of the fruit and there is a risk of spreading the infestation to sound fruit.

Evolving external damage include that caused by different types of fungi. Fungal pathogens can enter a fruit through wounds sustained during harvesting and the infestation is gradually spread over the whole fruit, depending on the temperature and humidity conditions, until the complete degradation of the fruit. Particularly, decay caused by *Penicillium* spp. fungi, such as *Penicillium digitatum* and *Penicillium italicum*, is among the main problems affecting postharvest and marketing processes of citrus fruit. Economic losses generated by these fungi are enormous, amounting to between 10% and 15% of total product value (Eckert and Eaks, 1989). Furthermore, since these fungal pathogens reproduce very rapidly and produce high amounts of spores that are readily disseminated by air currents, a small number of decayed fruit can infect a whole consignment, thus causing even more economic losses. This problem is aggravated when the fruit is stored for a long time or shipped to distant export markets. In addition to the associated economic losses, a high number of decayed fruit in the final destination can blacken the reputation of Spanish citrus producers.

Therefore, an issue of major concern in commercial packinghouses is to prevent the appearance of fungal infections and their spread in order to ensure an excellent quality and absolute absence of infected fruit. In practice, decay caused by fungi is controlled by application of conventional synthetic chemical fungicides, such as imazalil or thiabendazole, which delay or prevent the appearance of damage due to fungi. However, the widespread use of these fungicides has led to the resistance of the fungal pathogens (Eckert, 1990). In addition, fungal pathogens are sometimes already in the fruit before any fungicide treatment is applied in postharvest, since they can enter the fruit during harvesting (Obagwu and Korsten, 2003). Another drawback of fungicides is that export customers limit considerably their use due to the increasing social concerns about environmental contamination and human health risks associated with fungicides residues (Palou et al., 2008). In this context, effective early detection of fungal infections and removal of infected fruit in packinghouses can prevent the spread of the infections, thus leading to a potential reduction of the use of fungicides.

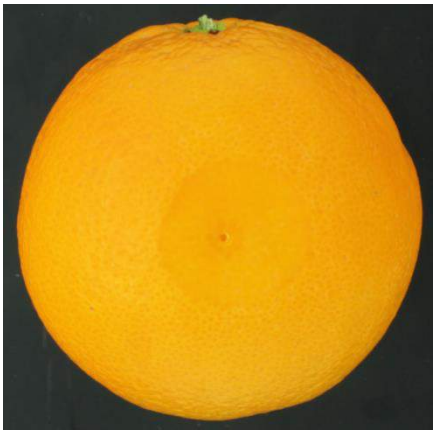

Figure 1.1. Orange presenting decay lesions caused by *P. digitatum* fungus.

Decay at its early stages (before sporulation) is hardly detectable because the appearance of the damage is virtually identical to sound skin, thus being barely visible to the human eye (Figure 1.1). Therefore, the detection of infected fruit is currently performed visually by trained workers examining each fruit individually in a dark room as it passes under ultraviolet (UV) illumination along a conveyor belt, since decay lesions produce visible fluorescence when being lit by this kind of light, and decayed fruits are removed manually (Figure 1.2).

Nevertheless, this method is potentially harmful for the workers and strictly regulated, since a long exposure to UV radiation can lead to several damaging effects to the human skin, such as premature aging and cancer (Lopes et al., 2010). As a direct consequence, the operators must work in shifts of just a few hours, thus leading to an operational inefficiency of the procedure that affects the assessment of the quality. Furthermore, as the decisions made by operators are affected by psychological factors such as acquired habits or fatigue caused by monotonous work, there is a high risk of human error. In this sense, since the efficiency of quality inspection processes determine the marketability of the product, automatic devices are being investigated as possible alternatives to manual inspection in order to enhance the detection of decay in packinghouses with the subsequent reduction in production costs, thus improving the competitiveness of citrus industry.

Figure 1.2. Operator examining citrus fruit under UV light to detect possible decay in a commercial packinghouse.

1.1.3. Optical systems

A possible solution to automate the detection of decay in citrus fruit could come from the development of systems based on optical sensing, such as computer imaging and spectroscopy. Nevertheless, this is not a simple task because automated inspection of agricultural produce shows certain particularities and problems that are not present in other fields due to their biological nature, such as the great variability of the objects inspected, due to differences between species and varieties as well as to individual differences between fruits belonging to the same variety. While manufactured products often present similar colours, shapes, sizes and other external features, fruit and vegetables may show different characteristics from one item to another. One single fruit can have a different colour, size and shape from another one, even though both of them were picked the same day from the same tree. Fruit and vegetables naturally change their colour or texture after being harvested, and these features depend on their maturity and how they are stored (ambient humidity and temperature, presence of volatiles, duration of the storage, etc.). Furthermore, the colour on a particular area of the skin of a healthy fruit may match the colour of a blemish on the surface of another fruit of the same variety. Moreover, it is essential that the presence of stem-ends, leaves, dirt or any extraneous material be identified and not confused with true skin defects.

Despite these difficulties, computer vision systems based on colour imaging have become widely used to automate the inspection of fruit and vegetables (Sun, 2007; Cubero et al., 2011). In most cases, their use is aimed at the inspection of external features related to quality, such as size, shape, colour or the presence of damage (Blasco et al., 2003; Costa et al., 2011). Currently, red-green-blue (RGB) computer vision systems are used in the citrus industry to detect external defects that are visible at first glance (Blasco et al., 2007b; Kim et al., 2009; López-García et al., 2010). Even though such systems offer important advantages like real-time operation, low cost or simulation of human processes, they also have some limitations, the main one being the fact that these vision systems are restricted to the visible part of the electromagnetic spectrum and miss important information that is outside these limits. This disadvantage derives from the fact that conventional vision systems try to imitate human perception of colour by capturing three images corresponding to the red, green and blue bands, and then combining these monochromatic images in order to obtain a colour image. In consequence, some defects, such as decay at very early stages, are very difficult to detect using standard artificial vision systems because they are hardly visible to the human eye and, consequently, by conventional colour cameras.

Therefore, other technologies have been proposed for automatically detecting decay in citrus fruit, such as vision systems that combine standard cameras and UV illumination (Kurita et al., 2009). The vision systems based on UV radiation imitate the fluorescence technique used in the citrus industry by humans. In these systems, UV sources induce visible fluorescence of essential oils present on the skin of citrus fruit produced by cell breakage. Fluorescence then augments the contrast of damage caused by fungal infestations, and this can be captured by standard cameras. Nevertheless, the utilisation of UV light presents some disadvantages because not all cultivars of citrus show the same autofluorescence phenomenon due to differences in the peel composition (Momin et al., 2011; Momin et al., 2012) and, in addition, other defects like chilling injury can also lead to some degree of fluorescence (Slaughter et al., 2008; Obenland et al., 2009), thus reducing the performance of these systems.

Other solution for detecting non-visible damage in citrus fruit, and without using UV illumination, could come from the use of optical technologies that are not limited to the visible part of the electromagnetic spectrum, ranging from 380 nm to 780 nm, unlike standard vision systems, but also operate in spectral areas where the human eye is not sensitive, such as in the UV (100-380 nm) and near-infrared (NIR; 780-2500 nm) regions. In this sense, some spectroscopic studies on citrus fruit in the visible and NIR regions (Gaffney, 1973) revealed that different external defects have different spectral signatures and show significant spectral differences with respect to the healthy areas, which can lead to the selection of certain sets of wavelengths at which the contrast between healthy and damaged skin is maximum, thus facilitating the detection of particularly

dangerous defects. As a consequence of these preliminary studies, technological advances to tackle the problem of detection of hardly-visible damage in citrus fruit, such as decay at early stages, are suggested to use optical approaches that also include spectral regions outside the visible electromagnetic spectrum, such as multispectral and hyperspectral vision systems, light backscattering imaging systems and spectroscopy systems, in order to enhance the capabilities of standard vision systems.

1.1.3.1. Multispectral and hyperspectral vision systems

In order to advance in the automatic detection of decay in citrus fruit, one way to enhance the possibilities of standard colour systems that seek to imitate the human eye is the use of multispectral computer vision systems. These systems can acquire a set of optimised monochromatic images at a few wavelengths that make it possible to estimate or discover features that are difficult with the traditional systems. Multispectral systems should not be confused with hyperspectral ones. Hyperspectral imaging involves a relatively large number of narrow spectral bands over a continuous spectral range, whereas a multispectral imaging deals with only a few spectral bands that do not necessarily have to be continuous nor narrow. An RGB camera could be considered a particular case of a multispectral system, since it captures three monochromatic, broad-band images to obtain a colour image. However, it is common to include also wavelengths outside the visible region of the electromagnetic spectrum, such as NIR, for detecting external damage in citrus fruit (Aleixos et al., 2002; Blasco et al., 2007a; Blanc et al., 2009; Blasco et al., 2009). The main advantages of multispectral imaging systems are the relatively low cost of the system in comparison with hyperspectral systems and the fact that they can be more specific for real applications. In fact, hyperspectral systems are sometimes used just to select the particular set of wavelengths that will finally be used in multispectral systems.

In this sense, the use of hyperspectral sensors makes it possible to conduct a more sophisticated analysis of the scene by acquiring a large set of monochromatic, narrow-band images corresponding to consecutive wavelengths. Although hyperspectral vision systems were originally developed for remote sensing and meteorology (Goetz et al., 1985; Lillesand et al., 2004), the gradual reduction in the price of these systems has allowed them to be incorporated in many laboratories of other research fields, such as precision agriculture (Erives and Fitzgerald, 2005; Muhammed, 2005) or food quality and safety control (Park et al., 2002; Sun, 2010; Elmasry et al., 2008b). In particular, the use of hyperspectral systems for internal and external quality assessment of fruit and vegetables has increased considerably in recent years (Gowen et al., 2007; Lorente et al., 2012). Hyperspectral sensors have been used successfully to identify external damage in

agricultural products (Liu et al., 2005; Elmasry et al., 2008a; Wang et al., 2011b; Vélez-Rivera et al., 2014). In the particular case of citrus fruit, several works have been carried out to detect skin defects (Martínez-Usó et al., 2005; Qin et al., 2009a, 2012). However, very limited research work has been conducted to detect decay caused by fungi in citrus fruit by means of hyperspectral imaging (Gómez-Sanchis et al., 2012, 2013).

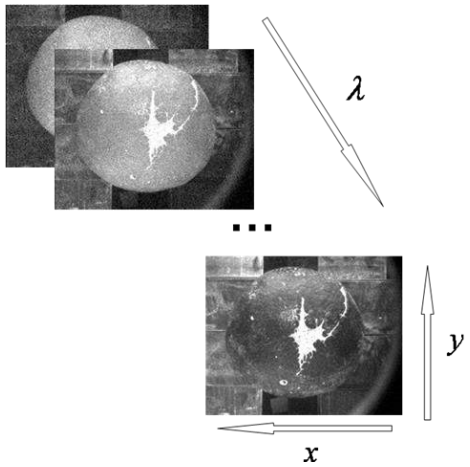

Figure 1.3. Illustration of a hyperspectral image cube. The two spatial dimensions are *x* and *y*, and the spectral dimension is *λ*.

As already commented, hyperspectral systems can acquire a large number of monochromatic images of the same scene at consecutive wavelengths, thus enabling simultaneous analysis of the spatial and spectral information from an object. Therefore, hyperspectral imaging integrates the main features of conventional imaging and spectroscopy. The set of monochromatic images that are captured constitutes a hyperspectral image. As they are made up of a large collection of images, hyperspectral images constitute a more extensive source of information than that provided by a single monochromatic image or a conventional RGB image. The number of images depends on the spectral resolution of the system used, and the images are combined by forming a cube in which two dimensions are spatial (pixels) and the third is the spectrum of each pixel, as shown in Figure 1.3. Without adequate processing, such a large amount of data, despite being one of the main advantages of hyperspectral systems, can complicate the extraction of useful information, since much of the information obtained is redundant or, by nature, irrelevant for the tackled problem, thus leading to the worsening of the quality assessment of fruit. In addition, the processing of the information can become excessively complex and time-consuming for such

high-dimensional data sets and the current acquisition times of the hyperspectral images are still slow, which make it difficult to incorporate hyperspectral vision systems into an industry that demands real-time inspection. All these problems are commonly alleviated by reducing the dimensionality of hyperspectral images by selecting a small set of wavelengths with the most relevant information. There are numerous methods for selecting particular wavelengths, and thus reducing the hyperspectral images to multispectral ones, which are easier to implement in systems suitable for the real-time product inspection. In this respect, further information can be found in Grahn and Geladi (2007).

Hyperspectral vision systems have three essential elements: light sources, usually halogen lamps placed in such an arrangement that diffuse illumination is provided and the scene is thus illuminated uniformly (Gómez-Sanchis et al., 2008a), an image sensor (also referred to as image detector), typically a monochromatic charge-coupled device (CCD) or complementary metal-oxide semiconductor (CMOS) camera, and a wavelength selection device. Although most of the hyperspectral systems work in the spectral range between 400 nm and 1000 nm (Lorente et al., 2012), these systems can be manufactured with a sensitivity up to about 2500 nm, and it is very important that both the wavelength selector and the image sensor are sensitive to the same spectral range (Cubero et al., 2011). The most popular wavelength selectors used in hyperspectral imaging systems are imaging spectrophotometers (Polder et al., 2004; Al-Mallahi et al., 2008; ElMasry et al., 2008a), liquid crystal tunable filters (LCTF; Evans et al., 1998; Gómez-Sanchis et al., 2008b; Wang et al., 2012) and, to a lesser extent, acousto-optic tunable filters (AOTF; Bei et al., 2004; Jiménez et al., 2008; Vila-Francés et al., 2011). Depending on the technology used, the selection of the wavelengths can be performed by separating the incident radiation into individual wavelengths (e.g. imaging spectrophotometer) or blocking the radiation in such a way that only the desired wavelength reaches the image sensor (e.g. LCTF and AOTF).

Imaging spectrophotometers separate the reflection of a very thin slice of the scene into its spectral components by using a prism or a diffraction grating and project the spectral information onto an image sensor. This kind of device generally operates in a line scanning mode, i.e. the object is scanned line-by-line as the entire field of view is acquired. One advantage of the imaging spectrophotometer is its high spectral resolution. On the other hand, the major drawback of the vision systems based on this technology is the need to move the object with respect to the spectrophotometer in order to acquire an entire image. An AOTF is basically an optical band-pass filter based on diffraction that can be rapidly tuned to discrete wavelengths by varying the frequency of an acoustic wave propagating through an anisotropic crystal medium (Chang, 1976). Unlike a classical diffraction grating, the AOTF only diffracts one specific wavelength of light, so that it acts more like a band-pass filter with a narrow bandwidth than a diffraction grating.

LCTF devices use electronically controlled liquid crystal elements to transmit light with a selectable wavelength whilst excluding all others. The LCTF is based on Lyot filters, which consist of several optical stages each composed of a liquid crystal layer sandwiched between two linear polarisers. Due to the birefringence of liquid crystal, as the incident linearly polarised light traverses the liquid crystal layer, it is split into two light rays (the ordinary and the extraordinary rays), which have different optical paths though the liquid crystal and emerge with a phase delay that is dependent on the wavelength. After transmission through the liquid crystal, only those wavelengths that are in phase are transmitted by the polariser to the next filter stage (Hecht, 2001). Tunability is provided by the relative alignment of the liquid crystals along an applied electric field between the two polarisers. Vision systems based on LCTFs and AOTFs acquire images with a high spatial resolution, but limited spectral resolution. On the contrary, systems based on imaging spectrophotometers can acquire images with high spectral resolution but low spatial resolution. When comparing the systems based on tunable filters, an important advantage of LCTF-based systems is that they offer a wider field of vision and better imaging quality than those based on AOTFs (Vila-Francés et al., 2010). On the other hand, LCTF hyperspectral technology presents, as its major drawback, a tuning time of tens of milliseconds, which is much longer than that required for AOTF technology, typically tens of microseconds. Further information on the principles of hyperspectral imaging and the recent advances and applications of this technology for fruit and vegetable quality assessment can be found in a review by Lorente et al. (2012).

1.1.3.2. Light backscattering imaging systems

Light backscattering imaging is another optical technique that has recently emerged as an alternative tool for fruit inspection, which combines spectroscopic and imaging approaches in the visible and NIR regions of the electromagnetic spectrum. Basic concepts related to light interaction with turbid biological materials, such as fruit, are first reviewed for a better understanding of this imaging technique. Light is properly the electromagnetic radiation that is visible to the human eye, which covers the range between 380 nm and 780 nm. However, radiation in some other ranges of the electromagnetic spectrum, especially in the UV and NIR regions, is also commonly referred to as light, since physical processes that are relevant for these ranges are similar to those for visible light. As shown in Figure 1.4, when a light beam interacts with a turbid media, such as a fruit, reflectance, absorption and transmittance happen (Birth, 1976). Particularly, light reflectance (scattering) is shown in two different geometries: specular or Fresnel reflectance and diffuse reflectance, the latter also referred to as backscattering. It is assumed that a small portion of incident light (only about 4-5%) is reflected on the surface of the sample (specular reflectance) and the rest penetrates into the tissue. In the tissue, most of the entering light is

scattered backwards to the exterior tissue surface after interacting with the internal components of the fruit (backscattering), whereas the remaining radiation is absorbed by the tissue or transmitted further out of the fruit in different direction (Meinke and Friebel, 2009).

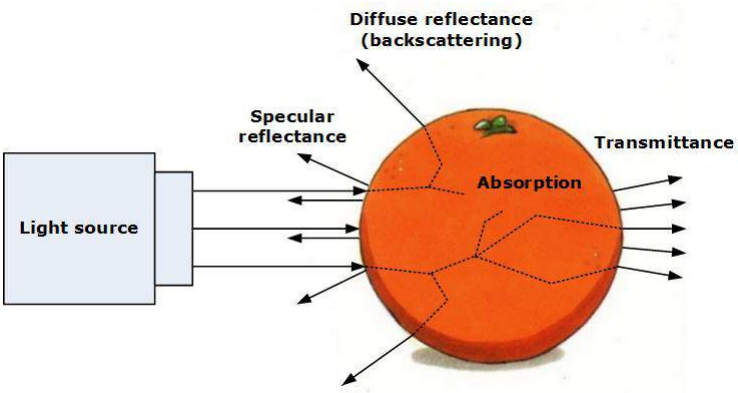

Figure 1.4. Modes of light interaction with fruit.

The modes of light interaction with biological tissues are specific to each material, and the relative contribution of each mode depends on the chemical constitution and structural properties of the sample. Therefore, the optical analyses can be used to characterise fruits (Salguero-Chaparro et al., 2014), particularly by means of the absorption and scattering properties, which are in turn described by the absorption coefficient (μ_a) and the reduced scattering coefficient (μ_s') (Tuchin, 2000). Light absorption is mainly related to the chemical components of the fruit, such as sugar, water or pigments (Williams and Norris, 2001). The chemical bonds of biological materials absorb light energy at particular wavelengths, thus the absorption properties are strongly dependent on light wavelength. In this sense, the conventional spectroscopy approach, which covers a wide range of wavelengths, is successfully used to measure chemical components of food and agricultural products, such as the soluble solids content (SSC) of fruit. By contrast, light scattering inside a fruit is affected by the structural properties of the tissue, such as density, particle size and cellular structures (Seifert et al., 2014a). In a strongly scattering material, such as fruit, photons often undergo multiple scattering before either being absorbed or exiting from the material, which largely determines the intensity of the scattered light that is emitted outside the fruit (McGlone et al., 1997). Hence, backscattered light, recorded by an imaging system, can be useful as an indirect measure of the histology of fruit, such as flesh firmness. Furthermore, if spectral information is added to the spatial imaging information, combined analyses of texture and chemical composition can be done. Accordingly, many research works have been focused on using light backscattering

imaging systems to assess quality of apples (Qing et al., 2007; Lu et al., 2010) and other fresh fruit (Lu and Peng, 2006; Romano et al., 2008); however, no research has been reported to detect decay in citrus fruit using this technique. The decaying process in citrus fruit is mainly characterised by the weakening of the cell walls due to changes in enzymatic activity (Barmore and Brown, 1979) and the subsequent early visible symptom such as the accumulation of liquid in the tissue (Barmore and Brown, 1981). In consequence, since structural changes in fruit tissue, as well as possible associated changes in chemical composition, and therefore changes in the optical properties, are expected, the light backscattering imaging technique may have the potential for decay detection.

Systems based on light backscattering imaging have two essential components: a light source and an imaging unit. According to the kind of light source and imaging device, light backscattering imaging is divided into two main approaches: laser-light backscattering imaging (LLBI) and broadband-light backscattering imaging. The latter approach in turn includes multispectral light backscattering imaging (MLBI) and hyperspectral light backscattering imaging (HLBI) (Mollazade et al., 2012). In the LLBI technique, the light source is a laser diode, which is the best monochromatic light source (Lu and Peng, 2007; Qing et al., 2007; Baranyai and Zude, 2009). Laser light can deliver more light per unit area for a specific wavelength than a broadband light source. Therefore, light penetrates deeper into the fruit and the backscattered photons contain more information. Furthermore, the image acquisition is fast. On the other hand, the acquired images carry information just in a specific wavelength, thus requiring multiple lasers to acquire backscattering images at multiple wavelengths, which can be expensive. In the MLBI and HLBI approaches, a broadband light, such as the light generated by a halogen lamp, is usually passed through an optic fibre with small diameter and then focused on the sample by a converging lens (Lu, 2004; Peng and Lu, 2006b; Qin et al., 2009b). The main advantage of broadband light is that this light source can provide all the required wavelengths. On the contrary, the major drawback is the low output power per unit area, thus leading to shallow light penetration and the subsequent loss of information. With regard to the imaging unit, the detector should have a high efficiency in the spectral areas covering the needed wavelengths, usually in the visible and short-wave NIR regions. In backscattering imaging systems, both colour and monochromatic cameras, commonly CCD-based cameras, are employed. However, colour cameras are much less sensitive and slower than monochromatic cameras. Therefore, monochromatic cameras are preferred over the colour ones in order to acquire higher-quality images in a faster way. In the LLBI approach, the imaging unit only consists of a camera. However, since a broadband-light source is used in the MLBI and HLBI techniques, in addition to an image detector, a wavelength selection device is also required for image acquisition, such as imaging spectrophotometers or tunable filters (earlier discussed in Section 1.1.3.1) in the HLBI and a few filters at specific wavelengths in the MLBI. Since the

HLBI technique is based on hyperspectral vision systems, this approach is expensive and time-consuming and, therefore, it is not suitable for real-time sorting applications. In consequence, the target of the HLBI is to find a limited number of wavelengths that provide the maximum information about the structural and chemical properties of a particular variety of fruit (Peng and Lu, 2006a). Then, to implement the backscattering imaging technique in practice, the selected wavelengths can be used in LLBI or MLBI systems in order to assess quality of fruit in a relatively cheap, simple and fast way. However, for practical applications, LLBI systems are more suitable than MLBI systems, since they obtain more information about the tissue, as commented above.

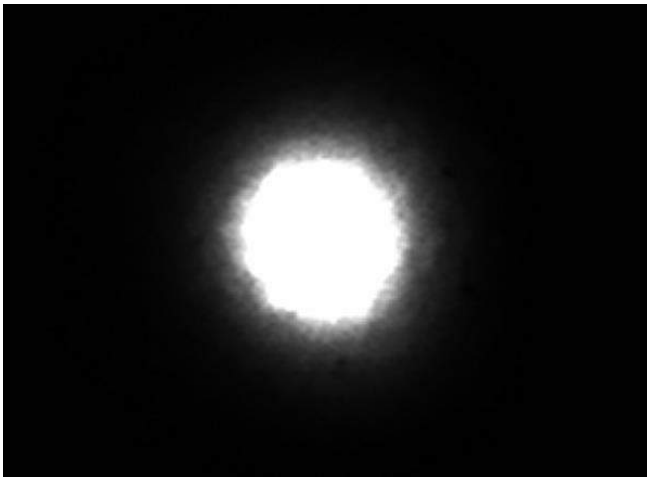

Figure 1.5. A typical raw backscattering image.

With regard to the position of the light source in the light backscattering imaging systems, the incident angle of the light beam should be chosen in such a way that the specular reflectance acquired by the detector is minimum, since the purpose of backscattering imaging is only to acquire the backscattered photons. Researchers recommended a small incident angle, approximately in the range between 5º and 25º with respect to the vertical axis (Lu, 2004; Qin and Lu, 2007). Furthermore, a small incident angle, coupled with a small beam size, allows the assumption that the light beam is almost perpendicular to the fruit surface, thus obtaining images that are symmetrical with respect to the incident point, as shown in Figure 1.5. Raw backscattering image data could be used directly as the input feature vector to predict the fruit quality by a calibration model. However, the dimension of the feature vector cannot be taken arbitrary large because an increase of the dimension leads to a decrease of performance in the predictions (Heijden et al., 2004). Due to the radial symmetry of the backscattering images, they are usually

reduced to one-dimensional profiles through radial averaging (Lu, 2004). To this end, each backscattering image is first divided into a number of concentric rings of a specified width, and the radial intensity of the backscattering profile is then calculated by averaging all pixels within each circular ring.

Afterwards, in order to get even higher performance predictions, a lower-size feature vector can be obtained by extracting new features from the one-dimensional profiles. For this purpose, two different methods are commonly employed to characterise backscattering profiles. One method is to find the parameters of symmetric distribution functions describing the behaviour of backscattering profiles. Different distribution functions have been investigated to fit the backscattering profiles of fruit, such as the Lorentzian function or the Gaussian function (Peng and Lu, 2005). The other method for characterising the backscattering profiles is a physical approach, instead of purely statistical as the previous one. This physical approach consists in extracting some optical properties (the absorption, μ_a, and reduced scattering, μ_s', coefficients) of fruit from Farrell's diffusion theory (Farrell et al., 1992), which provides a faithful description of the shape of the backscattering profiles (Qin and Lu, 2007; Qin et al., 2009b). Farrell's diffusion theory model is valid only for materials with scattering dominance, such as turbid biological materials (including fruit) in the visible and short-wave NIR spectral regions, approximately between 500 nm and 1300 nm. Similarly to the parameters of the distribution functions, the optical coefficients can be used for assessing quality attributes of fruit. However, the additional advantage of the physical model, compared to the statistical approach, is that it allows to measure and separate the absorption and scattering properties. Optical technologies such as conventional spectroscopy measure the combined effect of absorption and scattering properties in the sample without being able to separate scattering from absorption, since the two phenomena are intertwined (Meinke and Friebel, 2009). Particularly, the intensity level of the measured spectrum is strongly affected by the scattering process, while the shape is more related to the absorption process. In this sense, measurement and separation of the optical properties of a biological tissue by means of backscattering imaging, coupled with the physical approach for profile characterisation, are useful for quantitative analysis of light-tissue interactions, thus facilitating the future development of more effective optical sensing techniques for determining and quantifying the structural characteristics and chemical composition of food and agricultural products. More details about the theoretical and technical principles of light backscattering imaging, as well as the recent achievements and applications of this technology for food and agricultural produce quality evaluation, are given in a comprehensive review by Mollazade et al. (2012).

1.1.3.3. Spectroscopy systems

Conventional spectroscopy also appears to be a promising alternative for decay detection in citrus fruit since this technology can rapidly measure the optical properties of the samples, also in spectral regions outside the visible electromagnetic spectrum. This optical technique uses electromagnetic radiation covering a large number of narrow spectral bands over a continuous spectral range, usually in the visible and NIR spectral regions. Both spectroscopy and hyperspectral imaging involve a large amount of spectral data, and even share some acquisition equipment. Hence, similarly to hyperspectral imaging, in spectroscopy, it is necessary to extract essential information contained in the spectra using techniques for reducing the dimensionality of the data (Song et al., 2013), since the presence of irrelevant or redundant spectral information could lead to lower performance predictions of fruit quality. However, despite the similarities between both technologies, they should not be confused. Hyperspectral imaging acquires simultaneously spectral and spatial information from an object, while spectroscopy provides only spectral information captured at a particular spot on the sample, since the point detector used in this technology has size limitation. Conversely, this lack of spatial information makes spectroscopy much less time-consuming and more appropriate for real-time applications than hyperspectral imaging. Another difference between both techniques is the way in which they use the light source.

In this sense, contrary to the diffuse lighting used in hyperspectral imaging to illuminate the scene uniformly, in spectroscopy, light hits directly a product (e.g. fruit), and the reflected or transmitted radiation is measured by a light detector. When the radiation penetrates the fruit, its spectral characteristics change through wavelength. This change depends on the absorption properties of the fruit, strongly associated with the chemical composition, as well as on its light scattering properties, which are related to the microstructure, as further discussed in Section 1.1.3.2. In particular, the scattering process affects the intensity level of the measured spectrum rather than the shape, this being more related to the absorption process of chemical components in the fruit at specific wavelengths. Similarly to backscattering imaging, in spectroscopy, the light source is aimed towards the fruit. In backscattering imaging, the backscattered light is recorded by an imaging system, thus obtaining spatial information of the light signal on the sample. On the contrary, spectroscopy measures light without tracking spatial information of the light signals. Due to the commented dependences of the spectra with the absorption and scattering properties of fruit, measurements acquired using spectroscopy systems are useful for determining the textural and chemical properties of fruit, such as flesh firmness or SSC. In fact, spectroscopy is one of the most investigated techniques for non-destructive quality assessment of a wide range of food

products. Therefore, this technology is arguably the most advanced with regard to equipment and applications, and such technological progress has thus led to the development of spectroscopy systems with high acquisition speed used in the agro-food industry for real-time sorting of products according to their quality. Accordingly, many studies have been reported to assess the internal and external quality of different fresh fruit by spectroscopy systems (Schmilovitch et al., 2000; Liu and Ying, 2005; Han et al., 2006; Nicolaï et al., 2006; Xing et al., 2006). Most of the research studies using this technology on citrus fruit have been focused on evaluating the internal quality attributes, such as SSC, acid levels or vitamin C content (Lee et al., 2004; Guthrie et al., 2005; Xia et al., 2007; Sun et al., 2009; Liu et al., 2010b). However, very limited research work has been conducted to assess the external quality of citrus fruit, such as the presence of surface defects, by means of spectroscopy in the visible and NIR ranges (Gaffney, 1973; Zheng et al., 2010). With respect to spectroscopy research particularly aimed at decay detection, there has been reported a preliminary study conducted by Blasco et al. (2000) for early detection of *Penicillium digitatum* and *Alternaria citri* fungi in citrus fruit using NIR spectroscopy, pointing to differences in reflectance spectra between sound and infected areas in the peel of fruit. However, further research is still lacking for decay detection in citrus fruit using this technology. For further information, multiple applications of spectroscopy for quality assessment of citrus fruit and other fruit and vegetables can be consulted in the reviews by Nicolaï et al. (2007) and Magwaza et al. (2012), respectively.

Depending on the sample properties to be analysed, there are three different measurement setups frequently used for fresh fruit quality evaluation, shown in Figure 1.6: transmittance, reflectance and interactance (Schaare and Fraser, 2000). In the case of transmittance mode, the incident light illuminates perpendicularly to one side of the sample and the transmitted light is detected from the opposite side. In practice, this mode is frequently used to assess internal quality attributes, such as SSC or acid levels, of fruit, especially fruit with thick skin (e.g. citrus fruit), since it allows to obtain information on inner portion of the product (Lee et al., 2004; Han et al., 2006). However, very high intensity of incident illumination is needed in order to have at least some light transmitted, thus causing possible thermal damage to the fruit at the illuminated spot and the subsequent alteration of spectral properties. In reflectance mode, the detector receives both radiation specularly reflected from the sample, which contains no information about the internal composition of sample, and backscattered radiation that has interacted with the internal particles of sample. Therefore, in order to minimise specular reflectance acquired by the detector, light source and detector are often mounted under a specific angle, commonly 45º. In the case of interactance mode, the detector is shielded from receiving specular reflectance. To this end, the light source and detector are placed parallel to each other in such a way that specular reflectance cannot directly reach the detector. For example, this can be achieved by means of a bifurcated

probe in which fibres leading to the light source and detector are parallel to each other and in direct contact with the surface of the fruit sample. The main difference between reflectance and interactance modes is that the interactance setup guarantees that only backscattered light is detected. Some of the advantages of reflectance and interactance modes are that measurements are easier to obtain, lower intensity of illumination is required, and the intensity levels of the reflected radiation are much higher than those of transmitted radiation. On the other hand, the incident light cannot reach a deep position in the sample because of high absorption or multiple scattering and, therefore, the reflectance spectra do not contain a lot of information about the internal quality of the flesh, especially in thick-skinned fruit. However, reflectance and interactance modes are preferred over transmittance setup when only information of substances located on or just under the fruit surface is required. For example, measurements of reflectance are used to determine chemical components in fruit with thin skin and to assess the external quality of fruit, such as the colour of product surface and the presence of surface defects (Liu and Ying, 2005; Xing et al., 2006). In this sense, reflectance spectra acquired by spectroscopy systems may be also suitable for detecting decay in citrus fruit.

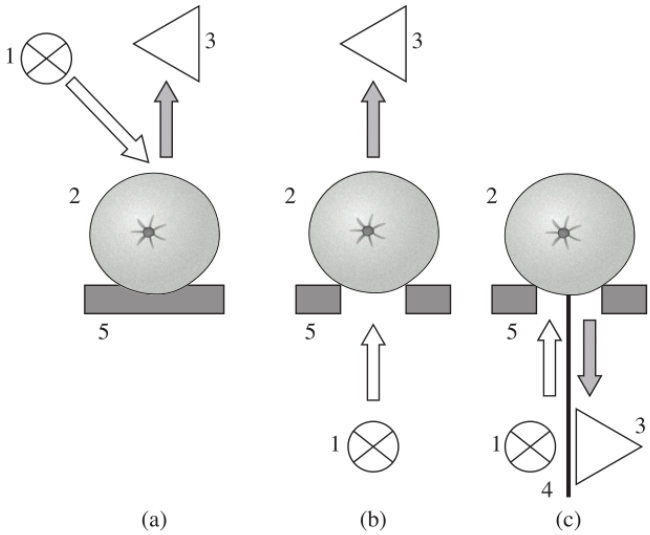

Figure 1.6. Measurement setups of spectra: (a) reflectance, (b) transmittance, and (c) interactance. 1: light source; 2: fruit sample; 3: light detector; 4: light shield; 5: sample holder.

With respect to the technological components in spectroscopy, a spectroscopy system mainly consists of a light source (usually a halogen light source), a wavelength selection device and a light detector. In addition, other optical components are usually required, such as optical fibres to conduct the light from the light source to the sample and from the sample to the detector, beam splitters, lenses and collimators. In spectroscopy, the most widespread devices to obtain monochromatic light at particular wavelengths are filters, which block the radiation in such a way that only the desired wavelength reaches the image detector, and monochromators, which separate spatially the incident radiation into individual wavelengths. However, although filters and monochromators are the most commonly-used wavelength selectors, there also exists other more sophisticated ways to select spectral information, which are used in modern spectroscopy systems. For example, laser-based spectroscopy systems have different laser light sources or a tunable laser. Other modern systems called Fourier-transform spectrophotometers use a Michelson interferometer to obtain spectral information, instead of using a monochromator or filter. In respect to filters, one relatively cheap option for performing spectral selection is the use of interference filters, such as Fabry-Perot filters; however, this equipment is limited to the use of discrete wavelengths. Other filters that can scan through a wide range of wavelengths are the tunable filters, such as AOTF and LCTF, earlier discussed in Section 1.1.3.1. Nevertheless, tunable filters are expensive and time-consuming. With regard to monochromators, although both prisms and diffraction gratings, like those used in imaging spectrophotometers, are frequently-employed in spectroscopy, the gratings are preferred over the prisms due to their higher spectral resolution. Among all the commented filters and monochromators, the main options to produce monochromatic light are interference filters, AOTF and gratings, with grating-based systems currently dominating the market. Depending on the required spectral ranges, different types of detectors that use different technologies and materials can be chosen. Common examples of detectors used in spectroscopy are photodiode arrays (PDA) and CCD arrays. For real-time fruit grading applications, the currently-preferred spectroscopy systems usually include a fixed grating, coupled with a silicon CCD array or PDA detector (400-1000 nm) or an indium-gallium-arsenide (InGaAs) PDA detector (800-1700 nm), since a typical acquisition time below 50 ms is thus achieved. More guidelines for selecting a spectroscopy system with appropriate components and measurement setup for each particular application are given by Herold et al. (2009).

1.1.4. Machine learning techniques

Agricultural products such as fruit and vegetables can be characterised by means of the measurements acquired with the different optical techniques commented in previous sections.

Particularly, in hyperspectral imaging, each pixel of the hyperspectral image of a particular piece of fruit or vegetable is characterised by its reflectance spectrum (i.e. reflectance levels at a large number of consecutive spectral bands). On the contrary, in backscattering imaging, instead of characterising each pixel individually, the whole backscattering image at each wavelength is usually featured by means of several parameters obtained from fitting the one-dimensional backscattering profile with a statistical or physical profile modelling approach. Therefore, the features characterising completely an agricultural product consist of the profile parameters obtained for all the backscattering images acquired at different wavelengths. In the case of spectroscopy, each fruit or vegetable is described by the reflectance or transmittance spectrum measured at a particular spot on the product.

After identifying or extracting features from the optical measurements, the problem encountered is how to predict the internal and external quality of agricultural products from their associated features. With the fast development of artificial intelligence, this process can be performed by using machine learning techniques. These mathematical algorithms are capable of learning the pattern of the input features from previous experience as humans do, that is, machine learning methods can accumulate experience through data and develop new knowledge so that their performance on specific tasks improves over time (Izenman, 2008). Machine learning algorithms can be divided into supervised and unsupervised methods. In supervised learning, there is a set of n samples, $\{\mathbf{x}_i, t_i\}_{i=1\ldots n}$, where $\mathbf{x}_i$ is the input m-dimensional feature vector for the i-th sample with a known desired output variable t_i, and the goal is to find a function of the input features to approximate the known outputs, which can be used to generate an output for future unseen inputs. On the other hand, in unsupervised learning, there is no information available to define an appropriate output variable, and the objective is to discover underlying patterns in the input data (e.g. by means of a cluster analysis), instead of finding a mapping from inputs to outputs. Both regression and classification models are supervised learning techniques. The main difference between both predictive models is the type of the output variable, which is continuous (i.e. a real number) in regression models and discrete or categorical in classification models. In quality evaluation of agricultural products, regression models are used to estimate a response value related to quality of fruit and vegetables (e.g. SSC or acid levels), whereas classifiers are employed to predict the class membership of the samples (e.g. the presence or absence of bruises or decaying parts in the product surface).

The above-commented features extracted from optical measurements could be employed directly as inputs of a regression or classification model for decision making in order to predict the quality of agricultural products. However, for high-dimensional data (i.e. feature vectors with more than 10 dimensions), some features may be irrelevant or redundant for the tackled problem and,

therefore, the reduction of the number of input features is usually performed prior to applying the predictive model. This pre-processing step involves several benefits, especially when using hyperspectral imaging or spectroscopy, which are characterised by a particularly large amount of spectral data. In most predictive algorithms, the complexity (i.e. the number of internal parameters) depends on the number of inputs, as well as on the size of the dataset, and, hence, the reduction of the input dimensionality usually leads to simpler models, which require less memory and computational operations (Alpaydin, 2004). In addition, simpler models tend to be more robust to the overfitting problem, especially on datasets with a limited number of samples, thus achieving higher performance predictions (Tian, 2010). Overfitting occurs when the predictive model memorises the known data rather than learning to generalise from trend and, therefore, models that have been overfitted will generally have poor performance when predicting unseen data. As an extreme example, the overfitting problem is accentuated when the number of internal parameters of the predictive model is the same as or greater than the number of samples (Izenman, 2008).

For overcoming these problems, there are numerous supervised and unsupervised machine learning techniques that reduce the dimensionality of the feature space without loss of information, which can be divided into feature extraction and feature selection methods according to the way in which the methods operate on the data for reduction purposes (Song et al., 2013). Feature extraction techniques, commonly referred as manifold learning techniques, transform the data in a high-dimensional space into a lower-dimensional space that preserves the observed properties of the data, generally known as manifold, and their goal is to recover the low-dimensional manifold embedded within the high-dimensional space. The main disadvantage of these techniques is that all the original features are required for computing the new ones. Particularly, principal component analysis (PCA; Jolliffe, 2002) is a popular manifold learning technique that has been widely used for data reduction in research focused on fruit and vegetables quality inspection by means of optical techniques (He et al., 2005; Liu et al., 2006; Omid et al., 2010). On the other hand, instead of creating new features, feature selection approaches try to find a subset of the original features that contains the least number of features with the most significant information. Feature selection techniques can be essentially categorised into wrapper and filter methods (Guyon and Elisseeff, 2003). Wrapper methods use as selection criterion the goodness of fit between the input features and the output provided by the predictive model under consideration, such as a neural network, thus presenting the advantage of optimising, by their nature, the performance of the prediction process. Within these methods, a traditional measure for evaluating classifiers is the classification success rate. On the contrary, filter methods use an indirect measure of the quality of the selected features that does not require the use of the predictive model (e.g. by evaluating the correlation function between each input feature and the

dependent variable). Therefore, filter techniques involve a faster convergence and greater robustness to changes in the classification or regression model.

Unlike feature extraction methods, feature selection techniques, by their nature, do not require all the original features for obtaining the essential information from data. Therefore, this kind of techniques is commonly employed for reducing the high-dimensional hyperspectral images to multispectral ones by selecting a small set of wavelengths (Gómez-Sanchis et al., 2012; Vélez-Rivera et al., 2014). As earlier stated in Section 1.1.3.1, this wavelength selection process is of main importance for the food quality industry, since multispectral images are easier to implement in vision systems suitable for the real-time product inspection, due to the fact that the acquisition time of these images is faster and the subsequent data analysis is simpler and less time-consuming than for hyperspectral images. Similarly, the HLBI systems, coupled with feature selection methods, are used for finding a limited number of wavelengths (Peng and Lu, 2006a), which can be then used in LLBI or MLBI systems for practical quality assessment applications based on backscattering imaging, as commented in Section 1.1.3.2. In LLBI or MLBI systems, which acquire images only at a few wavelengths, since the number of obtained features (typically profile parameters corresponding to the specific wavelengths) is not so high anymore, it is not strictly necessary to apply dimensionality reduction techniques (Qing et al., 2008; Romano et al., 2008). However, either feature selection or feature extraction methods are recommended to be used to obtain an even lower-size feature vector (Peng and Lu, 2007), thus possibly achieving higher performance predictions. In the case of spectroscopy, both types of dimensionality reduction methods can be employed (Guthrie et al., 2005; He et al., 2005), since the use of all the original features for obtaining the most useful information is not a limiting factor for commercial spectroscopy systems, which usually acquire the complete spectrum of a sample at high speed.

From all the aforementioned issues, it is reasonable to think that, when using optical techniques for quality assessment of agricultural products, a key step is the selection of appropriate machine learning techniques for both data dimensionality reduction and prediction purposes. Therefore, new research on agro-food quality assessment applications based on optical systems should be oriented towards not only technological equipment improvements, but also the development of powerful machine learning techniques capable of gathering useful information about quality from the optical measurements in a reliable way.

1.2. Objectives of the doctoral thesis

The overall goal of the present doctoral thesis is to advance in the automatic detection of early symptoms of decay caused by *Penicillium* spp. fungi in citrus fruit using optical systems and machine learning techniques, thus providing alternatives to manual inspection for accomplishing this detection task more efficiently and, consequently, leading to a potential reduction of the use of fungicides. For this purpose, in particular, three different optical techniques are investigated, including hyperspectral imaging, light backscattering imaging and spectroscopy. The systems based on these optical technologies are not limited to the visible part of the electromagnetic spectrum, unlike standard vision systems based on colour cameras. Specifically, in addition to the visible spectral region, the optical systems used in this thesis also operate in the NIR area, where the human eye is not sensitive. Therefore, these systems may have the potential for detecting hardly-visible damage in citrus fruit, such as decay at early stages.

When using optical techniques for fruit quality assessment, a key step is the selection of appropriate machine learning techniques capable of gathering useful information about quality from the optical measurements in a reliable way. In particular, the detection of decay in citrus fruit can be regarded as a classification problem, in which features obtained from the optical measurements of fruit, after possibly being subjected to a dimensionality reduction process, are used as input vectors of a classifier in order to discriminate fruit with symptoms of decay from sound fruit.

In order to reach the aforementioned overall goal, this can be subdivided into more specific objectives related to each optical technology. This is done due to the fact that each optical technique has a different inherent nature and, therefore, the treatment of the obtained data should be specific to each technology in order to detect decay in citrus fruit. The specific objectives are grouped according to the optical technologies in the following sections.

1.2.1. Hyperspectral imaging

In this doctoral thesis, in order to explore the possibilities of hyperspectral imaging for decay detection, it is used a hyperspectral vision system based on LCTFs operating in the visible and NIR spectral regions. This kind of hyperspectral systems can acquire images with high spatial resolution, and does not require the movement of the fruit sample with respect to the imaging system to acquire an entire image, unlike systems based on imaging spectrophotometers. In

addition, LCTF-based systems offer a wider field of vision and better imaging quality than those based on AOTFs.

The specific goals related to hyperspectral imaging are twofold:

- Due to the current need for reducing the high-dimensional hyperspectral images to multispectral ones for the subsequent implementation in real-time inspection systems, the main goal within this optical technology is to propose a novel feature selection methodology suitable for selecting a reduced set of wavelengths that are effective in the detection of decay in citrus fruit.
- Another important goal is to compare the proposed feature selection method with other common feature selection techniques in terms of the classification performance in the tackled problem of decay detection in citrus fruit using hyperspectral images.

1.2.2. Light backscattering imaging

In particular, a LLBI system with diode lasers emitting at several wavelengths in the visible and NIR ranges is used in this thesis, instead of a broadband-light backscattering imaging one, such as a MLBI or HLBI system. This system selection is mainly motivated by the fact that LLBI systems can obtain more information about the fruit tissue than MLBI and HLBI systems, since laser light penetrates deeper into the fruit than broadband light.

The specific objectives related to light backscattering imaging are enumerated as follows:

- Within this optical technique, the most important objective is undoubtedly to evaluate, for the first time, the potential of LLBI for detecting decay caused by fungi in citrus fruit, before the appearance of fruiting structures.
- Another objective is to combine and rank the different laser wavelengths used to acquire the backscattering images in terms of their contribution to the detection of decay, in order to figure out the most suitable combination of laser wavelengths to detect fruit with decay.
- In order to get high classification performance, each backscattering image is usually characterised by means of several parameters obtained from fitting the one-dimensional backscattering profiles with a statistical or physical profile modelling approach. The profile parameters obtained with both approaches can be then used for assessing quality attributes of fruit. In fact, this thesis also aims at evaluating and comparing the two kinds

of profile modelling approaches in terms of their classification performance in the addressed problem of decay detection in citrus fruit.

- The additional advantage of the physical profile modelling approach, compared to the statistical one, is that it also allows to measure and separate the absorption and scattering properties of biological products, which is useful for quantitative analysis of light-tissue interactions. In this sense, other goal of this thesis is the measurement and separation of the optical properties of sound and decaying tissues of citrus fruit at different wavelengths, in order to extract more knowledge about the underlying optical properties associated with the decaying process in citrus fruit.
- In addition, even though the number of features characterising completely a fruit sample with LLBI is not so high (i.e. profile parameters obtained for the backscattering images acquired at a few laser wavelengths), dimensionality reduction techniques are recommended to be used to obtain an even lower-size feature vector, thus possibly leading to higher performance predictions. Therefore, an ultimate goal related to this optical technology is to evaluate and compare different feature selection methods, in order to find out which technique leads to the best classification performance for decay detection in citrus fruit.

1.2.3. Spectroscopy

This doctoral thesis particularly makes use of a spectroscopy system in reflectance mode, operating in two different spectral ranges included in the visible and NIR regions. Reflectance mode is preferred over transmittance setup when only information of substances located on or just under the fruit surface is required. Therefore, this mode may be suitable for detecting decay in citrus fruit. Some of the advantages of this mode are that measurements are easier to obtain, lower intensity of illumination is required, and the intensity levels of the reflected radiation are much higher than those of transmitted radiation.

The specific objectives within spectroscopy are enumerated as follows:

- With respect to this popular optical technique, the main goal is to evaluate more thoroughly the feasibility of reflectance spectroscopy in the visible and NIR regions as a tool for the automatic detection of early decay symptoms caused by fungi in citrus fruit, since only a preliminary study has been reported about the use of spectroscopy for this purpose (Blasco et al., 2000) and, therefore, further research is still lacking for decay detection in citrus fruit using this technology.

- Regarding the different spectral regions in which the used spectroscopy system operates, this thesis intends to find out which of the two spectral ranges provides the best classification performance for decay detection in citrus fruit.
- In spectroscopy, pre-processing techniques are usually employed to remove possible noise from the measured spectra in order to improve the results of quality prediction. In this respect, this research work also aims at studying the influence of several pre-processing techniques commonly used in spectroscopy on the classification performance in the tackled problem.
- Due to the large amount of spectral data involved in spectroscopy, a step of particular interest when using this technology is to extract essential information contained in the spectra using techniques for reducing the dimensionality of the data, since the presence of irrelevant or redundant spectral information could lead to lower performance predictions of fruit quality. In this sense, an important goal of this thesis is to investigate and compare different feature extraction techniques (i.e. manifold learning techniques), which are able to transform the high-dimensional spectral data into meaningful representations of reduced dimensionality with the most relevant information, in terms of their classification performance for decay detection in citrus fruit. In practice, feature extraction methods are commonly employed in spectroscopy research, since the use of all the original spectral features for obtaining the most useful information is not a limiting factor for the commercial spectroscopy systems, such as that used in this thesis, which can acquire the complete spectrum of a sample at high speed.
- Prior to dimensionality reduction, a key step is to estimate the target dimensionality of the corresponding lower-dimensional data representations, since manifold learning methods need the dimensionality of data as an external parameter. Therefore, another objective of this thesis is to evaluate and compare several dimensionality estimators according to their classification performance for the decay detection problem.

1.3. Research framework of the doctoral thesis

The present doctoral thesis summarises the research efforts of its author, during the period 2010-2014, as a member of the Computer Vision Laboratory at the Agro-engineering Centre as part of the Valencian Institute for Agricultural Research (IVIA). Due to the great importance of the citrus industry in the Valencian Community, a substantial part of research conducted at the IVIA is

related to citrus fruit, such as the development of new citrus cultivars, introduction of improved techniques for cultivating and harvesting citrus fruit or the incorporation of new technologies to assess quality of citrus fruit.

In particular, the research topics of the thesis are embedded in the context of several research projects aimed at the development of new technologies based on computer vision (INIA-FEDER RTA2009-00118-C02-01 and MICINN-FEDER DPI2010-19457) and spectroscopy (INIA-FEDER RTA2012-00062-C04-01) for automatic quality inspection of agricultural products.

Furthermore, part of the research work dealing with machine learning techniques is in the framework of existing close collaboration between the Computer Vision Laboratory at the IVIA and the Intelligent Data Analysis Laboratory (IDAL) at the Electronic Engineering Department of the University of Valencia. The IDAL is concerned with the application of techniques coming from very different areas (e.g. statistics, data mining, machine learning or optimisation) to real-world data analysis problems. This research group applies those techniques to a wide range of applications in medicine, pharmacy, agriculture, marketing, etc.

In addition, it should also be highlighted that specific research related to backscattering imaging carried out in this doctoral thesis is the product of fruitful collaborative research with a German research group during two research stays abroad of three months each. Specifically, the foreign research team is the Sensor Technology Research Group at the Horticultural Engineering Department as part of the Leibniz-Institute for Agricultural Engineering Potsdam-Bornim (ATB). The overall mission of this research group is essentially the assessment of properties of fresh fruit by means of optical and electro-chemical analyses.

1.4. Structure of the doctoral thesis

This doctoral thesis is presented as a collection of research papers that address the goals listed in Section 1.2. In particular, the thesis consists of three papers previously published in peer-reviewed international journals, one paper accepted for publication and other paper submitted, but yet not accepted for publication, with the author of this doctoral thesis as the first author of the five papers. The journals in which the papers have been published (or accepted or submitted) have impact factors within the first quartile in their subject categories, according to the 2013 Journal Citation Reports (JCR) published by Thomson Reuters. The complete references of the research papers comprised in this thesis, as well as the impact factor and quartile in the subject category of interest for each journal, are listed as follows:

- Lorente, D., Aleixos, N., Gómez-Sanchis, J., Cubero, S., Blasco, J., 2013. Selection of optimal wavelength features for decay detection in citrus fruit using the ROC curve and neural networks. Food and Bioprocess Technology, 6, 530-541.

  Paper status in the journal: published.

  Journal information (2013): impact factor: 3.126; subject category: *Food Science & Technology*; journal rank in the subject category: 12/123; quartile in the subject category: Q1.

- Lorente, D., Blasco, J., Serrano, A.J., Soria-Olivas, E., Aleixos, N., Gómez-Sanchis, J., 2013. Comparison of ROC feature selection method for the detection of decay in citrus fruit using hyperspectral images. Food and Bioprocess Technology, 6, 3613-3619.

  Paper status in the journal: published.

  Journal information (2013): impact factor: 3.126; subject category: *Food Science & Technology*; journal rank in the subject category: 12/123; quartile in the subject category: Q1.

- Lorente, D., Zude, M., Regen, C., Palou, L., Gómez-Sanchis, J., Blasco, J., 2013. Early decay detection in citrus fruit using laser-light backscattering imaging. Postharvest Biology and Technology, 86, 424-430.

  Paper status in the journal: published.

  Journal information (2013): impact factor: 2.628; subject category: *Food Science & Technology*; journal rank in the subject category: 20/123; quartile in the subject category: Q1.

- Lorente, D., Zude, M., Idler, C., Gómez-Sanchis, J., Blasco, J. Laser-light backscattering imaging for early decay detection in citrus fruit using both a statistical and a physical model. Accepted for publication in Journal of Food Engineering.

  Paper status in the journal: accepted for publication.

  Journal information (2013): impact factor: 2.576; subject category: *Food Science & Technology*; journal rank in the subject category: 23/123; quartile in the subject category: Q1.

- Lorente, D., Escandell-Montero, P., Cubero, S., Gómez-Sanchis, J., Blasco, J. Visible-NIR reflectance spectroscopy and manifold learning methods applied to the detection of fungal infections on citrus fruit. Submitted to Journal of Food Engineering.

Paper status in the journal: submitted, but yet not accepted for publication.

Journal information (2013): impact factor: 2.576; subject category: *Food Science & Technology*; journal rank in the subject category: 23/123; quartile in the subject category: Q1.

Table 1.1. Organisation of chapters.

Part	Chapter
Part I: Introduction	Chapter 1: Introduction and objectives
Part II: Hyperspectral imaging	Chapter 2: Selection of optimal wavelength features for decay detection in citrus fruit using the ROC curve and neural networks
	Chapter 3: Comparison of ROC feature selection method for the detection of decay in citrus fruit using hyperspectral images
Part III: Light backscattering imaging	Chapter 4: Early decay detection in citrus fruit using laser-light backscattering imaging
	Chapter 5: Laser-light backscattering imaging for early decay detection in citrus fruit using both a statistical and a physical model
Part IV: Spectroscopy	Chapter 6: Visible-NIR reflectance spectroscopy and manifold learning methods applied to the detection of fungal infections on citrus fruit
Part V: Conclusions	Chapter 7: Conclusions and future work

The five research papers are presented as five different chapters that compose the body of this thesis report. Even though the research papers are intended to be maintained as faithful as possible to the published or submitted versions, they are slightly edited for their integration in this thesis report. In particular, despite the text of research papers in their original versions may have different size, fonts or styles, the formatting in the thesis is uniform among the chapters so that the thesis report as a whole has a homogeneous appearance. However, the internal headings, and therefore the structure, differ among the chapters.

Each of the chapters based on research papers can stand alone as an individual piece of research work, and therefore, can be read independently, and in whatever order. However, if possible, they should be read in the presented order, which is the chronological order of submission or publication in the corresponding journals, since this order is the most logical for acquiring a better understanding of the link among the different research papers. Furthermore, there are two additional chapters (including this first one and another one at the end) that frame the five internal chapters corresponding to research papers, and assist in establishing the thesis as a coherent whole. In addition, a list of references and an appendix containing the three published research papers in their respective journal formats are provided at the end of the thesis.

The seven chapters of this thesis report are organised into five different parts, as indicated in Table 1.1. A brief summary of each part follows:

- **Part I: Introduction.** This introductory part, consisting of only one chapter (Chapter 1), basically sets out the context of the thesis, and provides the background necessary to understand the remainder of the thesis. In particular, this part introduces in a general way the problem of the decay detection in citrus fruit, and gives an overview of the different optical techniques analysed in this thesis to automate this detection, with particular attention being paid on technical principles of these technologies and their applications for fruit and vegetable quality assessment. Furthermore, it is included a brief introduction to the use of machine learning techniques for quality assessment of agricultural products from the corresponding optical measurements. In addition, the objectives and the research framework of the doctoral thesis are also presented. As an additional remark, it should be commented that a large portion of the introductory part related to hyperspectral imaging (Section 1.1.3.1) is based on a review paper (Lorente et al., 2012), which is the result of the extensive bibliographic search developed during the first year of the research stage associated with this doctoral thesis, with the aim of acquiring a deeper knowledge about the state of art of this optical technology.
- **Part II: Hyperspectral imaging.** This part comprises Chapters 2 and 3, which correspond to two research papers related to hyperspectral imaging. In particular, the research paper in Chapter 2 proposes a novel feature selection methodology, in order to select an optimal set of wavelengths effective in the detection of decay in citrus fruit by means of hyperspectral images. In Chapter 3, the research paper compares the feature selection method proposed in Chapter 2 with other common feature selection techniques in terms of the classification performance in the tackled problem of decay detection.

- **Part III: Light backscattering imaging.** This part consists of Chapters 4 and 5, and includes two research papers related to light backscattering imaging. The research work presented in this part is the product of research during two stays in Germany, as commented in Section 1.3. The research paper in Chapter 4 evaluates the potential of LLBI for decay detection in citrus fruit. For this purpose, a statistical model is used to characterise backscattering profiles obtained from backscattering images. In this research work, the different laser wavelengths are combined and ranked in terms of their contribution to the detection of decay. In order to continue the research line of Chapter 4, the research paper presented in Chapter 5 reports new progress in the automatic detection of decay in citrus fruit by means of LLBI. Particularly, the two kinds of profile modelling approaches (statistical and physical) and different feature selection methods are compared according to their classification performance in the addressed problem.
- **Part IV: Spectroscopy.** This part with only one chapter (Chapter 6) includes a research paper dealing with spectroscopy. This research paper evaluates the feasibility of reflectance spectroscopy in the visible and NIR spectral regions for the automatic detection of decay in citrus fruit. For this purpose, this research investigates and compares two different spectral ranges included in the visible and NIR regions in which the reflectance measurements are acquired, as well as different spectral pre-processing techniques, dimensionality estimators and manifold learning methods for dimensionality reduction, in terms of their classification performance for the decay detection problem.
- **Part V: Conclusions.** This final part consists of Chapter 7, and presents the overall and specific conclusions drawn from this doctoral thesis. In addition, this part identifies possible lines for future research in order to continue the research work presented in this thesis. Finally, the scientific publications related to the thesis are also listed.

Part II

Hyperspectral imaging

Chapter 2

Selection of optimal wavelength features for decay detection in citrus fruit using the ROC curve and neural networks

D. Lorente[1], N. Aleixos[2], J. Gómez-Sanchis[3], S. Cubero[1], J. Blasco[1]

[1] Centro de Agroingeniería, Instituto Valenciano de Investigaciones Agrarias (IVIA), Cra. Moncada-Náquera km 5, 46113 Moncada (Valencia), Spain.

[2] Instituto Interuniversitario de Investigación en Bioingeniería y Tecnología Orientada al Ser Humano, Universitat Politècnica de València, Camino de Vera s/n, 46022 Valencia, Spain.

[3] Intelligent Data Analysis Laboratory (IDAL), Electronic Engineering Department, Universitat de València, Dr. Moliner 50, 46100 Burjassot (Valencia), Spain.

Published in: Food and Bioprocess Technology (2013), 6, 530-541.

Abstract

Early automatic detection of fungal infections in postharvest citrus fruits is especially important for the citrus industry because only a few infected fruits can spread the infection to a whole batch

during operations such as storage or exportation, thus causing great economic losses. Nowadays, this detection is carried out manually by trained workers illuminating the fruit with dangerous ultraviolet lighting. The use of hyperspectral imaging systems makes it possible to advance in the development of systems capable of carrying out this detection process automatically. However, these systems present the disadvantage of generating a huge amount of data, which must be selected in order to achieve a result that is useful to the sector. This work proposes a methodology to select features in multiclass classification problems using the receiver operating characteristic curve, in order to detect rottenness in citrus fruits by means of hyperspectral images. The classifier used is a multilayer perceptron, trained with a new learning algorithm called extreme learning machine. The results are obtained using images of mandarins with the pixels labelled in five different classes: two kinds of sound skin, two kinds of decay and scars. This method yields a reduced set of features and a classification success rate of around 89%.

Keywords: Computer vision; Citrus fruits; Decay; Non-destructive inspection; Hyperspectral imaging; ROC curve.

2.1. Introduction

Decay pathogens can enter fruit through wounds sustained during harvesting. This implies that the pathogen is already in the fruit before any treatment is applied in postharvest (Obagwu and Korsten, 2003). Early detection of fungal infections in citrus fruits is especially important in packinghouses because a very small number of infected fruits can spread the infection to a whole batch, thus causing great economic losses and affecting further operations, such as storage and transport. The most important postharvest damage in citrus packinghouses is caused by *Penicillium* spp. fungi (Eckert and Eaks, 1989). Nowadays, the detection of rotten fruit on citrus packing lines is carried out visually under dangerous ultraviolet (UV) illumination, and decay fruits are removed manually. This procedure, however, may be harmful for operators and operationally inefficient, since they must work in shifts of just a few hours. This rate of staff rotation affects the assessment of the quality. A possible solution arises from the use of automatic machine vision systems.

Computer vision has become widely used to automate the inspection of all different types of food commodities like meat (Du and Sun, 2009), fish (Quevedo and Aguilera, 2010; Quevedo et al., 2010), bakery products (Farrera-Rebollo et al., 2012), grains (Manickavasagan et al., 2010) or fruits (Karimi et al., 2012). In most cases, its use is aimed at the inspection of external features

related to quality, such as size, shape, colour or the presence of damage (Cubero et al., 2011). The use of technology based on colour cameras for the detection of external damage of citrus is currently under research. Kim et al. (2009) used colour texture features based on hue-saturation-intensity (HSI) and colour co-occurrence method to detect peel diseases in grapefruit. López-García et al. (2010) used multivariate image analysis with the same objective in citrus fruits. However, some defects, like decay or freeze damage, are very difficult to detect using standard artificial vision systems since they are hardly visible to the human eye and, consequently, by standard red-green-blue (RGB) cameras (Blasco et al., 2007a). Therefore, different technologies have to be incorporated, such as the use of UV-induced fluorescence (Slaughter et al., 2008; Obenland et al., 2009). In an attempt to automate the current manual tasks of detection of decay, Blanc et al. (2009, 2010) patented an automatic machine for decay detection using UV illumination, and Kurita et al. (2009) developed an inspection system based on simultaneous visible and UV illumination using light-emitting diodes. However, it would be desirable to avoid the use of UV radiation in these tasks, which could be achieved by finding out particular wavelengths in the visible or near-infrared (NIR) part of the electromagnetic spectrum.

Images acquired in visible and NIR simultaneously were used to detect different types of damage in citrus fruits by Aleixos et al. (2002), and more recently by Blasco et al. (2009), who attempted to detect common external defects and diseases, including decay, by combining NIR, visible and also UV-induced fluorescence. In this sense, the recent introduction of hyperspectral sensors for the inspection of food (Sun, 2010) makes it possible to carry out a more precise analysis of the problem by acquiring images for specific ranges of wavelengths to detect features non-visible features or to select particular sets of some wavelengths related to important physical properties, as indicated in the review of Lorente et al. (2012).

Using spectroscopy, Gaffney (1973) found that different external defects on citrus fruits have different spectral signatures, stated later in the review of Magwaza et al. (2012), which can lead to the selection of certain sets of wavelengths that facilitate the detection of particularly dangerous defects such as canker (Balasundaram et al., 2009). However, in real life, it is not enough just to distinguish between fruit affected by serious diseases and sound fruit. It is important to develop systems capable of separating also produce affected by scars on the rind, or other external defects that only downgrade the quality of the fruit but do not spread among other fruits and do not prevent its marketing in domestic markets (Blasco et al., 2009). If they are not taken into account, these cosmetic defects may be confused with the dangerous by an automatic system. Qin et al. (2009a) used a hyperspectral system with sensitivity in the range 450-930 nm to detect different kinds of damage that affect the skin of citrus, with particular attention being paid to the detection of canker

from other common defects. However, one of the main problems of these systems is the huge amount of data generated (Gómez-Sanchis et al., 2008b).

While a standard RGB image is composed of three images corresponding to the red, green and blue bands, a hyperspectral image consists of a set of monochromatic, narrow-band images that increases the complexity of the analysis and requires more computing time to analyse them with an automatic system, which prevent its use in real-time in-line inspection system. For this reason, it is very important to select only those bands with the most relevant information, while discarding those that do not contribute in any significant way to improve the results. With the aim of detecting different defects on the skin of oranges using a hyperspectral system, Li et al. (2011) used principal component analysis (PCA) to select two sets of six and three optimal wavelengths, and later applied PCA and band ratios to detect the defects in these multispectral images.

Generally, statistical methods to reduce dimensionality and select features can be divided into wrapper and filter methods (Guyon and Elisseeff, 2003). Filter methods use an indirect measure of the quality of the selected features (e.g. by evaluating the correlation function between each input feature and the dependent variable –class– of the classification problem), obtaining a faster convergence of the selection algorithm. On the other hand, the selection criteria used by wrapper methods are the goodness-of-fit between the inputs and the output provided by the learning machine under consideration, like for example, a neural network. Within these methods, a traditional measure for evaluating classifiers is the classification success rate. However, a more suitable way of measuring the quality of a classifier is the area under the receiver operating characteristic (ROC) curve, which is the measure used in the feature selection method proposed in this work. Basic concepts related to classification models are first reviewed for a better understanding of the ROC curve as feature selection method. The ROC curve is a graphical plot of the true positive rate vs. false positive rate for a binary classifier, as its discrimination threshold is varied, this value being defined as that from which a positive class prediction is made (Fawcett, 2006). The area under a ROC curve (AUC) is used as a global measure of classifier performance that is invariant to the classifier discrimination threshold and the class distribution (Bradley, 1997). Maximum classification accuracy corresponds to an AUC value of 1, while a random guess separation involves a minimum AUC value of 0.5.

With regard to classification methods, because of their flexibility and the possibility of working with unstructured and complex data like those obtained from biological products, artificial neural networks (ANN) have been applied in almost every aspect of food science, and it is a useful tool for performing food safety and quality analyses. For instance, a combination of principal components analysis and ANN was used by Bennedsen et al. (2007) to detect surface defects on apples. Unay and Gosselin (2006) used a multilayer perceptron (MLP) as a promising technique

for segmenting surface defects on apples. Ariana et al. (2006) presented an integrated approach using multispectral imaging in reflectance and fluorescence modes to acquire images of three varieties using two ANN-based classification schemes (binary and multiclass). In the case of citrus fruits, Kondo et al. (2000) used, among other methods, ANN to detect some external and internal features in oranges, while Gómez-Sanchis et al. (2012) used minimum redundancy maximum relevance as feature selection method, and MLP for pixel classification to detect rottenness in mandarins.

This paper advances in the automatic detection of a dangerous postharvest disease of citrus fruits, such as fungal decay, and to distinguish fruit with symptoms of decay from sound fruit and affected by minor defects. A feature selection methodology that expands the use of the ROC curve to multiclass classification problems is proposed. This methodology has been applied to the selection of an optimal set of features that are effective in the detection of common defects and decay in citrus fruits using hyperspectral images.

In particular, we have used computer vision for detection of two dangerous types of decay caused by *Penicillium digitatum* Sacc (green mould) and *Penicillium italicum* Wehmer (blue mould) because these pathogens occur in almost all regions of the world where citrus is grown, and cause serious postharvest losses annually (Palou et al., 2001). Furthermore, in order to explore the possibilities of the ROC method as a technique for selecting important wavelengths in fruit inspection, we used an ANN-based classifier trained with a new learning algorithm called extreme learning machine (ELM; Huang et al., 2006).

2.2. Feature selection methodology

2.2.1. Imaging system

In this work, a hyperspectral vision system based on liquid crystal tunable filters (LCTF) was employed. The set of monochrome images acquired by this system makes up a hyperspectral image from which spatial as well as spectral information can be obtained about the scene. A hyperspectral image can be interpreted as a hypercube, in which two dimensions are spatial (pixels) and the third is the spectrum of each pixel. The system consists of a monochrome camera (CoolSNAP ES, Photometrics) with a high level of sensitivity between 320 nm and 1020 nm. It was set to acquire 551×551 pixel images with a resolution of 3.75 pixels/mm. The camera transfers the images to a computer by means of a proprietary frame grabber based on peripheral

component interconnect (PCI) technology. The computer employed is based on a Pentium 4 processor with 1 Gb of random access memory (RAM). A lens capable of providing a uniform focus between 400 nm and 1000 nm was chosen for use with the system (Xenoplan 1.4/17MM, Schneider).

Two LCTF were used, one sensitive to the visible between 400 nm and 720 nm (Varispec VIS07, CRI, Inc.) and one sensitive to NIR in the 650- to 1100-nm range (Varispec NIR07, CRI, Inc.). Each fruit was illuminated individually by indirect light from twelve halogen lamps (20 W) inside an aluminium hemispherical diffuser in order to provide good spectral efficiency in the visible and NIR. The lamps were powered by a stabilised power supply (12 V/DC 350 W). Because the sum of efficiencies of the filter, camera and illumination system is different across the selected wavelengths, the acquisition software was programmed to correct the integration time for each particular band that is acquired. Hence, these differences in the efficiency of the filter for each band are offset by calculating the particular integration time for each image in each wavelength using a white reference, so that the spectral response of the system is flat over the whole spectral range.

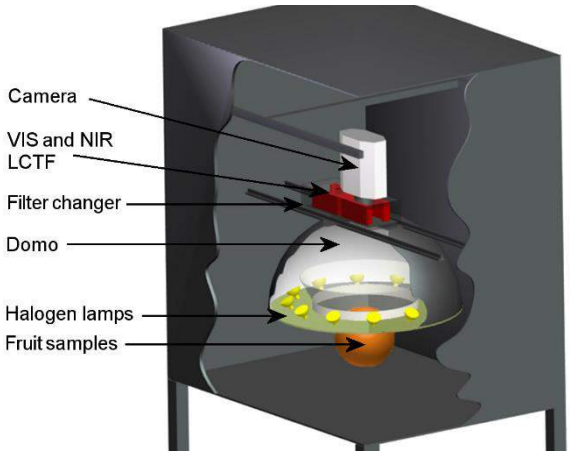

Figure 2.1. Scheme of the image acquisition system showing the arrangement of the visible and near-infrared liquid crystal tunable filters.

The filters were placed just in front of the camera lens. One of the main problems arose when it came to changing between visible and infrared filters, since the camera could move when handling the filters, which made it difficult to acquire the exactly same scene with both filters. This problem was solved by designing and installing a system to hold and guide the filters. The two filters were

fitted to the support and move on a sliding mechanism, thus allowing each filter to be set in the right place without handling the camera. The arrangement of the image acquisition system inside the inspection chamber is shown in Figure 2.1.

2.2.2. Fruit used in the experiments

The experiments were carried out using mandarins cv. 'Clemenules' (*Citrus clementina* Hort. ex Tanaka) with two kinds of defects: (1) minor defects represented by external scars affecting only the appearance of the fruit, and (2) serious diseases that can spread to other fruits caused by two different fungi; *P. digitatum* and *P. italicum*. The fruits affected by the first type of defects were chosen at random from the packing line of a trading company. On the other hand, damage produced by fungi was caused artificially in sound fruits using an inoculation of spores.

A total of 240 fruits were used: 60 sound fruits, 60 presenting external scars, 60 inoculated with spores of *P. digitatum* and 60 inoculated with spores of *P. italicum*. The inoculation was performed using a suspension of spores with a concentration of 10^6 spores/ml for both fungi, which is sufficient to cause infestation in laboratory conditions (Palou et al., 2001). From the point of view of the postharvest, it is probably not important to differentiate between both types of decay. However, in this paper, this distinction has been made to test the potential of this method to discriminate between defects that are virtually identical in their early stages to the naked human eye. The fruits were stored for three days in a controlled environment at 25 ºC and 99% relative humidity. After this period, all the inoculated fruits presented a characteristic patch of rottenness with a diameter between 10 mm and 35 mm. While rind scars are clearly visible, the colour of rotten skin is similar to the colour of the sound skin around it, thus making it difficult for a human inspector to detect it.

The images were acquired by placing the fruit manually in the inspection chamber and then presenting the damage to the camera. A total of 240 hyperspectral images were acquired from 460 nm to 1020 nm, with a spectral resolution of 10 nm. The hyperspectral image was therefore composed of 57 monochrome images of each fruit, which gives a total number of 13680 monochrome images. The analysis of images started by correcting the effects of illumination on spherical fruits following the methodology described in Gómez-Sanchis et al. (2008a). Then, in order to separate the fruit from the background in the image, the hyperspectral images were pre-processed using masking. The mask was created by thresholding the fruit image at 650 nm, since images at this wavelength provided the best contrast between fruit and background.

Figure 2.2 shows the RGB images of four fruits corresponding to a sound fruit, a fruit with scars on the rind, a fruit infected by *P. digitatum* and a fruit infected by *P. italicum*, respectively from top to bottom. The adjoining columns show example images of the same fruits acquired at 530, 640, 740 and 910 nm, respectively. These images were chosen at different wavelengths just to have an overall impression of what could be seen in hyperspectral images but not necessarily used in the experiments. In the RGB images, the damage caused by fungi is hardly visible to the naked human eye.

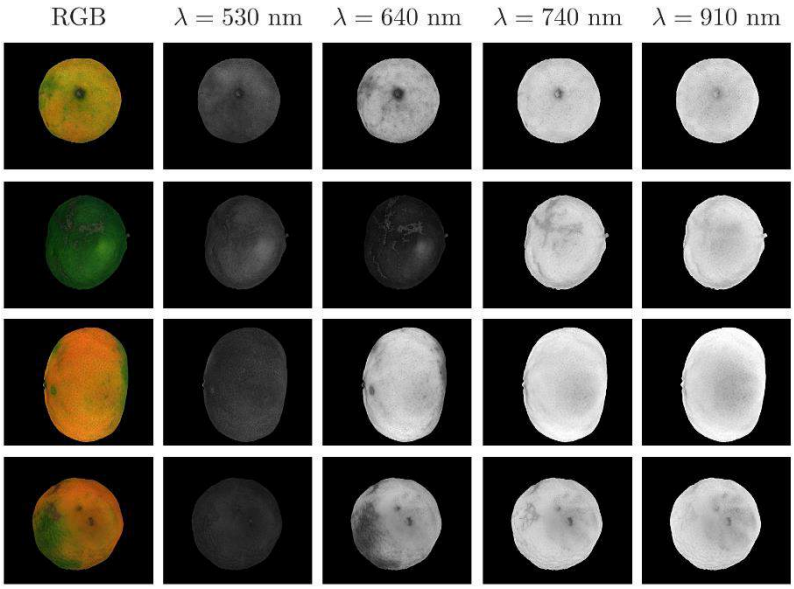

Figure 2.2. RGB and monochrome images (530, 640, 740 and 910 nm) of a sound mandarin and mandarins with scars, affected by *P. digitatum* and affected by *P. Italicum* (from *top* to *bottom*).

2.2.3. Labelled set

In supervised classification, there is a set of n labelled samples, $\{\mathbf{x}_i, y_i\}_{i=1...n}$, where $\mathbf{x}_i$ represents the m-dimensional feature vector for the i-th pixel with label y_i. Here, m represents the spectral bands and spectral indexes, and y defines the universe of all possible labelled classes in the image. In this work, the supervised nature of the problem presented here required the construction of a labelled data set, consisting of $m = 74$ features associated with each pixel, specifically 57 purely spectral variables (reflectance level of the pixel for each acquired band) and 17 spectral

indexes calculated by combining several reflectance values, as shown in Table 2.1. The spectral indexes were used to know if any of them could improve the decay detection in comparison to the use of only purely spectral variables. In order to build this labelled set, $n = 143095$ pixels were selected manually and then a human expert assigned them to one of the five classes considered in this work: green sound skin (GS), orange sound skin (OS), defective skin by scars (SC), decay caused by *P. digitatum* (PD) and decay caused by *P. italicum* (PI). Each sample pattern is therefore composed of 74 features and a class label. A background class was not included, since the background pixels were segmented earlier in the pre-processing step.

Table 2.1. Spectral indexes used in this work as input features. R_λ is the reflectance value at band λ.

Vegetative index	Estimation	Parameter values used in this work	Reference
Normalised difference vegetation index (NDVI)	$NDVI = \frac{R_{NIR} - R_{RED}}{R_{NIR} + R_{RED}}$	λ_{NIR} = 800 nm λ_{RED} = 640 nm	Tucker (1979)
Green normalised difference vegetation index (green NDVI). Version I	$Green\ NDVI\ I = \frac{R_{GREEN} - R_{RED}}{R_{GREEN} + R_{RED}}$	λ_{GREEN} = 550 nm λ_{RED} = 640 nm	Yang et al. (2007)
Green normalised difference vegetation index (green NDVI). Version II	$Green\ NDVI\ II = \frac{R_{NIR} - R_{GREEN}}{R_{NIR} + R_{GREEN}}$	λ_{NIR} = 800 nm λ_{GREEN} = 550 nm	Gitelson et al. (1996)
Water band index (WBI)	$WBI = \frac{R_{950nm}}{R_{900nm}}$		Xu et al. (2007)
Soil-adjusted vegetation index (SAVI)	$SAVI = \frac{(R_{NIR} - R_{RED})(1+L)}{R_{NIR} + R_{RED} + L}$	λ_{NIR} = 800 nm λ_{RED} = 640 nm L = 0.5	Yang et al. (2007)
Photochemical reflectance index (PRI)	$PRI = \frac{R_{531nm} - R_{570nm}}{R_{531nm} + R_{570nm}}$	$\lambda_{531nm} \approx$ 500 nm	Huang et al. (2007)
Red-edge vegetation stress index (RVSI)	$RVSI = \frac{R_{714nm} + R_{752nm}}{2 - R_{733nm}}$	$\lambda_{714nm} \approx$ 710 nm $\lambda_{752nm} \approx$ 750 nm $\lambda_{733nm} \approx$ 730 nm	Naidu et al. (2009)
Modified chlorophyll absorption in reflectance index (MCARI)	$MCARI = \left[(R_{700nn} - R_{670nm}) - 0.2(R_{700nn} - R_{550nm})\right] \times \frac{R_{700nm}}{R_{670nm}}$		Naidu et al. (2009)
Visible atmospherically resistant index (VARI)	$VARI = \frac{R_{GREEN} - R_{RED}}{R_{GREEN} + R_{RED} - R_{BLUE}}$	λ_{GREEN} = 550 nm λ_{RED} = 640 nm	Naidu et al. (2009)

		λ_{BLUE} = 480 nm	
Water index (WI)	$WI = \frac{R_{900nm}}{R_{970nm}}$		Naidu et al. (2009)
Transformed chlorophyll absorption in reflectance index (TCARI)	$TCARI = 3 \times \left[(R_{700nn} - R_{670nm}) - 0.2(R_{700nn} - R_{550nm}) \right] \times \frac{R_{700nm}}{R_{670nm}}$		Haboudane et al. (2002)
Optimised soil-adjusted vegetation index (OSAVI)	$OSAVI = \frac{(R_{NIR} - R_{RED})(1 + 0.16)}{R_{NIR} + R_{RED} + 0.16}$	λ_{NIR} = 800 nm λ_{RED} = 640 nm	Rondeaux et al. (1996)
Citrus colour index (CCI)	$CCI = \frac{a \times 1000}{L \times b}$	*a*, *b* and *L* are the coordinates of the CIELAB colour space	Jiménez-Cuesta et al. (1981)
Other indexes	$R_{NIR} - R_{RED}$	λ_{NIR} = 800 nm λ_{RED} = 640 nm	Yang et al. (2007)
	$\frac{R_{RED}}{R_{NIR}}$	λ_{NIR} = 800 nm λ_{RED} = 640 nm	Yang et al. (2007)
	$\frac{R_{GREEN}}{R_{RED}}$	λ_{GREEN} = 550 nm λ_{RED} = 640 nm	Yang et al. (2007)
	$\frac{R_{NIR}}{R_{RED}}$	λ_{NIR} = 800 nm λ_{RED} = 640 nm	Yang et al. (2007)

The labelled set was divided into a training set of 35774 samples (25% of the total), a validation set of 35774 samples (25% of the total) and a test set of 71547 samples (50% of the total). The first two sets were used to build the proposed statistical methods of feature selection and classification and the third one to evaluate classifier performance. The choice of a huge number of pixels in the test set was made in order to check the generalisation capability of the models.

2.2.4. Feature selection

The feature selection methodology proposed to expand the use of the ROC curve to multiclass classification problems consists of two parts: (1) obtaining a ranking of features ordered according to the discriminant relevance of the features, and (2) the choice of an optimal number of features from the feature ranking. Both this feature selection method and the classification procedure used in this work were implemented using Matlab 7.9 (Mathworks, Inc.).

Obtaining a feature ranking

The first step consists in obtaining a feature ranking for each class. The ROC curve is intended for binary classification problems. However, in this work, problems with more than two classes are considered. Therefore, the *one vs. all* (OVA) approach is employed to obtain a feature ranking for each class, which maximises the separation between that class and the others. The OVA structure consists in assuming that the problem has only two classes: a class from which the ranking is obtained and another class grouping the remaining classes (Rifkin and Klautau, 2004). In order to obtain these partial rankings, several steps were followed for each class, these steps being similar to the ones used by Serrano et al. (2010) in binary classification problems; the classifier is trained using all the features, taking into account the OVA structure, that is, considering a classification problem with only two classes. Then, the area under the ROC curve is obtained for the classification model using all features (AUC_0). The following parameters are obtained for each input feature x_i:

- Area under the ROC curve for the classifier without taking into account the effect of feature x_i (AUC_i). For this purpose, when using the classifier, the feature x_i is assumed to be constant for every sample, $x_i = 0$.
- Discriminant relevance of feature x_i (DR_i), which is defined as the difference between the area under the ROC curve of the classifier using all the features (AUC_0) and the area without taking into account the effect of feature x_i (AUC_i). This parameter indicates the importance of a feature for the discrimination process carried out by the classifier, considering that the higher the discriminant relevance of a feature is, the more discriminatory that feature will be.
- A z statistic of feature x_i (z_i) is calculated from the discriminant relevance of feature x_i (DR_i), as shown in Equation 2.1:

$$z_i = \frac{AUC_0 - AUC_i}{\sqrt{SE_0^2 + SE_i^2 + 2 \cdot \rho \cdot SE_0 \cdot SE_i}} \tag{2.1}$$

where SE_0 and SE_i are the standard errors of AUC_0 and AUC_i, respectively, and ρ is the correlation between AUC_0 and AUC_i. In this work, a feature is considered to be relevant for the problem when its corresponding z value exceeds a 95% significance level, this level being chosen empirically.

Features in each ranking are ordered according to the contribution each of them makes to the discriminant capability of the classification process, and the input features with the highest z values are considered the most discriminatory features.

The second step consists in obtaining a global feature ranking. After obtaining the partial rankings corresponding to each class, the next step is to perform a single global ranking that includes all the classes. The z values corresponding to the rankings for each class are combined by means of their weighted mean (Equation 2.2), which assigns a weight to each class in proportion to its relative importance in the classification problem. Thus, the global relevance of each feature is obtained, and then each input feature is ranked according to its global relevance. The ranking thus obtained maximises the global separation among all the classes.

$$\overline{z}_i = \frac{\sum_{k=1}^{N} z_{ik} \cdot w_k}{\sum_{k=1}^{N} w_k} \tag{2.2}$$

where $\overline{z}_i$ is the global relevance of feature x_i, N is the number of different classes, z_{ik} is the z value of feature x_i from the partial ranking for the *k*-th class and w_k is the weight for the *k*-th class.

Choice of an optimal number of features

In this stage, a minimum number of features leading to a saturation trend in the success rate of classification are chosen. The following steps are required to do this. The initial step is to obtain the evolution of the success rate of classification as a function of the number of features. For this purpose, the classifier is trained using the first feature of the global ranking and its success rate is evaluated, this process is then repeated including the next feature of the ranking, and so on, until all the features are employed sequentially. Then, the first number of input features n satisfying the two conditions in Equations 2.3 and 2.4 is chosen, where $success_n$ is the success rate of classification using n features, $success_{n+1}$ the success rate with $n+1$ input features and so on.

$$success_{n+1} - success_n \leq 1\% \tag{2.3}$$

$$success_{n+2} - success_{n+1} \leq 1\% \tag{2.4}$$

2.2.5. Classifier

The classifier used to explore the possibilities of the proposed feature selection methodology is a MLP with a single hidden layer, which is the simplest kind of ANN. However, the feature selection procedure is independent of the chosen classification method. ANN is considered to be a commonly used pattern recognition tool in hyperspectral image processing because it is capable of handling a large amount of heterogeneous data with considerable flexibility and has non-linear properties (Plaza et al., 2009).

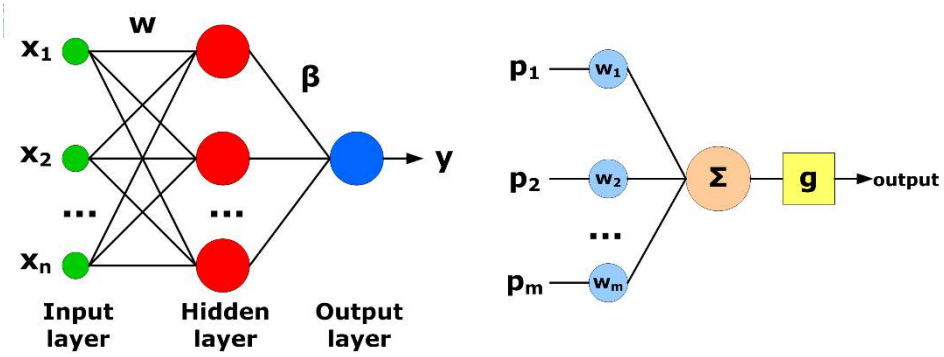

Figure 2.3. Structures of a multilayer perceptron with a single hidden layer (*left*) and an example of artificial neuron (*right*).

The most popular ANN is the MLP, which is a feed-forward ANN model that maps sets of input data onto a set of appropriate output, and consists of multiple layers of nodes (neurons) in a directed graph that is fully connected from one layer to the next. In particular, the MLP used in this work has an input layer, a single hidden layer and an output layer. MLP can use a large variety of learning techniques, the most popular being backpropagation, which is a supervised learning method based on gradient descent in error that propagates classification errors back through the network and uses those errors to update parameters (Shih, 2010). In these classical learning methods, the parameters of the ANN are normally tuned iteratively and thus entail several disadvantages, such a high degree of slowness and convergence to local minima. In order to avoid these problems, the MLP used in this work was trained using ELM, which is a new learning algorithm that determines the ANN parameters (not the optimal architecture) analytically in a faster way instead of tuning them iteratively. This increase of speed in the learning algorithm is very important in order to search the optimal features in our particular feature selection problem using ROC curve. Moreover, this learning algorithm for feed-forward neural networks with a

single hidden layer, like an MLP, provides good generalisation performance, as well as an extremely fast learning speed (Huang et al., 2006).

Considering a set of n patterns, $\{\mathbf{x}_i, t_i\}_{i=1..n}$, and M nodes in the hidden layer, the MLP output for the *i*-th sample is given by Equation 2.5, which is obtained in a straightforward way taking into account the structure of an artificial neuron, as well as the MLP structure (Figure 2.3).

$$y_i = \sum_{j=1}^{M} g(\mathbf{w}_j \cdot \mathbf{x}_i) \cdot \beta_j \tag{2.5}$$

where $\mathbf{w}_j$ is the weight vector connecting the *j*-th hidden node and the input nodes, β_j is the weight vector connecting the *j*-th hidden node and the output nodes and g is an activation function applied to the scalar product of the input vector and the hidden layer weights.

Equation 2.6 can be written compactly in matrix notation as $\mathbf{y} = \mathbf{G} \cdot \boldsymbol{\beta}$, where $\boldsymbol{\beta}$ is the weight vector of the output layer and $\mathbf{G}$ is given by:

$$\mathbf{G} = \begin{pmatrix} g(\mathbf{w}_1 \cdot \mathbf{x}_1) & \cdots & g(\mathbf{w}_M \cdot \mathbf{x}_1) \\ \vdots & \ddots & \vdots \\ g(\mathbf{w}_1 \cdot \mathbf{x}_n) & \cdots & g(\mathbf{w}_M \cdot \mathbf{x}_n) \end{pmatrix} \tag{2.6}$$

ELM proposes a random choice of the weights of the hidden layer, $\mathbf{w}_j$, thus making it necessary only to determine the weights of the output layer, $\boldsymbol{\beta}$, analytically through simple generalised inverse operation of the matrix $\mathbf{G}$ according to the Equation 2.7:

$$\boldsymbol{\beta} = \mathbf{G}^{\dagger} \cdot \mathbf{t} \tag{2.7}$$

where $\mathbf{G}^{\dagger} = (\mathbf{G}^T \cdot \mathbf{G})^{-1} \cdot \mathbf{G}^T$ is the Moore-Penrose generalised inverse of matrix $\mathbf{G}$ (Rao and Mitra, 1972), $\mathbf{G}^T$ being the transpose of matrix $\mathbf{G}$.

An important issue in practical applications of ELM is how to obtain an optimal number of the hidden nodes in the network architecture in order to achieve a good generalisation performance when training a neural network. The methodology used to select the optimum number of hidden neurons was to estimate the classification success rate for several models, obtained by varying the number of neurons in the hidden layer (Huang et al., 2006). In a first step, architectures with a variable number of hidden neurons from 25 to 1025 in increments of 100 elements were tested in order to obtain the range of the architectures that fit correctly the data maintaining the generalisation capabilities of the model. These limits were set because networks that are too small cannot model the data properly, while networks that are too large may lead to overfitting (Prechelt, 1996). Attending the curve of success rate, the optimum range was selected between 75 and 225

neurons. In a second step, architectures using 75 from 225 neurons were tested, selecting finally a MLP that used $M = 125$ neurons in the hidden layer and the sigmoid function as the activation function (g). The classification success rate for the model with 125 hidden neurons was 91.4%, while the success rate for the model with 1025 neurons was about 95.6%, thus improving by only 4% while the training time burst.

2.2.6. Approaches to the problem of decay detection

This work considers three different approaches to feature selection in the problem of the detection of decay in mandarins, depending on the number of classes involved in the problem and the weight or importance of each class. The typical problem involves the five classes described in the labelled set, all of them having equal importance or weight.

The first approach considers five different classes of similar importance in the classification problem. Therefore, when obtaining the global relevance of each feature, the weights of all the classes were considered to be equal. The aim of this approach is to know the behaviour of the method by considering a quality classification of the fruit, which separates sound fruits from those that only contain cosmetic defects that degrade the appearance, and from dangerous infections. However, it is reasonable to assume that in the real world, the classes belonging to decaying skin should be more important for the problem which is the detection of decay.

Therefore, the approach II rests on the idea that the problem has five classes of different importance in the classification. To know the behaviour of the proposed method to enhance the detection of the most important cases, empirical weights were assigned to the classes in Equation 2.2, more importance being given to decay classes $(w_{PD} = w_{PI} = 15)$, medium importance was given to the scar class $(w_{SC} = 5)$ and less to sound classes $(w_{GS} = w_{OS} = 1)$.

Moreover, decay is the disease whose detection is of most importance and which has not been still solved by automatic systems. Hence, since the actual aim of a potential inspection system would be to detect decay, it is also important to study the potential of the detection of just infected fruit, which leads to a binary problem: the separation between infected or not infected fruit (approach III). Two classes were defined:

- Decay. This class includes the two kinds of decay presented in this work: infection caused by *P. digitatum* and by *P. italicum*.
- Not decay. This class groups the remaining classes: green sound skin, orange sound skin and scars.

2.3. Results and discussion

2.3.1. Feature selection

Figure 2.4 shows the z statistic obtained for the 74 input features for each of the five classes. This statistic gives the same information as the variation in AUC. In addition, it makes it possible to study whether an input feature is discriminant or not.

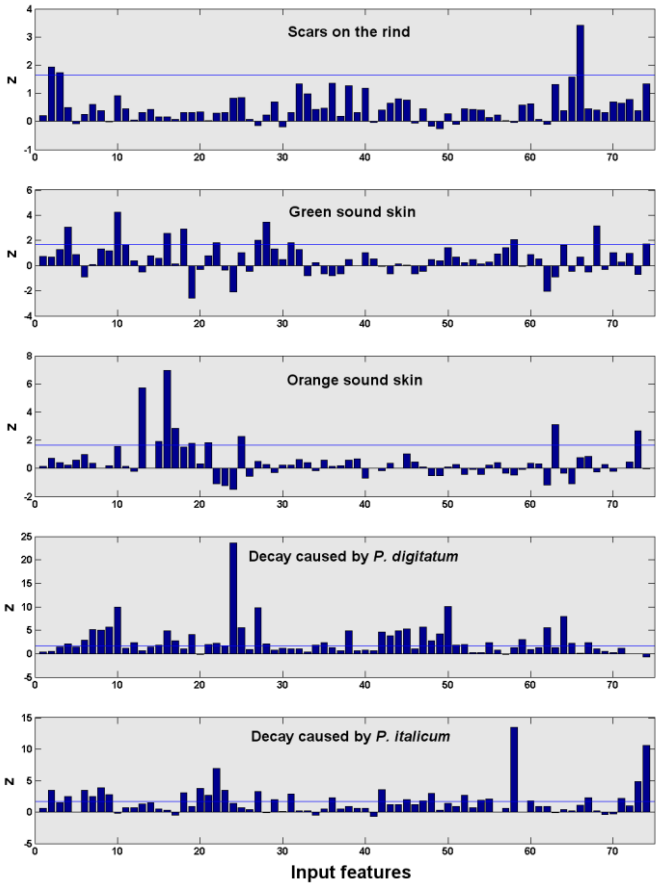

Figure 2.4. The *z* statistic of the 74 input features for each of the five classes: defects by scars on the rind, green sound skin, orange sound skin, decay caused by *P. digitatum*, and decay caused by *P. italicum*. *Horizontal solid lines* indicate the limit at the 95% significance level.

After obtaining the z values of the input features for each class, the global relevance of each feature was computed for approaches I and II, considering five classes of similar importance and five classes of different importance, respectively. The resulting optimal number of features according to the proposed mathematical criterion, shown in Equations 2.3 and 2.4, is six for the first approach and seven for the second. Table 2.2 shows the set of selected features for the first approach, as well as the correspondence between these features and the spectral indexes or reflectance values associated with them. Similarly, Table 2.3 shows the set of selected features, ordered according to their importance in the classification problem, for the second approach and the correspondence between the selected input features and the spectral indexes or reflectance values.

Table 2.2. Selected features and their correspondence with the spectral bands or indexes for approach I.

Input feature	Spectral index or reflectance value
24	Reflectance at 690 nm
10	Reflectance at 550 nm
58	NDVI
27	Reflectance at 720 nm
16	Reflectance at 610 nm
50	Reflectance at 950 nm

Table 2.3. Selected features and their correspondence with the spectral bands or indexes for approach II.

Input feature	Spectral index or reflectance value
24	Reflectance at 690 nm
58	NDVI
27	Reflectance at 720 nm
50	Reflectance at 950 nm
10	Reflectance at 550 nm
74	CCI
22	Reflectance at 670 nm

When comparing Tables 2.2 and 2.3, it can be noticed that most of the input features are coincident in both sets, except feature 16 for approach I and features 74 and 22 in the case of approach II.

This is due to the fact that these two features are really important for the detection of pixels belonging to the classes of decay, the highest weights being achieved when the global value of z is obtained, as can be straightforwardly seen from the z values for the *P. italicum* class in Figure 2.4.

Furthermore, feature 16 is not selected for the second approach, while in the first approach it is. This is due to the fact that, although this feature has a high level of importance for the classification of pixels belonging to the orange skin class, as shown in Figure 2.4, it is considered of low importance when obtaining the global relevance in the second approach. In addition, a general conclusion drawn from analysing the results for both approaches is that all the selected features are important for at least one of the five classes.

Finally, the z values were computed for the third approach, which considers the classification problem to be binary. Therefore, the z statistic values were obtained directly without employing the OVA structure which is only necessary in multiclass problems. The resulting optimal number of features was chosen according to the mathematical criterion shown in Equations 2.3 and 2.4, being a total of four. Table 2.4 shows the selected features for the third approach and the correspondence between these features and the spectral indexes or reflectance values.

Table 2.4. Selected features and their correspondence with the spectral indexes or reflectance values for approach III.

Input feature	Spectral index or reflectance value
23	Reflectance at 680 nm
60	Green NDVI, version II
28	Reflectance at 730 nm
15	Reflectance at 600 nm

2.3.2. Classifier performance evaluation

The MLP classifier, trained with the ELM algorithm, was evaluated using the selected features for each approach to the problem on the test set of labelled data. Table 2.5 shows the results for the first approach using the set of six input features provided by the proposed feature selection methodology. An average success rate of 87.5% is achieved with this approach, this parameter being calculated as the sum of the elements on the main diagonal of the obtained confusion matrix divided by the number of classes.

For the second approach, the evaluation of pixel classification using the set of seven optimal features leads to the confusion matrix shown in Table 2.6. This approach yields an average success rate of 89.1%.

When comparing the two confusion matrixes (Tables 2.5 and 2.6), it can be observed that the number of well-classified pixels of decay classes (PD and PI) for the second approach is greater than that obtained for the first approach. This is due to the fact that these two classes were given the highest weight when obtaining the global relevance for the second approach. Moreover, in the second approach, the classification of pixels with scars (SC) is improved, although to a lesser extent than the classification of the PD and PI classes. It can also be observed that the results for the classification of the sound classes (GS and OS) hardly vary between the two approaches, since these classes are considered of low importance when obtaining the global relevance in the second approach.

Table 2.5. Confusion matrix of the classification of pixels for approach I.

Prediction/reality	GS (%)	OS (%)	SC (%)	PD (%)	PI (%)
Green skin	96.91	0.13	0.06	0.03	0.00
Orange skin	2.42	94.69	0.01	2.77	1.22
Scars	0.11	0.03	97.34	0.17	0.83
P. digitatum	0.33	3.02	1.49	74.43	23.93
P. italicum	0.23	2.14	1.10	22.60	74.02

Average success rate = 87.5%

Table 2.6. Confusion matrix of the classification of pixels for approach II.

Prediction/Reality	GS (%)	OS (%)	SC (%)	PD (%)	PI (%)
Green skin	96.61	0.09	0.03	0.06	0.00
Orange skin	2.40	94.56	0.26	2.72	1.79
Scars	0.08	0.05	98.08	0.00	1.10
P. digitatum	0.82	2.38	0.17	75.90	16.83
P. italicum	0.09	2.92	1.47	21.32	80.28

Average success rate = 89.1%

Table 2.5 and 2.6 show, in both cases, that the most difficult task in the pixel-classification problem is to discriminate the PD class from the PI class, due to the similarity of the damage caused by the two fungi. On the other hand, the low percentage of sound pixels (GS and OS) classified as rotten pixels (PD and PI) in both approaches should also be highlighted. In practice, this is of great importance since most confusion is done between classes that could be grouped into the same category or commercial importance such as decay (PD and PI) and sound (GS and OS).

To conclude the comparison between approaches I and II, from the results obtained, it can be said that the second approach generally provides better results than the first one, with an increase in the average success rate from 87.5% to 89.1%. This improvement is obtained by taking into account classes with different degrees of importance in the classification problem.

Similarly, Table 2.7 shows the results of the evaluation of classifier performance for approach III using the set of four input features selected with the proposed method, where an average success rate of 95.5% was achieved. Better results are obtained for this approach, since similar classes are grouped into a single class, thus avoiding the confusion that occurs in the classification of these similar classes.

Table 2.7. Confusion matrix of the classification of pixels for approach III.

Prediction/Reality	Decay (%)	Not decay (%)
Decay	96.48	5.13
Not decay	3.52	94.87

Average success rate = 95.5%

2.4. Conclusions

In this work, a feature selection methodology has been proposed that expands the use of the ROC curve to multiclass classification problems, in order to select a reduced set of features that are effective in the detection of decay in citrus fruits using hyperspectral images. Once the optimal features have been selected, pixels from the images were classified using an MLP trained with a fast new learning algorithm (ELM).

This selection methodology was applied specifically to the detection of decay in citrus fruits caused by two different fungi, *P. digitatum* and *P. italicum*, and other common types of damage, such as scars. The conclusions drawn after performing several tests can be summarised as follows:

- A reduced number of features have been obtained for each of the three approaches to the problem, this number being six for the first approach, seven for the second approach and four for the third one. In addition, all the selected features for the first and second approaches are important for at least one of the five classes defined (two kinds of sound skin, two kinds of decay and scars).
- The set of features selected with the second approach provides better classification results than those obtained with the first one and increases the average success rate from 87.5% to 89.1% by taking into account classes with different degrees of importance in the classification problem. On the other hand, as expected, better results were obtained for the third approach (95.5%), specifically aimed at the detection of decay.

Acknowledgements

This work was partially funded by the Instituto Nacional de Investigación y Tecnologia Agraria y Alimentaria de España (INIA) through research project RTA2009-00118-C02-01 and by the Ministerio de Ciencia e Innovación de España (MICINN) through research project DPI2010-19457, both projects with the support of European FEDER funds. This work was also partially funded by the Universitat de València through project UV-INV-AE11-41271.

Chapter 3

Comparison of ROC feature selection method for the detection of decay in citrus fruit using hyperspectral images

D. Lorente[1], J. Blasco[1], A.J. Serrano[2], E. Soria-Olivas[2], N. Aleixos[3], J. Gómez-Sanchis[2]

[1]Centro de Agroingeniería, Instituto Valenciano de Investigaciones Agrarias (IVIA), Cra. Moncada-Náquera km 5, 46113 Moncada (Valencia), España.

[2]Intelligent Data Analysis Laboratory (IDAL), Electronic Engineering Department, Universitat de València, Avda. Universitat s/n, 46100 Burjassot (Valencia), España.

[3]Instituto en Bioingeniería y Tecnología Orientada al Ser Humano, Universitat Politècnica de València, Camino de Vera s/n, 46022 Valencia, España.

Published in: Food and Bioprocess Technology (2013), 6, 3613-3619.

Abstract

Hyperspectral imaging systems allow to detect the initial stages of decay caused by fungi in citrus fruit automatically, instead of doing it manually under dangerous ultraviolet illumination, thus preventing the fungal infestation of other sound fruit and, consequently, the enormous economical losses generated. However, these systems present the disadvantage of generating a huge amount of data, which is necessary to select for achieving some result useful for the sector. There are numerous feature selection methods to reduce dimensionality of hyperspectral images. This work compares a feature selection method using the area under the receiver operating characteristic (ROC) curve with other common feature selection techniques, in order to select an optimal set of wavelengths effective in the detection of decay in citrus fruit using hyperspectral images. This comparative study is done using images of mandarins with the pixels labelled in five different classes: two types of healthy skin, two types of decay and scars, ensuring that the ROC technique generally provides better results than the other methods.

Keywords: Computer vision; Citrus fruit; Decay; Non-destructive inspection; Hyperspectral imaging; ROC curve; Feature selection.

3.1. Introduction

Decay caused by fungi is among the main defects affecting the postharvest and marketing processes of citrus fruit. Infected fruit can be neither stored for a long time nor long-term transported during exportation since a small number of decay fruit can infect a whole consignment. Thus, fungal infections generate great economic losses to the citrus industry if damaged fruit are not early detected, being Penicillium spp. as the fungi that lead to the most postharvest losses in citrus packinghouses (Eckert and Eaks, 1989). In current packing lines, the detection of decayed fruit is made visually by trained operators examining the fruit as it passes under ultraviolet (UV) light. Nevertheless, this method is subjective and potentially dangerous for human skin. The use of automatic machine vision systems is a possible solution for preventing these drawbacks.

Technology based on colour cameras has spread rapidly for the detection of skin damage of fruit and vegetables (Zude, 2009; Cubero et al., 2011), being a common technique for the inspection of citrus fruit. For instance, Kondo et al. (2000) studied the possibility of detecting sugar content and acid content of oranges ‘Iyokan’ using a machine vision system and neural networks.

Slaughter et al. (2008) developed a non-contact method of detecting freeze-damaged oranges based on UV fluorescence, and López-García et al. (2010) used multivariate image analysis to detect peel diseases in citrus fruit. Nevertheless, decay lesions are difficult to detect using standard artificial vision systems since they are hardly visible to the human eye and, therefore, by standard colour cameras (Figure 3.1). Blasco et al. (2007a) used visible computer vision to detect different types of damages in citrus fruit including decay by green mould. While the success in other defects was high, the detection of decay was lower than 60% because the damages caused for this disease in the citrus skin are not clearly visible before sporulation. On the other hand, following the fluorescence technique used in the industry to detect decay by humans, Kurita et al. (2009) tried to detect decay in citrus using two lighting systems (visible and UV) changing between them while the fruit is under the view of the camera.

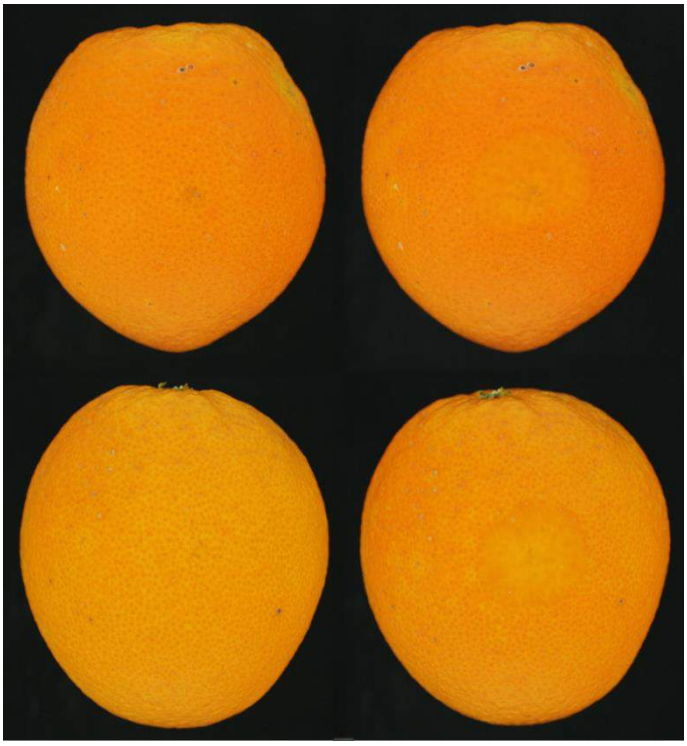

Figure 3.1. Sound orange (*left*) and the same fruit showing decay caused by *P. digitatum* (*right*).

Hyperspectral sensors have been used successfully as an alternative to detect non-visible damages on fruit (Lorente et al., 2012). In the particular case of citrus fruit, different works have been carried out to detect decay lesions (Qin et al., 2009a, 2012; Gómez-Sanchis et al., 2012). A hyperspectral image consists of a large number of consecutive monochromatic images of the same scene in each wavelength, becoming very important to select only those bands with the most relevant information, while discarding those that do not contribute in any significant way to improve the results, containing redundant information or exhibiting a high degree of correlation. There are numerous feature selection methods to reduce dimensionality that retain most of the original information in fewer bands.

For example, Gómez-Sanchis et al. (2008b) evaluated four feature selection methods with the aim of selecting an optimal set of wavelengths in the range 460-1020 nm for detecting decay in citrus fruit. Xing et al. (2005) used principal component analysis (PCA) to reduce data from a hyperspectral imaging system (400-1000 nm) for detecting bruises on 'Golden Delicious' apples. PCA was also used by Liu et al. (2005) to obtain spectral features for the detection of chilling injury in cucumbers imaged using a hyperspectral system (447-951 nm). More recently, Li et al. (2011) have used PCA to select most discriminant wavelengths in the range 400-1000 nm for detecting various common skin defects on oranges. Partial least squares (PLS) or artificial neural networks (ANN) are another techniques commonly used for feature selection purposes. ElMasry et al. (2008a) determined some important wavelengths for detecting bruises in 'McIntosh' apples using PLS on hyperspectral images in the range 400-1000 nm and ElMasry et al. (2009) used ANN to classify apples into injured and normal classes, and to detect changes in firmness due to chilling injury by selecting optimal wavelengths.

3.1.1. Objective

The method used by Lorente et al. (2013c) to select most relevant spectral features for detecting decay in citrus fruit was based on the area under the receiver operating characteristic (ROC) curve, which is a promising method to measure the quality of a binary classifier. A novel approach was presented to extend its use to multiclass problems, such as the automatic discrimination of decay lesions in citrus fruits, which is a problem still under research and very important from the agricultural point of view since the damages caused by fungi are hardly visible to the naked human eye and standard vision systems, and can be quickly spread to other sound fruits during storage. This work aims to compare our novel approach of the ROC feature selection method with other common feature selection techniques for agricultural multiclass classification problems. We use the detection of decay in citrus fruits using hyperspectral imaging as a benchmark problem by

selecting an optimal set of wavelengths effective in the discrimination between common defects and decay lesions in citrus fruit. The comparison of different feature selection techniques is aimed at knowing if the ROC method is a promising technique in multiclass classification problems relative to other commonly used methods in terms of classification accuracy.

3.2. Material and methods

3.2.1. Image acquisition

The hyperspectral imaging system used was based on liquid crystal tunable filters (LCTF; e.g. Lorente et al., 2013c). The system consists of a monochrome camera (CoolSNAP ES, Photometrics, Tucson, USA), a lens providing a uniform focus in the working range (Xenoplan 1.4/17MM, Jos. Schneider Optische Werke GmbH, Bad Kreuznach, Germany), and two LCTF (CRI Varispec VIS07 and NIR07, UK) sensitive to the visible (400-720 nm) and NIR (650-1100 nm), respectively. The scene was illuminated by halogen lamps placed inside an aluminium hemispherical domo.

For hyperspectral images, a total of 240 'Clemenules' mandarins (*Citrus clementina* Hort. ex Tanaka) collected from a local producer company were used, including 60 without visible damages, 60 presenting external scars, 60 inoculated with spores of *Penicillium digitatum* and 60 inoculated with spores of *Penicillium italicum*. The inoculation was performed using a suspension of spores with a concentration of 10^6 spores/ml for both fungi, which is sufficient to cause infestation in laboratory conditions (Palou et al., 2001). The images were acquired by presenting manually the damage on the fruit to the camera. A total of 240 hyperspectral images were taken in the range of 460-1020 nm, with a 10-nm spectral resolution. Each sample pattern in the labelled set consisted of 74 spectral features associated with each pixel (reflectance level for each acquired band –grey level in each monochromatic image– and several spectral indexes) and a class label assigned manually by a human expert. Five different classes were considered in this work: green sound skin (GS), orange sound skin (OS), defective skin by scars (SC), decay caused by *P. digitatum* (PD) and decay caused by *P. italicum* (PI).

3.2.2. Feature selection methods

The performance of the method based on the area under the ROC curve is compared with other common feature selection methods. The methods included in this comparative study are: correlation analysis (CA; Rodgers and Nicewander, 1988), mutual information (MI; Bonnlander and Weigend, 1994), Fisher's discriminant analysis (FDA; Venables and Ripley, 2002), t-test (TT; Li et al., 2006), Wilks' lambda (WL; Ouardighi et al., 2007), Bhattacharyya distance (BD; Choi and Lee, 2003), minimum redundancy maximum relevance difference criterion (MRMRd; Ponsa and López, 2007), minimum redundancy maximum relevance quotient criterion (MRMRq; Peng et al., 2005) and Kullback-Leibler divergence (KLD; Kullback, 1987; Abe et al., 2000). These feature selection techniques have been chosen because they are commonly applied to the analysis of hyperspectral imaging in the fields of pattern recognition and remote sensing, although they have not been used before for automatic fruit or vegetable inspection using computer vision. Therefore, it will also be studied if they are suitable and accurate methods for this kind of problems.

In order to get a feature selection for each method, two steps were followed: (1) to obtain a ranking of features ordered according to the discriminant relevance of the features, and (2) the selection of an optimal number of features from the feature ranking. The feature selection methods and the classification procedure used in this work were implemented using Matlab 7.9 (The Mathworks, Inc., Natick, USA).

Step I: Obtainment of a feature ranking

The obtainment of a feature ranking for each class is the initial step to follow. The feature selection techniques studied are intended for binary classification problems, but this work deals with problems with more than two classes. Therefore, the *one vs. all* approach (Rifkin and Klautau, 2004) is employed to obtain a feature ranking for each class, which maximises the separation between that class and the others. The second step consists in obtaining a single global feature ranking for each method that is achieved from the relevance values corresponding to the partial rankings for each class. These relevance values are weighted in proportion to the relative importance of the class in the problem, and combined using Equation 3.1.

$$\overline{r}_j = \frac{\sum_{k=1}^{N} r_{jk} \cdot w_k}{\sum_{k=1}^{N} w_k} \tag{3.1}$$

where $\bar{r}_j$ is the global relevance of feature x_j, N is the number of different classes, r_{jk} is the relevance value of feature x_j from the partial ranking for the *k*-th class and w_k is the weight for the *k*-th class.

After obtaining the global relevance of each feature, each input feature is ranked.

Step II: Selection of an optimal number of features

Once the global feature ranking has been obtained, a minimum number of features leading to a saturation trend in the success rate of classification is chosen for each method. The success rate is calculated using the first features in the ranking, then successive features are added in an iterative process until the increment of the success rate is lower than a certain threshold (1%). The n features that satisfy this condition are then selected.

3.2.2.1. Area under ROC curve

The ROC curve is a graphical plot of the true positive rate vs. false positive rate for a binary classifier, as its discrimination threshold is varied; this value being defined as that from which a positive class prediction is made (Fawcett, 2006). The area under a ROC curve (AUC) is used as a global measure of classifier performance that is invariant to the classifier discrimination threshold and the class distribution (Bradley, 1997). Maximum classification accuracy corresponds to an AUC value of 1, while a random guess separation involves an AUC value of 0.5. Basically, the ROC feature selection method for binary classification problems consists in calculating a z statistic from the discriminant relevance of each feature x_j, defined as the difference between the AUC of a classifier using all the features (AUC_0) and the AUC of a classifier without taking into account the effect of feature x_j (AUC_j) (Serrano et al., 2010).

3.2.3. Classifier

The classifier used in this comparative study is a multilayer perceptron (MLP) with a single hidden layer, being a type of ANN (Plaza et al., 2009). MLP can use a wide range of learning techniques for determining the network parameters, the most commonly used being backpropagation. In these classical learning methods, the parameters of the ANN are usually tuned iteratively, thus entailing several disadvantages, such a high computational complexity and convergence to local minima (Shih, 2010). To avoid this, the MLP used in this work avoids these problems by being trained

using extreme learning machine (ELM; Huang et al., 2006), in the same way as that used in Lorente et al. (2013c), which is a new learning algorithm that determines the MLP parameters analytically in a faster way instead of tuning them iteratively providing a good generalisation performance at an extremely fast learning speed.

3.2.4. Approaches to the problem of decay detection

In this work, three different approaches to the problem of the decay detection in mandarins are considered, depending on the number of classes implicated and the importance of each class (Lorente et al., 2013c). The approach I involves the five classes described in the labelled set, all of them having equal importance or weight. Therefore, the weights of all the classes were considered to be equal when obtaining the global relevance.

It is, however, realistic to assume that the classes belonging to decaying skin should be more important for decay detection. Hence, approach II gives more importance to decay classes $(w_{PD} = w_{PI} = 15)$, medium to the scar class $(w_{SC} = 5)$ and less to sound classes $(w_{GS} = w_{OS} = 1)$. Furthermore, since the actual objective of a potential inspection system would be to detect decay, it is also important to study the detection of just infected fruit, leading to a binary problem: the separation between infected or not infected fruit (approach III).

3.2.5. Methodology of comparison

Two different tests were carried out in order to compare the different selection techniques with the ROC feature selection method. The comparison, in both tests, is based on the performance evaluation of the classifier using the different sets of features provided by the methods. The first test (test I) consists in selecting an optimum number of features for each method and for each approach. Therefore, for each method, a different number of features that maximises the classification will be obtained. A different way to make the comparison is using a fixed number of features for all methods (test II). For this test, we have chosen the number of features obtained for the ROC method for each approach.

3.3. Results and discussion

The classification obtained using the ROC method is in general better than those obtained for the other methods in all cases, except for MRMRd and MRMRq using the third approach. These results could be expected since the MRMR criterion is recognised as one of the most powerful techniques for feature selection (Peng et al., 2005; Ponsa and López, 2007). The success of ROC approach is similar to that obtained using the rest of the methods tested. The differences are not significant and, therefore, we cannot say that our approach is better than the others in terms of decay detection accuracy. It is, however, important to highlight that the best results are achieved using the ROC method for all tests and all approaches. This result should to be taken into account because it is probably due to the fact that this method not only evaluates the features selection, but also optimises the performance of the classifier. Therefore, having similar results, ROC method can achieve slightly better scores.

Table 3.1. Results of the classifier performance evaluation using the features selected by the different methods for each approach, but being possible a different number of features for each case (test I).

Selection method	Approach I		Approach II		Approach III	
	Success rate (%)	Selected features	Success rate (%)	Selected features	Success rate (%)	Selected features
CA	85.94	5	82.44	3	95.02	2
MI	85.53	5	84.87	4	93.08	4
FDA	86.65	5	82.21	3	95.02	2
TT	85.67	5	79.43	2	95.00	2
WL	85.96	5	82.43	3	95.03	2
BD	83.61	3	81.59	4	94.34	3
MRMRd	85.69	5	85.58	5	96.06	2
MRMRq	85.39	4	88.30	7	95.86	3
KLD	85.55	5	87.48	7	95.43	4
ROC	87.46	6	89.07	7	95.52	4

Table 3.1 shows the results of the classifier performance evaluation using the different sets of features provided by the feature selection methods, described above, corresponding to the test I. The accuracy achieved with the ROC method is higher than that obtained with the other methods,

except for MRMR in approach III. However, on one hand, minimal redundancy methods try to extract the features with a high degree of relevance, avoiding those features with redundant information. On the other hand, ROC is a method that provides those bands that used in a classification problem fit a classifier in much robust way in terms of accuracy and significance of the model.

In general, the rest of the methods saturate the criterion of success with fewer bands than those selected by the ROC. This, in theory, means that, to reach more approximate results than ROC, the number of bands needed by these methods should be higher. Therefore, the test II was used in order to check the performance of the ROC method using the same number of bands, being six for the first approach, seven for the second approach and four for the third one. As shown in Table 3.2, the ROC feature method provides higher scores than most of the feature selection methods used in this study. As it happens in test I, the only two methods surpassing the ROC are MRMRd and MRMRq for the third approach. This fact shows that, in the most pessimistic scenario for ROC method (i.e. permitting an increase of the number of features for the rest of the methods), it obtains better results than the others, except in the case of MRMR methods in approach III. Even though the differences with the other methods are small since all of them are good feature selection methods, in the case of the approach II, which is probably the most realistic scenario in the real world, the ROC method is clearly the one that obtains better accuracy.

Table 3.2. Results of the classifier performance evaluation using the features selected by the different methods for each approach, but always employing the same number of features for each method (test II).

Selection method	Approach I (%) (6 features)	Approach II (%) (7 features)	Approach III (%) (4 features)
CA	86.48	83.39	95.09
MI	85.88	87.50	93.08
FDA	86.78	84.12	95.10
TT	85.72	82.92	95.10
WL	86.56	83.39	95.11
BD	85.18	83.59	94.93
MRMRd	86.72	86.37	97.18
MRMRq	86.53	88.30	96.42
KLD	85.77	87.48	95.43
ROC	87.46	89.07	95.52

3.4. Conclusions

In the first test, the classification average success rate obtained using the ROC method is greater than that obtained for the other methods in almost every case, except for MRMRd and MRMRq using the third approach. When we use the same number of features for all the methods, the ROC feature method provides generally better results than most of the feature selection methods used in this comparative study, being the average success rate for ROC almost always greater than that obtained for the other methods, only being surpassed by the MRMR methods for the third approach.

Therefore, the ROC feature selection method is a suitable feature selection technique that can be applied with success to multiclass classification problems with a huge amount of features, such as the segmentation of hyperspectral images to detect decay in citrus fruit, having at least similar results than other recognised feature selection methods but with the advantage of to optimise, by its nature, the performance of the classifier.

Acknowledgements

This work has been partially funded by the Universitat de València through project UV-INV-AE11-41271, by the Instituto Nacional de Investigación y Tecnología Agraria y Alimentaria de España (INIA) through research project RTA2009-00118-C02-01 and by the Ministerio de Ciencia e Innovación de España (MICINN) through research project DPI2010-19457, both projects with the support of European FEDER funds.

Part III

Light backscattering imaging

Chapter 4

Early decay detection in citrus fruit using laser-light backscattering imaging

D. Lorente[1], M. Zude[2], C. Regen[2], L. Palou[3], J. Gómez-Sanchis[4], J. Blasco[1]

[1]Centro de Agroingeniería, Instituto Valenciano de Investigaciones Agrarias (IVIA), Cra. Moncada-Náquera km 5, 46113 Moncada (Valencia), Spain.

[2]Leibniz-Institute for Agricultural Engineering Potsdam-Bornim (ATB), Max-Eyth-Allee 100, 14469 Potsdam-Bornim, Germany.

[3]Centro de Tecnología Poscosecha (CTP), Instituto Valenciano de Investigaciones Agrarias (IVIA), Cra. Moncada-Náquera km 5, 46113 Moncada (Valencia), Spain.

[4]Intelligent Data Analysis Laboratory (IDAL), Electronic Engineering Department, Universitat de València, Avda. Universitat s/n, 46100 Burjassot (Valencia), Spain.

Published in: Postharvest Biology and Technology (2013), 86, 424-430.

Abstract

Early detection of fungal infections in citrus fruit still remains as one of the major problems in postharvest technology. The potential of laser-light backscattering imaging was evaluated for detecting decay in citrus fruit after infection with the pathogen *Penicillium digitatum*, before the appearance of fruiting structures (green mould). Backscattering images of oranges cv. 'Navelate' with and without decay were obtained using diode lasers emitting at five different wavelengths in the visible and near infrared range for addressing the absorption of fruit carotenoids, chlorophylls and water/carbohydrates. The apparent region of backscattered photons captured by a camera had radial symmetry with respect to the incident point of the light, being reduced to a one-dimensional profile after radial averaging. The Gaussian-Lorentzian cross product (GL) distribution function with five independent parameters described radial profiles accurately with average R^2 values higher or equal to 0.998, pointing to differences in the parameters at the five wavelengths between sound and decaying oranges. The GL parameters at each wavelength were used as input vectors for classifying samples into sound and decaying oranges using a supervised classifier based on linear discriminant analysis. Ranking and combination of the laser wavelengths in terms of their contribution to the detection of decay resulted in the minimum detection average success rate of 80.4%, which was obtained using laser light at 532 nm that addresses differences in scattering properties of the infected tissue and carotenoid contents. However, the best results were achieved using the five laser wavelengths, increasing the classifier average success rate up to 96.1%. The results highlight the potential of laser-light backscattering imaging for advanced citrus grading.

Keywords: Fruit inspection; Citrus fruit; Decay; Laser-light backscattering imaging; LDA classifier; Gaussian-Lorentzian cross product function.

4.1. Introduction

Decay caused by *Penicillium* spp. is among the main problems affecting the postharvest and marketing processes of citrus fruit (Palou et al., 2011). Early detection of fungal infections still remains as one of the major issues in packinghouses because a small number of decayed fruit can cause the infection of a whole consignment during storage and distribution. Currently, the detection of decayed fruit in packing lines is carried out visually by trained workers inspecting each fruit individually as it passes under ultraviolet (UV) light along a conveyor belt. However, this procedure has a high risk of human error and is potentially harmful for operators (Lopes et

al., 2010). Machine vision systems potentially provide a means to detect decayed fruit automatically, thus preventing the drawbacks related to human inspection.

Although the use of technology based on colour cameras has spread rapidly for detecting skin damage of fruit and vegetables (c.f. Zude, 2009; Cubero et al., 2011), its application to the external inspection of citrus fruit is only currently under research. For example, Kim et al. (2009) detected peel diseases in grapefruit using colour texture features based on hue-saturation-intensity (HSI) and the colour co-occurrence method. Nevertheless, some defects, such as decay at very early stages, are virtually identical to the sound skin, thus being very difficult to detect them by the human eye and, consequently, by standard artificial vision systems, which are limited to the visible region of the electromagnetic spectrum (Blasco et al., 2009).

Various machine vision technologies have been incorporated for automatically detecting decay in citrus fruit imitating the fluorescence technique used in the industry by humans. Kurita et al. (2009) developed an inspection system based on two lighting systems (visible and UV) that should be powered alternatively using a stroboscopic mode since the fluorescence effect produced by UV light would be undetectable with a simultaneous use of both systems due to the high intensity of white light. However, the use of UV light has some limitations because not all decay lesions, and not all the citrus cultivars, present the same level of sensitivity to the fluorescence phenomenon, and, on the contrary, other defects like chilling injury can present some fluorescence (Slaughter et al., 2008), thus reducing the performance of these systems. In this sense, the recent introduction of hyperspectral sensors for food inspection is a successful alternative to detect non-visible damages on fruit (Lorente et al., 2012). In the particular case of citrus fruit, different research has been conducted to detect decay lesions. For instance, Gómez-Sanchis et al. (2012, 2013) and Lorente et al. (2013a, 2013c) studied the feasibility of a hyperspectral vision system based on liquid crystal tuneable filters (LCTF; 460-1020 nm) for detecting decay in citrus fruit in early stages of infection using halogen lighting instead of the traditional inspection using UV lighting.

Recently, light backscattering imaging (LBI) has been studied as an alternative machine vision technique for assessing fruit quality. When a light beam interacts with a fruit, reflectance, absorption and transmittance occur (Birth, 1976). Particularly, light reflectance (scattering) appears with two different geometries: Fresnel reflectance, which happens when photons are reflected on the surface of the sample; and diffuse reflectance (Meinke and Friebel, 2009). In the latter case, light enters the sample and interacts with the internal components of the fruit, and then it is scattered backward to the exterior tissue surface, thus carrying information related to the morphology and structures of the tissue additional to the absorption properties (Lu, 2004). In recent years, much work has focused on using LBI systems to assess quality of apples and other fresh fruit; however, no research has been reported to detect decay in citrus fruit using this

technique. For example, Lu (2004) analysed backscattering images from apples at multiple wavelengths in the visible and the near-infrared (NIR) regions for predicting firmness and soluble solids content (SSC). In another study, the variation of moisture content of banana slices subjected to different drying conditions was evaluated by taking backscattering images at 670 nm (Romano et al., 2008). From experiments on bruised apples, Lu et al. (2010) suggested that the scattering analysis would provide good results.

Decay process in citrus fruit implies changes in the enzymatic activity, resulting in an enhanced water-soluble pectin fraction and, consequently, weakening of the cell wall (Barmore and Brown, 1979). The subsequent water soaking of the tissue is an early visible symptom of infection in citrus (Barmore and Brown, 1981). Hence, since later changes in the pigment contents, and therefore in the optical properties of fruit tissue, can be expected, LBI technique could be a promising tool for detecting decay in citrus fruit. The main objective of this research work was to evaluate the potential of laser-light backscattering imaging (LLBI) as a tool for the automatic detection of green mould caused by *P. digitatum* on citrus fruit. For this purpose, diode lasers emitting in the visible and NIR ranges were used to obtain backscattering images of citrus fruit aiming for the classification of fruit into two classes (sound and decaying oranges). The ultimate aim of this work was to evaluate and compare laser wavelengths in terms of their contribution to the detection of decay.

4.2. Materials and methods

4.2.1. Fruit and fungal inoculation

The experiments were carried out using sweet oranges (*Citrus sinensis* L. Osbeck) cv. 'Navelate' collected during the 2012 harvest season from the field collection of the Citrus Germplasm Bank at the IVIA (Spain) (Navarro et al., 2002). A total of 100 fruits were used for the experiments: 50 oranges were superficially injured on the rind and inoculated with spores of *P. digitatum* and the other 50 were injured in the same way but treated with sterilised water for control purposes. *P. digitatum* isolate NAV-7, from the fungal culture collection of the IVIA CTP, was cultured on potato dextrose agar (PDA; Sigma-Aldrich Chemical Co., St. Louis, MA, USA) plates at 25 ºC. Conidia from 7 to 14 day old cultures were taken from the agar surface with a sterile glass rod and transferred to a sterile aqueous solution of 0.05% Tween® 80 (Panreac, S.A.U., Spain). The conidial suspension was filtered through two layers of cheesecloth to separate hyphal fragments

and adjusted to a concentration of 10^6 spores/ml using a haemocytometer. For inoculation, 20 µl of the conidial suspension was placed on the equator of each fruit by immersing the tip of a stainless steel rod, 1 mm wide and 2 mm in length, in the suspension and inserting it in the fruit rind. A concentration of 10^6 spores/ml of *P. digitatum* is the most appropriate to effectively infect citrus fruit in laboratory conditions (Palou et al., 2001). The fruits were stored for four days in a controlled environment at 20 °C and 65% relative humidity. After this period, all the inoculated fruit presented lesions due to decay of an average diameter of 30 mm. Figure 4.1 shows the images of a sound control orange and an infected orange.

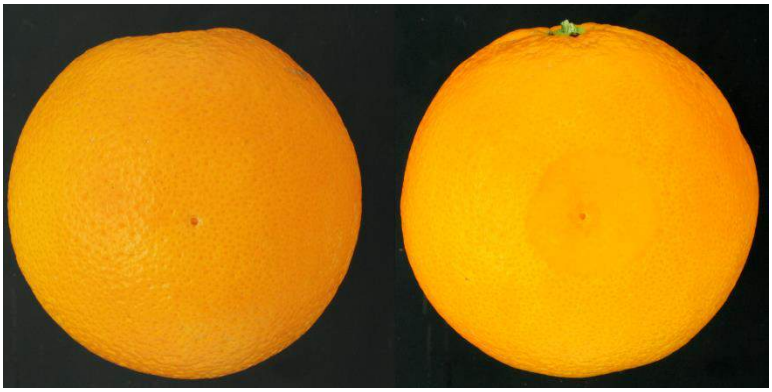

Figure 4.1. RGB images of a sound orange used for control (*left*) and an orange showing early decay symptom caused by *P. digitatum* (*right*).

4.2.2. Imaging system

In this work, a LLBI system was employed. This system mainly consisted of a CCD (charge-coupled device) based camera (JAI CV-A50 IR) with a zoom lens (F2.5 and focal lengths of 18-108 mm), five solid-state laser diode modules emitting at different wavelengths (532, 660, 785, 830 and 1060 nm) used alternately as light sources and a computer for controlling the camera. After penetrating into the fruit tissue, the fraction of the light backscattered to the fruit surface was recorded by the camera and transferred to the computer. A typical raw backscattering image is shown in Figure 4.2.

The imaging system was set up in a dark room in order to prevent the influence of ambient light. It was configured to acquire 720×576 pixel images with a resolution of 0.073 mm/pixel. Parameters of laser sources are shown in Table 4.1. The incident angle of the light beam was set

to 7º with respect to the vertical axe for all the laser sources and the distance from the laser sources to the fruit sample was chosen according to the focus of each laser (Qing et al., 2007). This setting allowed for the assumption that the light beam was almost perpendicular to the fruit surfaces, thus obtaining images symmetric with respect to the incident point (Mollazade et al., 2012). The arrangement of the image acquisition system is pictured in Figure 4.3. The backscattering images were acquired by placing the fruit manually in the imaging system presenting the damage to the camera. A total of five images were acquired for each of the 100 orange samples at the five laser wavelengths, which gave a total number of 500 backscattering images.

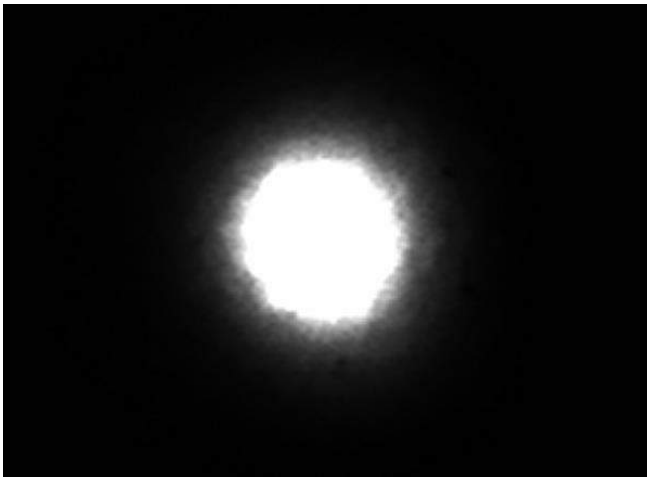

Figure 4.2. Example of a raw backscattering image.

Table 4.1. Parameters of laser sources.

Wavelength (nm)	Output (mW)	Beam size (mm)
532	10	2.5×2.5
660	2	4.0×4.0
785	45	1.0×1.0
830	30	1.0×1.0
1060	85	1.5×5.25

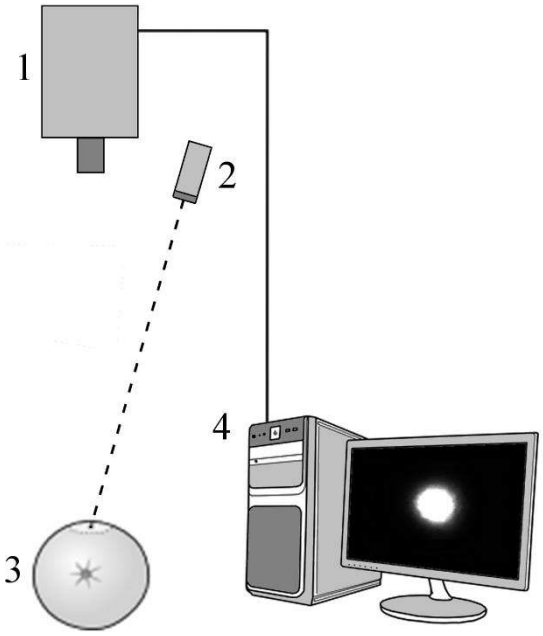

Figure 4.3. Scheme of the laser-light backscattering system. 1: CCD camera with lens; 2: laser source; 3: fruit sample; 4: computer.

4.2.3. Function for describing backscattering profiles

Backscattering images had radial symmetry with respect to the light incident point and their intensity decreases with increasing distance from the incident point (Figure 4.2). The images were reduced to one-dimensional profiles after radial averaging (Lu, 2004). For this purpose, the centre of beam incident point was identified for each backscattering image using the weighted centre of gravity method (Weeks, 1996), which considers that the centre is a point in which the maximum light intensity occurs. The radial intensity of the backscattering profiles was then calculated by obtaining the average value of all pixels within each circular ring with one pixel size (0.073 mm).

Backscattering profiles thus obtained could be used directly as a feature vector to predict the presence of damage on the skin of the fruit by a multivariate calibration model. In order to get more robust and fast predictions, data reduction was targeted. One method for this is to find the parameters of symmetric distribution functions describing the backscattering profiles.

Moreover, it is advisable to perform some pre-processing on the profiles to fit the backscattering profiles more accurately, such as removing the data points within and adjacent to the light incident area since these points are saturated, or shifting the profiles towards the profile centre by a distance equal to the number of removed data points in the saturation area (Peng and Lu, 2005). In this work, all the data points with a greyscale level (0-255) higher than 253 were removed.

Subsequently to pre-tests using various distribution functions (data not shown), the Gaussian-Lorentzian cross product (GL) function was applied. This distribution function is a Voigt approximation that combines a Gaussian and a Lorentzian in a multiplicative form. GL is commonly used in spectroscopy; also for describing laser profiles (Penache et al., 2002; Limandri et al., 2008; Stace et al., 2012). The GL function is mathematically expressed by Equation 4.1:

$$I(x) = a + \frac{b}{\left[1 + e\left(\frac{x-c}{d}\right)^2\right] \exp\left[\frac{1-e}{2}\left(\frac{x-c}{d}\right)^2\right]} \tag{4.1}$$

where I is the light intensity of each circular band after radial averaging; x is the scattering distance expressed as number of data points (pixels); a is the asymptotic value of light intensity when x approaches infinity; b is the peak value of estimated light intensity at the centre; c is the centre parameter; d is the full scattering width that produces the half maximum peak value; e is related to the shape. The shape parameter e varies from 0 to 1; a value of 0 results in the pure Gaussian function, whereas the pure Lorentzian occurs with a value of 1. Figure 4.4 shows a backscattering profile described by this GL distribution function with five parameters.

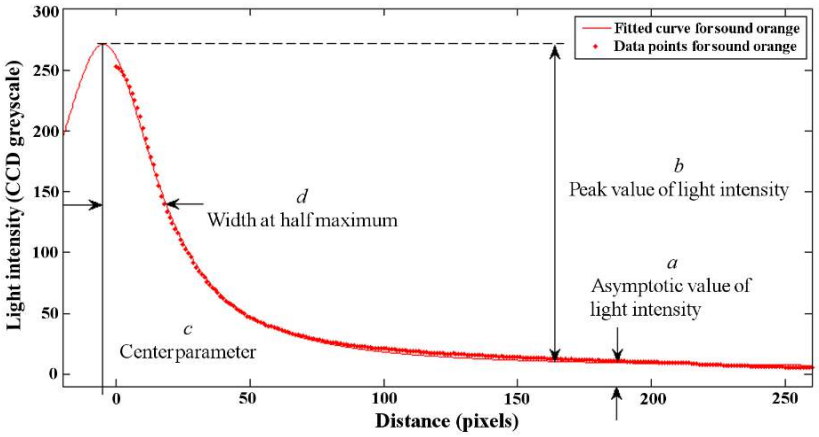

Figure 4.4. Gaussian-Lorentzian cross product distribution model for backscattering profiles.

The GL function was used to fit the backscattering profiles at the five laser wavelengths for each fruit sample. A program based on non-linear least squares regression analysis (Gelman and Hill, 2006) was written using Curve Fitting Toolbox of Matlab 7.9 (Mathworks, Inc.) in order to fit the backscattering profiles to the GL function and to estimate the five GL parameters for each sample at each laser wavelength. The remaining algorithms in this work, such as classification methods, were also implemented using Matlab environment.

4.2.4. Classifier

Linear discriminant analysis (LDA), also known as Fisher discriminant analysis (Fisher, 1936), is a supervised method of dimensionality reduction and classification used in statistics, pattern recognition and machine learning (Sierra, 2002; Wang et al., 2011a). LDA aims to find a linear projection of high-dimensional data onto a lower dimensional space ($c-1$ dimensions in a problem with c classes) where the class separation is maximised. This is achieved by maximising the ratio of the variance between the classes and variance within the classes (Duda et al., 2001). LDA has no free parameters to be adjusted and the extracted features are potentially interpretable under linearity assumptions. Furthermore, LDA is closely related to principal component analysis (PCA). The main difference between both linear projection techniques is that LDA explicitly attempts to model the difference between the classes of data, while PCA does not take into account any difference in class due to its unsupervised nature. LDA method therefore performs better for classification purposes (Martínez and Kak, 2001).

4.2.5. Labelled set

In supervised classification, there is a set of n labelled samples, $\{\mathbf{x}_i, t_i\}_{i=1..n}$, where $\mathbf{x}_i$ represents the *m*-dimensional feature vector for the *i*-th sample with label t_i. In this work, the supervised nature of the LDA classifier required the construction of a labelled data set, consisting of $m=25$ features associated with each orange sample, specifically the five GL parameters at each of the five laser wavelengths obtained from fitting the profiles.

In order to build this labelled set, the $n=100$ oranges were assigned to one of the two classes considered in this work: sound oranges and oranges presenting decay. Each sample pattern was therefore composed by 25 features and a class label. The labelled set was divided into a calibration set of 50 samples (50% of the total) and a validation set of 50 samples (50% of the total). The first set was used to build the proposed classification method and the second one to evaluate its

performance. In the validation set, the same number of samples as in the calibration set was chosen in order to check the generalisation capability of the classifier.

4.2.6. Development and validation of the classification models

LDA classification method and parameters obtained with GL at five laser wavelengths were used to classify fruit samples. Laser wavelengths were ranked in terms of their contribution to decay detection. In order to rank wavelengths, the LDA classifier was first built and evaluated using the five GL parameters corresponding to each individual wavelength as feature vector. Laser wavelengths were then ranked in ascending order of classification average success rate values. The best single wavelength that had the highest success rate was selected. The next step is to obtain the best two wavelengths. Each of the remaining wavelengths was individually added to the best single wavelength, and the corresponding success rate values were computed for all two-wavelength combinations. The best two wavelengths were chosen when they had the highest success rate among all two-wavelength combinations. This procedure was then repeated for obtaining the best three wavelengths and so on, until all wavelengths were ranked.

The calibration set of labelled data was used to build the classification models and the validation set to evaluate classifier performance. Apart from calculating the classification average success rates to assess the performance of classification, Cohen's kappa statistic values were computed to evaluate the classification bias (Fleiss, 1981). Classification average success rate provided a measure for classification accuracy with a range from 0% to 100%, this parameter being calculated as the number of correctly classified samples divided by the total number of samples. Cohen's kappa statistic gave information about if the classifier was biased towards one of the two classes, varying from 0 to 1, with a value of 1 representing a completely unbiased classifier.

4.3. Results and discussion

4.3.1. Description of backscattering profiles

For the five laser wavelengths, the GL function described backscattering profiles with average determination coefficients (R^2) values higher or equal to 0.998 and average root mean squared errors (RMSE) lower or equal to 2.54 (CCD greyscale) (Table 4.2). These values were calculated

by averaging the coefficients of determination and the RMSEs corresponding to the 100 orange samples at each laser wavelength.

Table 4.2. Average determination coefficients (R^2) and average root mean squared errors (RMSE) from fitting backscattering profiles by the GL function for all samples at the five laser wavelengths.

Wavelength (nm)	R^2 (unitless)	RMSE (CCD greyscale)
532	0.998	2.14
660	0.999	0.61
785	0.998	2.48
830	0.998	2.54
1060	0.998	2.32

The average GL parameters and the resulting average fitted curves obtained for the backscattering profiles of sound oranges and oranges with decay at the five laser wavelengths are shown in Figure 4.5. A significance test (p-value < 0.05 , one-tailed unpaired t-test) was applied to the data in order to determine if the differences between average parameters of sound oranges and decaying oranges were statistically significant. Some GL parameters presented a general trend at all the laser wavelengths (parameters b , c and e). The sound oranges had lower peak values (parameter b) than the oranges with decay at all wavelengths. By contrast, an opposite trend for centre values (parameter c) was observed, these being consistently higher for the sound oranges. However, the differences between both kinds of fruit for these two parameters were not significant enough at 660 nm. Furthermore, for both backscattering profiles, shape parameter (parameter e) generally had an almost constant value close to 1, even though this was slightly higher for the oranges with decay at 660 nm.

On the other hand, the asymptotic values (parameter a) and scattering widths (parameter d) showed a different trend between both backscattering profiles according to the laser wavelength. The sound oranges presented lower asymptotic values than the decaying oranges at almost every wavelength, except at 532 nm (parameter a was higher for the sound oranges) and at 1060 nm (parameter a did not present significant differences between both kinds of oranges). With regard to scattering widths, for the sound oranges, these values were lower than for the decaying oranges at 532 nm, 785 nm and 830 nm and, conversely, higher at 660 nm and 1060 nm. From these results, it can be said that backscattering profiles, and consequently GL parameters, were dependent on the orange state: sound or decaying, since GL parameters differed between both states at the five laser wavelengths.

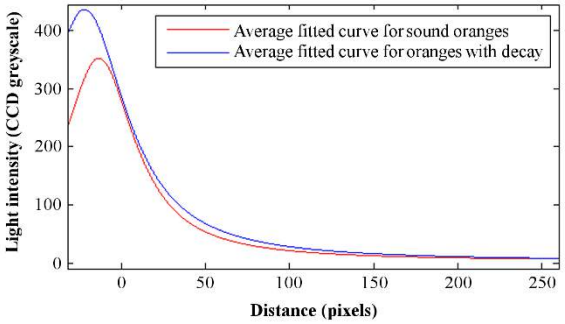

	Sound	Decaying
a (greyscale)*	3.72	2.99
b (greyscale)*	348.80	433.64
c (pixels)*	-13.30	-21.84
d (pixels *	25.97	30.27
e (unitless)	1.000	0.999

(a)

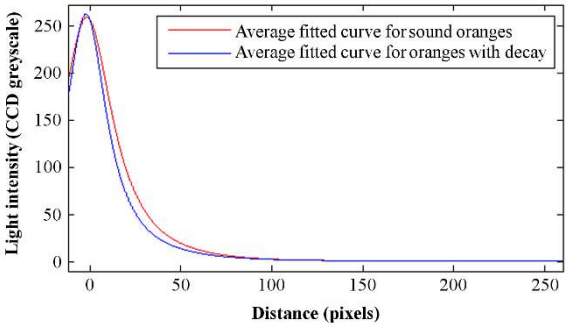

	Sound	Decaying
a (greyscale)*	0.97	0.98
b (greyscale)	257.75	261.57
c (pixels)	-1.65	-2.13
d (pixels)*	16.97	13.67
e (unitless)*	0.921	0.960

(b)

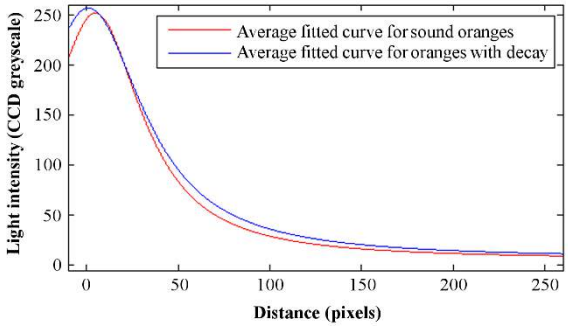

	Sound	Decaying
a (greyscale)*	6.22	7.60
b (greyscale)*	245.53	249.10
c (pixels)*	4.90	1.26
d (pixels)*	30.75	36.14
e (unitless)	0.998	0. 993

(c)

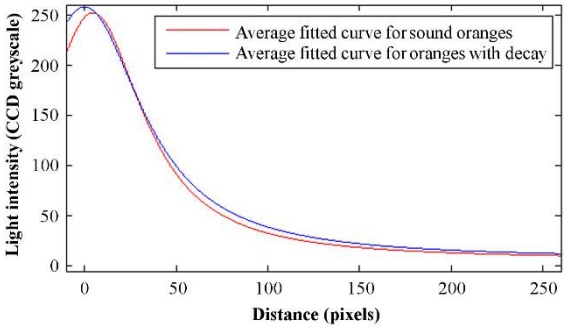

	Sound	Decaying
a (greyscale)*	6.83	7.38
b (greyscale)*	245.23	250.57
c (pixels)*	4.73	0.29
d (pixels)*	33.09	38.08
e (unitless)	0. 998	0. 999

(d)

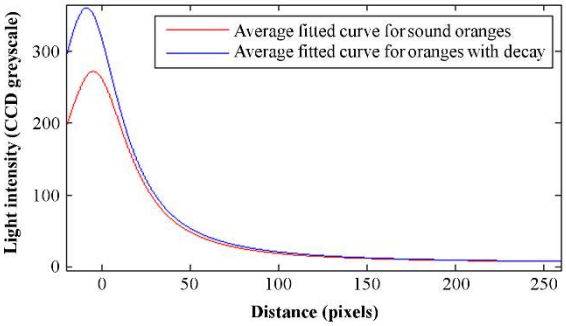

	Sound	Decaying
a (greyscale)	5.23	5.14
b (greyscale)*	266.93	355.48
c (pixels)*	-4.50	-8.40
d (pixels)*	24.16	23.42
e (unitless)	1.000	0.99

(e)

Figure 4.5. Average Gaussian-Lorentzian cross product (GL) parameters and average GL distribution curves for the backscattering profiles of sound oranges and oranges with decay at: (a) 532 nm, (b) 660 nm, (c) 785 nm, (d) 830 nm, and (e) 1060 nm. Parameters marked with * presented statistically significant differences between sound and decaying oranges.

4.3.2. Classifier performance evaluation

Table 4.3 shows the classification results for the ranked wavelength combinations, obtained from the validation set of labelled data. Values of classification average success rate and Cohen's kappa statistic, as well as the corresponding confusion matrixes, are shown for all wavelength combinations. According to the scale proposed by Landis and Kock (1977), Cohen's kappa values were interpreted as follows: 0.00-0.20 regarded as slight, 0.21-0.40 as fair, 0.41-0.60 as moderate, 0.61-0.80 as good and 0.81-1.00 as very good.

When comparing the classification results, it can be noticed that the minimum average success rate of 80.39% and the lowest Cohen's kappa value of 0.610 were obtained for the single

wavelength. In contrast, the best classification results were achieved using the five laser wavelengths with an average success rate of 96.08% and a value of Cohen's kappa of 0.921. As shown in the confusion matrix for this classification model using all the wavelengths, the percentage of well-classified fruit samples exceeded 95% for both classes despite the evident similarity between sound oranges and oranges with decay.

Table 4.3. Classification results for the ranked wavelength combinations.

Number of wavelengths	Wavelength combination (nm)	Average success rate (%)	Cohen's kappa	Confusion matrix
1	532	80.39	0.610	Sound (%) / Decay (%): Sound 87.50 / 25.93; Decay 12.50 / 74.07
2	532, 660	90.20	0.803	Sound (%) / Decay (%): Sound 87.50 / 7.41; Decay 12.50 / 92.59
3	532, 660, 1060	92.16	0.843	Sound (%) / Decay (%): Sound 91.67 / 7.41; Decay 8.33 / 92.59
4	532, 660, 1060, 830	94.12	0.882	Sound (%) / Decay (%): Sound 95.83 / 7.41; Decay 4.17 / 92.59
5	532, 660, 1060, 830, 785	96.08	0.921	Sound (%) / Decay (%): Sound 95.83 / 3.70; Decay 4.17 / 96.30

Moreover, the increase in the average success rate of around 10% from the single wavelength (80.39%) to the two-wavelength combination (90.20%) should be highlighted. Both wavelengths are in the visible wavelength range. Therefore, we assume that the visible wavelength range may provide more robust information on the differences in the scattering properties of the tissue, due to (i) higher scattering coefficients and resulting increased signal to noise ratio, and (ii) increased perturbation in the NIR range due to highly variable water and carbohydrates contents that absorb in the NIR. From the corresponding confusion matrixes, it can be also observed that, while the number of well-classified sound oranges remained the same (87.50%) for both cases, the classification of oranges with decay was greatly improved for the two-wavelength combination,

increasing from 74.07% to 92.59%. In practice, this reduction of the number of badly-classified oranges with decay is of major importance for a potential inspection system since only a reduced number of infected and sporulated fruit can be the source for important spread of fungal infections to healthy fruit handled or stored in the packinghouse, thus causing great economic losses.

On the other hand, for all the other cases, from one wavelength combination to another, the increase in the average success rate was only approximately 2% by including one wavelength more in the model.

Effective control of green mould and other citrus postharvest diseases has relied for many years on the application of conventional synthetic chemical fungicides such as imazalil or thiabendazole. However, there is currently a clear need to find and implement alternative control methods because of increasing concerns about environmental contamination and human health risks associated with fungicide residues (Palou et al., 2008). Findings from this research are a significant step for the adoption by the citrus industry of non-polluting alternative control methods, because early decay detection is an effective tool to reduce fungicide usage in the context of integrated disease management (IDM) programs.

4.4. Conclusions

The feasibility of LLBI was proved for detecting superficial decay in citrus fruit caused by *P. digitatum*. Backscattering images of oranges at five laser wavelengths in the visible and NIR ranges were used for non-destructive detection. The GL distribution function with five independent parameters described backscattering profiles accurately, with average R^2 values higher or equal to 0.998. GL parameters were dependent on the orange state (sound or decaying), observing differences between both states at all wavelengths.

In the classification of sound and decaying oranges, all wavelengths contributed to the highest average success rate of 96.1%. The increase in the average success rate of around 10% from the single wavelength (80.4%) to the two-wavelength combination (90.2%), both in the visible range, should be highlighted.

Therefore, the early detection of decaying fruit by means of backscattering imaging analysis has a high potential for its integration in a commercial system. Nevertheless, for future setting up on a sorting line, perhaps a line laser should be applied on rotating fruit, instead of point lasers.

Acknowledgements

This work has been partially funded by the Instituto Nacional de Investigación y Tecnología Agraria y Alimentaria de España (INIA) through research project RTA2012-00062-C04-01 with the support of European FEDER funds. Delia Lorente thanks INIA for the support through grant FPI-INIA number 42.

Chapter 5

Laser-light backscattering imaging for early decay detection in citrus fruit using both a statistical and a physical model

D. Lorente[1], M. Zude[2], C. Idler[2], J. Gómez-Sanchis[3], J. Blasco[1]

[1]Centro de Agroingeniería, Instituto Valenciano de Investigaciones Agrarias (IVIA), Ctra. Moncada-Náquera km 5, 46113 Moncada (Valencia), Spain.

[2]Leibniz-Institute for Agricultural Engineering Potsdam-Bornim (ATB). Max-Eyth-Allee 100, 14469 Potsdam-Bornim, Germany.

[3]Intelligent Data Analysis Laboratory (IDAL), Electronic Engineering Department, Universitat de València. Avda. Universitat s/n, 46100 Burjassot (Valencia), Spain.

Accepted for publication in: Journal of Food Engineering.

Abstract

The early detection of decay caused by fungi in citrus fruit is a primary concern in the postharvest phase, the automation of this task still being a challenge. This work reports new progress in the

automatic detection of early symptoms of decay in citrus fruit after infection with the pathogen *Penicillium digitatum* using laser-light backscattering imaging. Backscattering images of sound and decaying parts of the surface of oranges cv. 'Valencia late' were obtained using laser diode modules emitting at five wavelengths in the visible and near-infrared regions. The images of backscattered light captured by a camera had radial symmetry with respect to the incident point of the laser beam, these being reduced to a one-dimensional profile through radial averaging. Two models were used to characterise backscattering profiles: a statistical model using the Gaussian-Lorentzian cross product (GL) distribution function with five parameters and a physical approach calculating the absorption, μ_a, and reduced scattering, μ_s', coefficients from Farrell's diffusion theory. Models described radial profiles accurately, with slightly better curve-fitting results ($R^2 \geq 0.996$) for the GL model compared to Farrell's model ($R^2 \geq 0.982$), both indicating significant differences in the parameters between sound and decaying orange skin at the five wavelengths. For dimensionality reduction purposes, feature selection methods were employed to select the most relevant backscattering profile parameters for the detection of early decay lesions. The feature vectors obtained were used to discriminate between sound and decaying skin using a supervised classifier based on linear discriminant analysis. The best classification results were achieved using a reduced set of GL parameters, yielding a maximum overall classification accuracy of 93.4%, with a percentage of well-classified sound and decaying samples of 92.5% and 94.3%, respectively. Results also pointed out application limits of Farrell's diffusion theory at 532 nm laser wavelength, for which high absorption of pigments occurred.

Keywords: Fruit inspection; Citrus fruit; Decay detection; Laser-light backscattering imaging; LDA classifier; Gaussian-Lorentzian cross product distribution function; Farrell's diffusion theory model; Feature selection.

5.1. Introduction

Postharvest decay in citrus fruit, due to *Penicillium* spp. fungi, causes severe economic losses world-wide in almost all regions where citrus is grown (Eckert and Eaks, 1989). Decayed fruit can propagate the fungal infection in the production, during long-term storage or fruit shipping to export markets. In practice, these infections are controlled by applying synthetic chemical fungicides, such as imazalil or thiabendazole. However, the widespread use of these fungicides has led to the resistance of the fungal pathogens (Eckert, 1990). Therefore, early detection of infected citrus fruit is regarded as a primary concern in commercial packinghouses. At present, the detection of infected fruit is performed visually by trained workers examining each fruit under

ultraviolet (UV) illumination inside a dark chamber, since UV light triggers the excitation of fungal products, thus causing fluorescence emission in the blue (Momin et al., 2012). Nevertheless, this method has a high risk of human error and is harmful for the workers, since long exposure to UV radiation can lead to damage to the human skin, such as premature aging or cancer (Lopes et al., 2010).

The automation of these tasks using modern machine vision systems can be considered a valuable alternative to human inspection (Cubero et al., 2011). In this sense, vision systems based on colour cameras are currently used in the citrus industry to detect external defects that are visible at first glance (Blasco et al., 2007b; Kim et al., 2009). However, decay in its early stages (before sporulation) is hardly detectable, since the appearance of the damage is very similar to sound skin, thus being barely visible to the human eye (Figure 5.1). Other machine vision technologies have been proposed, such as the use of automated readings of UV-induced fluorescence. The systems based on UV radiation imitate the fluorescence technique used in the industry to detect decay in citrus by humans (Kurita et al., 2009). Nevertheless, the utilisation of UV light presents some disadvantages because not all cultivars of citrus show the same autofluorescence phenomenon due to differences in the peel composition (Momin et al., 2011; Momin et al., 2012) and, in addition, other defects like chilling injury can also lead to some degree of fluorescence (Slaughter et al., 2008). An alternative for detecting non-visible damage on citrus fruits is provided by hyperspectral and multispectral vision systems (Blasco et al., 2009; Gómez-Sanchis et al., 2012; Lorente et al., 2013c), since these systems are not limited to the visible part of the electromagnetic spectrum (Qin et al., 2013).

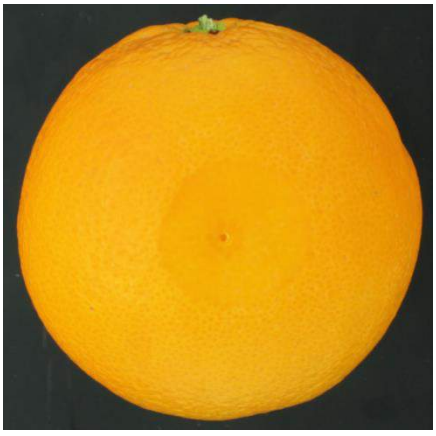

Figure 5.1. Orange showing early decay symptoms caused by *Penicillium digitatum* fungus.

Light backscattering imaging (LBI) has recently emerged as an alternative machine vision technique for fruit inspection combining spectroscopic and imaging approaches. The spatial modes of light interaction with turbid biological materials can provide distinct information related to the chemical and structural properties of the sample. It is assumed that, when a light beam interacts with a fruit, a small portion of only about 4-5% is reflected on the surface of the sample (Fresnel scattering) and the rest penetrates into the tissue (Birth, 1976). In the tissue, the entering light is partly scattered backwards to the exterior tissue surface after interacting with the internal components of the fruit (diffuse scattering or backscattering), whereas the remaining radiation is absorbed by tissue or transmitted further out of the fruit in different direction (Meinke and Friebel, 2009). The optical analyses can be used to characterise fruits (Salguero-Chaparro et al., 2014), particularly by two optical properties: the absorption coefficient (μ_a) and the reduced scattering coefficient (μ_s') (Tuchin, 2000). Light absorption is mainly related to the chemical components of the fruit, such as amino acids, inorganic ions, carbohydrates, water or pigments (Williams and Norris, 2001). The spectroscopic technology has been successfully used to classify fruits in sorting lines, considering e.g. the soluble solids content (SSC). In contrast, light scattering is affected by the structural properties of the tissue, such as density, particle size and cellular structures (Seifert et al., 2014a). Here, light scattering, recorded by an imaging system, can be useful as an indirect measure of the histology of fruit, such as flesh firmness. If spectral and additional spatial imaging information is available, combined analyses of texture and chemical composition can be done. Accordingly, many studies have reported work on assessing the quality of different fresh fruit by LBI systems. For example, Qing et al. (2007) predicted firmness and SSC in apples from backscattering images acquired using laser light at five different wavelengths in the visible and near-infrared (NIR) regions (680, 780, 880, 940 and 980 nm). In other research, the variation of moisture content of banana slices subjected to different drying conditions was evaluated by taking backscattering images using a laser diode emitting at 670 nm (Romano et al., 2008). In order to detect bruises on apples, Lu et al. (2010) determined the optical properties (the absorption and the reduced scattering coefficients) of normal and bruised tissues, as well as their changes with time after bruising, using backscattering images acquired in the range of 500-1000 nm with a hyperspectral imaging system.

The process of decay in citrus fruit is characterised by the weakening of the cell walls due to changes in enzymatic activity (Barmore and Brown, 1979). Thus, the subsequent accumulation of liquid in the apoplast of the epidermis is an early visible symptom of infection in citrus (Barmore and Brown, 1981). In consequence, since structural changes in fruit tissue, and therefore changes in the optical properties, are expected, the LBI technique may have the potential for decay detection. In previous research (Lorente et al., 2013b), backscattering images obtained using laser light at several wavelengths in the visible and NIR ranges (532, 660, 785, 830 and 1060 nm) were

analysed, for the first time, in order to detect decay caused by fungi in citrus fruit. The Gaussian-Lorentzian cross product (GL) distribution function with five independent parameters was used to describe backscattering profiles from backscattering images in that research. However, there also exists a physical, instead of statistical model for characterising the backscattering profiles. This physical approach consists in extracting optical properties (the absorption and reduced scattering coefficients) of fruits by Farrell's diffusion theory (Farrell et al., 1992), which provides a faithful description of the shape of the backscattering profiles (Qin and Lu, 2007; Qin et al., 2009b). In order to continue the research line of the previous work (Lorente et al., 2013b), the present study advances in the automatic detection of an economically dangerous postharvest disease of citrus fruit, such as fungal decay caused by *Penicillium digitatum*, by means of laser-light backscattering imaging (LLBI). Particularly, this research aimed at evaluating and comparing the two profile modelling approaches (statistical and physical) and different feature selection methods in terms of their performance in the classification of orange skin into sound or decaying in an early stage, this appearing as the next step in the direction towards a potential automation. The additional advantage of the physical profile modelling approach, compared to the statistical one, is that it also allows to measure and separate the absorption and scattering properties of biological products, which is useful for quantitative analysis of light-tissue interactions. In this sense, an ultimate objective of this research work was the measurement and separation of the optical properties of sound and decaying skin of citrus fruit at different wavelengths, in order to extract more knowledge about the underlying optical properties associated with the decaying process in citrus fruit.

5.2. Material and methods

5.2.1. Fruit used in the experiments

Sweet oranges (*Citrus sinensis* L. Osbeck) cv. 'Valencia late', grown in Spain, were purchased from a local market in Potsdam (Germany). These oranges came from organic production, thus ensuring the absence of chemicals, such as synthetic waxes or fungicides, commonly applied on fruit during the postharvest phase in conventional crop production. For the experiments, a total of 40 fruits were superficially punctured on the rind and inoculated with spores of *P. digitatum* fungus. The *P. digitatum* strain DSM-2750, from the Collection of Microorganisms and Cell Cultures (DSMZ, Germany), was cultured on potato dextrose agar (PDA; Sigma-Aldrich Chemical Co., Germany) plates at 24 °C in the dark. Conidia from 10 day old cultures were taken

from the agar surface with a sterile glass rod and transferred to a sterile aqueous solution of 0.05% Tween® 80. The conidial suspension was filtered through two layers of cheesecloth to separate hyphal fragments and then adjusted to a concentration of 1.4×10^6 spores/ml using a haemocytometer, which is sufficient to cause infestation in laboratory conditions (Palou et al., 2001). For inoculation, the oranges were wounded with a steel needle by making a 1 mm wide by 2 mm deep injury on the equatorial zone, and then 20 µl of the conidial suspension was placed on each wound using a micropipette. The fruits were stored in an environment-controlled chamber at 22 °C and relative humidity of 55% for a period of time that was long enough for decay lesions with a diameter of about 25 mm to appear on all the fruits. This storage period was different for each fruit, since the development of the decay varied from one fruit to another, with the first patches of decay appearing on some oranges after four days' storage and the latest after 12 days. Backscattering images of a particular orange were acquired as soon as that orange presented decay damage with the aforementioned diameter dimension and, then, the fruit was removed from the experiments. Two different parts of the surface of each of the 40 oranges were analysed: the one presenting decay lesions and the opposite side of the orange, where the skin was thoroughly checked to be completely sound. Therefore, a total of 80 samples of orange skin were examined with the backscattering imaging system.

5.2.2. Imaging system

The LLBI system (Figure 5.2) developed in the Leibniz-Institute for Agricultural Engineering Potsdam-Bornim (ATB) was used in this research. This system mainly consisted of a monochrome charge-coupled device (CCD) camera (CV-A50IR, JAI Ltd., Japan) with a zoom lens (12VG1040ASIR-SQ, Tamron Co. Ltd., Japan), a computer for controlling the camera and storing the images, and five solid-state laser diode modules used alternately emitting at different wavelengths: 532 nm (HK-5616-02, Shimadzu, Japan), 660 nm (LPM-660-60C, Newport, USA), 785 nm (LPM-785-45C, Newport, USA), 830 nm (LPM-830-30C, Newport, USA) and 1060 nm (LPM-1060-85E, Newport, USA), ranging from 10 mW to 85 mW to provide high contrast images. Lasers wavelengths were chosen by reaching a compromise between the main absorbing molecules in oranges and available hardware: 532 nm is related to the absorption of light by the carotenoids, 660 nm relates to chlorophyll and its degradation products, 785 nm is commonly used as a reference wavelength, while 830 nm and 1060 nm respond to the water absorption, and also absorption of other molecules with e.g. C-H or C-OH bonds. After entering into the fruit tissue, the portion of the light backscattered to the fruit surface was recorded by the camera and

transferred to the computer using a frame-grabber board (VRmAVC-1, VRmagic Holding AG, Germany).

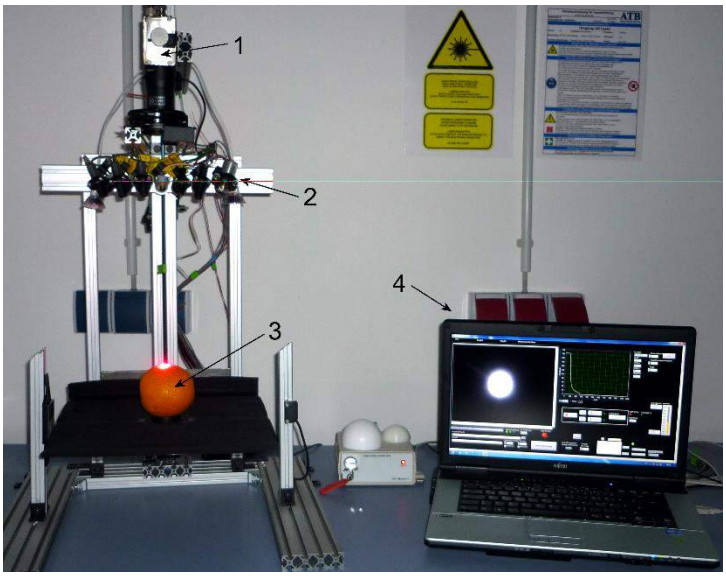

Figure 5.2. Picture of the laser-light backscattering system. 1: CCD camera with lens; 2: laser sources; 3: fruit sample; 4: computer.

Image acquisition took place in a dark room in order to avoid the interference of ambient illumination. The imaging system was configured to acquire 720×576 pixel images with a resolution of 0.133 mm/pixel. The distance from the lens to the fruit was set to 340 mm and the laser diode modules were placed in a fixed position in such a way that all the laser beams were aimed towards the top of the fruit. Therefore, the incident angle of the light beam was different for each laser, varying marginally in the range between 5º and 15º with respect to the vertical axis. The small incident angle and small beam size allowed to assume that the light beam was almost perpendicular to the fruit surfaces, thus obtaining images that were symmetrical with respect to the incident point (Mollazade et al., 2012). The backscattering images were acquired by placing each fruit manually in the imaging system so that the part of the fruit under study was facing the camera. A total of five images were taken for each of the 80 samples of orange skin at the five laser wavelengths, thereby resulting in 400 backscattering images.

5.2.3. Processing of backscattering images

Since the backscattering images had radial symmetry with respect to the light incident point, they were reduced to one-dimensional profiles through radial averaging. To this end, the centre of the beam incident point was first identified for each backscattering image using the weighted centre of gravity method (Weeks, 1996), which considers the centre to be the point with the maximum light intensity. The radial intensity of the backscattering profiles was then calculated by averaging all pixels within each circular ring with one pixel size (0.133 mm).

Before fitting the backscattering profiles with the GL distribution model and the Farrell's diffusion theory model, some pre-processing was performed on the profiles to fit them more accurately, thereby leading to better predictions. The data points within and adjacent to the light incident area were first removed without losing essential scattering information since these points were saturated (Peng and Lu, 2005). In particular, all the data points with a greyscale level (0-255) higher than 253 were eliminated from the profiles. Later, each backscattering profile was normalised by its actual maximum value of light intensity that occurred at the closest point to the light incident centre (r_{norm}), thus avoiding the need to measure absolute reflectance intensities (Peng and Lu, 2007). In addition, a third pre-processing step was also necessary only before using the GL model. The profiles were shifted towards the profile centre by a distance equal to the number of removed data points in the saturation area, thus allowing the statistical model to fit the backscattering profiles more precisely without the influence of light saturation in the incident area (Peng and Lu, 2005).

5.2.3.1. Gaussian-Lorentzian cross product distribution model

The GL distribution function is a Voigt approximation combining a Gaussian and a Lorentzian in a multiplicative form and is commonly used in spectroscopy (Limandri et al., 2008). The GL function with five parameters is expressed mathematically by Equation 5.1:

$$R_{GL}(r) = a + \frac{b}{\left[1+e\left(\frac{r-c}{d}\right)^2\right]\exp\left[\frac{1-e}{2}\left(\frac{r-c}{d}\right)^2\right]} \quad (5.1)$$

where R_{GL} is the light intensity of each circular ring after radial averaging; r is the scattering distance (mm); a is the asymptotic value of the light intensity when r approaches infinity; b is the peak value of the light intensity at the centre; c is the centre parameter; d is the full scattering width that produces the half maximum peak value; and e is related to the shape. The shape

parameter e ranges from 0 to 1; the pure Gaussian function occurs with a value of 0, whereas the pure Lorentzian has a value of 1. Figure 5.3(a) shows how this GL distribution function fits a backscattering profile.

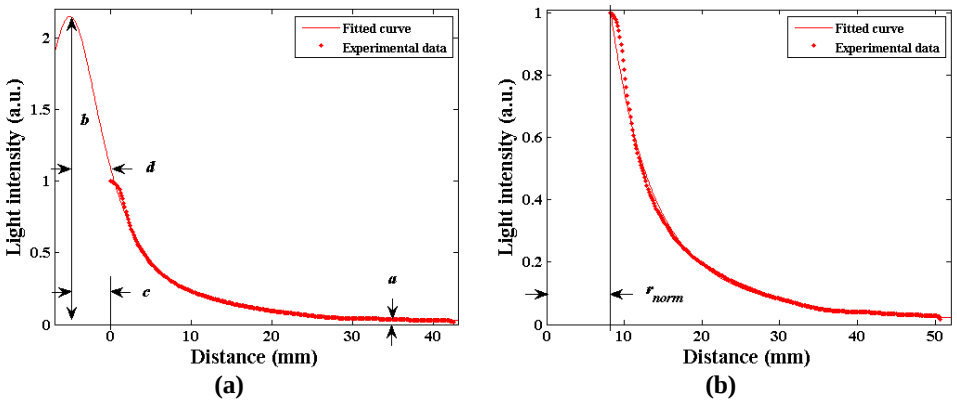

Figure 5.3. Models for fitting backscattering profiles: (a) Gaussian-Lorentzian cross product (GL) distribution model and (b) Farrell's diffusion theory model.

After pre-processing the backscattering profiles, the GL function was employed to fit the profiles at the five laser wavelengths for each sample. For this purpose, a program based on the Levenberg-Marquardt non-linear least squares regression analysis (Gelman and Hill, 2006) was written using the Curve Fitting Toolbox of Matlab 7.9 (Mathworks, Inc.). The curve fitting process was performed by minimising the sum of the squares of the differences between the experimental data and the GL model. Each backscattering profile was thus uniquely characterised by the five GL parameters. The performance of curve fitting was evaluated by computing the coefficients of determination (R^2) and the root mean squared errors (RMSE) corresponding to each of the 80 samples of orange skin at each laser wavelength, and then averaging these values. Moreover, a significance test (p-value < 0.05, one-tailed Wilcoxon rank-sum test) (Wilcoxon, 1945) was applied to the data in order to determine if the differences between the median values of the fitting parameters of sound and decaying skin were statistically significant. In addition to the fitting models, the remaining algorithms used in this work, such as feature selection methods and classification models, were also implemented using the Matlab environment.

5.2.3.2. Farrell's diffusion theory model

Light propagation in a turbid material can be described by the Boltzmann equation (Tuchin, 2000), which is rather complicated to solve analytically. Nevertheless, when scattering is dominant $(\mu_s' >> \mu_a)$, this equation can be simplified to an approximate diffusion equation, which has an analytical solution under certain assumptions. Farrell et al. (1992) found an analytical solution for the approximate diffusion equation to describe diffuse reflectance at the surface of a semi-infinite homogeneous turbid material when an infinitely small light beam strikes the surface vertically. In Farrell's diffusion theory model, diffuse reflectance is expressed as a function of distance from the light source and the optical properties of the material, such as the absorption (μ_a) and reduced scattering coefficients (μ_s') and the relative refractive index (Equation 5.2):

$$R_F(r) = \frac{a'}{4\pi}\left[\frac{1}{\mu_t'}\left(\mu_{eff}+\frac{1}{r_1}\right)\frac{\exp(-\mu_{eff}r_1)}{r_1^2}+\left(\frac{1}{\mu_t'}+\frac{4A}{3\mu_t'}\right)\left(\mu_{eff}+\frac{1}{r_2}\right)\frac{\exp(-\mu_{eff}r_2)}{r_2^2}\right] \qquad (5.2)$$

where r is the distance from the light incident centre (mm); a' is the transport albedo, $a' = \mu_s'/(\mu_a+\mu_s')$; μ_{eff} is the effective attenuation coefficient, $\mu_{eff} = [3\mu_a(\mu_a+\mu_s')]^{1/2}$; μ_t' is the total interaction coefficient, $\mu_t' = \mu_a + \mu_s'$; the variables r_1 and r_2 are given by the equations $r_1 = [(1/\mu_t')^2 + r^2]^{1/2}$ and $r_2 = [((1/\mu_t')+(4A/3\mu_t'))^2 + r^2]^{1/2}$, respectively; A is an internal reflection coefficient that can be computed by this empirical equation (Groenhuis et al., 1983): $A = (1+r_d)/(1-r_d)$, in which $r_d \approx -1.440n_{rel}^{-2} + 0.710n_{rel}^{-1} + 0.668 + 0.0636n_{rel}$ and n_{rel} is the relative refractive index of the material-air interface, $n_{rel} = n_m / n_{air}$. Figure 5.3(b) shows how Farrell's diffusion theory model fits a backscattering profile.

In this work, an orange fruit was assumed to be a semi-infinite homogeneous turbid material with scattering dominance in order to apply Farrell's diffusion theory model for describing the diffuse reflectance (or backscattering) at the surface of the fruit generated by the light beam of the different laser sources. For many biological materials, scattering is dominant in the visible and short-wave NIR spectral regions (approximately 500-1300 nm), in which the diode lasers used in this research emitted. Moreover, although the refractive index for biological materials varies slightly with wavelength (Mourant et al., 1997), a constant value of $n_m = 1.40$ was assumed for oranges. This value is commonly used for the simulation of light propagation in fruit tissue (Baranyai and Zude, 2009).

After determining A, Farrell's model was used to fit the pre-processed backscattering profiles and to estimate μ_a and μ_s' for each sample at all laser wavelengths. Because of non-uniformity in the scale of experimental backscattering profiles and Farrell's diffusion theory model, the model was also normalised at a specific distance with respect to the light incident centre (r_{norm}), equal

to that chosen for the normalisation of the experimental profiles (Qin and Lu, 2007). The normalised Farrell's model was then fitted to the pre-processed experimental profiles using the same curve-fitting algorithm as that employed for the GL model. Thus, each backscattering profile was uniquely described by the two optical coefficients. In addition, the performance of the curve fitting was evaluated and a significance test was applied to the data, similarly to that done for the GL model.

5.2.4. Labelled sets

Supervised machine learning methods require the use of a set of n labelled samples, $\{\mathbf{x}_i, t_i\}_{i=1..n}$, where $\mathbf{x}_i$ is the *m*-dimensional feature vector for the *i*-th sample with label t_i. Due to the supervised nature of the statistical techniques used in this research, it was necessary to construct two labelled data sets with different feature vectors. The features belonging to the first labelled set were obtained from the GL model and the features of the second set from Farrell's model. The first labelled set consisted of $m = 25$ features associated with each sample of orange skin (the five GL parameters at each of the five laser wavelengths obtained from fitting the GL model to the backscattering profiles). Similarly, the second labelled set was composed of $m = 10$ features (the absorption and reduced scattering coefficients for each sample extracted from Farrell's model at the five laser wavelengths). For both labelled data sets, the $n = 80$ samples of orange skin were assigned to one of the two classes considered in this work: sound and decaying skin. Each sample pattern was therefore composed of 25 features and a class label for the labelled set from the GL model, and 10 features and a class label for the labelled set from Farrell's model.

5.2.5. Feature selection methods

For optimisation purposes, some feature selection methods were used to find a subset of the original features that contains the least number of features with the most significant information, resulting in an improvement in the classification of orange skin into sound and decaying (Dash and Liu, 1997). The feature selection methods used were: correlation analysis (CA; Rodgers and Nicewander, 1988), mutual information (MI; Battiti, 1994), Fisher's discriminant analysis (FDA; Cheng et al., 2004), t-test (TT; Li et al., 2006), Wilks' lambda (WL; Ouardighi et al., 2007), Bhattacharyya distance (BD; Choi and Lee, 2003), minimum redundancy maximum relevance difference criterion (MRMRd; Ponsa and López, 2007), minimum redundancy maximum relevance quotient criterion (MRMRq; Peng et al., 2005) and Kullback-Leibler divergence (KLD; Kullback, 1987). These supervised methods are intended for binary classification problems, like

the proposed here, and were chosen because they have been successfully tested in previous studies related to fruit inspection using computer vision (Gómez-Sanchis et al., 2013; Lorente et al., 2013a). Furthermore, these feature selection techniques are filter-type methods, which use an indirect measure of the quality of the selected features as a selection criterion, instead of optimising the success of a particular classifier as in the so-called wrapper methods (Guyon and Elisseeff, 2003). Thus, filter methods involve a faster convergence and greater robustness to changes in the classification method.

5.2.6. Development and validation of the classification models

Features that best distinguished between sound and decaying samples were chosen by selecting a minimum set of features for each selection method, and for both labelled sets, that maximised classifier performance. Feature vectors from the GL model and the Farrell's model labelled sets were used to discriminate between both kinds of samples using a classifier based on linear discriminant analysis (LDA; Fisher, 1936). For each feature selection method, the performance of the classifier was evaluated using the first feature in the feature ranking provided by the corresponding selection method, and then successive features were added in an iterative process until all the features were employed sequentially.

A cross-validation procedure was used to evaluate and compare the performance of the classification models. In particular, the experiments were performed with 5-fold cross-validation, consisting in dividing the data randomly into five subsets of equal size and class proportions (Kohavi, 1995), and using four data subsets as the calibration set to build the classification models and the remaining one as the validation set to evaluate classifier performance (Hastie et al., 2009). This process was repeated five times leaving one different subset each time and the whole 5-fold cross-validation process was performed 100 times to reduce variability due to random partitioning and obtain reliable performance estimation. Therefore, a total of 500 iterations of calibration and validation were performed for each classification model. The validation results were subsequently averaged over all iterations, thus obtaining a mean confusion matrix created by computing the element-wise mean of the individual confusion matrices for each iteration.

In order to assess the classification performance, overall accuracy (Fleiss, 1981) and the value of Cohen's kappa statistic (Sim and Wright, 2005) were computed for each classification model from its associated mean confusion matrix. Overall accuracy of classification was calculated as the number of correctly-classified samples divided by the total number of samples, varying from 0% to 100%. Unlike the overall accuracy, Cohen's kappa statistic took into account whether the classifier was biased towards one of the two classes when measuring the classifier performance.

Perfect classifier performance corresponds to a kappa value of 1, while a random guess classification involves a kappa value of 0. A kappa statistic value much lower than the overall accuracy suggests that the overall accuracy is inflated due to the classification bias.

5.3. Results and discussion

5.3.1. Description of backscattering profiles

Table 5.1 shows the average determination coefficients (R^2) and the average root mean squared errors (RMSE) obtained from fitting backscattering profiles by the GL model and the Farrell's model at the five laser wavelengths. Values related to light intensity were expressed in arbitrary units (a.u.) after normalisation. Both profile models described backscattering profiles with high coefficients of determination and low errors. However, the GL approach provided slightly better curve-fitting results.

Table 5.1. Average determination coefficients (R^2) and average root mean squared errors (RMSE) from fitting backscattering profiles by the GL model and Farrell's model for all samples at the five laser wavelengths.

Wavelength (nm)	Gauss-Lorentzian cross product distribution model		Farrell's diffusion theory model	
	R^2 (unitless)	RMSE (a.u.)	R^2 (unitless)	RMSE (a.u.)
532	0.9987	0.0044	0.9864	0.0144
660	0.9963	0.0118	0.9816	0.0250
785	0.9977	0.0087	0.9869	0.0205
830	0.9972	0.0097	0.9855	0.0218
1060	0.9989	0.0071	0.9893	0.0221

The median values of the five GL parameters and the absorption and reduced scattering coefficients obtained for the backscattering profiles of sound and decaying skin samples at the five laser wavelengths are shown in Table 5.2. The table also shows if the differences between fitting parameters of sound and decaying orange skin were statistically significant (p-value < 0.05). Considering the statistical GL approach, the parameters a and e showed a general trend at all wavelengths. The sound skin presented higher asymptotic values (parameter

a) than the decay lesions at all wavelengths. Furthermore, for both kinds of orange skin samples, the shape parameter (parameter e) generally had a nearly constant value close to 1, even though this was slightly higher for the decaying samples at 785 nm. Therefore, the shape of all profiles was similar to a pure Lorentzian. On the other hand, peak values (parameter b), centre values (parameter c) and scattering widths (parameter d) presented a different trend between both kinds of samples depending on the laser wavelength. The differences between both kinds of samples were significant at only two wavelengths for the peak values and also at two wavelengths for the centre values. The sound samples had higher peak values than the decaying samples at 660 nm and, conversely, lower ones at 785 nm. Moreover, the centre values for the sound samples were higher than for the decaying samples at 785 nm and 830 nm. With regard to scattering widths, the values for the sound samples were lower than for the decaying samples at almost every wavelength, except at 532 nm, for which parameter d was higher for the sound samples.

With regard to the physical approach, the differences in the absorption and reduced scattering coefficients between sound and decaying skin at the different wavelengths were justified by reasons connected with the decaying process, since the calculated coefficients provided a real connection with the optical properties of citrus fruit. With respect to the differences in the μ_a values, the absorption coefficient values for the sound samples appeared higher than those obtained for the decaying samples at almost every wavelength, except at 532 nm. The absorption properties depend on the chemical bonds of the biological materials, which absorb light energy at particular wavelengths. In this sense, at 532 nm, the absorption of carotenoids was captured. The carotenoids content was not expected to change in early symptoms. At 660 nm, the absorption of fruit chlorophyll was measured (Zude, 2003). Therefore, the enhanced μ_a for sound samples pointed to an increase in the chlorophyll content –either chlorophyll *a* or its degradation product pheophytin (Seifert et al., 2014b). An explanation for the difference measured at 780 nm is lacking, since almost no absorption of native fruit compounds appears at this passband. Due to the water soaking of the decaying tissue and the associated enhanced transpiration rate, the μ_a values for decaying samples were expected to appear lower than those obtained for sound samples at 830 nm and 1060 nm, since these two wavelengths are mainly related to the water absorption, as reported by Walsh and Kawano (2009). This was therefore confirmed in the present study.

With respect to the differences in the μ_s' values, the reduced scattering coefficient values were significantly lower for the decaying samples at 830 nm and 1060 nm, which may be explained by the difference in the refractive index or by the decreased amount of scatters in the fruit tissue due to the weakening of the cell walls during the decaying process (Barmore and Brown, 1979).

Table 5.2. Median values of the GL parameters and the absorption and reduced scattering coefficients for the backscattering profiles of sound and decaying skin samples at the five laser wavelengths. Parameters marked with * presented statistically significant differences between samples of sound and decaying orange skin.

Wavelength (nm)	Gauss-Lorentzian cross product distribution model			Farrell's diffusion theory model		
		Sound	Decaying		Sound	Decaying
532	*a* (a.u.)*	0.0046	0.0039	μ_a (mm^{-1})	0.0948	0.1048
	b (a.u.)	1.0284	1.0318	μ_s' (mm^{-1})	0.3820	0.3991
	c (mm)	-0.1393	-0.1365			
	d (mm)*	1.0452	0.9806			
	e (unitless)	1.00000	1.00000			
660	*a* (a.u.)*	0.0173	0.0046	μ_a (mm^{-1})*	0.0095	0.0051
	b (a.u.)*	24.3932	8.5176	μ_s' (mm^{-1})	0.1955	0.1945
	c (mm)	-5.3157	-5.4000			
	d (mm)*	1.1592	2.0492			
	e (unitless)	1.00000	1.00000			
785	*a* (a.u.)*	0.0100	0.0053	μ_a (mm^{-1})*	0.0280	0.0177
	b (a.u.)*	1.2127	1.4227	μ_s' (mm^{-1})	0.2289	0.2283
	c (mm)*	-1.0289	-1.6437			
	d (mm)*	2.4823	2.7051			
	e (unitless)*	0.99998	1.00000			
830	*a* (a.u.)*	0.0127	0.0068	μ_a (mm^{-1})*	0.0224	0.0113
	b (a.u.)	1.4197	1.7274	μ_s' (mm^{-1})*	0.2241	0.2151
	c (mm)*	-1.5893	-2.2958			
	d (mm)*	2.6570	2.9267			
	e (unitless)	1.00000	1.00000			
1060	*a* (a.u.)*	0.0152	0.0116	μ_a (mm^{-1})*	0.0131	0.0108
	b (a.u.)	2.6976	2.4552	μ_s' (mm^{-1})*	0.2020	0.1983
	c (mm)	-3.8149	-3.6906			
	d (mm)*	2.9060	3.1250			
	e (unitless)	0.99999	1.00000			

The values of μ_a and μ_s' obtained for citrus fruit in this study were comparable in order of magnitude with those for other fresh fruits and vegetables reported in the literature. For example, Qin and Lu (2008) determined μ_a and μ_s' of apple (three different varieties), peach, pear,

kiwifruit, plum, cucumber, zucchini squash and tomato over the spectral range of 500-1000 nm, resulting in values with magnitude orders similar to those obtained for oranges in this work. As can be straightforwardly seen from Figure 5.4, the values of μ_s' were at least one order higher than the μ_a values for both kinds of samples at all wavelengths, except at 532 nm, thereby highlighting the dominant effect of scattering for light propagation in oranges in the visible and short-wave NIR spectral regions (approximately 500-1300 nm). Consequently, the prerequisite of $\mu_s' >> \mu_a$ was given and the diffusion theory approach could be applied. Another aspect that should be highlighted is that the maximum values of μ_s' were obtained at 532 nm. This could be due to the fact that more interactions usually occur at short wavelengths than at long ones (Meinke and Friebel, 2009), thus leading to an increase in the amount of scattering events especially at 532 nm, which was the shortest wavelength of the five used in this work. Moreover, the maximum values of μ_a also occurred at 532 nm, which is due to the absorption of carotenoids, these compounds predominating in the skin of citrus fruits in the mature stage, as described by Ladaniya (2008). Therefore, the difference between the absorption and reduced scattering coefficients was less evident at 532 nm, and the diffusion theory could not be properly applied. This assumption was supported by the high variance in the calculated coefficients (Figure 5.4).

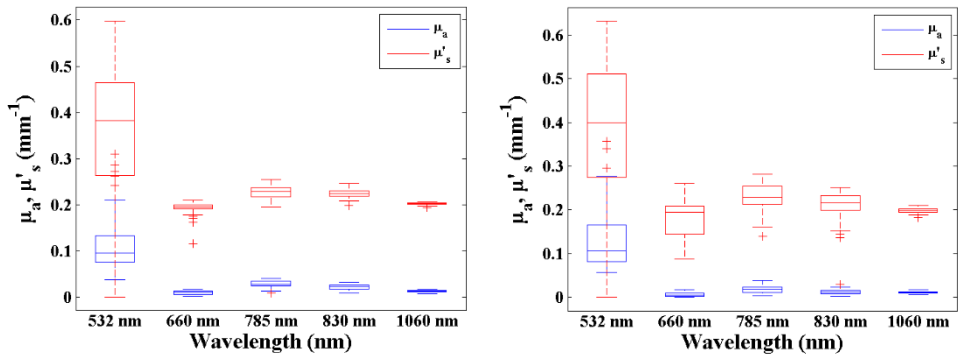

Figure 5.4. Boxplots of the absorption and reduced scattering coefficients for the backscattering profiles of (a) sound and (b) decaying skin samples at the five laser wavelengths.

Overall, the GL parameters and the absorption and reduced scattering coefficients differed between the two states of orange skin (sound or decaying) at the five laser wavelengths. Therefore, it can be said that backscattering profiles, and consequently GL parameters and the optical coefficients, were dependent on the laser wavelengths and the state of the skin. In previous

research (Lorente et al., 2013b), only the GL statistical model was used; however, the GL parameters presented different statistical significances and trends between sound and decaying oranges from those reported in the present work. This could be due to certain differences between both studies that could influence on the measured data, such as the orange cultivar and the pre-processing of backscattering profiles. In any case, in both research studies, for each laser wavelength, some of the associated GL parameters showed significant differences between both fruit states, this being an important indicator of potential success in the further separation of the tissue into sound and decaying by an automated system. However, the comparison of the results from GL model and physical model performed in this work was more interesting, since more causal effects could be extracted compared to exclusively statistical approach.

5.3.2. Classifier performance evaluation

Figure 5.5 shows the evolution of the overall accuracy of the LDA classifier as a function of the number of ranked features for each feature selection method using the GL model and Farrell's model labelled sets. It is observed that all feature selection methods showed similar performance. However, two similar maximum overall accuracies of 93.38% and 93.39% were obtained for the GL model. The maximum value of 93.38% was achieved using the first three features ranked with the MRMRd and MRMRq methods (GL feature selection I). Similarly, the maximum value of 93.39% was obtained using the first seven features provided by the CA, FDA, TT and WL methods (GL feature selection II). For the Farrell's model labelled set, the overall accuracy reached a maximum value of 92.42% using the first eight features ranked with the MI, BD and KLD feature selection methods. It is noticeable that several selection methods gave exactly the same results due to the fact that the selected features coincided for those methods.

For further discussion, Table 5.3 shows the selected features leading to the best classification performance for both labelled sets, as well as the classification results for these feature selections, including overall accuracies, Cohen's kappa values and the associated mean confusion matrices. In accordance with the scale proposed by Landis and Kock (1977), Cohen's kappa values can be interpreted as follows: 0.00-0.20 values indicated slight classification performance, 0.20-0.40 fair performance, 0.40-0.60 moderate performance, 0.60-0.80 good performance and 0.80-1.00 very good performance.

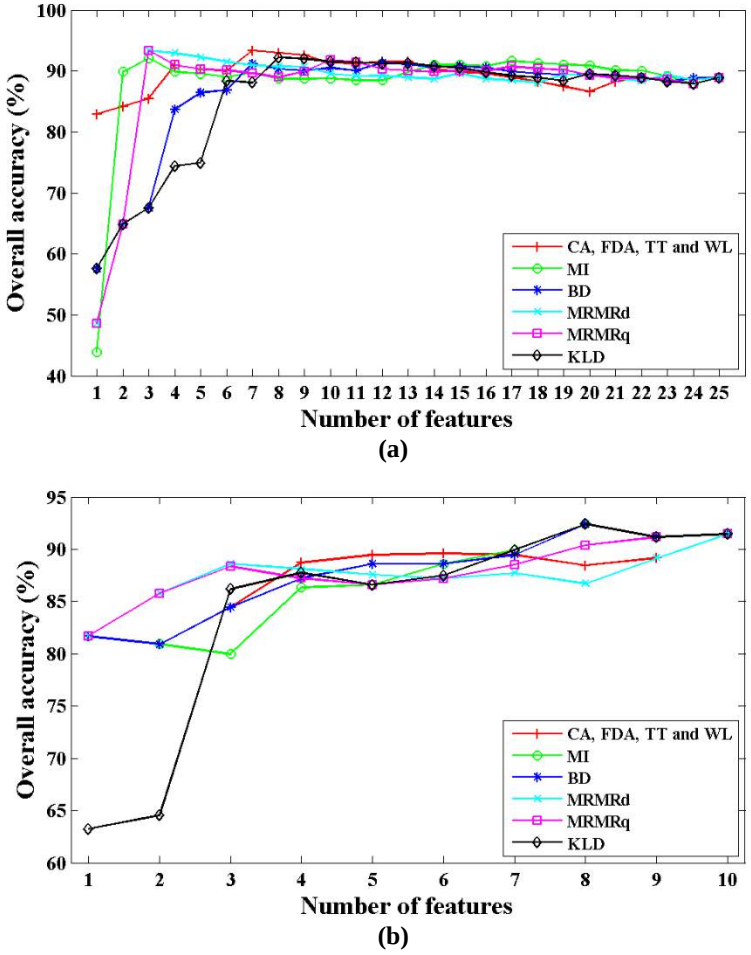

Figure 5.5. Evolution of the classifier overall accuracy with the number of ranked features for each selection method using the GL model (a) and Farrell's model (b) labelled sets.

Table 5.3. Selected features and the corresponding classification results for the labelled sets from the GL model and Farrell's model.

	Gauss-Lorentzian cross product distribution model		Farrell's diffusion theory model
	GL feature selection I	GL feature selection II	
Selection methods	MRMRd, MRMRq	CA, FDA, TT, WL	MI, BD, KLD
Selected features	d at 532 nm a at 785 nm d at 830 nm	d at 532 nm a at 660 nm d at 660 nm a at 785 nm c at 785 nm a at 830 nm c at 830 nm	μ_a at 660 nm μ_s' at 660 nm μ_a at 785 nm μ_s' at 785 nm μ_a at 830 nm μ_s' at 830 nm μ_a at 1060 nm μ_s' at 1060 nm
Overall accuracy (%)	93.38	93.39	92.43
Cohen's kappa	0.868	0.869	0.849
Mean confusion matrix			

	Sound (%)	Decay (%)
Sound	95.33	8.58
Decay	4.67	91.42

	Sound (%)	Decay (%)
Sound	92.53	5.75
Decay	7.47	94.25

	Sound (%)	Decay (%)
Sound	90.60	5.75
Decay	9.40	94.25

When comparing the two sets of selected features for the GL model, it can be noticed that parameters b and e were not selected in any of the selections. This suggests that parameters a, c and d were more valuable for discriminating between sound and decaying orange skin than parameters b and e. Furthermore, all the features in these two selections presented statistically significant differences between samples of sound and decaying skin, as shown in Table 5.2. For Farrell's model, the resulting set of selected features included the absorption and reduced scattering coefficients at four laser wavelengths, the optical coefficients at 532 nm remaining outside the feature selection. In addition, the two optical coefficients at 532 nm did not present significant differences between the two kinds of samples (Table 5.2), which could be related to

their little impact on the detection of decay in oranges, as well as to the inappropriateness to apply Farrell's model when μ_s' did not exceed μ_a.

Comparison of the classification results using the two feature selections for the GL model shows that, even though the overall accuracies and Cohen's kappa values for both selections were almost identical, the corresponding mean confusion matrices were slightly different. It can be observed that the number of well-classified sound samples for GL feature selection I (95.33%) was higher than that obtained for GL feature selection II (92.53%). In contrast, the classification of decaying samples was improved when using GL feature selection II, with the success rate increasing from 91.42% to 94.25%. In practice, this increase in the number of well-classified decaying samples is of major importance for a potential inspection system, since just a few infected fruits can spread the infection to a whole batch, thus causing great economic losses. A general conclusion drawn from analysing the results is that GL feature selection II generally provided better results than GL feature selection I for the decay detection problem, with only four more features being included in the classification model. With regard to the classification results using the selected features for Farrell's model, it can be observed from the mean confusion matrix that the classification results were quite similar to those obtained using GL feature selection II. Nevertheless, the number of well-classified sound samples for GL feature selection II (92.53%) was higher than that obtained using the feature selection for Farrell's model (90.60%).

In the light of these results, this work lays the foundation for the future implementation of an automatic system based on LLBI capable of detecting decay in early stages, which is very important from the agricultural point of view. However, further research on backscattering imaging in other cultivars of citrus fruits is still required before commercial application. Some issues should be taken into account for future setting-up on a commercial fruit sorter. For example, line lasers should be applied on rotating fruit in order to explore the whole surface of each fruit. In addition, imaging systems must be capable of taking images at several wavelengths simultaneously and at a fast speed.

5.4. Conclusions

This research article reports new progress in the automation of the detection of early decay symptoms caused by *P. digitatum* fungus in citrus fruit by means of the LLBI technique. Backscattering images of oranges at five laser wavelengths in the visible and NIR range were used for this detection. Farrell's diffusion theory model and the GL distribution function described

backscattering profiles accurately at the five laser wavelengths using the absorption and reduced scattering coefficients and five fitting parameters, respectively. However, the GL model had slightly better curve-fitting results, with average R^2 values higher than or equal to 0.996, compared with values higher than or equal to 0.982 obtained with Farrell's model. Overall, the GL parameters and the optical coefficients differed between sound and decaying orange skin at all wavelengths.

The comparison of the results from GL model and physical model allowed to extract more causal effects compared to exclusively statistical approach, pointing to changes in the structural fruit properties due to decay. The results showed the feasibility of wavelengths in the visible and NIR ranges when applying GL model, while the Farrell's approach was most successful when addressing passbands in the NIR range. Particularly, laser at 532 nm provided difficulties for the physical approach. Although curve-fitting results showed high R^2 values, the high variance found for μ_a and μ_s' at 532 nm and the results of the feature selection pointed to the limitations of Farrell's model in the case of high absorption coefficient due to high carotenoids absorbance in oranges.

The classification results using the eight selected optical coefficients for Farrell's model were quite similar to those obtained using the GL selection with seven features, with a similar percentage of well-classified decaying samples of 94.2% and the classification of sound samples being better for the GL selection, increasing from 90.6% to 92.5%. In conclusion, the optimal sets of features for the GL and Farrell's models resulted in good classification results, with a percentage of well-classified samples above 90% for both classes despite the similarity between sound and decaying orange skin. The next step will be the development of a prototype for in-line real-world tests.

Acknowledgements

This work has been partially funded by INIA through research project RTA2012-00062-C04-01 with the support of European FEDER funds. Delia Lorente thanks INIA for the support through grant FPI-INIA number 42.

Part IV

Spectroscopy

Chapter 6

Visible-NIR reflectance spectroscopy and manifold learning methods applied to the detection of fungal infections on citrus fruit

D. Lorente[1], P. Escandell-Montero[2], S. Cubero[1], J. Gómez-Sanchis[2], J. Blasco[1]

[1]Centro de Agroingeniería, Instituto Valenciano de Investigaciones Agrarias (IVIA), Cra. Moncada-Náquera km 5, 46113 Moncada (Valencia), Spain.

[2]Intelligent Data Analysis Laboratory (IDAL), Electronic Engineering Department, Universitat de València, Avda. Universitat s/n, 46100 Burjassot (Valencia), Spain.

Submitted to: Journal of Food Engineering.

Abstract

The development of systems for automatically detecting decay in citrus fruit during quality control is still a challenge for the citrus industry. The feasibility of reflectance spectroscopy in the visible

and near infrared (NIR) regions was evaluated for the automatic detection of the early symptoms of decay caused by *Penicillium digitatum* fungus in citrus fruit. Reflectance spectra of sound and decaying surface parts of mandarins cv. 'Clemenvilla' were acquired in two different spectral regions, from 650 nm to 1050 nm (visible-NIR) and from 1000 nm to 1700 nm (NIR), pointing to significant differences in spectra between sound and decaying skin for both spectral ranges. Three different manifold learning methods (principal component analysis, factor analysis and Sammon mapping) were investigated to transform the high-dimensional spectral data into meaningful representations of reduced dimensionality containing the essential information, this step being of particular interest in spectroscopy research in order to achieve better performance predictions of fruit quality. The low-dimensional data representations were used as input feature vectors to discriminate between sound and decaying skin using a supervised classifier based on linear discriminant analysis. The best classification results were achieved by employing factor analysis on the NIR spectra, yielding a maximum overall classification accuracy of 97.8%, with a percentage of well-classified sound and decaying samples of 100% and 94.4%, respectively. These results lay the foundation for the future implementation of reflectance spectroscopy technology on a commercial fruit sorter for the purpose of detecting decay in citrus fruit.

Keywords: Manifold learning methods; Dimensionality reduction; LDA classifier; Citrus fruit; Decay detection; Visible-NIR reflectance spectroscopy.

6.1. Introduction

Citrus production is one of the most important agricultural activities in the world, in economic terms. However, the presence of postharvest decay due to *Penicillium* spp. fungi is among the main problems affecting citrus production (Palou et al., 2011). Early detection of fungal infections and removal of infected fruit are issues of major concern in commercial packinghouses because a small number of infected fruits can rapidly spread the fungal infection over all the production. Detection of infected fruit has traditionally been carried out manually using ultraviolet (UV) light, which induces visible fluorescence of fungal products (Kondo et al., 2009). This method, however, is potentially harmful for the workers, since long exposure to UV illumination can cause damage to human skin, such as cancer or premature aging (Lopes et al., 2010). Various technologies are being investigated for the automatic detection of decay in citrus fruit as alternatives to human inspection, including vision systems based on UV-induced fluorescence (Kurita et al., 2009), hyperspectral and multispectral vision systems (Gómez-Sanchis et al., 2012, 2013; Lorente et al., 2013c) and laser-light backscattering imaging systems (Lorente et al., 2013b).

In this sense, spectroscopy also appears to be a promising alternative for decay detection in citrus fruit since this technology can rapidly measure the optical properties of the samples, which are related to their chemical and physical properties (Khanmohammadi et al., 2014). When light interacts with a fruit, a small portion is reflected on the surface of the sample (specular or Fresnel reflectance) and the rest penetrates into the tissue (Birth, 1976). Most of the entering light interacts with the internal components of the fruit, and then it is scattered backwards to the exterior tissue surface (diffuse reflectance), thus carrying information related to the morphology and structures of the tissue in addition to its chemical composition. The rest of the entering radiation is absorbed by tissue or transmitted out from the fruit in different directions (Meinke and Friebel, 2009). Therefore, reflectance measurements acquired using visible-NIR spectroscopy systems can be useful for measuring the textural and chemical properties of fruit (Sánchez et al., 2012) Accordingly, many studies have been reported that assess the quality of different fresh fruit by visible-NIR spectroscopy systems in reflectance mode (Fu et al., 2007; Jha et al., 2014; Wang et al., 2014; Wang and Xie, 2014). Most of the research studies using this technology on citrus fruit have been focused on evaluating the internal quality attributes, such as soluble solids content (SSC), pH or vitamin C content (Gómez et al., 2006; Xia et al., 2007; Cayuela, 2008; Antonucci et al., 2011; Kohno et al., 2011). However, very limited research work has been conducted to assess the external quality of citrus fruit, such as the presence of surface damages or diseases, by means of reflectance spectroscopy in the visible and NIR ranges (Gaffney, 1973; Blasco et al., 2000; Zheng et al., 2010).

One of the main problems of multispectral systems is the large volume of data. Hence, it is necessary to extract essential information about quality attributes contained in the spectra using techniques for reducing the dimensionality of the data (Garrido-Novell et al., 2012), since the presence of irrelevant spectral variables could lead to lower performance predictions of fruit quality. Generally, dimensionality of the spectral feature space can be reduced by using either feature selection or feature extraction. Feature selection approaches try to find a subset of the original variables that contains the least number of variables with the most significant information. On the other hand, feature extraction techniques –commonly referred to as manifold learning techniques– transform the data in the high-dimensional space into a lower-dimensional space that preserves the observed properties of the data, generally known as a manifold. Particularly, some popular manifold learning techniques, such as principal component analysis (PCA), have been widely used for data reduction in spectroscopy research focused on fruit quality inspection (Xie et al., 2009; Liu et al., 2010a).

The present research work emerged from the need for a more thorough evaluation of the potential of reflectance spectroscopy in the visible and NIR regions as a tool for automatically detecting

decay lesions caused by *P. digitatum* fungus in citrus fruit during quality control. For this purpose, two spectrophotometers operating in different spectral ranges within the visible and NIR regions were used to acquire reflectance spectra of citrus fruit. Some spectral pre-processing techniques were then applied to the spectra in order to remove any irrelevant information. In order to achieve better decay detection results, several manifold learning methods were investigated to transform the high-dimensional spectral data into meaningful representations of reduced dimensionality, this step being of particular interest in spectroscopy research. Prior to dimensionality reduction, different methods were employed to estimate the target dimensionality of the corresponding lower-dimensional data representations. The ultimate aim of this research work was to evaluate and compare the reflectance measurements acquired in the two different spectral ranges, the pre-processing techniques, the dimensionality estimators and the dimensionality reduction methods in terms of their performance in the classification of citrus fruit skin into sound or decaying at an early stage.

6.2. Material and methods

6.2.1. Fruit and fungal inoculation

Mandarins cv. 'Clemenvilla' (*Citrus reticulata* Hort. ex Tanaka) were selected for the experiments due to their great economic impact in the Spanish agro-food industry. These fruits were collected during the 2012 harvest season from the field collection of the Citrus Germplasm Bank at the IVIA (Spain) (Navarro et al., 2002) before any commercial postharvest treatments were applied. For the experiments, a total of 117 mandarins were used: 67 fruits were superficially punctured on the rind and inoculated with spores of *P. digitatum* fungus and the other 50 were injured in the same way but treated with sterilised water for control purposes. The *P. digitatum* strain NAV-7, from the fungal culture collection of the IVIA CTP, was cultured on potato dextrose agar (PDA; Sigma-Aldrich Chemical Co., St. Louis, MA, USA) plates in the dark at 25 °C. Conidia from 7 to 14-day-old cultures were taken from the agar surface with a sterile glass rod and transferred to a sterile aqueous solution of 0.05% Tween® 80 (Panreac, S.A.U., Spain). The conidial suspension was filtered through two layers of cheesecloth to separate hyphal fragments and then adjusted to a concentration of 10^6 spores/ml using a haemocytometer, which is commonly used to produce infestation in laboratory conditions (Palou et al., 2001). The mandarins were inoculated in the equatorial zone with 20 μl of the spore suspension by immersing the tip of a stainless steel rod, 1 mm wide and 2 mm deep, into the suspension and inserting it in the fruit rind afterwards. After

inoculation, the fruits were kept in a controlled environment at 24 °C and relative humidity of 24% for a period of time that was long enough for decay lesions with diameters equal to or higher than 10 mm to appear on all the infected fruits. This period was different for each fruit, since the development of the decay varied from one fruit to another, the first patches of decay thus appearing on some mandarins after three days' storage and the latest after six days. All the inoculated mandarins presented decay lesions in the early stages of infection (before sporulation) with a variable diameter ranging from 10 mm to 40 mm. Images of a sound mandarin and a mandarin showing decay lesions are shown in Figure 6.1.

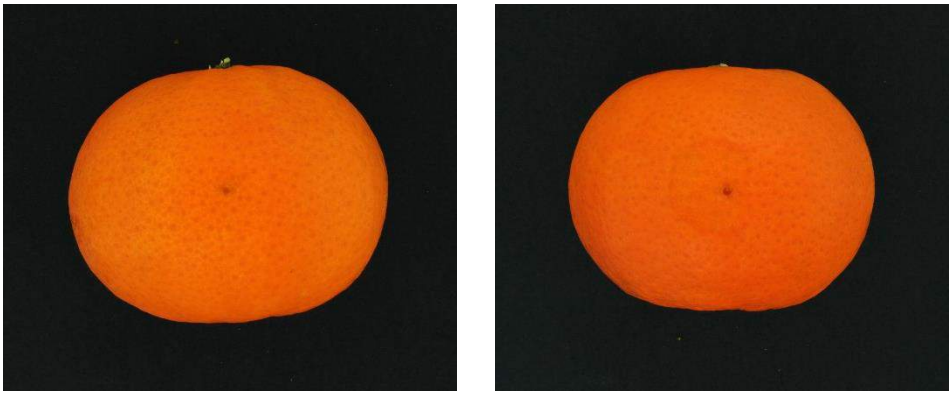

(a) **(b)**

Figure 6.1. A sound mandarin (a) and a mandarin presenting decay lesions caused by P. digitatum (b).

The control fruits inoculated with just water were used to evaluate how the physical changes produced in the rind by the inoculation procedure influenced the spectral measurements. To this end, two different parts of the surface of each of the 50 control mandarins were analysed: one close to the inoculation puncture and the other on the opposite side of the mandarin, where there was no hole. The spectral measurements of both kinds of sound skin samples were expected to be similar in order to confirm that the inoculation process did not affect the measurements. In addition, spectra were also acquired for the surface part presenting decay lesions of the 67 infected mandarins. Therefore, a total of 167 skin samples were analysed in this work: 100 sound skin samples (50 samples of sound skin close to the inoculation hole and 50 samples of sound skin further away from the hole) and 67 decaying skin samples.

6.2.2. Spectroscopy system

In this research, a system based on two spectrophotometers used alternately (Figure 6.2) was employed to acquire spectra in reflectance mode. The system consisted mainly of a multichannel spectrophotometer platform (AvaSpec-USB2-DT, Avantes, Inc.) on which two spectrophotometers were mounted, a stabilised halogen light source (AvaLight-HAL-S, Avantes, Inc.), a Y-shaped fibre-optic reflectance probe (FCR-7IR200-2-45-ME, Avantes, Inc.), a holder for positioning the sample properly over the probe, and a personal computer equipped with commercial software (AvaSoft version 7.2, Avantes, Inc.) for controlling both spectrophotometers and acquiring the spectra.

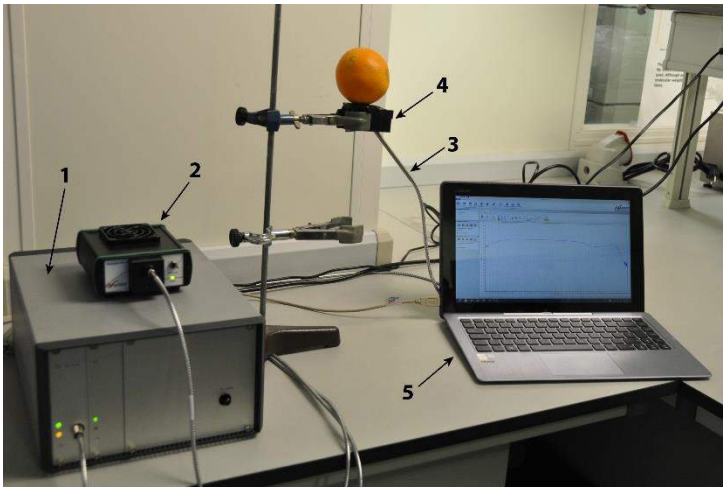

Figure 6.2. Picture of the spectroscopy system. 1: Spectrophotometer platform with two spectrophotometers; 2: Light source; 3: Reflectance probe; 4: Sample holder; 5: Computer with acquisition software.

The first spectrophotometer (AvaSpec-ULS2048-USB2, Avantes, Inc.) included a 2048 pixel charge-coupled device (CCD) detector, a 50 µm entrance slit and a 600 lines/mm diffraction grating covering the visible-NIR range from 600 nm to 1100 nm with a spectral sampling interval of 0.255 nm. The second spectrophotometer (AvaSpec-NIR256-1.7, Avantes, Inc.) was equipped with a 256 pixel non-cooled indium-gallium-arsenide (InGaAs) detector, a 100 µm entrance slit and a 300 lines/mm diffraction grating covering the NIR range of 900 nm to 1750 nm with a sampling interval of 3.535 nm. Both spectrophotometers were connected to the computer through

a single USB cable. The light source emitted light from a 10 W tungsten halogen lamp that provided good spectral efficiency in the visible and NIR regions. In order to stabilise the light emitted by the lamp, the light source was turned on 15 minutes before each measurement session. The reflection probe, consisting of seven fibres with a diameter of 200 µm, delivered the light to the sample through a bundle of six fibres and collected the reflectance from the sample, which was carried by a single fibre to the spectrophotometer in use. The probe tip was designed to provide reflectance measurements at an angle of 45º so as to minimise specular reflectance.

The integration time was adjusted for each spectrophotometer using a 99% reflective white reference, so that the maximum reflectance value over the wavelength range was around 90% of saturation. Thus, the integration times were set to 90 ms and 700 ms for the visible-NIR spectrophotometer and the NIR spectrophotometer, respectively. For both spectrophotometers, each spectrum was obtained as the average of five scans to reduce the thermal noise of the detector (Nicolaï et al., 2007). The average reflectance measurements of each sample (S) were then converted into relative reflectance values (R) with respect to the white reference (the so-called raw spectra in this work) using dark reflectance values (D) and the reflectance values of the white reference (W), as shown in Equation 6.1:

$$R = \frac{S - D}{W - D} \tag{6.1}$$

The dark spectrum and the spectrum of the white reference were recorded with each spectrophotometer prior to the acquisition of spectra of each batch of samples. The white reference spectrum was acquired at the same integration time as the spectrum of the corresponding sample. The dark spectrum was obtained by turning off the light source and completely covering the tip of the reflectance probe at the same integration time. Due to the high level of noise on the edges of the spectra, further analysis was performed only on data in the 650 nm to 1050 nm range for the visible-NIR measurements, and in the 1000 nm to 1700 nm range for the NIR spectra. Therefore, since each visible-NIR spectrum had a spectral sampling interval of 0.255 nm, each raw spectrum was composed of 1570 spectral data points. Similarly, each raw spectrum obtained using the NIR spectrophotometer consisted of 198 data points. These raw spectra were acquired by placing each fruit manually on the sample holder so that the part of the fruit under study was facing the tip of the reflectance probe. In this work, two raw spectra (visible-NIR and NIR) were recorded for each of the 167 skin samples, a total of 334 spectra thus being acquired.

6.2.3. Spectral pre-processing

Different physical characteristics of the fruits, such as the size or the shape of the particles, affect light reflectance (scattering). These variations between samples can be observed as additive (baseline shift) and multiplicative effects (tilt) in the spectra. These effects create noise problems when analysing fruit quality parameters for which such physical information is irrelevant. Several pre-processing techniques are aimed at removing physical phenomena in the spectra in order to improve the subsequent quality prediction step using a regression or classification model (Candolfi et al., 1999).

Two of the most commonly used scatter-correction techniques in spectroscopy are multiplicative scatter correction (MSC; Geladi et al., 1985) and standard normal variate (SNV; Barnes et al., 1989). MSC aims to reduce the scattering effects by fitting each spectrum of a group of samples to a reference spectrum, which usually corresponds to the mean spectrum of the data set. Each spectrum is fitted by linear least squares regression. This technique depends on the data set. Therefore, if the raw data set is modified, the reference spectrum is certain to change, thus making it necessary to perform the pre-processing on the spectra again. On the other hand, SNV corrects each spectrum individually by subtracting the mean of the spectrum and dividing by the standard deviation of the spectrum. Thus, SNV normalises each individual spectrum to zero mean and unit standard deviation. Figure 6.3 shows a set of raw spectra and the corresponding spectra pre-processed with MSC and SNV as an illustrative example of how these scatter-correction methods work. More particularly, the NIR spectra of all mandarin skin samples involved in this research are shown. Values related to relative reflectance were expressed in arbitrary units (a.u.).

In this work, the raw spectra acquired with both spectrophotometers were pre-processed using MSC and SNV to reduce spectral variability. In addition, due to the underlying nature of most of the techniques used in this work, such as PCA, the raw spectra and the corresponding spectra pre-processed with MSC and SNV were mean centred by subtracting the mean spectrum of each data set from each spectrum. However, the normalisation scaling of data according to the standard deviation (standardisation), commonly used in techniques dependent on the relative scale of the variables such as PCA, was not required in this work. This was due to the fact that the spectral data were measured in the same units and had similar ranges. The pre-processing techniques and the remaining algorithms in the present work were implemented using Matlab 8.1 (Mathworks, Inc., USA).

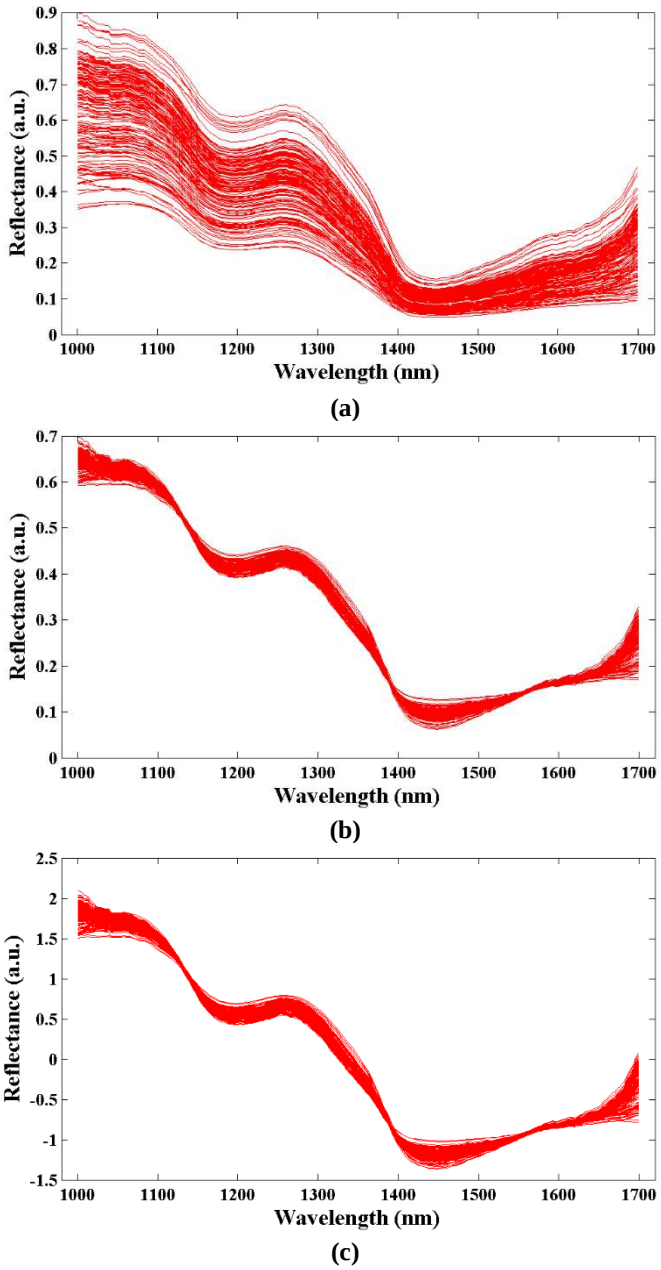

Figure 6.3. Representative raw spectra (a) and the corresponding spectra pre-processed with MSC (b) and SNV (c).

6.2.4. Dimensionality reduction

The spectral features (variables) from the pre-processed spectra could be employed directly as inputs of classification algorithms in order to discriminate between sound and decaying skin. Nevertheless, most of the spectral features from these high-dimensional spectra are irrelevant or redundant for the classification task, leading to the overfitting problem and consequently decreasing the performance of the classifier (Tian, 2010). To overcome these problems, manifold learning methods can be used to reduce the dimensionality of the spectral feature space. These techniques transform the data in the high-dimensional space into a lower-dimensional space that preserves the observed properties of the data, generally known as a manifold, and their goal is to recover the low-dimensional manifold embedded within the high-dimensional space. The manifold should have a dimensionality corresponding to the intrinsic dimensionality of the data, defined as the minimum number of parameters needed to describe all the information in the data. The estimation of the intrinsic dimensionality of data is a key step in the process of dimensionality reduction, since manifold learning methods need the intrinsic dimensionality as an external and user-defined parameter (Lee and Verleysen, 2007).

In this work, three popular unsupervised manifold learning methods were investigated for dimensionality reduction: principal component analysis (PCA; Jolliffe, 2002), factor analysis (FA; Lawley and Maxwell, 1971) and Sammon mapping (Sammon, 1969). The data transformation is linear in PCA and FA, while Sammon mapping is a non-linear method, thus being capable of handling more complex data with non-linear relationships. On the other hand, unlike PCA and FA, the Sammon method is unable to generalise the mapping to new data without performing the dimensionality reduction again due to its non-parametric nature. These three methods based on simple models were chosen due to their suitability for the available data sets, following the guidelines given by Lee and Verleysen (2007). If the data set is small, the use of more complex dimensionality reduction methods is questionable, since the limited number of samples could be insufficient to identify the large number of parameters involved in these complex methods. Furthermore, for data with very high dimensionality, more complex methods can become confused due to the curse of dimensionality and, consequently, provide meaningless results. Therefore, methods with the simplest models are more suitable for small data sets with high dimensionality, such as those used in this work. With regard to intrinsic dimensionality estimation, four different approaches were employed in this work: eigenvalue-based estimator (EB; Fukunaga and Olsen, 1971), maximum likelihood estimator (ML; Levina and Bickel, 2005), correlation dimension estimator (CD; Camastra and Vinciarelli, 2002) and geodesic minimum spanning tree estimator (GMST; Costa and Hero, 2004).

All the techniques for dimensionality reduction and intrinsic dimensionality estimation were implemented using the Matlab Toolbox for Dimensionality Reduction (version 0.8.1; van der Maaten, et al., 2009). In the case of the intrinsic dimensionality estimation methods, their implementations in the toolbox are parameterless. For the implementations of dimensionality reduction, only the intrinsic dimensionality needs to be specified by the user as an external parameter. The free parameters related to the iterative nature of FA and Sammon mapping, such as the maximum number of iterations and the convergence constant, are already optimally fixed by default and embedded in the toolbox implementations, thus not requiring further user-defined parameters.

6.2.5. Data sets

Supervised classification requires the use of a set of n labelled samples, $\{\mathbf{x}_i, t_i\}_{i=1..n}$, where $\mathbf{x}_i$ is the *m*-dimensional feature vector for the *i*-th sample with label t_i. Due to the supervised nature of the problem presented in this research, six labelled data sets with different feature vectors had to be constructed. Particularly, the spectral features were obtained from the raw spectra and the spectra pre-processed with MSC and SNV associated with each of the two spectrophotometers, all the spectra also being mean centred. The three labelled sets based on the visible-NIR spectra consisted of $m = 1570$ spectral features associated with each sample of mandarin skin, while the three labelled sets corresponding to the NIR spectra were composed of $m = 198$ spectral features. For all the labelled data sets, the $n = 167$ samples of mandarin skin were assigned to one of the two classes considered in this work: sound and decaying skin. Each sample pattern was therefore composed of 1570 features and a class label for the data sets from the visible-NIR spectra, and 198 features and a class label for the data sets from the NIR spectra.

6.2.6. Development and validation of the classification models

In this work, four different unsupervised techniques were used to estimate the intrinsic dimensionality of the six different data sets, associated with the visible-NIR and the NIR spectra pre-processed with different scatter-correction methods. Each of the three unsupervised methods for dimensionality reduction were then applied on the data sets using the different intrinsic dimensionality estimations as target dimensionalities of the corresponding lower-dimensional data representations. Subsequently, the low-dimensional data representations were used as input feature vectors to classify samples of mandarin skin into sound and decaying using a supervised classifier based on linear discriminant analysis (LDA; Fisher, 1936). Tests were aimed at

evaluating and comparing the spectral ranges (visible-NIR and NIR), the scatter-correction methods (no pre-processing, MSC and SNV), the intrinsic dimensionality estimators (EB, ML, CD and GMST) and the dimensionality reduction techniques (PCA, FA and Sammon mapping) in terms of their classification performance. In particular, the main interest of this work lies in finding out which combination of spectral range, pre-processing technique, estimator of intrinsic dimensionality and dimensionality reduction method provided the best classification performance for decay detection in citrus fruit.

A cross-validation procedure was used to evaluate and compare the performance of the classification models. In particular, the experiments were performed with five-fold cross-validation, consisting in dividing the data randomly into five folds (subsets) of equal size, and using four folds as the calibration set to build the classification models and the remaining one as the validation set to assess classifier performance (Hastie et al., 2009). This process was repeated five times leaving one different fold each time. Thus, all samples were used for both calibration and validation. Furthermore, the folds were stratified so that they had approximately the same class proportions as the original labelled sets (Kohavi, 1995). The whole five-fold cross-validation process was repeated 100 times in order to reduce variability due to random partitioning and obtain reliable performance estimations. Therefore, a total of 500 iterations of calibration and validation were performed for each classification model. The validation results were then averaged over all the iterations, thereby obtaining a mean confusion matrix created by computing the element-wise mean of the individual confusion matrices for each iteration.

For the purpose of evaluating the classification performance, overall accuracy (Fleiss, 1981) and the value of Cohen's kappa statistic (Sim and Wright, 2005) were computed for each classification model from its associated mean confusion matrix. The overall accuracy of classification was calculated as the number of correctly classified samples divided by the total number of samples, ranging from 0% to 100%. Unlike the overall accuracy, Cohen's kappa statistic took into account whether the classifier was biased towards one of the two classes when measuring classifier performance. Perfect classifier performance resulting in completely unbiased classification corresponds to a kappa value of 1, whereas a random guess classification involves a kappa value of 0. A kappa value much lower than the overall accuracy means that the overall accuracy is inflated due to the classification bias.

6.3. Results and discussion

6.3.1. Analysis of spectra

Before going ahead with the dimensionality reduction and classification tasks on the spectra, the effect of the inoculation procedure on the spectral measurements was evaluated. For this purpose, the raw spectra of the two kinds of sound skin samples (sound skin close to the hole caused by the inoculation and sound skin further away from the hole) were tested to see if they were similar. Figure 6.4 shows the mean spectra of both kinds of sound skin samples for the visible-NIR and the NIR spectral ranges. The mean spectra were calculated by averaging each spectral variable obtained from the visible-NIR and the NIR raw spectra corresponding to all the samples for each kind of sound skin. A significance test (p-value < 0.05 , two-tailed unpaired t-test) was applied to the raw spectra acquired with both spectrophotometers in order to determine whether the mean spectra of the two types of sound skin did not present statistically significant differences. According to the results of the significance test, the differences between the mean spectra of both kinds of sound skin samples were not statistically significant for any of the 1570 spectral variables in the visible-NIR range. For the spectra in the NIR range, the mean spectra of the two types of sound skin presented statistically significant differences for only 6 out of 198 (3.0%) spectral variables, ranging from 1364 nm to 1382 nm, thereby resulting in a great majority of 192 of the 198 (97.0%) spectral variables without significant differences. Therefore, since the majority of the mean values of the spectral variables did not present any significant differences between the two kinds of sound skin, the subsequent experiments in this work considered the spectra of sound skin close to the inoculation hole and sound skin further away for both spectral ranges as belonging to the same kind of skin samples (the so-called sound class).

The same significance test was applied to the raw spectra acquired in the two spectral ranges in order to examine whether the raw spectra of decaying skin samples and samples of sound skin, grouping together the two kinds of sound skin, had significantly different means for all the spectral variables. The mean spectra of sound and decaying skin samples for the visible-NIR and the NIR spectral ranges are shown in Figure 6.5. In accordance with the results concerning statistical significance, the mean spectra of sound and decaying skin samples presented statistically significant differences for all spectral variables in the visible-NIR and the NIR ranges. Mean spectra were significantly lower for the decaying samples, which may be explained by the lower amount of scattering in the fruit tissue due to the weakening of the cell walls during the decaying process (Barmore and Brown, 1979). From these spectral differences between the two states of

mandarin skin (sound and decaying), it can be said that the spectra acquired in both spectral ranges were dependent on the state of the skin. Therefore, the spectral measurements could be potentially useful for decay detection in subsequent classification tasks.

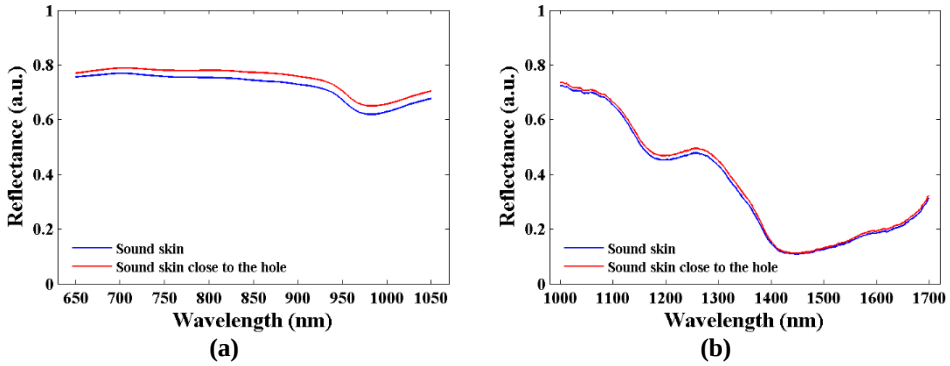

Figure 6.4. Mean spectra of the two kinds of sound skin samples obtained from the visible-NIR (a) and NIR (b) raw spectra.

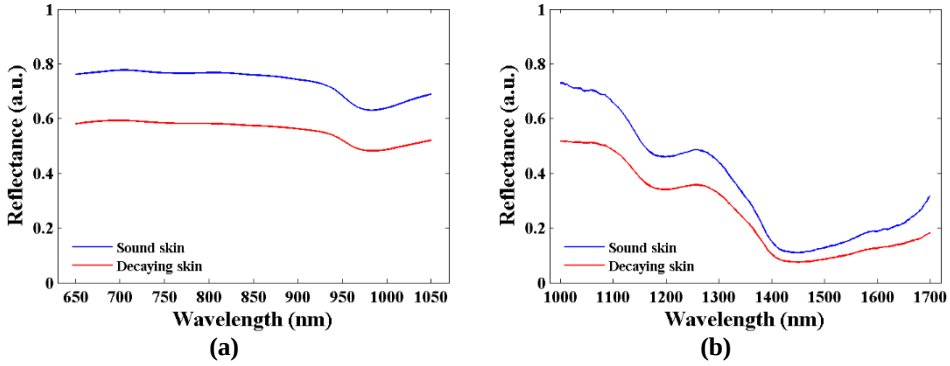

Figure 6.5. Mean spectra of sound and decaying skin samples obtained from the visible-NIR (a) and NIR (b) raw spectra.

6.3.2. Classifier performance evaluation

Table 6.1 shows the overall accuracies of the LDA classifier for the visible-NIR and the NIR spectra after applying the different scatter-correction techniques and the dimensionality reduction methods, using the different intrinsic dimensionality estimations as target dimensionalities of the

lower-dimensional data representations. It can be observed that the scatter-correction methods had an influence on classifier performance. In general, the spectra without scatter-correction led to better classification results than the spectra that were pre-processed with MSC and SNV for both spectral ranges. This could be due to the fact that the scatter-correction techniques are aimed at removing the variations in spectra due to the structural and physical characteristics of the fruit tissue, while retaining the absorption properties related to the chemical components in the spectra. Therefore, the results obtained suggested that the process of decay in citrus fruit may be more characterised by structural changes in fruit tissue, such as the weakening of the cell walls due to changes in enzymatic activity (Barmore and Brown, 1979) and the subsequent water soaking of the tissue (Barmore and Brown, 1981), rather than changes in chemical composition. In consequence, MSC and SNV probably removed important information for decay detection from the spectral measurements.

With regard to the intrinsic dimensionality estimations, results revealed that EB and CD estimated lower intrinsic dimensionalities than ML and GMST, thus leading to poorer classifier performances. Overall, the classification accuracies using the intrinsic dimensionalities obtained by ML and GMST were quite similar. Nevertheless, classification results for ML were clearly better than for GMST in a few cases, such as when using the uncorrected spectra and the spectra pre-processed with MSC in the visible-NIR range. Furthermore, when using the same number of target dimensions, Sammon mapping led to different overall accuracies. This was due to the random initialisation of this technique, thus giving rise to different classification results for several runs. Similarly, it is noticeable that FA sometimes resulted in slightly different overall accuracies for a similar number of dimensions, also due to its random initialisation. In contrast, PCA gave exactly the same results when using the same target dimensionalities.

When comparing classifier performance for the three dimensionality reduction techniques on the visible-NIR spectra, it can be noticed that PCA and FA outperformed Sammon mapping for most of the cases. These results agree with van der Maaten et al. (2009) in that non-linear dimensionality reduction techniques were often incapable of outperforming traditional linear methods on real-world data despite their ability to handle more complex data with non-linear relationships. For the spectra in the visible-NIR range, the maximum overall accuracy of 95.1% was obtained by employing PCA on the uncorrected spectra, using the intrinsic dimensionality estimation provided by ML. However, this classification result was almost identical to the overall accuracy of 95.1% obtained with FA on the same spectra using the same dimensionality estimation. With respect to the comparison of the performance for dimensionality reduction methods on the NIR spectra, the three methods yielded similar classification results. Nevertheless, the maximum classification accuracy of 97.8% was obtained by employing FA on the uncorrected spectra, using the intrinsic

dimensionality estimation provided by ML or GMST. This result was closely followed by the overall accuracy of 97.7% obtained with PCA using the uncorrected spectra and the same dimensionality estimation.

Table 6.1. Overall classifier accuracies for the visible-NIR and NIR spectra using the different scatter-correction methods, intrinsic dimensionality estimators and dimensionality reduction techniques.

		Visible-NIR spectra				NIR spectra			
		Intrinsic dimension	PCA (%)	FA (%)	Sammon (%)	Intrinsic dimension	PCA (%)	FA (%)	Sammon (%)
No pre-processing	EB	1	89.68	89.70	88.89	1	92.47	92.51	92.87
	ML	3	95.07	95.05	88.68	3	97.69	97.76	96.63
	CD	1	89.68	89.70	89.66	2	94.90	96.72	95.20
	GMST	2	89.16	89.07	88.61	3	97.69	97.76	97.59
MSC	EB	3	56.90	54.46	59.69	2	88.56	89.01	89.07
	ML	15	73.12	83.44	69.05	3	93.92	92.61	94.42
	CD	1	62.01	61.90	52.67	2	88.56	89.01	89.06
	GMST	11	70.27	80.80	62.84	3	93.92	94.26	93.72
SNV	EB	4	75.93	72.47	61.13	2	88.56	88.96	89.05
	ML	14	78.02	84.84	71.29	3	93.95	94.04	93.44
	CD	2	59.09	57.26	61.10	2	88.56	88.96	89.05
	GMST	12	79.41	83.17	71.50	3	93.95	94.04	94.32

For further discussion, Table 6.2 shows the combinations of pre-processing technique, estimator of intrinsic dimensionality and dimensionality reduction method leading to the best classification performance for the visible-NIR and the NIR spectra, as well as the classification results using these winning combinations of methods, including overall accuracies, Cohen's kappa values and the associated mean confusion matrices. In accordance with the scale proposed by Landis and Kock (1977), Cohen's kappa values were interpreted as follows: 0.00-0.20 values indicated slight classification performance, 0.20-0.40 fair performance, 0.40-0.60 moderate performance, 0.60-0.80 good performance, and 0.80-1.00 very good performance.

When comparing the two winning combinations of techniques, it is noticeable that the winning dimensionality reduction techniques for the visible-NIR and NIR spectra were PCA and FA, respectively. Unlike the Sammon method, and due to their parametric nature, these two linear techniques have the advantage of being able to generalise the mapping to new data without performing the dimensionality reduction again. Comparison of the classification results using the

winning combinations of techniques shows that the winning combination for the visible-NIR spectra led to higher overall classification accuracy than the winning combination for the NIR spectra, increasing from 95.1% to 97.8%. Moreover, it can be observed that the Cohen's kappa value of 0.896 (or equivalently, 89.6%) for the visible-NIR spectra was much lower than the corresponding overall accuracy. This means that the overall accuracy was inflated due to the classification bias towards one of the two classes. In contrast, the kappa value of 0.953 (or equivalently, 95.3%) for the NIR spectra was notably closer to the corresponding overall accuracy, thus the NIR spectra entailed more balanced classification results for both classes than the visible-NIR spectra. In fact, this can be seen straightforwardly from the mean confusion matrices for both spectral ranges. It can be noticed that the number of well-classified sound samples for the NIR spectra (100.0%) was higher than that obtained for the visible-NIR spectra (98.0%). Furthermore, when using the NIR spectra, the classification of decaying samples was improved to a greater extent than the classification of sound classes, with the success rate increasing from 90.7% to 94.4%. In practice, this increase in the number of well-classified decaying samples is of major importance for a potential inspection system, since just a small number of infected fruits can spread the fungal infection to healthy fruit in the batch, thus entailing great economic losses. Therefore, a general conclusion drawn from analysing these classification results is that the winning combination of techniques for the NIR spectra provided better results than the winning combination corresponding to the visible-NIR spectra for the decay detection problem.

Table 6.2. Classification results for the visible-NIR and NIR spectra using the winning combinations of techniques.

<table>
<tr><th></th><th>Visible-NIR spectra</th><th>NIR spectra</th></tr>
<tr><td>Winning combination of techniques</td><td>No pre-processing, ML, PCA</td><td>No pre-processing, ML (or GMST), FA</td></tr>
<tr><td>Overall accuracy (%)</td><td>95.07</td><td>97.76</td></tr>
<tr><td>Cohen's kappa</td><td>0.896</td><td>0.953</td></tr>
<tr><td>Mean confusion matrix</td><td>
<table>
<tr><th></th><th>Sound (%)</th><th>Decay (%)</th></tr>
<tr><td>Sound</td><td>98.01</td><td>9.31</td></tr>
<tr><td>Decay</td><td>1.99</td><td>90.69</td></tr>
</table>
</td><td>
<table>
<tr><th></th><th>Sound (%)</th><th>Decay (%)</th></tr>
<tr><td>Sound</td><td>100.00</td><td>5.58</td></tr>
<tr><td>Decay</td><td>0.00</td><td>94.42</td></tr>
</table>
</td></tr>
</table>

In view of these results, the present research lays the foundation for the future development of an automatic system based on reflectance spectroscopy in the visible and NIR regions that is capable of detecting early symptoms of decay in citrus fruit, which is extremely important from the economic point of view. However, further investigation on the use of the spectral measurements, coupled with the corresponding winning combinations of multivariate techniques, for decay detection in other cultivars of citrus fruit is still needed for commercial application. Moreover, some issues should be taken into account in order to be able to establish spectroscopy technology on a commercial fruit sorter aimed at the detection of decay. For example, spectrophotometers should be applied on rotating fruit in order to explore the whole surface of each fruit.

6.4. Conclusions

This work has shown the potential of visible-NIR reflectance spectroscopy for detecting early decay symptoms caused by *P. digitatum* fungus in citrus fruit. Reflectance spectra of mandarin skin samples acquired in two different spectral regions, from 650 nm to 1050 nm (visible-NIR) and from 1000 nm to 1700 nm (NIR), were used for this detection, significant differences in spectra between sound and decaying skin being observed for both spectral ranges.

The evaluation of performance in the classification of sound and decaying skin was obtained for the visible-NIR and NIR spectra using the different scatter-correction techniques, intrinsic dimensionality estimators and manifold learning techniques for dimensionality reduction. For the spectra in the visible-NIR range, the maximum overall accuracy of 95.1% was obtained by employing PCA on the uncorrected spectra, using the intrinsic dimensionality estimation provided by ML. In the case of the NIR range spectra, a maximum classification accuracy of 97.8% was achieved by employing FA on the uncorrected spectra, using the intrinsic dimensionality estimation provided by ML or GMST. From these results, it can be said that, for both spectral ranges, the linear manifold learning techniques for dimensionality reduction (PCA and FA) outperformed the non-linear technique (Sammon mapping). Moreover, it should be highlighted that the spectra without scatter-correction led to better classification results than the spectra pre-processed with MSC and SNV, since these techniques probably removed important information for decay detection from the spectra.

The winning combination of techniques for the NIR spectra provided better results than the winning combination corresponding to the visible-NIR spectra, with an increase in the overall classification accuracy from 95.1% to 97.8%. Furthermore, when using the NIR spectra, the

percentage of well-classified samples was improved for both skin classes, with the success rate increasing from 98.0% to 100.0% for sound samples and from 90.7% to 94.4% for decaying samples. In conclusion, even though the best classification results were obtained using the winning combination of techniques for the NIR spectra, the two optimal combinations of techniques obtained for the visible-NIR and NIR spectra resulted in good classification results for the problem of decay detection, with a percentage of well-classified samples above 90% for both classes in spite of the similarity between sound and decaying skin. Nevertheless, despite these optimistic results, further research is still needed to be able to establish spectroscopy technology on a commercial fruit sorter aimed at decay detection in citrus fruit.

Acknowledgements

This work has been partially funded by the Instituto Nacional de Investigación y Tecnología Agraria y Alimentaria de España (INIA) through research project RTA2012-00062-C04-01 with the support of European FEDER funds. Delia Lorente thanks INIA for the support through grant FPI-INIA number 42.

Part V

Conclusions

Chapter 7

Conclusions and future work

This final chapter presents the overall and specific conclusions drawn from this doctoral thesis. In addition, this chapter identifies possible lines for future research in order to continue the research work presented in this thesis. At the end of this chapter, a list of the scientific publications related to the thesis is also provided.

7.1. Overall conclusions

Decay caused by *Penicillium* spp. fungi is among the main problems affecting postharvest and marketing processes of citrus fruit because a small number of decayed fruit can infect a whole consignment, during long-term storage or fruit shipping to export markets, thus involving enormous economic losses and the blackening of the reputation of citrus producers. Therefore, effective early detection of fungal infections and removal of infected fruit are issues of major importance in commercial packinghouses in order to prevent the spread of the infections, thus ensuring an excellent fruit quality and absolute absence of infected fruit.

In this sense, the research efforts associated with this doctoral thesis have been oriented towards addressing such an important challenge for the citrus industry as the automation of the detection of early symptoms of decay, in order to provide alternatives to manual inspection using dangerous UV illumination, thus accomplishing this detection task more efficiently and, consequently, leading to a possible reduction of the use of fungicides. As a direct consequence of the conducted research work, this doctoral thesis has advanced in the field of the automatic detection of decay

in citrus fruit using optical systems and machine learning methods, thus fulfilling the overall goal of this doctoral research study. In particular, three different optical techniques operating in the visible and NIR spectral regions have been investigated, including hyperspectral imaging, light backscattering imaging and spectroscopy. Since the optical systems used in this thesis have not been limited to the visible part of the electromagnetic spectrum, they have shown capabilities beyond those of the naked human eye and traditional computer vision systems based on colour cameras, this fact being of special interest for detecting hardly-visible damage in citrus fruit, such as decay at early stages. In addition, a vast number of machine learning techniques aimed at data dimensionality reduction and classification has been explored for dealing with the optical measurements of citrus fruit in order to discriminate fruit with symptoms of decay from sound fruit. Due to the different inherent nature of each of the optical techniques used in this thesis, the treatment of the obtained data, and therefore the machine learning methods, has been specific to each optical technology in order to handle the particularities of each one.

The three optical technologies, coupled with suitable machine learning methods, investigated in this doctoral thesis have provided good results in the classification of skin of citrus fruit into sound or decaying in an early stage, with a percentage of well-classified samples above 90% for both classes despite their similarity. Therefore, these results represent an improvement on those obtained in previous works using traditional computer vision systems based on colour cameras and visible lighting for decay detection in citrus fruit, with a limited success rate of only around 65% in the identification of decaying fruits (Blasco et al., 2007a). Thus, in view of the results, this doctoral thesis has laid the foundation for the future implementation of an automatic system based on whatever of the studied optical technologies capable of detecting decay in early stages.

However, for future commercial application, the knowledge of the particularities of each optical technology would be useful in order to take advantage of some favourable characteristics specific to each technology or address the associated limitations. In this respect, in order to have a better understanding of the connections between the different technologies, some characteristics of the investigated optical techniques associated with their practical application for fruit inspection have been compared and compiled from the experience acquired through the development of this doctoral thesis. These characteristics, as well as the main connections between technologies, are summarised as follows, paying special attention on the specific systems used in this thesis: a hyperspectral vision system based on LCTFs, a spectroscopy system in reflectance mode and a LLBI system.

For example, although both spectroscopy and hyperspectral imaging cover a large number of narrow spectral bands over a continuous spectral range, hyperspectral imaging acquires simultaneously spectral and spatial information from a fruit, while spectroscopy provides only

spectral information captured at a particular spot on the sample, since the point detector used in this technology has size limitation. Conversely, this lack of spatial information makes spectroscopy much less time-consuming and more appropriate for real-time applications than hyperspectral imaging. In fact, hyperspectral systems are so time-consuming that, in practice, they are used just as a means for selecting the particular set of wavelengths that will finally be used in multispectral systems suitable for the real-time product inspection, as done in this doctoral thesis. Another important difference between spectroscopy and hyperspectral imaging is the way in which they use the light source. In this sense, contrary to the diffuse lighting used in hyperspectral imaging to illuminate the scene uniformly, in reflectance spectroscopy, light hits directly a fruit, partly penetrating into the tissue, and a light detector measures the reflected radiation, which contains information about the internal components of the fruit.

Similarly to reflectance spectroscopy, in backscattering imaging, the light source is also aimed towards the fruit. However, in backscattering imaging, the backscattered light is recorded by an imaging system, thus tracking spatial information of the light signal on the sample, unlike spectroscopy. In addition, in the particular case of LLBI systems, as that used in this doctoral thesis, laser light penetrates deeper into the fruit than broadband light (e.g. light generated by a halogen lamp), as that usually used in a reflectance spectroscopy system, thus obtaining more information about the fruit tissue. On the other hand, LLBI systems provide information just in a few wavelengths, unlike spectroscopy systems, which cover a large number of consecutive wavelengths. In addition, although LLBI systems can be potentially used to assess quality of fruit in a relatively cheap, simple and fast way, further advances in equipment are still required before commercial application. For example, future LLBI systems must be capable of taking images at several wavelengths simultaneously and at a faster speed than that obtained with the current LLBI systems, thus making it easier to incorporate this technology into an industry that demands real-time inspection. Moreover, instead of point lasers, perhaps line lasers should be applied on rotating fruit in order to explore the whole surface of each fruit. On the contrary, since spectroscopy is arguably the most advanced optical technology with regard to equipment and applications, such technological progress has already led to the development of spectroscopy systems with high acquisition speed used in the agro-food industry for real-time sorting of products according to their quality. However, despite such advances in spectroscopy systems, a few issues should be considered for the specific application of this technology for decay detection in citrus fruit. For example, spectrophotometers should be applied on rotating fruit in order to examine the whole fruit surface. Although rotation of fruit is also suggested for all the systems that inspect external defects in citrus fruit, this is of particular importance in spectroscopy systems for overcoming the pronounced lack of spatial information and, consequently, ensuring an exceptional fruit quality.

7.2. Specific conclusions

This doctoral report has been presented as a collection of research papers, from Chapter 2 to 6. The research work presented in each chapter has been aimed at addressing the specific objectives related to each optical technology listed in Section 1.2, thus leading to its own conclusions and contributions to knowledge in the research field of this thesis. In the following sections, the specific conclusions of this doctoral thesis are grouped according to the different optical technologies, with emphasis on linking the knowledge extracted from the different chapters in order to establish the thesis as a coherent whole.

7.2.1. Hyperspectral imaging

This section presents the conclusions drawn from Part II of this thesis report (Chapters 2 and 3), which has included two research papers related to hyperspectral imaging. Both research papers have used the same hyperspectral system based on two LCTFs operating in the visible and NIR spectral regions, thus allowing the acquisition of hyperspectral images in the range of 460-1020 nm, with a spectral resolution of 10 nm.

Due to the current need for reducing the high-dimensional hyperspectral images to multispectral ones for the subsequent implementation in real-time inspection systems, the research paper in Chapter 2 has proposed a novel wrapper feature selection methodology for multiclass classification problems that uses the area under the ROC curve as measure of classifier performance, in order to select a reduced set of wavelengths that are effective in the detection of decay in citrus fruit. The specific conclusions drawn from Chapter 2 are the following:

- The proposed feature selection method has expanded the use of the ROC curve from binary classification problems to multiclass classification problems. Therefore, this methodology has been applied to select an optimal set of wavelengths that are effective not only in the discrimination between fruit affected by serious diseases (decay lesions) and sound fruit, but also capable of separating fruit affected by cosmetic defects (scars), which only affect the appearance of the fruit but do not spread among other fruits and do not prevent its commercialisation in the internal market as fresh product or its use in the processed citrus industry. Cosmetic defects have been taken into account to prevent them to be confused with the dangerous ones by an automatic system, thus avoiding the economic losses associated with the removal of fruit affected only by minor defects. In particular, the proposed feature selection methodology has been applied to the problem

of classification of pixels from hyperspectral images of mandarins cv. 'Clemenules', in order to separate the pixels into five different classes: decay caused by two different fungi (*P. digitatum and P. italicum*), two kinds of sound skin (green and orange) and scars.

- Although the ROC feature selection technique is independent of the chosen classification method, the classifier used to explore the possibilities of this wrapper selection method has been a MLP with a single hidden layer, trained with a new learning algorithm called ELM. The use of this learning algorithm has involved a much faster learning speed than that obtained using classical learning methods (e.g. backpropagation), since ELM has determined the ANN parameters analytically instead of tuning them iteratively. This increase in speed has been very important in order to facilitate the search of the optimal features using the proposed feature selection method. In addition, once selected the optimal features, the same classifier has been also used for classifying the pixels from the hyperspectral images.
- The proposed feature selection method has been applied considering three different approaches to the problem of decay detection in mandarins, depending on the number of classes implicated and the importance of each class. As a result, a reduced number of spectral features (including purely spectral variables and spectral indexes) have been obtained for each approach: six for the first approach (i.e. five classes of similar importance), seven for the second approach (i.e. five classes of different importance, with decay classes having the maximum importance) and four for the third one (i.e. binary classification problem: infected and not infected).
- The set of features selected for the second approach has provided better classification results than that obtained for the first one, with an increase in the average success rate from 87.5% to 89.1% by taking into account classes with different importance in the classification problem. This improvement has been especially due to the increase in the number of well-classified pixels of decay classes, this fact being of major importance for a potential inspection system. Furthermore, for these two approaches, due to the similarity of the damage caused by the two fungi, most confusion has been done between both decay classes, which could be grouped into the same category or commercial importance. In this sense, as expected, better results have been obtained for the third approach (average success rate of 95.5% with classification rates above 94% for both classes), which is a simplified approach to the problem, specifically aimed at the detection of decay.

In Chapter 3, the research paper has compared the feature selection method proposed in Chapter 2 with other common feature selection techniques (CA, MI, FDA, TT, WL, BD, MRMRd, MRMRq and KLD) in terms of the classification performance in the tackled problem of decay detection in citrus fruit. All the methods have been applied to the same hyperspectral images of mandarins, with the pixels labelled in five classes, using the same approaches to the problem and the same classifier for separating the pixels as those employed in Chapter 2 with the ROC feature selection method. The specific conclusions extracted from Chapter 3 are enumerated as follows:

- After carrying out two different tests to perform the comparison (i.e. a test selecting an optimal number of features for each method and for each approach that could be different for each case and other test using a fixed number of features for all cases), the ROC feature selection method has generally provided better results than most of the feature selection methods used in the comparative study. In particular, the average success rate obtained using the ROC method in both tests have been greater than that obtained for the other methods, only being surpassed by the MRMR methods for the third approach.
- The proposed feature selection technique based on the area under the ROC has shown to be a suitable feature selection method for multiclass classification problems with a huge amount of features, such as the selection of wavelengths effective in the decay detection in citrus fruit, providing at least similar results as those obtained with other feature selection methods but with the additional advantage of optimising, by its nature, the classifier performance.

7.2.2. Backscattering imaging

The conclusions extracted from the third part of this thesis (Chapters 4 and 5), which has comprised two research papers dealing with backscattering imaging, are presented in this section. In both research papers, a LLBI system with five diode lasers emitting at different wavelengths in the visible and NIR ranges (532, 660, 785, 830 and 1060 nm) has been employed to acquire backscattering images.

In Chapter 4, the research paper has evaluated, for the first time, the potential of LLBI for decay detection in citrus fruit. For this purpose, backscattering images of oranges cv. 'Navelate' in two different states (sound oranges and oranges presenting decay lesions caused by *P. digitatum* fungus) have been acquired in the research work. The specific conclusions drawn from Chapter 4 are the following:

- In order to get higher performance classification results, each backscattering image have been characterised by means of five parameters obtained from fitting the one-dimensional backscattering profile with a statistical modelling approach using the Gaussian-Lorentzian cross product (GL) distribution function. As a result, the GL function has described the radial profiles accurately with average R^2 higher or equal to 0.998, pointing to differences in the parameters at the five wavelengths between sound and decaying oranges.
- In order to classify oranges into sound and decaying, the GL parameters at each wavelength have been used as input vectors of a LDA classifier. In this sense, ranking and combination of the laser wavelengths in terms of their contribution to the detection of decay have led to a maximum average success rate of 96.1% when using the five laser wavelengths, with a percentage of well-classified oranges above 95% for both classes despite the similarity between sound oranges and oranges presenting decay lesions. Moreover, it has been observed an increase in the average success rate of around 10% from the single wavelength (80.4%) to the two-wavelength combination (90.2%), with both wavelengths being in the visible range (532 nm and 660 nm), thus assuming that this range may provide more information on the differences in scattering properties of the tissue. In particular, this increase has been due to the improvement in the classification of oranges with decay, this fact being of major importance for a potential inspection system aimed at detecting decay in citrus fruit.
- From all the obtained results, the research paper in Chapter 4 has proved the feasibility of LLBI for detecting superficial decay in citrus fruit, thus having a high potential to be integrated in a future commercial system after further investigation.

In order to continue the research line of Chapter 4, the research paper presented in Chapter 5 has reported new progress in the automatic detection of decay caused by *P. digitatum* fungus in citrus fruit by means of LLBI. Particularly, the two kinds of profile modelling approaches (statistical and physical) and different feature selection methods, also used in the comparison study performed in Chapter 3, have been compared according to their classification performance in the addressed problem, this appearing as the next step in the direction towards the automation. In this research paper, backscattering images of sound and decaying parts of the surface of oranges cv. 'Valencia late' have been analysed. The specific conclusions extracted from Chapter 5 are enumerated as follows:

- In particular, the two models investigated to characterise backscattering profiles have been the statistical model using the GL distribution function with five parameters, also

employed in Chapter 4, and a physical approach calculating the absorption, μ_a, and reduced scattering, μ_s', coefficients from Farrell's diffusion theory. As a result, the two models have described radial profiles accurately, with slightly better curve-fitting results ($R^2 \geq 0.996$) for the GL model compared to Farrell's model ($R^2 \geq 0.982$). In addition, both profile modelling approaches have shown significant differences in the parameters between sound and decaying skin at the five wavelengths, thus indicating the suitability of these two models for characterising differences in the tissue of citrus fruit due to the decaying process.

- In the case of the statistical model, the GL parameters have presented different statistical significances and trends between sound and decaying oranges from those reported in the research paper in Chapter 4, which could be explained due to some differences between both studies that could influence on the measured data, such as the orange cultivar and the pre-processing of backscattering profiles. In any case, in both research studies, for each laser wavelength, some of the associated GL parameters have shown significant differences between both fruit states, this being an important indicator of potential success in the further separation of the tissue into sound and decaying by an automated system.

- In addition to characterising backscattering profiles, the physical profile modelling approach has offered the additional advantage, compared to the statistical approach, of allowing the measurement and separation of the optical properties of sound and decaying tissues of citrus fruit at the different wavelengths, thus facilitating the extraction of more knowledge about the underlying optical properties associated with the decaying process. In particular, the differences in the absorption and reduced scattering coefficients between sound and decaying skin at the different wavelengths have been justified by reasons connected with the decaying process, since the calculated coefficients have provided a real connection with the optical properties of citrus fruit. In addition, the values of μ_s' have been generally at least one order higher than the μ_a values for both states, thereby highlighting the dominant effect of scattering for light propagation in oranges in the studied wavelengths and, consequently, the fulfilment of the prerequisite for the application of the diffusion theory approach. However, the difference between both optical coefficients has been less evident at 532 nm due to the high absorption of carotenoids in oranges and the high variance in the calculated coefficients, this fact suggesting the inappropriateness to apply Farrell's model at this wavelength.

- Despite the fact that statistical significance may provide a general idea whether a variable should be included in a classification model, it is sometimes possible to have an

insignificant variable that is useful for forecasting or to have a significant variable that is better omitted when forecasting. Therefore, methods intended and optimised specifically for feature selection purposes have been preferred over significance tests in order to select a reduced number of backscattering profile parameters relevant for the detection of decay lesions. As a result, seven features have been selected for the GL model using the CA, FDA, TT and WL methods, this feature selection suggesting that parameters b and e have been the least valuable for discriminating between sound and decaying orange skin. In the case of Farrell's model, the resulting set of eight features selected with the MI, BD and KLD methods have included the absorption and reduced scattering coefficients at four laser wavelengths, with the optical coefficients at 532 nm remaining outside the feature selection, this fact also pointing out the limitations of Farrell's model at this wavelength.

- The selected features have been used to discriminate between sound and decaying skin using a LDA classifier, as that used in Chapter 4. The classification results using the selected optical coefficients for Farrell's model (average success rate of 92.4%) have been quite similar to those obtained using the GL selection (average success rate of 93.4%), with both approaches yielding a similar percentage of well-classified decaying samples of 94.2% and the classification of sound samples being better for the GL selection, increasing from 90.6% to 92.5%. Therefore, the optimal sets of features for both profile modelling approaches have resulted in good classification results, with a percentage of well-classified samples above 90% for both classes despite the similarity between sound and decaying orange skin.
- In the light of the results, the research paper presented in this chapter has laid the foundation for the future implementation of an automatic system based on LLBI capable of detecting decay in early stages. However, some issues should be taken into account for future setting-up on a commercial fruit sorter. For example, line lasers should be applied on rotating fruit in order to explore the whole surface of each fruit. In addition, imaging systems must be capable of taking images at several wavelengths simultaneously and at a fast speed.

7.2.3. Spectroscopy

This section summarises the conclusions extracted from Part IV (Chapter 6), which has consisted of one research paper related to spectroscopy. This research paper has evaluated more thoroughly the feasibility of reflectance spectroscopy in the visible and NIR regions for the automatic

detection of decay caused by *P. digitatum* fungus in citrus fruit. For this purpose, this research has investigated and compared two different spectral ranges included in the visible and NIR regions in which the reflectance measurements have been acquired, as well as different spectral pre-processing techniques, dimensionality estimators and manifold learning methods for dimensionality reduction, in terms of their classification performance for the decay detection problem. The specific conclusions drawn from Chapter 6 are the following:

- In this research, reflectance spectra of sound and decaying surface parts of mandarin cv. 'Clemenvilla' have been acquired in two different spectral regions, from 650 nm to 1050 nm (visible-NIR) and from 1000 nm to 1700 nm (NIR), pointing to significant differences in spectra between sound and decaying skin for both spectral ranges, this fact suggesting the potential suitability of the spectral measurements for decay detection in subsequent classification tasks.

- The effect of the inoculation procedure on the spectral measurements has been evaluated. To this end, the spectra of the two kinds of sound skin samples (sound skin close to the hole caused by the inoculation and sound skin further away from the hole) have been tested to check their similarity. As a result, the spectra have not presented significant differences between both kinds of sound skin for both spectral ranges, thus confirming that the inoculation process have not affected the measurements. In addition, although this statement has been made using measurements acquired with a spectroscopy system, it can be also extrapolated to the other optical technologies, this finding being of main interest for research on detecting decay in citrus fruit using optical techniques.

- Some spectral pre-processing techniques aimed at scatter-correction have been investigated to remove possible noise from the measured spectra. In order to achieve better decay detection results, several manifold learning methods have been then used to transform the high-dimensional spectral data into meaningful representations of reduced dimensionality, this step being of particular interest in spectroscopy research due to the large amount of spectral data involved in this technology. Prior to dimensionality reduction, different methods for estimating the target dimensionality of the corresponding lower-dimensional data representations have been employed. The low-dimensional data representations have been used as input feature vectors to discriminate between sound and decaying skin using a LDA classifier. In this sense, the spectral ranges (visible-NIR and NIR), the scatter-correction techniques (no pre-processing, MSC and SNV), the dimensionality estimators (EB, ML, CD and GMST) and the manifold learning methods for dimensionality reduction (PCA, FA and Sammon) have been evaluated and compared in terms of their classification performance

- For the spectra in the visible-NIR range, the maximum average success rate of 95.1% has been obtained by employing PCA on the uncorrected spectra, using the intrinsic dimensionality estimation provided by ML. In the case of the NIR range spectra, a maximum average success rate of 97.8% has been achieved by employing FA on the uncorrected spectra, using the intrinsic dimensionality estimation provided by ML or GMST. These results have indicated that, for both spectral ranges, the linear manifold learning techniques for dimensionality reduction (PCA and FA) have outperformed the non-linear technique (Sammon). Moreover, the spectra without scatter-correction have led to better classification results than the spectra pre-processed with MSC and SNV, since these techniques have probably removed important information for decay detection from the spectra, this fact suggesting that decaying process in citrus fruit may be more characterised by structural changes in fruit tissue, rather than changes in chemical composition. In addition, results have revealed that ML and GMST have estimated higher intrinsic dimensionalities than EB and ML, thus leading to better classifier performances.

- The winner combination of techniques for the NIR spectra has provided better results than the winner combination corresponding to the visible-NIR spectra, with an increase in the average success rate from 95.1% to 97.8%. Furthermore, when using the NIR spectra, the percentage of well-classified samples has been improved for both skin classes, with the success rate increasing from 98.0% to 100.0% for sound samples and from 90.7% to 94.4% for decaying samples. However, the two optimal combinations of techniques obtained for the visible-NIR and NIR spectra have resulted in good classification results for the decay detection problem, with a percentage of well-classified samples above 90% for both classes.

- From all the obtained results, the research paper presented in Chapter 6 has shown the high potential of reflectance spectroscopy in the visible and NIR regions for detecting decay in citrus fruit, thus laying the foundation for the future development of an automatic system based on this technology. However, despite the optimistic results, further research on spectroscopy technology is still needed before its commercial application. Moreover, some issues should be taken into account for future setting-up of this technology on a commercial sorter. For example, spectrophotometers should be applied on rotating fruit in order to explore the whole surface of each fruit.

7.3. Future research work

This doctoral thesis has presented advances in the field of the automatic detection of decay in citrus fruit using optical systems and machine learning methods. However, further investigation is still needed for the future establishment of the explored optical technologies, coupled with the suggested machine learning techniques, on a real-time fruit sorter. In this sense, several research lines regarded as the logical continuation of the research work presented in this doctoral thesis are enumerated as follows:

- The methodology proposed for each of the investigated optical techniques to detect decay in citrus fruit has been applied only to a limited number of cultivars of citrus fruit. Therefore, a natural way to continue the research line started in this doctoral thesis would be to test the efficiency of the use of the different optical measurements, coupled with the suggested multivariate techniques, over a wider range of citrus fruit cultivars with great economic importance for the agro-food industry. In this sense, a new research work on decay detection in citrus fruit has been recently started in the Computer Vision Laboratory at the IVIA. In particular, optical measurements of eight different cultivars of citrus fruit, including several cultivars of oranges and mandarins, have been acquired using the same hyperspectral vision system and the same spectroscopy system as those employed in this doctoral thesis.

- In addition to evolving decay lesions caused by fungi, future research on spectroscopy and backscattering imaging should also take into account other common defects appearing in citrus fruit (e.g. oleocellosis, scars caused by branch frictions and chilling injury), similarly to that done in the feature selection methodology using hyperspectral images proposed in this doctoral thesis. The inclusion of more external defects would enable the automatic separation of citrus fruit into different commercial categories according to the kind of defect appearing on the fruit surface, thus avoiding the economic losses associated with the removal of fruit affected only by cosmetic defects, which do not affect the organoleptic properties.

- An aspect to be taken into account in further research on backscattering imaging is the influence of the shape of citrus fruit on the measurement of actual reflectance intensities. In this doctoral thesis, backscattering images have been treated as if surface of citrus fruit was approximately flat, instead of spherical, and, therefore, no corrections have been applied on the images in order to take into consideration the effect of the shape. However, due to the curvature of the fruit surface, the reflectance captured by the

imaging system for a location at the fruit surface away from the light incident point tends to underestimate the actual light intensity for that location. Therefore, in order to achieve higher classification performance for decay detection in citrus fruit, correction of the backscattering images would be needed to reduce the degradation of light intensity from the centre to the borders of the images, similarly to that done with the hyperspectral images in this doctoral thesis. In this sense, some method based on Lambert's cosine law could be used for correcting the undesirable effect produced by the curvature of citrus fruit on backscattering images, such as those described in Peng and Lu (2006b) and Qing et al. (2007).

- The different pieces of research conducted in this doctoral thesis have provided methodologies to classify only a particular part of the surface of citrus fruit as being either decaying or sound (e.g. spatial region of the fruit surface corresponding to a pixel in the case of hyperspectral imaging). However, in order to ensure absolute absence of infected fruit, it would be interesting to develop a methodology for classifying each piece of fruit as a whole from the different optical measurements obtained after examining the whole fruit surface. In theory, since decay lesions evolve over the time, even though only a small surface part of a fruit was suspected of presenting decay, the fruit as a whole should be considered to be infected and, consequently, removed automatically from the commercial line in order to prevent the spread of the fungal infections. However, due to the fact that the classification performed by the machine learning methods is not a totally accurate process, the possibility of classification errors must be taken into account when developing the fruit classifier that will decide whether the fruit should be removed or not. In this sense, a possible idea could be the establishment of a reasonable minimum limit of the amount of decaying surface, with respect to the total fruit area, required to classify a fruit as infected. Therefore, only if the infected area of a fruit exceeded this limit, the fruit would be classified as an infected fruit.

- The present doctoral thesis has proposed particular wavelengths important for the decay detection in citrus fruit using different optical techniques. However, the different research works in this thesis have suggested slightly different sets of wavelengths for the same problem. This is probably due to the fact that the results are usually dependent on the cultivar, the optical techniques, the laboratory conditions (e.g. lighting and calibration) and the machine learning techniques. In this respect, an important challenge to be addressed in future research is to relate the selected wavelengths to internal compounds or physical-chemical properties that could thus support and justify the results from the point of view of the product. Although the physical approach used to

characterise the backscattering profiles in this doctoral thesis has attempted the extraction of more knowledge about the underlying absorption and scattering properties associated with decaying process in citrus fruit, destructive physical-chemical analyses are still required to find out the real changes in chemical composition more thoroughly. In this sense, the increasing interdisciplinary nature of research groups offers the possibility of combining genetic, biological and physiological knowledge with optical research, thus facilitating the advance towards integrated solutions for the fruit and vegetable industry. In fact, a research work is being currently conducted in collaboration with the Agro-food Technology Department of the Miguel Hernández University of Elche (UMH) in order to determine physical-chemical properties of citrus fruit during decaying process by means of analytical techniques such as gas chromatography-mass spectrometry (GC-MS) and high performance liquid chromatography (HPLC). In the framework of this research, some preliminary tests on sound and decaying skin samples of several cultivars of citrus fruit have shown some evidence of changes in chemical composition occurring during the decaying process. Therefore, in the near future, the existing relationships between the associated biological processes and the wavelengths selected using the different optical technologies may be found.

- Although this doctoral thesis has shown the feasibility of different optical techniques for detecting decay in citrus fruit by means of several pieces of research, comparison of the optical techniques has not been carried out. This has been due to the fact that direct comparison of the results from the different experiments is inappropriate because the measured values could be influenced by aspects such as the cultivar of citrus fruit or the laboratory conditions. In this sense, a further step in the framework of this research line would be to conduct a general experiment that use the three optical technologies at the same time on the same samples of citrus fruit, trying to homogenise the laboratory conditions for all technologies as much as possible, thus making it possible to compare the different optical techniques in terms of their classification performance for the decay detection problem. This future research should overcome a problem such as the difficulty for a research group of managing to gather the three different optical systems at the same laboratory.

- The most important challenge that should be faced in future research is certainly the development of a prototype for in-line real-world tests based on each of the studied optical technologies, coupled with the suggested machine learning methods, as early introduced in Section 7.1. The performance of the resulting prototypes for decay detection in citrus fruit should be evaluated in terms of quality fulfilments, speed and

robustness to check if these developing automatic systems are comparable to actual inspection systems used in the agro-food industry. In particular, a multispectral vision system suitable for real-time inspection could be implemented using the particular set of wavelengths selected using hyperspectral imaging, as a result of the research conducted in this doctoral thesis, coupled with the steady development of multispectral systems. In the case of spectroscopy, similarly to multispectral imaging, the technological progress has led to the development of spectroscopy systems with high acquisition speed used in the agro-food industry for real-time sorting of products according to their quality, which could be also employed for the detection of decay. However, a few issues should be considered for the specific application of optical systems for decay detection in citrus fruit, such as the rotation of fruit in order to inspect the whole fruit surface. In addition, in the case of backscattering imaging, since LLBI systems are less developed than multispectral vision systems and spectroscopy systems, still much more advances in equipment are required for the future implementation of LLBI systems that assess fruit quality. For example, future LLBI systems must be capable of taking images at several wavelengths simultaneously and at a faster speed, thus making it easier to incorporate this technology into an industry demanding real-time inspection. Moreover, instead of point lasers, perhaps line lasers should be applied on fruit in order to facilitate the inspection of the whole surface. In general, the incorporation of these optical technologies in the citrus industry with the aim of detecting decay is quite promising, due not only to continuous technological advances in optical systems leading to an increase in the acquisition speed, but also to the constant reduction in the price of equipment, as well as to the increasing computational capacity that will facilitate the real-time analysis of the optical measurements by means of machine learning methods.

7.4. Scientific publications related to the doctoral thesis

In the research stage associated with this doctoral thesis during the period 2010-2014, several scientific results have been produced, thus leading to publications in the research field of this thesis. Among these publications, those directly derived from the research results presented in this thesis report, with the author of this doctoral thesis as the first author, should be highlighted.

In addition to the publications directly arising from the results here presented, the knowledge acquired during these years has led to collaborations in other important publications related to the field of the automatic quality inspection of agricultural products using the optical techniques

analysed in this thesis report, among others, and machine learning methods. These research publications have been focused not only on decay detection in citrus fruit, but also on the assessment of other quality parameters in other agricultural products. Furthermore, machine learning methods different from those used in this thesis report have been also employed in these publications.

The following sections list all the scientific publications related to this doctoral thesis in chronological order, including those directly derived from the scientific results presented in this thesis report and those co-authored during the research stage associated with the doctoral studies, but not directly emerged from the results here presented.

7.4.1. Publications in international journals indexed in the JCR

- **Lorente, D.**, Aleixos, N., Gómez-Sanchis, J., Cubero, S., García-Navarrete, O.L., Blasco, J., 2012. Recent advances and applications of hyperspectral imaging for fruit and vegetable quality assessment. Food and Bioprocess Technology, 5, 1121-1142.
- **Lorente, D.**, Aleixos, N., Gómez-Sanchis, J., Cubero, S., Blasco, J., 2013. Selection of optimal wavelength features for decay detection in citrus fruit using the ROC curve and neural networks. Food and Bioprocess Technology, 6, 530-541.
- Gómez-Sanchis, J., Blasco, J., Soria-Olivas, E., **Lorente, D.**, Escandell-Montero, P., Martínez-Martínez, J.M., Martínez-Sober, M., Aleixos, N., 2013. Hyperspectral LCTF-based system for classification of decay in mandarins caused by *Penicillium digitatum* and *Penicillium italicum* using the most relevant bands and non-linear classifiers. Postharvest Biology and Technology, 82, 76-86.
- **Lorente, D.**, Blasco, J., Serrano, A.J., Soria-Olivas, E., Aleixos, N., Gómez-Sanchis, J., 2013. Comparison of ROC feature selection method for the detection of decay in citrus fruit using hyperspectral images. Food and Bioprocess Technology, 6, 3613-3619.
- **Lorente, D.**, Zude, M., Regen, C., Palou, L., Gómez-Sanchis, J., Blasco, J., 2013. Early decay detection in citrus fruit using laser-light backscattering imaging. Postharvest Biology and Technology, 86, 424-430.
- Gómez-Sanchis, J., **Lorente, D.**, Soria-Olivas, E., Aleixos, N., Cubero, S., Blasco, J., 2014. Development of a hyperspectral computer vision system based on two liquid crystal tuneable filters for fruit inspection. Application to detect citrus fruits decay. Food and Bioprocess Technology, 7, 1047-1056.

- Vélez-Rivera, N., Gómez-Sanchis, J., Chanona-Pérez, J., Carrasco, J.J., Millán-Giraldo, M., **Lorente, D.**, Cubero, S., Blasco, J., 2014. Early detection of mechanical damage in mango using NIR hyperspectral images and machine learning. Biosystems Engineering, 122, 91-98.

7.4.2. Book chapters

- Blasco, J., Aleixos, N., Cubero, S., **Lorente, D.**, 2012. Fruit, vegetable and nut quality evaluation and control using computer vision. In: Sun, D.W. (Ed.), Computer vision technology in the food and beverage industries. Woodhead Publishing, Cambridge, UK, pp. 379-399.
- Blasco, J., Aleixos, N., Cubero, S., Albert, F., **Lorente, D.**, Gómez-Sanchis, J., 2012. In-line sorting of processed fruit using computer vision. Application to the inspection of satsuma segments and pomegranate arils. In: Magdalena-Benedito, R., Martínez-Sober, M., Martínez-Martínez, J.M., Escandell-Montero, P., Vila-Francés, J. (Eds.), Intelligent data analysis for real-life applications: theory and practice. IGI Global, Hershey, USA, pp. 124-145.
- Gómez-Sanchis, J., Soria-Olivas, E., **Lorente-Garrido, D.**, Martínez-Martínez, J.M., Escandell-Montero, P., Guimerá-Tomás, J., Blasco, J., 2012. Decay detection in citrus fruits using hyperspectral computer vision. In: Magdalena-Benedito, R., Martínez-Sober, M., Martínez-Martínez, J.M., Escandell-Montero, P., Vila-Francés, J. (Eds.), Intelligent data analysis for real-life applications: theory and practice. IGI Global, Hershey, USA, pp. 104-123.

7.4.3. Communications in conferences

- **Lorente, D.**, Gómez-Sanchis, J., Aleixos, N., Cubero, S., García-Navarrete, O.L., Serrano, A., Soria, E., Blasco, J., 2011. Uso de la curva ROC para la selección de longitudes de onda óptimas en la detección de podredumbres de cítricos. In: VI Congreso Ibérico de Agroingeniería, September 2011, Évora, Portugal. Best Communication Award.
- Gómez-Sanchis, J., **Lorente, D.**, Aleixos, N., Martínez-Martínez, J.M., Escandell-Montero, P., Vila-Francés, J., Blasco, J., 2012. Detección automática de podredumbres en cítricos mediante técnicas de aprendizaje automático y visión hiperespectral. In: VIII

Congreso Español de Metaheurísticas, Algoritmos Evolutivos y Bioinspirados (MAEB), February 2012, Albacete, Spain, Proceedings, pp. 645-650.

- **Lorente, D.**, Gómez-Sanchis, J., Aleixos, N., Cubero, S., García-Navarrete, O.L., Serrano, A., Soria, E., Blasco, J., 2012. Selection of optimal wavelength features for decay detection in citrus fruit using the ROC curve. In: IV International Workshop on Computer Image Analysis in Agriculture, July 2012, Valencia, Spain.
- Blasco, J., Aleixos, N., Cubero, S., **Lorente, D.**, 2012. Computer vision systems for the nondestructive quality evaluation of agricultural products: techniques and applications. In: The 8th International Workshop on Nondestructive Quality Evaluation of Agricultural, Livestock and Fishery Products, November 2012, Taipei, Taiwan, Proceedings, pp. 3-34.
- **Lorente, D.**, Blasco, J., Zude, M., 2013. Automatische erkennung on verderb bei citrusfrüchten mit bildgebender, multispektraler rückstreumessung. In: 19 Workshop Computer-Bildanalyse in der Landwirtschaft, May 2013, Berlin, Germany.
- Blasco, J., Aleixos, N., Cubero, S., **Lorente, D.**, 2013. Automatic inspection of the quality of the citrus production using computer vision. In: II International Workshop on Multivariate Image Analysis, May 2013, Valencia, Spain, Book of abstracts, pp. 13-26.
- **Lorente, D.**, Zude, M., Gómez-Sanchis, J., Regen, C., Blasco, J., 2013. Detección de podredumbres en cítricos mediante análisis de imágenes backscattering. In: VII Congreso Ibérico de Agroingeniería y Ciencias Hortícolas, August 2013, Madrid, Spain, Book of abstracts, p. 48.
- Vélez-Rivera, N., Carrasco, J.J., Chanona-Pérez, J., **Lorente, D.**, Gómez-Sanchis, J., Millán-Giraldo, M., Farrera, R., Blasco, J., 2013. Detección de daños no perceptibles en frutos climatéricos a través del análisis de imágenes hiperespectrales. In: VII Congreso Ibérico de Agroingeniería y Ciencias Hortícolas, August 2013, Madrid, Spain, Book of abstracts, p. 50.
- Vélez-Rivera, N., Carrasco, J.J., Chanona-Pérez, J., Cardenas-Pérez, S., **Lorente, D.**, Gómez-Sanchis, J., Millán-Giraldo, M., Farrera, R., Blasco, J., 2013. Unnoticeable damage detection in climacteric fruit via hyperspectral imaging. In: 8th CIGR International Technical Symposium – Section VI "Advanced Food Processing and Quality Management", November 2013, Guangzhou, China.
- Cubero, S., Alegre, S., Aleixos, N., **Lorente, D.**, Blasco, J., 2013. Autonomous computer vision system for outdoors quality inspection and sorting of fruit after

harvesting. In: 8th CIGR International Technical Symposium – Section VI "Advanced Food Processing and Quality Management", November 2013, Guangzhou, China.

- Frutos, M.J., Wojdylo, A., Carbonell-Barrachina, A.A., Hernández-Herrero, J.A., Pastor, J.J., **Lorente-Garrido, D.**, Blasco, J., 2014. Characterization of flavonoids and antioxidant activity in Citrus peels as a commercial source of bioactive compounds. In: International Conference of the Institute of Food Technologists (IFT14), June 2014, New Orleans, LA, USA.
- **Lorente, D.**, Zude, M., Regen, C., Juste, F., Gómez-Sanchis, J., Blasco, J., 2014. Detection of decay in citrus fruit using absorption and scattering properties. In: International Conference on Agricultural Engineering (AgEng 2014), July 2014, Zurich, Switzerland.
- Cubero, S., Alegre, S., Aleixos, N., **Lorente, D.**, Blasco, J., 2014. Autonomous computer vision system for quality grading of fruit on mobile platforms. In: Applications of Computer Image Analysis and Spectroscopy in Agriculture, July 2014, Montreal, QC, Canada.
- **Lorente, D.**, Gómez-Sanchis, J., Aleixos, N., Cubero, S., Blasco, J., 2014. Hyperspectral system based on two liquid cristal tuneable filters for early detection of citrus fruits decay. In: 5th IASIM Conference in Spectral Imaging, December 2014, Rome, Italy, Book of abstracts, p. 39.

7.4.4. Publications in scientific divulgation journals

- **Lorente, D.**, Cubero, S., Blasco, J., Zude, M., Regen, C., Palou, L., Gómez-Sanchis, J., 2013. Detección automática de podredumbres en cítricos mediante análisis de imágenes backscattering. Horticultura, 309, 88-92.
- Blasco, J., Mellado, M., Aleixos, N., Frutos, M.J., Talens, P., Ortiz, C., Cubero, S., Pastor, J., Blanes, C., Carbonell, A., Albert, F., **Lorente, D.**, 2014. Técnicas avanzadas de inspección y manipulación aplicadas a la determinación automática de la calidad y seguridad de la producción agroalimentaria. Levante Agrícola, 422, 156-160.

References

Abe, N., Kudo, M., Toyama, J., Shimbo, M., 2000. A divergence criterion for classifier independent feature selection. Lecture Notes in Computer Science. Advances in Pattern Recognition, 1876, 668-676.

Aleixos, N., Blasco, J., Navarrón, F., Moltó, E., 2002. Multispectral inspection of citrus in real time using machine vision and digital signal processors. Computers and Electronics in Agriculture, 33, 121-137.

Al-Mallahi, A., Kataoka, T., Okamoto, H., 2008. Discrimination between potato tubers and clods by detecting the significant wavebands. Biosystems Engineering, 100, 329-337.

Alpaydin, E., 2004. Introduction to machine learning. The MIT Press, Cambridge, MA, USA.

Antonucci, F., Pallottino, F., Paglia, G., Palma, A., D'Aquino, S., Menesatti, P., 2011. Non-destructive estimation of mandarin maturity status through portable VIS-NIR spectrophotometer. Food and Bioprocess Technology, 4, 809-813.

Ariana, D.P., Guyer, D.E., Shrestha, B., 2006. Integrating multispectral reflectance and fluorescence imaging for defect detection on apples. Computers and Electronics in Agriculture, 50, 148-161.

Balasundaram, D., Burks, T.F., Bulanona, D.M., Schubert, T., Lee, W.S., 2009. Spectral reflectance characteristics of citrus canker and other peel conditions of grapefruit. Postharvest Biology and Technology, 51, 220-226.

Baranyai, L., Zude, M., 2009. Analysis of laser light propagation in kiwifruit using backscattering and Monte Carlo simulation. Computers and Electronics in Agriculture, 69, 33-39.

Barmore, C.R., Brown, G.E., 1979. Role of pectolytic enzymes and galacturonic acid in citrus fruit decay caused by *Penicillium digitatum*. Phytopathology, 69, 675-678.

Barmore, C.R., Brown, G.E., 1981. Polygalacturonase from citrus fruit infected with *Penicillium italicum*. Phytopathology, 71, 328-331.

Barnes, R.J., Dhanoa, M.S., Lister, S.J., 1989. Standard normal variate transformation and de-trending of near-infrared diffuse reflectance spectra. Applied Spectroscopy, 43, 772-777.

Battiti, R., 1994. Using mutual information for selecting features in supervised neural net learning. IEEE Transactions on Neural Networks, 5, 537-550.

Bei, L., Dennis, G.I., Miller, H.M., Spaine, T.W., Carnahan, J.W., 2004. Acousto-optic tunable filters: fundamentals and applications as applied to chemical analysis techniques. Progress in Quantum Electronics, 28, 67-87.

Bennedsen, B.S., Peterson, D.L., Tabb, A., 2007. Identifying apple surface defects using principal components analysis and artificial neural networks. Transactions of the ASABE, 50, 2257-2265.

Birth, G.S., 1976. How light interacts with foods. In: Gaffney, J.J. (Ed.), Quality detection in foods. ASAE, St. Joseph, USA, pp. 6-11.

Blanc, P.G.R., Blasco, J., Moltó, E., Gómez-Sanchis, J., Cubero, S., 2009. System for the automatic selective separation of rotten citrus fruit. European patent EP2133157A1.

Blanc, P.G.R., Blasco, J., Moltó, E., Gómez-Sanchis, J., Cubero, S., 2010. System for the automatic selective separation of rotten citrus fruit. United States patent US2010/0121484A1.

Blasco, J., Ortiz, C., Sabater, M.D., Moltó, E., 2000. Early detection of fungi damage in citrus using NIR spectroscopy. In: Proceedings of the SPIE, Biological Quality and Precision Agriculture II, Boston, USA, vol. 4203, pp. 47-54.

Blasco, J., Aleixos, N., Moltó, E., 2003. Machine vision system for automatic quality grading of fruit. Biosystems Engineering, 85, 415-423.

Blasco, J., Aleixos, N., Gómez, J., Moltó, E., 2007a. Citrus sorting by identification of the most common defects using multispectral computer vision. Journal of Food Engineering, 83, 384-393.

Blasco, J., Aleixos, N., Moltó, E., 2007b. Computer vision detection of peel defects in citrus by means of a region oriented segmentation algorithm. Journal of Food Engineering, 81, 535-543.

Blasco, J., Aleixos, N., Gómez-Sanchis, J., Moltó, E., 2009. Recognition and classification of external skin damage in citrus fruits using multispectral data and morphological features. Biosystems Engineering, 103, 137-145.

Bonnlander, B.V., Weigend, A.S., 1994. Selecting input variables using mutual information and nonparametric density estimation. In: *Proceedings of the 1994 International Symposium on Artificial Neural Networks* (ISANN'94), Tainan, Taiwan, pp. 42-50.

Bradley, A.P., 1997. The use of the area under the ROC curve in the evaluation of machine learning algorithms. Pattern Recognition, 30, 1145-1159.

Camastra, F., Vinciarelli, A., 2002. Estimating the intrinsic dimension of data with a fractal-based approach. IEEE Transactions on Pattern Analysis and Machine Intelligence, 24, 1404-1407.

Candolfi, A., De Maesschalck, R., Jouan-Rimbaud, D., Hailey, P.A., Massart, D.L., 1999. The influence of data pre-processing in the pattern recognition of excipients near-infrared spectra. Journal of Pharmaceutical and Biomedical Analysis, 21, 115-132.

Cayuela, J.A., 2008. Vis-NIR soluble solids prediction in intact oranges (*Citrus sinensis* L.) cv. Valencia Late by reflectance. Postharvest Biology and Technology, 47, 75-80.

Chang, C., 1976. Acousto-optic devices and applications. IEEE Transactions on Sonics Ultrasound, 23, 2-22.

Cheng, X., Chen, Y., Tao, Y., Wang, C., Kim, M.S., Lefcourt, A., 2004. A novel integrated PCA and FLD method on hyperspectral image feature extraction for cucumber chilling damage inspection. Transactions of the ASAE, 47, 1313-1320.

Choi, E., Lee, C., 2003. Feature extraction based on the Bhattacharyya distance. Pattern Recognition, 36, 1703-1709.

Costa, C., Antonucci, F., Pallottino, F., Aguzzi, J., Sun, D.W., Menesatti, P., 2011. Shape analysis of agricultural products: a review of recent research advances and potential application to computer vision. Food and Bioprocess Technology, 4, 673-692.

Costa, J.A., Hero, A.O., 2004. Geodesic entropic graphs for dimension and entropy estimation in manifold learning. IEEE Transactions on Signal. Processing, 52, 2210-2221.

Cubero, S., Aleixos, N., Moltó, E., Gómez-Sanchis, J., Blasco, J., 2011. Advances in machine vision applications for automatic inspection and quality evaluation of fruits and vegetables. Food and Bioprocess Technology, 4, 487-504.

Dash, M., Liu, H., 1997. Feature selection for classification. Intelligent Data Analysis, 1, 131-156.

Du, C.J., Sun, D.W., 2009. Retrospective shading correlation of confocal laser scanning microscopy beef images for three-dimensional visualization. Food and Bioprocess Technology, 2, 167-176.

Duda, R.O., Hart, P.E., Stork, D.G., 2001. Pattern classification (second ed.). Wiley-Interscience, New York, NY, USA.

Eckert, J.W., Eaks, I.L., 1989. Postharvest disorders and diseases of citrus fruit. In: Reuter, W., Calavan, E.C., Carman, G.E. (Eds.), The citrus industry. University California Press, Berkeley, CA, USA, pp. 179-260.

Eckert, J.W., 1990. Impact of fungicide resistance on citrus fruit decay control. In: Green, M.B., Le Baron, H.M., Moberg, W.K. (Eds.), Managing resistance to agrochemicals. From fundamental research to practical strategies. ACS Symposium Series, American Chemical Society, Washington, DC, USA, vol. 421, pp. 286-302.

ElMasry, G., Wang, N., Vigneault, C., Qiao, J., ElSayed, A., 2008a. Early detection of apple bruises on different background colors using hyperspectral imaging. LWT –Food Science and Technology, 41, 337-345.

ElMasry, G., Nassar, A., Wang, N., Vigneault, C., 2008b. Spectral methods for measuring quality changes of fresh fruits and vegetables. Stewart Postharvest Review, 4, 1-13.

ElMasry, G., Wang, N., Vigneault, C., 2009. Detecting chilling injury in Red Delicious apple using hyperspectral imaging and neural networks. Postharvest Biology and Technology, 52, 1-8.

Erives, H., Fitzgerald, G., 2005. Automated registration of hyperspectral images for precision agriculture. Computer and Electronics in Agriculture, 47, 103-119.

Evans, M.D., Thai, C.N., Grant, J.C., 1998. Development of a spectral imaging system based on a liquid crystal tunable filter. Transactions of the ASABE, 41, 1845-1852.

FAO, 2012. Citrus: statistics –fresh and processed citrus fruit. Food and Agriculture Organization of the United Nations (FAO).

Farrell, T.J., Patterson, M.S., Wilson, B., 1992. A diffusion-theory model of spatially resolved steady-state diffuse reflectance for the noninvasive determination of tissue optical-properties in vivo. Medical Physics, 19, 879-888.

Farrera-Rebollo, R.R., Salgado-Cruz, M.P., Chanona-Pérez, J., Gutiérrez-López, G.F., Alamilla-Beltrán, L., Calderón-Domínguez, G., 2012. Evaluation of image analysis tools for characterization of sweet bread crumb structure. Food and Bioprocess Technology, 5, 474-484.

Fawcett, T., 2006. An introduction to ROC analysis. Pattern Recognition Letters, 27, 861-874.

Fisher, R., 1936. The use of multiple measurements in taxonomic problems. Annals of Eugenics. 7, 179-188.

Fleiss, J.L., 1981. Statistical methods for rates and proportions (second ed.). Wiley-Interscience, New York, NY, USA.

Fu, X., Ying, Y., Lu, H., Xu, H., 2007. Comparison of diffuse reflectance and transmission mode of visible-near infrared spectroscopy for detecting brown heart of pear. Journal of Food Engineering, 83, 317-323.

Fukunaga, K., Olsen, D.R., 1971. An algorithm for finding intrinsic dimensionality of data. IEEE Transactions on Computers, 20, 176-183.

Gaffney, J.J., 1973. Reflectance properties of citrus fruit. Transactions of the ASAE, 16, 310-314.

Garrido-Novell, C., Pérez-Marin, D., Amigo, J.M., Fernández-Novales, J., Guerrero, J.E., Garrido-Varo, A., 2012. Grading and color evolution of apples using RGB and hyperspectral imaging vision cameras. Journal of Food Engineering, 113, 281-288.

Geladi, P., MacDougall, D., Martens, H., 1985. Linearization and scatter-correction for near-infrared reflectance spectra of meat. Applied Spectroscopy, 39, 491-500.

Gelman, A., Hill, J., 2006. Data analysis using regression and multilevel/hierarchical models. Cambridge University Press, Cambridge, UK.

Gitelson, A., Merzyak, M.N., Lichtenthaler, H.K., 1996. Detection of red-edge position and chlorophyll content by reflectance measurements near 700 nm. Journal of Plant Physiology, 148, 501-508.

Goetz, A., Vane, G., Solomon, J., Rock, B., 1985. Imaging spectrometry for Earth remote sensing. Science, 228, 1147-1153.

Gómez, A.H., He, Y., Pereira, A.G., 2006. Non-destructive measurement of acidity, soluble solids and firmness of Satsuma mandarin using VIS-NIR spectroscopy techniques. Journal of Food Engineering, 77, 313-319.

Gómez-Sanchis, J., Moltó, E., Camps-Valls, G., Gómez-Chova, L., Aleixos, N., Blasco, J., 2008a. Automatic correction of the effects of the light source on spherical objects. An application to the analysis of hyperspectral images of citrus fruits. Journal of Food Engineering, 85, 191-200

Gómez-Sanchis, J., Gómez-Chova, L., Aleixos, N., Camps-Valls, G., Montesinos-Herrero, C., Moltó, E., Blasco, J., 2008b. Hyperspectral system for early detection of rottenness caused by *Penicillium digitatum* in mandarins. Journal of Food Engineering, 89, 80-86.

Gómez-Sanchis, J., Martín-Guerrero, J.D., Soria-Olivas, E., Martínez-Sober, M., Magdalena-Benedito, R., Blasco, J., 2012. Detecting rottenness caused by *Penicillium* in citrus fruits using machine learning techniques. Expert Systems with Applications, 39, 780-785.

Gómez-Sanchis, J., Blasco, J., Soria-Olivas, E., Lorente, D., Escandell-Montero, P., Martínez-Martínez, J.M., Martínez-Sober, M., Aleixos, N., 2013. Hyperspectral LCTF-based system for classification of decay in mandarins caused by *Penicillium digitatum* and *Penicillium italicum* using the most relevant bands and non-linears classifiers. Postharvest Biology and Technology, 82, 76-86.

Gowen, A.A., O'Donnell, C.P., Cullen, P.J., Downey, G., Frias, J.M., 2007. Hyperspectral imaging –an emerging process analytical tool. Trends in Food Science & Technology, 18, 590-598.

Grahn, H.F., Geladi, P., 2007. Techniques and applications of hyperspectral image analysis. Wiley, Chichester, UK.

Groenhuis, R.A.J., Ferwerda, H.A., Ten Bosch, J.J., 1983. Scattering and absorption of turbid materials determined from reflection measurements. 1: Theory. Applied Optics, 22, 2456-2462.

Guthrie, J.A., Walsh, K.B., Reid, D.J., Liebenberg, C.J., 2005. Assessment of internal quality attributes of mandarin fruit. 1. NIR calibration model development. Australian Journal of Agricultural Research, 56, 405-416.

Guyon, I., Elisseeff, A., 2003. An introduction to variable and feature selection. Journal of Machine Learning Research, 3, 1157-1182.

Haboudane, D., Miller, J.R., Tremblay, N., Zarco-Tejada, P.J., Dextraze, L., 2002. Integrated narrow-band vegetation índices for prediction agricultura. Remote Sensing of Environment, 81, 416-426.

Han, D., Tu, R., Lu, C., Liu, C., Wen, Z., 2006. Nondestructive detection of brown core in the Chinese pear 'Yali' by transmission visible-NIR spectroscopy. Food Control, 17, 604-608.

Hastie, T., Tibshirani, R., Friedman, J.H., 2009. The elements of statistical learning: data mining, inference, and prediction (second ed.). Springer, New York, NY, USA.

He, Y., Li, X., Shao, Y., 2005. Quantitative analysis of the varieties of apple using near infrared spectroscopy by principal component analysis and BP model. Lecture Notes in Computer Science, 3809, 1053-1056.

Hecht, E., 2001. Optics (fourth ed.). Addison-Wesley, Reading, MA, USA.

Heijden, F.V.D., Duin, R.P.W., Ridder, D.D., Tax, D.M.J., 2004. Classification, parameter estimation and state estimation: an engineering approach using MATLAB. John Wiley & Sons, Cornwall, UK.

Herold, B., Kawano, S., Sumpf, B., Tillmann, P., Walsh, K.B., 2009. VIS/NIR Spectroscopy. In: Zude, M. (Ed.), Optical monitoring of fresh and processed agricultural crops. CRC Press, Boca Raton, USA, pp. 141-250.

Huang, G.B., Zhu, Q.Y., Siew, C.K., 2006. Extreme learning machine: theory and applications. Neurocomputing, 70, 489-501.

Huang, Y., Kangas, L.J., Rasco, B.A., 2007. Applications of artificial neural networks (ANNs) in food science. Critical Reviews in Food Science and Nutrition, 47, 113-126.

IVACE, 2013. Cítricos de la Comunidad Valenciana. Instituto Valenciano de Competitividad Empresarial (IVACE).

Izenman, A.J., 2008. Modern multivariate statistical techniques: regression, classification and manifold learning. Springer, New York, NY, USA.

Jha, S.N., Narsaiah, K., Jaiswal, P., Bhardwaj, R., Gupta, M., Kumar, R., Sharma, R., 2014. Nondestructive prediction of maturity of mango using near infrared spectroscopy. Journal of Food Engineering, 124, 152-157.

Jiménez, A., Beltrán, G., Aguilera, M.P., Uceda, M., 2008. A sensor-software based on artificial neural network for the optimization of olive oil elaboration process. Sensors and Actuators B, 129, 985-990.

Jiménez-Cuesta, M., Cuquerella, J., Martínez-Jávega, J.M., 1981. Determination of a color index for citrus fruit degreening. In: Proceedings of the International Society of Citriculture, vol. 2, pp. 750-753.

Jolliffe, I.T., 2002. Principal component analysis (second ed.). Springer, New York, NY, USA.

Karimi, Y., Maftoonazad, N., Ramaswamy, H.S., Prasher, S.O., Marcotte, M., 2012. Application of hyperspectral technique for color classification avocados subjected to different treatments. Food and Bioprocess Technology, 5, 252-264.

Kays, S.J., 1999. Preharvest factors affecting appearance. Postharvest Biology and Technology, 15, 233-247.

Khanmohammadi, M., Karami, F., Mir-Marqués, A., Bagheri Garmarudi, A., Garrigues, S., de la Guardia, M., 2014. Classification of persimmon fruit origin by near infrared spectrometry and least squares-support vector machines. Journal of Food Engineering, 142, 17-22.

Kim, D.G., Burks, T.F., Qin, J., Bulanon, D.M., 2009. Classification of grapefruit peel diseases using color texture feature analysis. International Journal of Agricultural and Biological Engineering, 2, 41-50.

Kohavi, R., 1995. A study of cross-validation and bootstrap for accuracy estimation and model selection. In: International Joint Conference on Artificial Intelligence (IJCAI), Morgan Kaufmann Publishers, San Mateo, CA, USA, pp. 1137-1143.

Kohno, Y., Kondo, N., Iida, M., Kurita, M., Shiigi, T., Ogawa, Y., Kaichi, T., Okamoto, S., 2011. Development of a mobile grading machine for citrus fruit. Engineering in Agriculture, Environment and Food, 4, 7-11.

Kondo, N., Ahmad, U., Monta, M., Murase, H., 2000. Machine vision based quality evaluation of Iyokan orange fruit using neural networks. Computers and Electronics in Agriculture, 29, 135-147.

Kondo, N., Kuramoto, M., Shimizu, H., Ogawa, Y., Kurita, M., Nishizu, T., Chong, V.K., Yamamoto, K., 2009. Identification of fluorescent substance in mandarin orange skin for machine vision system to detect rotten citrus fruits. Engineering in Agriculture, Environment and Food, 2, 54-59.

Kullback, S., 1987. The Kullback-Leibler distance. The American Statistician, 41, 340-341.

Kurita, M., Kondo, N., Shimizu, H., Ling, P., Falzea, P.D., Shiigi, T., Ninomiya, K., Nishizu, T., Yamamoto, K., 2009. A double image acquisition system with visible and UV LEDs for citrus fruit. Journal of Robotics and Mechatronics, 21, 533-540.

Ladaniya, M.S., 2008. Citrus fruit: biology, technology and evaluation. Elsevier Academic Press, San Diego, CA, USA.

Landis, J.R., Kock, G.G., 1977. The measurement of observer agreement for categorical data. Biometrics, 33, 159-174.

Lawley, D.N., Maxwell, A.E., 1971. Factor analysis as a statistical method (second ed.). Butterworth Co Publishers Ltd., London, UK.

Lee, K.J., Kim, G.Y., Kang, S.W., Son, J.R., Choi, D.S., Choi, K.H., 2004. Measurement of sugar content in citrus using near infrared transmittance. Key Engineering Materials, 270-273, 1014-1019.

Lee, J.A., Verleysen, M., 2007. Nonlinear dimensionality reduction. Springer, New York, NY, USA.

Levina, E., Bickel, P.J., 2005. Maximum likelihood estimation of intrinsic dimension. In: Saul, L.K., Weiss, Y., Bottou, L. (Eds.), Advances in neural information processing systems. The MIT Press, Cambridge, MA, USA, vol. 17.

Li, S., Liao, C., Kwok, J., 2006. Gene feature extraction using t-test statistics and kernel partial least squares. Lecture Notes in Computer Science. Neural Information and Processing, 4234, 11-20.

Li, J., Rao, X., Ying, Y., 2011. Detection of common defects on oranges using hyperspectral reflectance imaging. Computers and Electronics in Agriculture, 78, 38-48.

Lillesand, T.M., Kiefer, R.W., Chipman, J.W., 2004. Remote sensing and image interpretation (fifth ed.). John Wiley, New York, USA.

Limandri, S.P., Bonetto, R.D., Di Rocco, H.O., Trincavelli, J.C., 2008. Fast and accurate expression for the Voigt function. Application to the determination of uranium M linewidths. Spectrochimica Acta Part B: Atomic Spectroscopy, 63, 962-967.

Liu, Y., Chen, Y.R., Wang, C.Y., Chan, D.E., Kim, M.S., 2005. Development of a simple algorithm for the detection of chilling injury in cucumbers from visible/near-infrared hyperspectral imaging. Applied Spectroscopy, 59, 78-85.

Liu, Y., Ying, Y., 2005. Use of FT-NIR spectrometry in non-invasive measurements of internal quality of 'Fuji' apples. Postharvest Biology and Technology, 37, 65-71.

Liu, Y., Chen, Y.R., Wang, C.Y., Chan, D.E., Kim, M.S., 2006. Development of hyperspectral imaging technique for the detection of chilling injury in cucumbers; spectral and image analysis. Applied Engineering in Agriculture, 22, 101-111.

Liu, Y., Sun, X., Ouyang, A., 2010a. Nondestructive measurements of soluble solid content of navel orange fruit by visible-NIR spectrometric technique with PLSR and PCA-BPNN. LWT –Food Science and Technology, 43, 602-607.

Liu, Y., Sun, X., Zhang, H., Aiguo, O., 2010b. Nondestructive measurement of internal quality of Nanfeng mandarin fruit by charge coupled device near infrared spectroscopy. Computers and Electronics in Agriculture, 71, S10-S14.

Lopes, L.B., VanDeWall, H., Li, H.T., Venugopal, V., Li, H.K., Naydin, S., Hosmer, J., Levendusky, M., Zheng, H., Bentley, M.V., Levin, R., Hass, M.A., 2010. Topical delivery of lycopene using microemulsions: enhanced skin penetration and tissue antioxidant activity. Journal of Pharmaceutical Sciences, 99, 1346-1357.

López-García, F., Andreu-García, A., Blasco, J., Aleixos, N., Valiente, J.M., 2010. Automatic detection of skin defects in citrus fruits using a multivariate image analysis approach. Computers and Electronics in Agriculture, 71, 189-197.

Lorente, D., Aleixos, N., Gómez-Sanchis, J., Cubero, S., García-Navarrete, O.L., Blasco, J., 2012. Recent advances and applications of hyperspectral imaging for fruit and vegetable quality assessment. Food and Bioprocess Technology, 5, 1121-1142.

Lorente, D., Blasco, J., Serrano, A.J., Soria-Olivas, E., Aleixos, N., Gómez-Sanchis, J., 2013a. Comparison of ROC feature selection method for the detection of decay in citrus fruit using hyperspectral images. Food and Bioprocess Technology, 6, 3613-3619.

Lorente, D., Zude, M., Regen, C., Palou, L., Gómez-Sanchis, J., Blasco, J., 2013b. Early decay detection in citrus fruit using laser-light backscattering imaging. Postharvest Biology and Technology, 86, 424-430.

Lorente, D., Aleixos, N., Gómez-Sanchis, J., Cubero, S., Blasco, J., 2013c. Selection of optimal wavelength features for decay detection in citrus fruit using the ROC curve and neural networks. Food and Bioprocess Technology, 6, 530-541.

Lu, R., 2004. Multispectral imaging for predicting firmness and soluble solids content of apple fruit. Postharvest Biology and Technology, 31, 147-157.

Lu, R., Peng, Y., 2006. Hyperspectral scattering for assessing peach fruit firmness. Biosystems Engineering, 93, 161-171.

Lu, R., Peng, Y., 2007. Development of a multispectral imaging prototype for real-time detection of apple fruit firmness. Optical Engineering, 46, 123201.

Lu, R., Cen, H., Huang, M., Ariana, D.P., 2010. Spectral absorption and scattering properties of normal and bruised apple tissue. Transactions of the ASABE, 53, 263-269.

Magwaza, L.S., Opara, U.L., Nieuwoudt, H., Cronje, P.J.R., Saeys, W., Nicolaï, B., 2012. NIR spectroscopy applications for internal and external quality analysis of citrus fruit –a review. Food and Bioprocess Technology, 5, 425-444.

Manickavasagan, A., Jayas, D.S., White, N.D.G., Paliwal, J., 2010. Wheat class identification using thermal imaging. Food and Bioprocess Technology, 3, 450-460.

Martínez, A.M., Kak, A.C., 2001. PCA versus LDA. IEEE Transactions on Pattern Analysis and Machine Intelligence, 23, 228-233.

Martínez-Usó, A., Pla, F., García-Sevilla, P., 2005. Multispectral Segmentation by energy minimization for fruit quality estimation. In: Pattern Recognition and Image Analysis: Second Iberian Conference (IbPRIA 2005), June 2005, Estoril, Portugal, LNCS, vol. 3523, pp. 689-696.

McGlone, V.A., Abe, H., Kawano, S., 1997. Kiwifruit firmness by near infrared light scattering. Journal of Near Infrared Spectroscopy, 5, 83-89.

Meinke, M., Friebel, M., 2009. Determination of optical properties of turbid media: continuous wave approach. In: Zude, M. (Ed.), Optical monitoring of fresh and processed agricultural crops. CRC Press, Boca Raton, USA, pp. 44-55.

Mollazade, K., Omid, M., Tab, F.A., Mohtasebi, S.S., 2012. Principles and applications of light backscattering imaging in quality evaluation of agro-food products: a review. Food and Bioprocess Technology, 5, 1465-1485.

Momin, A., Kondo, N., Makoto, K., Ogawa, Y., Yamamoto, K., Shiigi, T., Ninomiya, K., 2011. Evaluation of the reasons why freshly appearing citrus peel fluorescence during automatic inspection by fluorescent imaging technique. In: Proceedings of the SPIE, Tenth International Conference on Quality Control by Artificial Vision, vol. 8000.

Momin, A., Kondo, N., Makoto, K., Ogawa, Y., Yamamoto, K., Shiigi, T., 2012. Investigation of excitation wavelength for fluorescence emission of citrus peels based on UV-VIS spectra. Engineering in Agriculture, Environment and Food, 5, 126-132.

Mourant, J.R., Fuselier, T., Boyer, J., Johnson, T.M., Bigio, I.J., 1997. Predictions and measurements of scattering and absorption over broad wavelength ranges in tissue phantoms. Applied Optics, 36, 949-957.

Muhammed, H., 2005. Hyperspectral crop reflectance data for characterising and estimating fungal disease severity in wheat. Biosystems Engineering, 91, 9-20.

Naidu, R.A., Perry, E.M., Pierce, F.J., Mekuria, T., 2009. The potential of spectral reflectance technique for the detection of Grapevine leafroll-associated virus-3 in two redberried wine grape cultivars. Computers and Electronics in Agriculture, 66, 38-45.

Navarro, L., Pina, J.A., Juarez, J., Ballester-Olmos, J.F., Arregui, J.M., Ortega, C., Navarro, A., Duran-Vila, N., Guerri, J., Moreno, P., Cambra, M., Zaragoza, S., 2002. The citrus variety improvement program in Spain in the period 1975-2001. In: Proceedings of the 15th Conference of the International Organization of Citrus Virologists (IOCV), Riverside, pp. 306-316.

Nicolaï, B.M., Theron, K.I., Lammertyn, J., 2006. Kernel PLS regression on wavelet transformed NIR spectra for prediction of sugar content of apple. Chemometrics and Intelligent Laboratory Systems, 85, 243-252.

Nicolaï, B.M., Beullens, K., Bobelyn, E., Peirs, A., Saeys, W., Theron, I. K., Lammertyn, J., 2007. Non-destructive measurement of fruit and vegetable quality by means of NIR spectroscopy: a review. Postharvest Biology and Technology, 46, 99-118.

Obagwu, J., Korsten, L., 2003. Integrated control of citrus green and blue molds using *Bacillus subtilis* in combination with sodium bicarbonate or hot water. Postharvest Biology and Technology, 28, 187-194.

Obenland, D., Margosan, D., Collins, S., Sievert, J., Fjeld, K., Arpaia, M.L., Thompson, J., Slaughter, D., 2009. Peel fluorescence as a means to identify freeze-damaged navel oranges. HortTechnology, 19, 379-384.

Omid, M., Mahmoudi, A., Omid, M.H., 2010. Development of pistachio sorting system using principal component analysis (PCA) assisted artificial neural network (ANN) of impact acoustics. Expert Systems with Applications, 37, 7205-7212.

Ouardighi, A., Akadi, A., Aboutajdine, D., 2007. Feature selection on supervised classification using Wilks lambda statistic. In: International Symposium on Computational Intelligence and Intelligent Informatics (ISCIII07), vol. 1, pp. 51-55.

Palou, L., Smilanick, J., Usall, J., Viñas, I., 2001. Control postharvest blue and green molds of oranges by hot water, sodium carbonate, and sodium bicarbonate. Plant Disease, 85, 371-376.

Palou, L., Smilanick, J.L., Droby, S., 2008. Alternatives to conventional fungicides for the control of citrus postharvest green and blue molds. Stewart Postharvest Review, 2, 1-16.

Palou, L., Smilanick, J.L., Montesinos-Herrero, C., Valencia-Chamorro, S., Pérez-Gago, M.B., 2011. Novel approaches for postharvest preservation of fresh citrus fruits. In: Slaker, D.A. (Ed.), Citrus fruits: properties, consumption and nutrition. Nova Science Publishers, Inc., New York, NY, USA, pp. 1-45.

Park, B., Lawrence, K., Windhand, W., Buhr, R., 2002. Hyperspectral imaging for detecting fecal and ingesta contaminants on poultry carcasses. Transactions of the ASAE, 45, 2017-2026.

Penache, C., Miclea, M., Bräuning-Demian, A., Hohn, O., Schössler, S., Jahnke, T., Niemax, K., Schmidt-Böcking, H., 2002. Characterization of a high-pressure microdischarge using diode laser atomic absorption spectroscopy. Plasma Sources Science and Technology, 11, 476-483.

Peng, H., Long, F., Ding, C., 2005. Feature selection based on mutual information: criteria of max-dependency, max-relevance, and min-redundancy. IEEE Transactions on Pattern Analysis and Machine Intelligence, 27, 1226-1238.

Peng, Y., Lu, R., 2005. Modeling multispectral scattering profiles for prediction of apple fruit firmness. Transactions of the ASAE, 48, 235-242.

Peng, Y., Lu, R., 2006a. An LCTF-based multispectral imaging system for estimation of apple fruit firmness: Part I: Acquisition and characterization of scattering images. Transactions of ASAE, 49, 259-267.

Peng, Y., Lu, R., 2006b. Improving apple fruit firmness predictions by effective correction of multispectral scattering images. Postharvest Biology and Technology, 41, 266-274.

Peng, Y., Lu, R., 2007. Prediction of apple fruit firmness and soluble solids content using characteristics of multispectral scattering images. Journal of Food Engineering, 82, 142-152.

Plaza, A., Benediktsson, J.A., Boardman, J.W., Brazile, J., Bruzzone, L., Camps-Valls, G., Chanussot, J., Fauvel, M., Gamba, P., Gualtieri, A., Marconcini, M., Tilton, J.C., Trianni, G., 2009. Recent advances in techniques for hyperspectral image processing. Remote Sensing of Environment, 113, S110-S122.

Polder, G., van der Heijden, G.W.A.M., van der Voet, H., Young, I.T., 2004. Measuring surface distribution of carotenes and chlorophyll in ripening tomatoes using imaging spectrometry. Postharvest Biology and Technology, 34, 117-129.

Ponsa, D., López, A., 2007. Feature selection based on a new formulation of the minimal-redundancy-maximal-relevance criterion. Lecture Notes in Computer Science. Pattern Recognition and Image Analysis, 4477, 47-54.

Prechelt, L., 1996. A quantitative study of experimental evaluations of neural network learning algorithms: current research practice. Neural Networks, 9, 457-462.

Qin, J., Lu, R., 2007. Measurement of the absorption and scattering properties of turbid liquid foods using hyperspectral imaging. Applied Spectroscopy, 61, 388-396.

Qin, J., Lu, R., 2008. Measurement of the optical properties of fruits and vegetables using spatially resolved hyperspectral diffuse reflectance imaging technique. Postharvest Biology and Technology, 49, 355-365.

Qin, J., Burks, T.F., Ritenour, M.A., Bonn, W.G., 2009a. Detection of citrus canker using hyperspectral reflectance imaging with spectral information divergence. Journal of Food Engineering, 93, 183-191.

Qin, J., Lu, R., Peng, Y., 2009b. Prediction of apple internal quality using spectral absorption and scattering properties. Transactions of the ASABE, 52, 499-507.

Qin, J., Burks, T.F., Zhao, X., Niphadkar, N., Ritenour, M.A., 2012. Development of a two-band spectral imaging system for real-time citrus canker detection. Journal of Food Engineering, 108, 87-93.

Qin, J., Chao, K., Kim, M.S., Lu, R., Burks, T.F., 2013. Hyperspectral and multispectral imaging for evaluating food safety and quality. Journal of Food Engineering, 118, 157-171.

Qing, Z., Ji, B., Zude, M., 2007. Predicting soluble solid content and firmness in apple fruit by means of laser light backscattering image analysis. Journal of Food Engineering, 82, 58-67.

Qing, Z., Ji, B., Zude, M., 2008. Non-destructive analysis of apple quality parameters by means of laser-induced light backscattering imaging. Postharvest Biology and Technology, 48, 215-222.

Quevedo, R., Aguilera, J.M., 2010. Color computer vision and stereoscopy for estimating firmness in the salmon (Salmon salar) fillets. Food and Bioprocess Technology, 3, 561-567.

Quevedo, R., Aguilera, J.M., Pedreschi, F., 2010. Color of salmon fillets by computer vision and sensory panel. Food and Bioprocess Technology, 3, 637-643.

Rao, C.R., Mitra, S.K., 1972. Generalized inverse of matrices and its applications. Wiley-Interscience, New York, NY, USA.

Rifkin, R., Klautau, A., 2004. In defense of one-vs-all classification. Journal of Machine Learning Research, 5, 101-141.

Rodgers, J.L., Nicewander, A.W., 1988. Thirteen ways to look at the correlation coefficient. The American Statistician, 42, 59-66.

Romano, G., Baranyai, L., Gottschalk, K., Zude, M., 2008. An approach for monitoring the moisture content changes of drying banana slices with laser light backscattering imaging. Food and Bioprocess Technology, 1, 410-414.

Rondeaux, G., Steven, M., Baret, F., 1996. Optimization of soil-adjusted vegetation indices. Remote Sensing of Environment, 55, 95-107.

Salguero-Chaparro, L., Baeten, V., Abbas, O., Peña-Rodríguez, F., 2014. On-line analysis of intact olive fruits by vis-NIR spectroscopy: optimisation of the acquisition parameters. Journal of Food Engineering, 112, 152-157.

Sammon, J.W., 1969. A nonlinear mapping for data structure analysis. IEEE Transactions on Computers, 18, 401-409.

Sánchez, M.T., De la Haba, M.J., Benítez-López, M., Fernández-Novales, J., Garrido-Varo, A., Pérez-Marín, D., 2012. Non-destructive characterization and quality control of intact strawberries based on NIR spectral data. Journal of Food Engineering, 110, 102-108.

Schaare, P.N., Fraser, D.G., 2000. Comparison of reflectance and transmission modes of visible-near infrared spectroscopy for measuring internal properties of kiwifruit (*Actinidia chinensis*). Postharvest Biology and Technology, 20, 175-184.

Schmilovitch, Z., Mizrach, A., Hoffman, A., Egozi, H., Fuchs, Y., 2000. Determination of mango physiological indices by near-infrared spectrometry. Postharvest Biology and Technology, 19, 245-252.

Seifert, B., Zude, M., Spinelli, L., Torricelli, A., 2014a. Optical properties of developing pip and stone fruit reveal underlying structural changes. Physiologia Plantarum, doi:10.1111/ppl.12232.

Seifert, B., Pflanz, M., Zude, M., 2014b. Spectral shift as advanced index for fruit chlorophyll breakdown. Food and Bioprocess Technology, 7, 2050-2059.

Serrano, A.J., Soria, E., Martín, J.D., Magdalena, R., Gómez, J., 2010. Feature selection using ROC curves on classification problems. In: International Joint Conference on Neural Networks (IJCNN 2010), July 2010, Barcelona, Spain, Proceedings, pp. 1980-1985

Shih, F.Y., 2010. Image processing and pattern recognition: fundamentals and techniques. Wiley-IEEE Press, New York, NY, USA.

Sierra, A., 2002. High-order Fisher's discriminant analysis. Pattern Recognition, 35, 1291-1302.

Sim, J., Wright, C.C., 2005. The kappa statistic in reliability studies: use, interpretation, and sample size requirements. Physical Therapy, 85, 257-268.

Slaughter, D.C., Obenland, D.M., Thompson, J.F., Arpaia, M.L., Margosan, D.A., 2008. Non-destructive freeze damage detection in oranges using machine vision and ultraviolet fluorescence. Postharvest Biology and Technology, 48, 341-346.

Song, M., Yang, H., Siadat, S.H., Pechenizkiy, M., 2013. A comparative study of dimensionality reduction techniques to enhance trace clustering performances. Expert Systems with Applications, 40, 3722-3737.

Stace, T.M., Truong, G.W., Anstie, J., May, E.F., Luiten, A.N., 2012. Power-dependent line-shape corrections for quantitative spectroscopy. Physical Review A: Atomic, Molecular and Optical Physics, 86, 012506.

Sun, D.W. (Ed.), 2007. Computer vision technology for food quality evaluation. Academic Press, Elsevier Science, London, UK.

Sun, X., Zhang, H., Liu, Y., 2009. Nondestructive assessment of quality of Nanfeng mandarin fruit by a portable near infrared spectroscopy. International Journal of Agricultural and Biological Engineering, 2, 65-71.

Sun, D.W. (Ed.), 2010. Hyperspectral imaging for food quality analysis and control. Academic Press, Elsevier Science, London, UK.

Tian, T.S., 2010. Dimensionality reduction for classification with high-dimensional data. PhD thesis, VDM Verlag, Saarbrücken, Germany.

Tuchin, V., 2000. Tissue optics: ligh scattering methods and instruments for medical diagnosis. SPIE Press, Bellingham, WA, USA.

Tucker, C.J., 1979. Red and photographic infrared linear combinations for monitoring vegetation. Remote Sensing of Environment, 8, 127-150.

Unay, D., Gosselin, B., 2006. Automatic defect segmentation of 'Jonagold' apples on multi-spectral images: a comparative study. Postharvest Biology and Technology, 42, 271-79.

Van der Maaten, L.J.P., Postma, E.O., van den Herik, H.J., 2009. Dimensionality reduction: a comparative review. Tilburg University Technical Report, TiCC-TR 2009-005.

Vélez-Rivera, N., Gómez-Sanchis, J., Chanona-Pérez, J., Carrasco, J.J., Millán-Giraldo, M., Lorente, D., Cubero, S., Blasco, J., 2014. Early detection of mechanical damage in mango using NIR hyperspectral images and machine learning. Biosystems Engineering, 122, 91-98.

Venables, W.N., Ripley, B.D., 2002. Modern applied statistics with S (fourth ed.). Springer, New York, NY, USA.

Vila-Francés, J., Calpe-Maravilla, J., Gómez-Chova, L., Amorós-López, J., 2010. Analysis of acousto-optic tunable filter performance for imaging applications. Optical Engineering, 49, 113203.

Vila-Francés, J., Calpe-Maravilla, J., Gómez-Chova, L., Amorós-López, J., 2011. Design of a configurable multispectral imaging system based on an AOTF. IEEE Transactions on Ultrasonics, Ferroelectrics, and Frequency Control, 58, 259-262.

Walsh, K.B., Kawano, S., 2009. Near infrared spectroscopy. In: Zude, M. (Ed.), Optical monitoring of fresh and processed agricultural crops. CRC Press, Boca Raton, USA, pp. 192-239.

Wang, S., Li, D., Song, X., Wei, Y., Li, H., 2011a. A feature selection method based on improved Fisher's discriminant ratio for text sentiment classification. Expert Systems with Applications, 38, 8696-8702.

Wang, J., Nakano, K., Ohashi, S., Kubota, Y., Takizawa, K., Sasaki, Y., 2011b. Detection of external insect infestations in jujube fruit using hyperspectral reflectance imaging. Biosystems Engineering, 108, 345-351.

Wang, W., Li, C., Tollner, E.W., Gitaitis, R.D., Rains, G.C., 2012. Shortwave infrared hyperspectral imaging for detecting sour skin (*Burkholderiacepacia*)-infected onions. Journal of Food Engineering, 109, 36-48.

Wang, A., Hu, D., Xie, L., 2014. Comparison of detection modes in terms of the necessity of visible region (VIS) and influence of the peel on soluble solids content (SSC) determination of navel orange using VIS-SWNIR spectroscopy. Journal of Food Engineering, 126, 126-132.

Wang, A., Xie, L., 2014. Technology using near infrared spectroscopic and multivariate analysis to determine the soluble solids content of citrus fruit. Journal of Food Engineering, 143, 17-24.

Weeks, A.R., 1996. Fundamentals of electronic image processing. Wiley-IEEE Press, New York, NY, USA.

Wilcoxon, F., 1945. Individual comparisons by ranking methods. Biometrics Bulletin, 1, 80-83.

Williams, P.C., Norris, K.H. (Eds.), 2001. Near-infrared technology in the agricultural and food industries (second ed.). American Association of Cereal Chemists, St. Paul, Minnesota, USA.

Xia, J., Li, X., Li, P., Ma, Q., Ding, X., 2007. Application of wavelet transform in the prediction of navel orange vitamin C content by near-infrared spectroscopy. Agricultural Sciences in China, 6, 1067-1073.

Xie, L., Ying, Y., Ying, T., 2009. Classification of tomatoes with different genotypes by visible and short-wave near-infrared spectroscopy with least-squares support vector machines and other chemometrics. Journal of Food Engineering, 94, 34-39

Xing, J., Bravo, C., Jancsók, P.T., Ramon, H., De Baerdemaeker, J., 2005. Detecting bruises on 'Golden Delicious' apples using hyperspectral imaging with multiple wavebands. Biosystems Engineering, 90, 27-36.

Xing, J., Bravo, C., Moshou, D., Ramon, H., De Baerdemaeker, J., 2006. Bruise detection on 'Golden Delicious' apples by vis/NIR spectroscopy. Computers and Electronics in Agriculture, 52, 11-20.

Xu, H.R., Ying, Y.B., Fu, X.P., Zhu, S.P., 2007. Near-infrared spectroscopy in detecting leaf miner damage on tomato leaf. Biosystems Engineering, 96, 447-454.

Yang, C.M., Cheng, C.H., Chen, R.K., 2007. Changes in spectral characteristics of rice canopy infested with brown planthopper and leaffolder. Crop Science, 47, 329-335.

Zheng, Y., He, S., Yi, S., Zhou, Z., Mao, S., Zhao, X., Deng, L., 2010. Predicting oleocellosis sensitivity in citrus using VNIR reflectance spectroscopy. Scientia Horticulturae, 125, 401-405.

Zude, M., 2003. Comparison of indices and multivariate models to non-destructively predict the fruit chlorophyll by means of visible spectrometry in apple fruit. Analytica Chimica Acta, 481, 119-126.

Zude, M. (Ed.), 2009. Optical monitoring of fresh and processed agricultural crops. CRC Press, Boca Raton, USA.

Appendix

Published papers in their journal formats

Food Bioprocess Technol (2013) 6:530–541
DOI 10.1007/s11947-011-0737-x

ORIGINAL PAPER

Selection of Optimal Wavelength Features for Decay Detection in Citrus Fruit Using the ROC Curve and Neural Networks

Delia Lorente · Nuria Aleixos · Juan Gómez-Sanchis · Sergio Cubero · Jose Blasco

Received: 11 July 2011 / Accepted: 13 November 2011 / Published online: 2 December 2011
© Springer Science+Business Media, LLC 2011

Abstract Early automatic detection of fungal infections in post-harvest citrus fruits is especially important for the citrus industry because only a few infected fruits can spread the infection to a whole batch during operations such as storage or exportation, thus causing great economic losses. Nowadays, this detection is carried out manually by trained workers illuminating the fruit with dangerous ultraviolet lighting. The use of hyperspectral imaging systems makes it possible to advance in the development of systems capable of carrying out this detection process automatically. However, these systems present the disadvantage of generating a huge amount of data, which must be selected in order to achieve a result that is useful to the sector. This work proposes a methodology to select features in multi-class classification problems using the receiver operating characteristic curve, in order to detect rottenness in citrus fruits by means of hyperspectral images. The classifier used is a multilayer perceptron, trained with a new learning algorithm called extreme learning machine. The results are obtained using images of mandarins with the pixels labelled in five different classes: two kinds of sound skin, two kinds of decay and scars. This method yields a reduced set of features and a classification success rate of around 89%.

Keywords Computer vision · Citrus fruits · Decay · Non-destructive inspection · Hyperspectral imaging · ROC curve

D. Lorente · S. Cubero · J. Blasco (✉)
Centro de Agroingeniería,
Instituto Valenciano de Investigaciones Agrarias (IVIA),
Cra. Moncada-Náquera km 5,
46113 Moncada, Valencia, Spain
e-mail: blasco_josiva@gva.es

N. Aleixos
Instituto Interuniversitario de Investigación en Bioingeniería y Tecnología Orientada al Ser Humano,
Universitat Politècnica de València,
Camino de Vera s/n,
46022 Valencia, Spain

J. Gómez-Sanchis
Intelligent Data Analysis Laboratory, IDAL,
Electronic Engineering Department, Universitat de València,
Dr. Moliner 50,
46100 Burjassot, Valencia, Spain

Introduction

Decay pathogens can enter fruit through wounds sustained during harvesting. This implies that the pathogen is already in the fruit before any treatment is applied in post-harvest (Obagwu and Korsten 2003). Early detection of fungal infections in citrus fruits is especially important in packing-houses because a very small number of infected fruits can spread the infection to a whole batch, thus causing great economic losses and affecting further operations, such as storage and transport. The most important post-harvest damage in citrus packinghouses is caused by *Penicillium* sp. fungi (Eckert and Eaks 1989). Nowadays, the detection of rotten fruit on citrus packing lines is carried out visually under dangerous ultraviolet (UV) illumination, and decay fruits are removed manually. This procedure, however, may be harmful for operators and operationally inefficient, since they must work in shifts of just a few hours. This rate of staff rotation affects the assessment of the quality. A possible solution arises from the use of automatic machine vision systems.

Computer vision has become widely used to automate the inspection of all different types of food commodities like meat (Du and Sun 2009), fish (Quevedo and Aguilera

2010; Quevedo et al. 2010), bakery products (Farrera-Rebollo et al. 2011), grains (Manickavasagan et al. 2010) or fruits (Karimi et al. 2009). In most cases, its use is aimed at the inspection of external features related with quality, such as size, shape, colour or the presence of damage (Cubero et al. 2011). The use of technology based on colour cameras for the detection of external damage of citrus is currently under research. Kim et al. (2009) used colour texture features based on HSI and colour co-occurrence method to detect peel diseases in grapefruit. López-García et al. (2010) used multivariate image analysis with the same objective in citrus fruits. However, some defects, like decay or freeze damage, are very difficult to detect using standard artificial vision systems since they are hardly visible to the human eye and, consequently, by standard red–green–blue (RGB) cameras Blasco et al. (2007). Therefore, different technologies have to be incorporated, such as the use of UV-induced fluorescence (Slaughter et al. 2008; Obenland et al. 2009). In an attempt to automate the current manual tasks of detection of decay, Blanc et al. (2009, 2010) patented an automatic machine for decay detection using UV illumination, and Kurita et al. (2009) developed an inspection system based on simultaneous visible and UV illumination using light-emitting diodes. However, it would be desirable to avoid the use of UV radiation in these tasks which could be achieved by finding out particular wavelengths in the visible or near-infrared (NIR) part of the electromagnetic spectrum.

Images acquired in visible and NIR simultaneously were used to detect different types of damage in citrus fruits by Aleixos et al. (2002) and more recently by Blanc et al. (2009), who attempted to detect common external defects and diseases, including decay, by combining NIR, visible and also UV-induced fluorescence. In this sense, the recent introduction of hyperspectral sensors for the inspection of food (Sun 2010) makes it possible to carry out a more precise analysis of the problem by acquiring images for specific ranges of wavelengths to detect features non-visible features or to select particular sets of some wavelengths related to important physical properties, as indicated in the review of Lorente et al. (2011).

Using spectroscopy, Gaffney (1973) found that different external defects on citrus fruits have different spectral signatures, stated later in the review of Magwaza et al. (2011), which can lead to the selection of certain sets of wavelengths that facilitate the detection of particularly dangerous defects such as canker (Balasundaram et al. 2009). However, in real life, it is not enough just to distinguish between fruit affected by serious diseases and sound fruit. It is important to develop systems capable of separating also produce affected by scars on the rind, or other external defects that only downgrade the quality of the fruit but do not spread among other fruits and do not prevent its marketing in domestic markets Blasco et al. (2009). If they are not taken into account, these cosmetic defects may be confused with the dangerous by an automatic system. Qin et al. (2009) used a hyperspectral system with sensitivity in the range 450–930 nm to detect different kinds of damage that affect the skin of citrus, with particular attention being paid to the detection of canker from other common defects. However, one of the main problems of these systems is the huge amount of data generated (Gómez-Sanchis et al. 2008a).

While a standard RGB image is composed of three images corresponding to the red, green and blue bands, a hyperspectral image consists of a set of monochromatic, narrow-band images that increases the complexity of the analysis and requires more computing time to analyse them with an automatic system, which prevent its use in real-time in-line inspection system. For this reason, it is very important to select only those bands with the most relevant information, while discarding those that do not contribute in any significant way to improve the results. With the aim of detecting different defects on the skin of oranges using a hyperspectral system, Li et al. (2011) used principal component analysis (PCA) to select two sets of six and three optimal wavelengths and later applied PCA and band ratios to detect the defects in these multispectral images.

Generally, statistical methods to reduce dimensionality and select features can be divided into wrapper and filter methods (Guyon and Elisseeff 2003). Filter methods use an indirect measure of the quality of the selected features (e.g. by evaluating the correlation function between each input feature and the dependent variable—class—of the classification problem), obtaining a faster convergence of the selection algorithm. On the other hand, the selection criteria used by wrapper methods are the goodness of fit between the inputs and the output provided by the learning machine under consideration, like, for example, a neural network. Within these methods, a traditional measure for evaluating classifiers is the classification success rate. However, a more suitable way of measuring the quality of a classifier is the area under the receiver operating characteristic (ROC) curve, which is the measure used in the feature selection method proposed in this work. Basic concepts related to classification models are first reviewed for a better understanding of the ROC curve as feature selection method. The ROC curve is a graphical plot of the true positive rate vs. false positive rate for a binary classifier, as its discrimination threshold is varied, this value being defined as that from which a positive class prediction is made (Fawcett 2006). The area under the ROC curve (AUC) is used as a global measure of classifier performance that is invariant to the classifier discrimination threshold and the class distribution (Bradley 1997). Maximum classification accuracy corresponds to an AUC value

of 1, while a random guess separation involves a minimum AUC value of 0.5.

With regard to classification methods, because of their flexibility and the possibility of working with unstructured and complex data like that obtained from biological products, artificial neural networks (ANN) have been applied in almost every aspect of food science, and it is a useful tool for performing food safety and quality analyses. For instance, a combination of principal components analysis and ANN was used by Bennedsen et al. (2007) to detect surface defects on apples. Unay and Gosselin (2006) used a multilayer perceptron (MLP) as a promising technique for segmenting surface defects on apples. Ariana et al. (2006) presented an integrated approach using multispectral imaging in reflectance and fluorescence modes to acquire images of three varieties using two ANN-based classification schemes (binary and multi-class). In the case of citrus fruits, Kondo et al. (2000) used, among other methods, ANN to detect some external and internal features in oranges while Gómez-Sanchis et al. (2012) used minimum redundancy maximum relevance as feature selection method and MLP for pixel classification to detect rottenness in mandarins.

This paper advances in the automatic detection of a dangerous post-harvest disease of citrus fruits, such as fungal decay, and to distinguish fruit with symptoms of decay from sound fruit and affected by minor defects. A feature selection methodology that expands the use of the ROC curve to multi-class classification problems is proposed. This methodology has been applied to the selection of an optimal set of features that are effective in the detection of common defects and decay in citrus fruits using hyperspectral images.

In particular, we have used computer vision for detection of two dangerous types of decay caused by *Penicillium digitatum* Sacc (green mould) and *Penicillium italicum* Wehmer (blue mould) because these pathogens occur in almost all regions of the world where citrus is grown and cause serious post-harvest losses annually (Palou et al. 2001). Furthermore, in order to explore the possibilities of the ROC method as a technique for selecting important wavelengths in fruit inspection, we used an ANN-based classifier trained with a new learning algorithm called extreme learning machine (ELM; Huang et al. 2006).

Feature Selection Methodology

Imaging System

In this work, a hyperspectral vision system based on liquid crystal tunable filters (LCTF) was employed. The set of monochrome images acquired by this system makes up a hyperspectral image from which spatial as well as spectral information can be obtained about the scene. A hyperspectral image can be interpreted as a hypercube, in which two dimensions are spatial (pixels) and the third is the spectrum of each pixel. The system consists of a monochrome camera (CoolSNAP ES, Photometrics) with a high level of sensitivity between 320 and 1,020 nm. It was set to acquire 551×551 pixel images with a resolution of 3.75 pixels/mm. The camera transfers the images to a computer by means of a proprietary frame grabber based on PCI technology. The computer employed is based on a Pentium 4 processor with 1 Gb of random access memory. A lens capable of providing a uniform focus between 400 and 1,000 nm was chosen for use with the system (Xenoplan 1.4/17MM, Schneider).

Two LCTF were used, one sensitive to the visible between 400 and 720 nm (Varispec VIS07, CRI Inc) and one sensitive to NIR in the 650- to 1,100-nm range (Varispec NIR07, CRI Inc). Each fruit was illuminated individually by indirect light from 12 halogen lamps (20 W) inside an aluminium hemispherical diffuser in order to provide good spectral efficiency in the visible and NIR. The lamps were powered by a stabilised power supply (12 V/DC 350 W). Because the sum of efficiencies of the filter, camera and illumination system is different across the selected wavelengths, the acquisition software was programmed to correct the integration time for each particular band that is acquired. Hence, these differences in the efficiency of the filter for each band are offset by calculating the particular integration time for each image in each wavelength using a white reference, so that the spectral response of the system is flat over the whole spectral range.

The filters were placed just in front of the camera lens. One of the main problems arose when it came to changing between visible and infrared filters, since the camera could move when handling the filters, which made it difficult to acquire the exactly same scene with both filters. This problem was solved by designing and installing a system to hold and guide the filters. The two filters were fitted to the support and move on a sliding mechanism, thus allowing each filter to be set in the right place without handling the camera. The arrangement of the image acquisition system inside the inspection chamber is shown in Figure 1.

Fruit Used in the Experiments

The experiments were carried out using mandarins cv. Clemenules (*Citrus clementina* Hort. ex Tanaka) with two kinds of defects: (1) minor defects represented by external scars affecting only the appearance of the fruit and (2) serious diseases that can spread to other fruits caused by

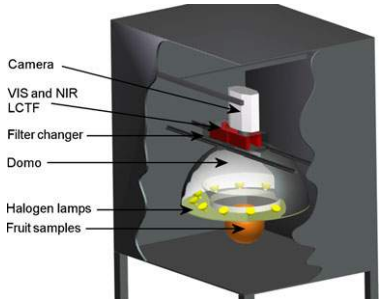

Fig. 1 Scheme of the image acquisition system showing the arrangement of the visible and near-infrared liquid crystal tunable filters

two different fungi; *P. digitatum* and *P. italicum*. The fruits affected by the first type of defects were chosen at random from the packing line of a trading company. On the other hand, damage produced by fungi was caused artificially in sound fruits using an inoculation of spores.

A total of 240 fruits were used: 60 sound fruits, 60 presenting external scars, 60 inoculated with spores of *P. digitatum* and 60 inoculated with spores of *P. italicum*. The inoculation was performed using a suspension of spores with a concentration of 10^6 spores/ml for both fungi, which is sufficient to cause infestation in laboratory conditions (Palou et al. 2001). From the point of view of the post-harvest, it is probably not important to differentiate between both types of decay. However, in this paper, this distinction has been made to test the potential of this method to discriminate between defects that are virtually identical in their early stages to the naked human eye. The fruits were stored for 3 days in a controlled environment at 25 °C and 99% relative humidity. After this period, all the inoculated fruits presented a characteristic patch of rottenness with a diameter between 10 and 35 mm. While rind scars are clearly visible, the colour of rotten skin is similar to the colour of the sound skin around it, thus making it difficult for a human inspector to detect it.

The images were acquired by placing the fruit manually in the inspection chamber and then presenting the damage to the camera. A total of 240 hyperspectral images were acquired from 460 to 1,020 nm, with a spectral resolution of 10 nm. The hyperspectral image was therefore composed of 57 monochrome images of each fruit, which gives a total number of 13,680 monochrome images. The analysis of images started by correcting the effects of illumination on spherical fruits following the methodology described in Gómez-Sanchis et al. (2008b). Then, in order to separate the fruit from the background in the image, the hyperspectral images were pre-processed using masking. The mask was created by thresholding the fruit image at 650 nm, since images at this wavelength provided the best contrast between fruit and background.

Figure 2 shows the RGB images of four fruits corresponding to a sound fruit, a fruit with scars on the rind, a fruit infected by *P. digitatum* and a fruit infected by *P. italicum*, respectively, from top to bottom. The adjoining columns show example images of the same fruits acquired at 530, 640, 740 and 910 nm, respectively. These images were chosen at different wavelengths just to have an overall impression of what could be seen in hyperspectral images but not necessarily used in the experiments. In the RGB images, the damage caused by fungi is hardly visible to the naked human eye.

Labelled Set

In supervised classification, there is a set of n labelled samples, $\{x_i, y_i\}_{i=1..n}$, where x_i represents the m-dimensional feature vector for the ith pixel with label y_i. Here, m represents the spectral bands and spectral indexes, and y defines the universe of all possible labelled classes in the image. In this work, the supervised nature of the problem presented here required the construction of a labelled data set, consisting of m=74 features associated to each pixel, specifically 57 purely spectral variables (reflectance level of the pixel for each acquired band) and 17 spectral indexes calculated by combining several reflectance values, as shown in Table 1. The spectral indexes were used to know if any of them could improve the decay detection in comparison to the use of only purely spectral variables. In order to build this labelled set, n=143,095 pixels were selected manually, and then a human expert assigned them to one of the five classes considered in this work: green sound skin (GS), orange sound skin (OS), defective skin by scars (SC), decay caused by *P. digitatum* (PD) and decay caused by *P. italicum* (PI). Each sample pattern is therefore composed of 74 features and a class label. A background class was not included, since the background pixels were segmented earlier in the pre-processing step.

The labelled set was divided into a training set of 35,774 samples (25% of the total), a validation set of 35,774 samples (25% of the total) and a test set of 71,547 samples (50% of the total). The first two sets were used to build the proposed statistical methods of feature selection and classification and the third one to evaluate classifier performance. The choice of a huge number of pixels in the test set was made in order to check the generalisation capability of the models.

Feature Selection

The feature selection methodology proposed to expand the use of the ROC curve to multi-class classification

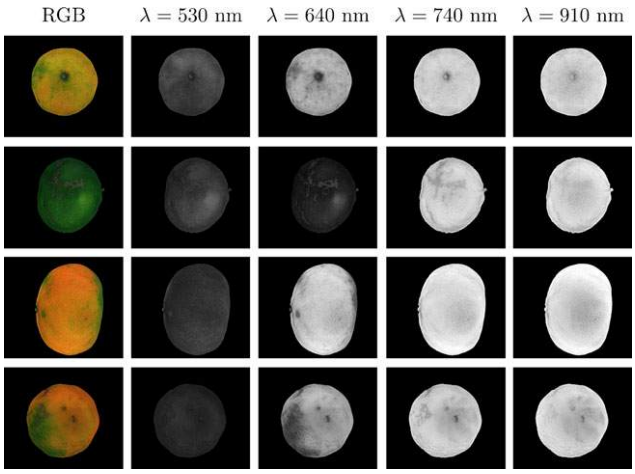

Fig. 2 RGB and monochrome images (530, 640, 740 and 910 nm) of a sound mandarin and mandarins with scars, affected by *P. digitatum* and affected by *P. italicum* (from *top* to *bottom*)

problems consists of two parts: (1) obtaining a ranking of features ordered according to the discriminant relevance of the features and (2) the choice of an optimal number of features from the feature ranking. Both this feature selection method and the classification procedure used in this work were implemented using Matlab 7.9 (Mathworks, Inc.).

Obtaining a Feature Ranking

The first step consists in obtaining a feature ranking for each class. The ROC curve is intended for binary classification problems. However, in this work, problems with more than two classes are considered. Therefore, the *one* vs. *all* (OVA) approach is employed to obtain a feature ranking for each class, which maximises the separation between that class and the others. The OVA structure consists in assuming that the problem has only two classes: a class from which the ranking is obtained and another class grouping the remaining classes (Rifkin and Klautau 2004). In order to obtain these partial rankings, several steps were followed for each class, these steps being similar to the ones used by Serrano et al. (2010) in binary classification problems; the classifier is trained using all the features, taking into account the OVA structure, that is, considering a classification problem with only two classes. Then, the area under the ROC curve is obtained for the classification model using all features (AUC_0). The following parameters are obtained for each input feature x_i:

- Area under the ROC curve for the classifier without taking into account the effect of feature x_i (AUC_i). For this purpose, when using the classifier, the feature x_i is assumed to be constant for every sample, x_i=0.
- Discriminant relevance of feature x_i (DR_i), which is defined as the difference between the area under the ROC curve of the classifier using all the features (AUC_0) and the area without taking into account the effect of feature x_i (AUC_i). This parameter indicates the importance of a feature for the discrimination process carried out by the classifier, considering that the higher the discriminant relevance of a feature is, the more discriminatory that feature will be.
- A z statistic of feature x_i (z_i) is calculated from the discriminant relevance of feature x_i (DR_i), as shown in Eq. 1:

$$z_i = \frac{AUC_0 - AUC_i}{\sqrt{SE_0^2 + SE_i^2 + 2 \cdot \rho \cdot SE_0 \cdot SE_i}} \quad (1)$$

where SE_0 and SE_i are the standard errors of AUC_0 and AUC_i, respectively, and ρ is the correlation between AUC_0 and AUC_i. In this work, a feature is considered to be relevant for the problem when its corresponding z value exceeds 95%, this level being chosen empirically.

Features in each ranking are ordered according to the contribution each of them makes to the discriminant capability of the classification process, and the input features with the highest z values are considered the most discriminatory features.

The second step consists in obtaining a global feature ranking. After obtaining the partial rankings corresponding to each class, the next step is to perform a single global ranking that includes all the classes. The z values corresponding to the rankings for each class are combined by means of their weighted mean (Eq. 2), which assigns a weight to each class in proportion to its relative importance

Table 1 Spectral indexes used in this work as input features

Vegetative index	Estimation	Parameter values used in this work	Reference
NDVI	$\mathrm{NDVI}=\frac{R_{\mathrm{NIR}}-R_{\mathrm{RED}}}{R_{\mathrm{NIR}}+R_{\mathrm{RED}}}$	λ_{NIR}=800 nm λ_{RED}=640 nm	Tucker (1979)
Green NDVI. Version I	$\text{Green NDVI I}=\frac{R_{\mathrm{GREEN}}-R_{\mathrm{RED}}}{R_{\mathrm{GREEN}}+R_{\mathrm{RED}}}$	λ_{GREEN}=550 nm λ_{RED}=640 nm	Yang et al. (2007)
Green NDVI. Version II	$\text{Green NDVI II}=\frac{R_{\mathrm{NIR}}-R_{\mathrm{GREEN}}}{R_{\mathrm{NIR}}+R_{\mathrm{GREEN}}}$	λ_{NIR}=800 nm λ_{GREEN}=550 nm	Gitelson et al. (1996)
WBI	$\mathrm{WBI}=\frac{R_{950\,\mathrm{nm}}}{R_{900\,\mathrm{nm}}}$		Xu et al. (2007)
SAVI	$\mathrm{SAVI}=\frac{(R_{\mathrm{NIR}}-R_{\mathrm{RED}})(1+L)}{R_{\mathrm{NIR}}+R_{\mathrm{RED}}+L}$	λ_{NIR}=800 nm λ_{RED}=640 nm L=0.5	Yang et al. (2007)
PRI	$\mathrm{PRI}=\frac{R_{531\,\mathrm{nm}}-R_{570\,\mathrm{nm}}}{R_{531\,\mathrm{nm}}+R_{570\,\mathrm{nm}}}$	$\lambda_{531\ \mathrm{nm}}\approx$500 nm	Huang et al. (2007)
RVSI	$\mathrm{RVSI}=\frac{R_{714\,\mathrm{nm}}+R_{752\,\mathrm{nm}}}{2}-R_{733\,\mathrm{nm}}$	$\lambda_{714\ \mathrm{nm}}\approx$710 nm $\lambda_{752\ \mathrm{nm}}\approx$750 nm $\lambda_{733\ \mathrm{nm}}\approx$730 nm	Naidu et al. (2009)
MCARI	$\mathrm{MCARI}=[(R_{700\,\mathrm{nm}}-R_{670\,\mathrm{nm}})-0.2(R_{700\,\mathrm{nm}}-R_{550\,\mathrm{nm}})]\times\frac{R_{700\,\mathrm{nm}}}{R_{670\,\mathrm{nm}}}$		Naidu et al. (2009)
VARI	$\mathrm{VARI}=\frac{R_{\mathrm{GREEN}}-R_{\mathrm{RED}}}{R_{\mathrm{GREEN}}+R_{\mathrm{RED}}-R_{\mathrm{BLUE}}}$	λ_{GREEN}=550 nm λ_{RED}=640 nm λ_{BLUE}=480 nm	Naidu et al. (2009)
WI	$\mathrm{WI}=\frac{R_{900\,\mathrm{nm}}}{R_{970\,\mathrm{nm}}}$		Naidu et al. (2009)
TCARI	$\mathrm{TCARI}=3\times[(R_{700\,\mathrm{nm}}-R_{670\,\mathrm{nm}})-0.2(R_{700\,\mathrm{nm}}-R_{550\,\mathrm{nm}})]\times\frac{R_{700\,\mathrm{nm}}}{R_{670\,\mathrm{nm}}}$		Haboudane et al. (2002)
OSAVI	$\mathrm{OSAVI}=\frac{(R_{\mathrm{NIR}}-R_{\mathrm{RED}})(1+0.16)}{R_{\mathrm{NIR}}+R_{\mathrm{RED}}+0.16}$	λ_{NIR}=800 nm λ_{RED}=640 nm	Rondeaux et al. (1996)
CCI	$\mathrm{CCI}=\frac{a\times1{,}000}{L\times b}$	a, b and L are the coordinates of the CIELAB colour space	Jiménez-Cuesta et al. (1981)
Other indexes	$R_{\mathrm{NIR}}-R_{\mathrm{RED}}$	λ_{NIR}=800 nm λ_{RED}=640 nm	Yang et al. (2007)
	$\frac{R_{\mathrm{RED}}}{R_{\mathrm{NIR}}}$	λ_{NIR}=800 nm λ_{RED}=640 nm	Yang et al. (2007)
	$\frac{R_{\mathrm{GREEN}}}{R_{\mathrm{RED}}}$	λ_{GREEN}=550 nm λ_{RED}=640 nm	Yang et al. (2007)
	$\frac{R_{\mathrm{NIR}}}{R_{\mathrm{RED}}}$	λ_{NIR}=800 nm λ_{RED}=640 nm	Yang et al. (2007)

R_λ is the reflectance value at band λ

NDVI normalised difference vegetation index, *WBI* water band index, *SAVI* soil-adjusted vegetation index, *PRI* photochemical reflectance index, *RVSI* red-edge vegetation stress index, *MCARI* modified chlorophyll absorption in reflectance index, *VARI* visible atmospherically resistant index, *WI* water index, *TCARI* transformed chlorophyll absorption in reflectance index, *OSAVI* optimised soil-adjusted vegetation index, *CCI* citrus colour index

in the classification problem. Thus, the global relevance of each feature is obtained, and then each input feature is ranked according to its global relevance. The ranking thus obtained maximises the global separation among all the classes.

$$\overline{z}_i=\frac{\sum_{k=1}^{N} z_{ik}\cdot w_k}{\sum_{k=1}^{N} w_k} \tag{2}$$

where $\overline{z}_i$ is the global relevance of feature x_i, N is the number of different classes, z_{ik} is the z value of feature x_i from the partial ranking for the kth class and w_k is the weight for the kth class.

Choice of an Optimal Number of Features

In this stage, a minimum number of features leading to a saturation trend in the success rate of classification are chosen. The following steps are required to do this:

The initial step is to obtain the evolution of the success rate of classification as a function of the number of features. For this purpose, the classifier is trained using

the first feature of the global ranking and its success rate is evaluated, this process is then repeated including the next feature of the ranking and so on, until all the features are employed sequentially. Then, the first number of input features n satisfying the two conditions in Eqs. 3 and 4 is chosen, where success_n is the success rate of classification using n features, success_{n+1} the success rate with $n+1$ input features and so on.

$$\text{success}_{n+1} - \text{success}_n \leq 1\% \tag{3}$$

$$\text{success}_{n+2} - \text{success}_{n+1} \leq 1\% \tag{4}$$

Classifier

The classifier used to explore the possibilities of the proposed feature selection methodology is a MLP with a single hidden layer, which is the simplest kind of ANN. However, the feature selection procedure is independent of the chosen classification method. ANN is considered to be a commonly used pattern recognition tool in hyperspectral image processing because it is capable of handling a large amount of heterogeneous data with considerable flexibility and has non-linear properties (Plaza et al. 2009).

The most popular ANN is the MLP, which is a feed-forward ANN model that maps sets of input data onto a set of appropriate output and consists of multiple layers of nodes (neurons) in a directed graph that is fully connected from one layer to the next. In particular, the MLP used in this work has an input layer, a single hidden layer and an output layer. MLP can use a large variety of learning techniques, the most popular being backpropagation, which is a supervised learning method based on gradient descent in error that propagates classification errors back through the network and uses those errors to update parameters (Shih 2010). In these classical learning methods, the parameters of the ANN are normally tuned iteratively and thus entail several disadvantages, such a high degree of slowness and convergence to local minima. In order to avoid these problems, the MLP used in this work was trained using ELM, which is a new learning algorithm that determines the ANN parameters (not the optimal architecture) analytically in a faster way instead of tuning them iteratively. This increase of speed in the learning algorithm is very important in order to search the optimal features in our particular feature selection problem using ROC curve. Moreover, this learning algorithm for feed-forward neural networks with a single hidden layer, like an MLP, provides good generalisation performance, as well as an extremely fast learning speed (Huang et al. 2006).

Considering a set of n patterns, $\{x_i, t_i\}_{i=1..n}$ and M nodes in the hidden layer, the MLP output for the ith sample is given by Eq. 5, which is obtained in a straightforward way taking into account the structure of an artificial neuron, as well as the MLP structure (Fig. 3).

$$y_i = \sum_{j=1}^{M} g(\mathbf{w}_j \cdot \mathbf{x}_i) \cdot \beta_j \tag{5}$$

where $\mathbf{w}_j$ is the weight vector connecting the jth hidden node and the input nodes, β_j is the weight vector connecting the jth hidden node and the output nodes and g is an activation function applied to the scalar product of the input vector and the hidden layer weights.

Equation 6 can be written compactly in matrix notation as $\mathbf{y}=\mathbf{G}\cdot\boldsymbol{\beta}$, where $\boldsymbol{\beta}$ is the weight vector of the output layer and $\mathbf{G}$ is given by:

$$\mathrm{G} = \begin{pmatrix} g(\mathbf{w}_1 \cdot \mathbf{x}_1) & \cdots & g(\mathbf{w}_M \cdot \mathbf{x}_1) \\ \vdots & \ddots & \vdots \\ g(\mathbf{w}_1 \cdot \mathbf{x}_n) & \cdots & g(\mathbf{w}_M \cdot \mathbf{x}_n) \end{pmatrix} \tag{6}$$

ELM proposes a random choice of the weights of the hidden layer, $\mathbf{w}_j$, thus making it necessary only to determine the weights of the output layer, $\boldsymbol{\beta}$, analytically through simple generalised inverse operation of the matrix $\mathbf{G}$ according to the Eq. 7:

$$\beta = G^{\dagger} \cdot t \tag{7}$$

where $G^{\dagger} = (G^T \cdot G)^{-1} \cdot G^T$ is the Moore–Penrose generalised inverse of matrix $\mathbf{G}$ (Rao and Mitra 1972), $\mathbf{G}^T$ being the transpose of matrix $\mathbf{G}$.

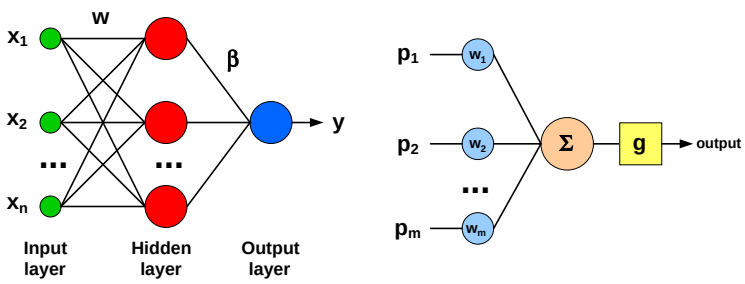

Figure 3 Structures of a multilayer perceptron with a single hidden layer (*left*) and an example of artificial neuron (*right*)

An important issue in practical applications of ELM is how to obtain an optimal number of the hidden nodes in the network architecture in order to achieve a good generalisation performance when training a neural network. The methodology used to select the optimum number of hidden neurons was to estimate the classification success rate for several models, obtained by varying the number of neurons in the hidden layer (Huang et al. 2006). In a first step, architectures with a variable number of hidden neurons from 25 to 1,025 in increments of 100 elements were tested in order to obtain the range of the architectures that fit correctly the data maintaining the generalisation capabilities of the model. These limits were set because networks that are too small cannot model the data properly, while networks that are too large may lead to overfitting (Prechelt 1996). Attending the curve of success rate, the optimum range was selected between 75 and 225 neurons. In a second step, architectures using 75 from 225 neurons were tested selecting finally a MLP that used M=125 neurons in the hidden layer and the sigmoid function as the activation function (g). The classification success rate for the model with 125 hidden neurons was 91.4%, while the success rate for the model with 1,025 neurons was about 95.6%, thus improving by only 4% while the training time burst.

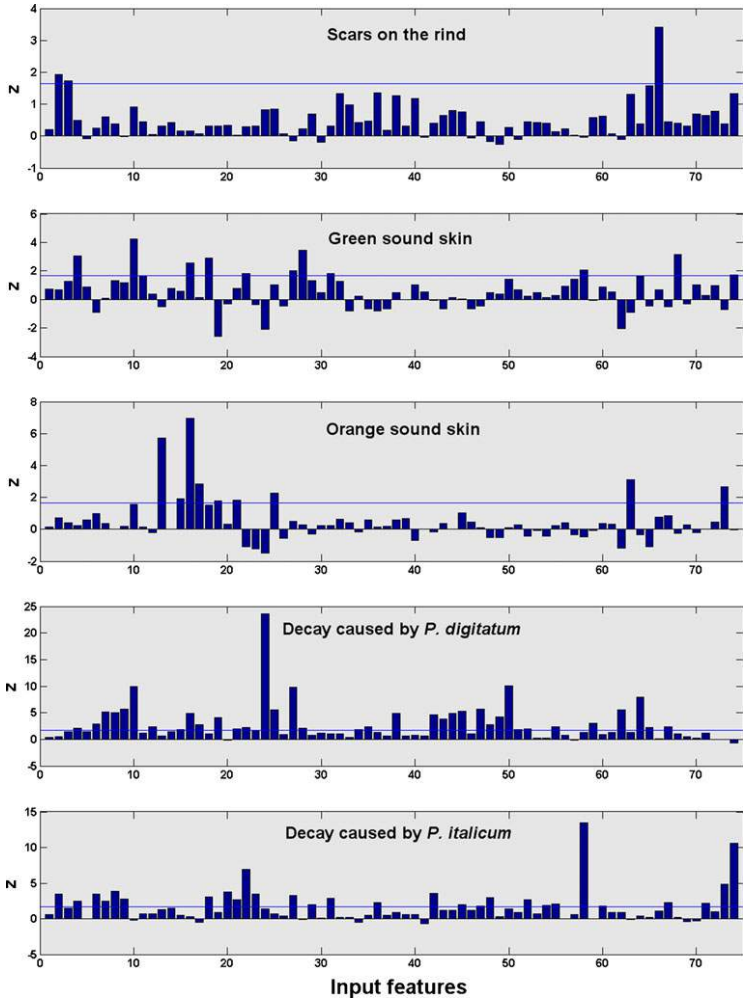

Figure 4 The z statistic of the 74 input features for each of the five classes: defects by scars on the rind, green sound skin, orange sound skin, decay caused by *P. digitatum* and decay caused by *P. italicum*. *Horizontal solid lines* indicate the limit at the 95% level

Table 2 Selected features and their correspondence with the spectral bands or for approach I

Input feature	Spectral index or reflectance value
24	Reflectance at 690 nm
10	Reflectance at 550 nm
58	NDVI
27	Reflectance at 720 nm
16	Reflectance at 610 nm
50	Reflectance at 950 nm

NDVI normalised difference vegetation index

Approaches to the Problem of Decay Detection

This work considers three different approaches to feature selection in the problem of the detection of decay in mandarins, depending on the number of classes involved in the problem and the weight or importance of each class. The typical problem involves the five classes described in the labelled set, all of them having equal importance or weight.

The first approach considers five different classes of similar importance in the classification problem. Therefore, when obtaining the global relevance of each feature, the weights of all the classes were considered to be equal. The aim of this approach is to know the behaviour of the method by considering a quality classification of the fruit, which separates sound fruits from those that only contain cosmetic effects that degrade the appearance and from dangerous infections. However, it is reasonable to assume that in the real world, the classes belonging to decaying skin should be more important for the problem which is the detection of decay.

Therefore, the approach II rests on the idea that the problem has five classes of different importance in the classification. To know the behaviour of the proposed method to enhance the detection of these most important cases, empirical weights were assigned to the classes in Eq. 2, more importance being given to decay classes (w_{PD}=w_{PI}=15), medium importance was given to the scar class (w_{SC}=5) and less to sound classes (w_{GS}=w_{OS}=1).

Moreover, decay is the disease whose detection is of most importance and which has still not been solved by automatic systems. Hence, since the actual aim of a potential inspection system would be to detect decay, it is also important to study the potential of the detection of just infected fruit, which leads to a binary problem: the separation between infected or not infected fruit (approach III). Two classes were defined:

- Decay. This class includes the two kinds of decay presented in this work: infection caused by *P. digitatum* and by *P. italicum*
- Not decay. This class groups the remaining classes: green sound skin, orange sound skin and scars

Results and Discussion

Feature Selection

Figure 4 shows the z statistic obtained for the 74 input features for each of the five classes. This statistic gives the same information as the variation in *AUC*. In addition, it makes it possible to study whether an input feature is discriminant or not.

After obtaining the z values of the input features for each class, the global relevance of each feature was computed for approaches I and II, considering five classes of similar importance and five classes of different importance, respectively. The resulting optimal number of features according to the proposed mathematical criterion, shown in Eqs. 3 and 4, is six for the first approaches and seven for the second. Table 2 shows the set of selected features for the first approach, as well as the correspondence between these features and the spectral indexes or reflectance values associated to them. Similarly, Table 3 shows the set of selected features, ordered according to their importance in the classification problem, for the second approach and the correspondence between the selected input features and the spectral indexes or reflectance values.

When comparing Tables 2 and 3, it can be noticed that most of the input features are coincident in both sets, except feature 16 for approach I and features 74 and 22 in the case of approach II. This is due to the fact that these two features are really important for the detection of pixels belonging to the classes of decay, the highest weights being achieved when the global value of z is obtained, as can be straightforwardly seen from the z values for the *P. italicum* class in Fig. 4.

Furthermore, feature 16 is not selected for the second approach, while in the first approach it is. This is due to the

Table 3 Selected features and their correspondence with the spectral bands or indexes for approach II

Input feature	Spectral index or reflectance value
24	Reflectance at 690 nm
58	NDVI
27	Reflectance at 720 nm
50	Reflectance at 950 nm
10	Reflectance at 550 nm
74	CCI
22	Reflectance at 670 nm

NDVI normalised difference vegetation index, *CCI* citrus colour index

Table 4 Selected features and their correspondence with the spectral indexes or reflectance values for approach III

Input feature	Spectral index or reflectance value
23	Reflectance at 680 nm
60	Green NDVI, version II
28	Reflectance at 730 nm
15	Reflectance at 600 nm

NDVI normalised difference vegetation index

fact that, although this feature has a high level of importance for the classification of pixels belonging to the orange skin class, as shown in Fig. 4, it is considered of low importance when obtaining the global relevance in the second approach. In addition, a general conclusion drawn from analysing the results for both approaches is that all the selected features are important for at least one of the five classes.

Finally, the z values were computed for the third approach, which considers the classification problem to be binary. Therefore, the z statistic values were obtained directly without employing the OVA structure which is only necessary in multi-class problems. The resulting optimal number of features was chosen according to the mathematical criterion shown in Eqs. 3 and 4, being a total of four. Table 4 shows the selected features for the third approach and the correspondence between these features and the spectral indexes or reflectance values.

Classifier Performance Evaluation

The MLP classifier, trained with the ELM algorithm, was evaluated using the selected features for each approach to the problem on the test set of labelled data. Table 5 shows the results for the first approach using the set of six input features provided by the proposed feature selection methodology. An average success rate of 87.5% is achieved with this approach, this parameter being calculated as the sum of the elements on the main diagonal of the obtained confusion matrix divided by the number of classes.

Table 5 Confusion matrix of the classification of pixels for approach I

Prediction/reality	GS (%)	OS (%)	SC (%)	PD (%)	PI (%)
Green skin	96.91	0.13	0.06	0.03	0.00
Orange skin	2.42	94.69	0.01	2.77	1.22
Scars	0.11	0.03	97.34	0.17	0.83
P. digitatum	0.33	3.02	1.49	74.43	23.93
P. italicum	0.23	2.14	1.10	22.60	74.02

Average success rate=87.5%

Table 6 Confusion matrix of the classification of pixels for approach II

Prediction/reality	GS (%)	OS (%)	SC (%)	PD (%)	PI (%)
Green skin	96.61	0.09	0.03	0.06	0.00
Orange skin	2.40	94.56	0.26	2.72	1.79
Scars	0.08	0.05	98.08	0.00	1.10
P. digitatum	0.82	2.38	0.17	75.90	16.83
P. italicum	0.09	2.92	1.47	21.32	80.28

Average success rate=89.1%

For the second approach, the evaluation of pixel classification using the set of seven optimal features leads to the confusion matrix shown in Table 7. This approach yields an average success rate of 89.1%.

When comparing the two confusion matrixes (Tables 5 and 6), it can be observed that the number of well-classified pixels of decay classes (PD and PI) for the second approach is greater than that obtained for the first approach. This is due to the fact that these two classes were given the highest weight when obtaining the global relevance for the second approach. Moreover, in the second approach, the classification of pixels with scars (SC) is improved, although to a lesser extent than the classification of the PD and PI classes. It can also be observed that the results for the classification of the sound classes (GS and OS) hardly vary between the two approaches, since these classes are considered of low importance when obtaining the global relevance in the second approach.

Tables 5 and 6 show, in both cases, that the most difficult task in the pixel classification problem is to discriminate the PD class from the PI class, due to the similarity of the damage caused by the two fungi. On the other hand, the low percentage of sound pixels (GS and OS) classified as rotten pixels (PD and PI) in both approaches should also be highlighted. In practice, this is of great importance since most confusion is done between classes that could be grouped into the same category or commercial importance such as decay (PD and PI) and sound (GS and OS).

To conclude the comparison between approaches I and II, from the results obtained, it can be said that the second

Table 7 Confusion matrix of the classification of pixels for approach III

Prediction/reality	Decay (%)	Not decay (%)
Decay	96.48	5.13
Not decay	3.52	94.87

Average success rate=95.5%

approach generally provides better results than the first one, with an increase in the average success rate from 87.5% to 89.1%. This improvement is obtained by taking into account classes with different degrees of importance in the classification problem.

Similarly, Table 7 shows the results of the evaluation of classifier performance for approach III using the set of four input features selected with the proposed method, where an average success rate of 95.5% was achieved. Better results are obtained for this approach, since similar classes are grouped into a single class, thus avoiding the confusion that occurs in the classification of these similar classes.

Conclusions

In this work, a feature selection methodology has been proposed that expands the use of the ROC curve to multi-class classification problems, in order to select a reduced set of features that are effective in the detection of decay in citrus fruits using hyperspectral images. Once the optimal features have been selected, pixels from the images were classified using an MLP trained with a fast new learning algorithm (ELM).

This selection methodology was applied specifically to the detection of decay in citrus fruits caused by two different fungi, *P. digitatum* and *P. italicum*, and other common types of damage, such as scars. The conclusions drawn after performing several tests can be summarised as follows:

- A reduced number of features have been obtained for each of the three approaches to the problem, these numbers being six for the first approach, seven for the second approach and four for the third one. In addition, all the selected features for the first and second approaches are important for at least one of the five classes defined (two kinds of sound skin, two kinds of decay and scars).
- The set of features selected with the second approach provides better classification results than those obtained with the first one and increases the average success rate from 87.5% to 89.1% by taking into account classes with different degrees of importance in the classification problem. On the other hand, as expected, better results were obtained for the third approach (95.5%), specifically aimed at the detection of decay.

Acknowledgements This work was partially funded by the Instituto Nacional de Investigación y Tecnologia Agraria y Alimentaria de España (INIA) through research project RTA2009-00118-C02-01 and by the Ministerio de Ciencia e Innovación de España (MICINN) through research project DPI2010-19457, both projects with the support of European FEDER funds. This work was also been partially funded by Universitat de València through project UV-INVAE11-41271.

References

Aleixos, N., Blasco, J., Navarrón, F., & Moltó, E. (2002). Multispectral inspection of citrus in real time using machine vision and digital signal processors. *Computers and Electronics in Agriculture, 33*(2), 121–137.

Ariana, D. P., Guyer, D. E., & Shrestha, B. (2006). Integrating multispectral reflectance and fluorescence imaging for defect detection on apples. *Computers and Electronics in Agriculture, 50*, 148–161.

Balasundaram, D., Burks, T. F., Bulanona, D. M., Schubert, T., & Lee, W. S. (2009). Spectral reflectance characteristics of citrus canker and other peel conditions of grapefruit. *Postharvest Biology and Technology, 51*, 220–226.

Bennedsen, B. S., Peterson, D. L., & Tabb, A. (2007). Identifying apple surface defects using principal components analysis and artificial neural networks. *Transactions of the ASABE, 50*(6), 2257–2265.

Blanc, P. G. R., Blasco, J., Moltó, E., Gómez-Sanchis, J., Cubero. S. (2009). System for the automatic selective separation of rotten citrus fruit. European patent EP2133157A1.

Blanc, P. G. R., Blasco, J., Moltó, E., Gómez-Sanchis, J., Cubero, S. (2010). System for the automatic selective separation of rotten citrus fruit. United States patent US2010/0121484A1.

Blasco, J., Aleixos, N., Gómez, J., & Moltó, E. (2007). Citrus sorting by identification of the most common defects using multispectral computer vision. *Journal of Food Engineering, 83*(3), 384–393.

Blasco, J., Aleixos, N., Gómez-Sanchis, J., & Moltó, E. (2009). Recognition and classification of external skin damage in citrus fruits using multispectral data and morphological features. *Biosystems Engineering, 103*, 137–145.

Bradley, A. P. (1997). The use of the area under the ROC curve in the evaluation of machine learning algorithms. *Pattern Recognition, 30*(7), 1145–1159.

Cubero, S., Aleixos, N., Moltó, E., Gómez-Sanchis, J., & Blasco, J. (2011). Advances in machine vision applications for automatic inspection and quality evaluation of fruits and vegetables. *Food and Bioprocess Technology, 4*(4), 487–504.

Du, C.-J., & Sun, D.-W. (2009). Retrospective shading correlation of confocal laser scanning microscopy beef images for three-dimensional visualization. *Food and Bioprocess Technology, 2*, 167–176.

Eckert, J., & Eaks, I. (1989). *Postharvest disorders and diseases of citrus. The citrus industry.* Berkeley: University California Press.

Farrera-Rebollo, R. R., Salgado-Cruz, M. P., Chanona-Pérez, J., Gutiérrez-López, G. F., Alamilla-Beltrán, L., & Calderón-Domínguez, G. (2011). Evaluation of image analysis tools for characterization of sweet bread crumb structure. *Food and Bioprocess Technology.* doi:10.1007/s11947-011-0513-y.

Fawcett, T. (2006). An introduction to ROC analysis. *Pattern Recognition Letters, 27*(8), 861–874.

Gaffney, J. J. (1973). Reflectance properties of citrus fruits. *Transactions of the ASAE, 16*(2), 310–314.

Gitelson, A., Merzyak, M. N., & Lichtenthaler, H. K. (1996). Detection of red-edge position and chlorophyll content by reflectance measurements near 700 nm. *Journal of Plant Physiology, 148*, 501–508.

Gómez-Sanchis, J., Gómez-Chova, L., Aleixos, N., Camps-Valls, G., Montesinos-Herrero, C., Moltó, E., & Blasco, J. (2008). Hyperspectral system for early detection of rottenness caused by *Penicillium digitatum* in mandarins. *Journal of Food Engineering, 89*(1), 80–86.

Gómez-Sanchis, J., Moltó, E., Camps-Valls, G., Gómez-Chova, L., Aleixos, N., & Blasco, J. (2008). Automatic correction of the effects of the light source on spherical objects. An application to

the analysis of hyperspectral images of citrus fruits. *Journal of Food Engineering, 85*(2), 191–200.

Gómez-Sanchis, J., Martín-Guerrero, J. D., Soria-Olivas, E., Martínez-Sober, M., Magdalena-Benedito, R., & Blasco, J. (2012). Detecting rottenness caused by *Penicillium* in citrus fruits using machine learning techniques. *Expert Systems with Applications, 39*(1), 780–785.

Guyon, I., & Elisseeff, A. (2003). An introduction to variable and feature selection. *Journal of Machine Learning Research, 3*, 1157–1182.

Haboudane, D., Miller, J. R., Tremblay, N., Zarco-Tejada, P. J., & Dextraze, L. (2002). Integrated narrow-band vegetation indices for prediction of crop chlorophyll content for application to precision agriculture. *Remote Sensing of Environment, 81*, 416–426.

Huang, G. B., Zhu, Q. Y., & Siew, C. K. (2006). Extreme learning machine: Theory and applications. *Neurocomputing, 70*, 489–501.

Huang, Y., Kangas, L. J., & Rasco, B. A. (2007). Applications of artificial neural networks (ANNs) in food science. *Critical Reviews in Food Science and Nutrition, 47(2)*, 113–126.

Jiménez-Cuesta, M., Cuquerella, J., & Martínez-Jávega, J. M. (1981). Determination of a color index for citrus fruit degreening. In: Proceedings of the International Society of Citriculture, 2, 750–753.

Karimi, Y., Maftoonazad, N., Ramaswamy, H. S., Prasher, S. O., & Marcotte, M. (2009). Application of hyperspectral technique for color classification avocados subjected to different treatments. *Food and Bioprocess Technology*. doi:10.1007/s11947-009-0292-x.

Kim, D. G., Burks, T. F., Qin, J., & Bulanon, D. M. (2009). Classification of grapefruit peel diseases using color texture feature analysis. *International Journal of Agricultural and Biological Engineering, 2*(3), 41–50.

Kondo, N., Ahmad, U., Monta, M., & Murase, H. (2000). Machine vision based quality evaluation of Iyokan orange fruit using neural networks. *Computers and Electronics in Agriculture, 29*, 135–147.

Kurita, M., Kondo, N., Shimizu, H., Ling, P., Falzea, P. D., Shiigi, T., Ninomiya, K., Nishizu, T., & Yamamoto, K. (2009). A double image acquisition system with visible and UV LEDs for citrus fruit. *Journal of Robotics and Mechatronics, 21*(4), 533–540.

Li, J., Rao, X., & Ying, Y. (2011). Detection of common defects on oranges using hyperspectral reflectance imaging. *Computers and Electronics in Agriculture, 78*(1), 38–48.

López-García, F., Andreu-García, A., Blasco, J., Aleixos, N., & Valiente, J. M. (2010). Automatic detection of skin defects in citrus fruits using a multivariate image analysis approach. *Computers and Electronics in Agriculture, 71*, 189–197.

Lorente, D., Aleixos, N., Gómez-Sanchis, J., Cubero, S., García-Navarrete, O. L., & Blasco, J. (2011). Recent advances and applications of hyperspectral imaging for fruit and vegetable quality assessment. *Food and Bioprocess Technology*. doi:10.1007/s11947-011-0725-1.

Magwaza, L. S., Opara, U. L., Nieuwoudt, H., Cronje, P. J. R., Saeys, W., & Nicolaï, B. (2011). NIR spectroscopy applications for internal and external quality analysis of citrus fruit—a review. *Food and Bioprocess Technology.*. doi:10.1007/s11947-011-0697-1.

Manickavasagan, A., Jayas, D. S., White, N. D. G., & Paliwal, J. (2010). Wheat class identification using thermal imaging. *Food and Bioprocess Technology, 3*(3), 450–460.

Naidu, R. A., Perry, E. M., Pierce, F. J., & Mekuria, T. (2009). The potential of spectral reflectance technique for the detection of Grapevine leafroll-associated virus-3 in two redberried wine grape cultivars. *Computers and Electronics in Agriculture, 66*, 38–45.

Obagwu, J., & Korsten, L. (2003). Integrated control of citrus green and blue molds using *Bacillus subtilis* in combination with sodium bicarbonate or hot water. *Postharvest Biology and Technology, 28*(1), 187–194.

Obenland, D., Margosan, D., Collins, S., Sievert, J., Fjeld, K., Arpaia, M. L., Thompson, J., & Slaughter, D. (2009). Peel fluorescence as a means to identify freeze-damaged navel oranges. *HortTechnology, 19*(2), 379–384.

Palou, L., Smilanik, J., Usall, J., & Viñas, I. (2001). Control postharvest blue and green molds of oranges by hot water, sodium carbonate, and sodium bicarbonate. *Plant Disease, 85*, 371–376.

Plaza, A., Benediktsson, J. A., Boardman, J. W., Brazile, J., Bruzzone, L., Camps-Valls, G., Chanussot, J., Fauvel, M., Gamba, P., Gualtieri, A., Marconcini, M., Tilton, J. C., & Trianni, G. (2009). Recent advances in techniques for hyperspectral image processing. *Remote Sensing of Environment, 113*(1), S110–S122.

Prechelt, L. (1996). A quantitative study of experimental evaluations of neural network learning algorithms: Current research practice. *Neural Networks, 9*(3), 457–462.

Qin, J., Burks, T. F., Ritenour, M. A., & Bonn, W. G. (2009). Detection of citrus canker using hyperspectral reflectance imaging with spectral information divergence. *Journal of Food Engineering, 93*, 183–191.

Quevedo, R., & Aguilera. (2010). Color computer vision and stereoscopy for estimating firmness in the salmon (*Salmon salar*) fillets. *Food and Bioprocess Technology, 3*(4), 561–567.

Quevedo, R., Aguilera, J. M., & Pedreschi, F. (2010). Color of salmon fillets by computer vision and sensory panel. *Food and Bioprocess Technology, 3*(5), 637–643.

Rao, C. R., & Mitra, S. K. (1972). *Generalized inverse of matrices and its applications*. New York: Wiley.

Rifkin, R., & Klautau, A. (2004). In defense of one-vs-all classification. *Journal of Machine Learning Research, 5*, 101–141.

Rondeaux, G., Steven, M., & Baret, F. (1996). Optimization of soil-adjusted vegetation indices. *Remote Sensing of Environment, 55*, 95–107.

Serrano AJ, Soria E, Martín JD, Magdalena R & Gómez J (2010) Feature selection using ROC curves on classification problems. In: *International Joint Conference on Neural Networks, IJCNN 2010, 28th–30th July 2010*. Barcelona, Spain. Proceedings, pp 1980–1985.

Shih, F. Y. (2010). *Image processing and pattern recognition: Fundamentals and techniques*. New York: Wiley-IEEE.

Slaughter, D. C., Obenland, D. M., Thompson, J. F., Arpaia, M. L., & Margosan, D. A. (2008). Non-destructive freeze damage detection in oranges using machine vision and ultraviolet fluorescence. *Postharvest Biology and Technology, 48*, 341–346.

Sun, D.-W. (Ed.). (2010). *Hyperspectral imaging for food quality analysis and control*. London: Academic.

Tucker, C. J. (1979). Red and photographic infrared linear combinations for monitoring vegetation. Remote Sensing of Environment, 8(2), 127–150.

Unay, D., & Gosselin, B. (2006). Automatic defect segmentation of 'Jonagold' apples on multi-spectral images: A comparative study. *Postharvest Biology and Technology, 42*, 271–279.

Xu, H. R., Ying, Y. B., Fu, X. P., & Zhu, S. P. (2007). Near-infrared spectroscopy in detecting leaf miner damage on tomato leaf. *Biosystems Engineering, 96*(4), 447–454.

Yang, C. M., Cheng, C. H., & Chen, R. K. (2007). Changes in spectral characteristics of rice canopy infested with brown planthopper and leaffolder. *Crop Science, 47*, 329–335.

Food Bioprocess Technol (2013) 6:3613–3619
DOI 10.1007/s11947-012-0951-1

COMMUNICATION

Comparison of ROC Feature Selection Method for the Detection of Decay in Citrus Fruit Using Hyperspectral Images

D. Lorente · J. Blasco · A. J. Serrano · E. Soria-Olivas · N. Aleixos · J. Gómez-Sanchis

Received: 11 April 2012 / Accepted: 5 August 2012 / Published online: 18 August 2012
© Springer Science+Business Media, LLC 2012

Abstract Hyperspectral imaging systems allow to detect the initial stages of decay caused by fungi in citrus fruit automatically, instead of doing it manually under dangerous ultraviolet illumination, thus preventing the fungal infestation of other sound fruit and, consequently, the enormous economical losses generated. However, these systems present the disadvantage of generating a huge amount of data, which is necessary to select for achieving some result useful for the sector. There are numerous feature selection methods to reduce dimensionality of hyperspectral images. This work compares a feature selection method using the area under the receiver operating characteristic (ROC) curve with other common feature selection techniques, in order to select an optimal set of wavelengths effective in the detection of decay in a citrus fruit using hyperspectral images. This comparative study is done using images of mandarins with the pixels labelled in five different classes: two types of healthy skin, two types of decay and scars, ensuring that the ROC technique generally provides better results than the other methods.

D. Lorente · J. Blasco
Centro de Agroingeniería, Instituto Valenciano de Investigaciones Agrarias (IVIA),
Cra. Moncada-Náquera km 5,
46113 Moncada, Valencia, Spain

A. J. Serrano · E. Soria-Olivas · J. Gómez-Sanchis (✉)
Intelligent Data Analysis Laboratory, IDAL, Electronic Engineering Department, Universitat de València,
Avda. Universitat s/n,
46100 Burjassot, Valencia, Spain
e-mail: juango3@uv.es

N. Aleixos
Instituto en Bioingeniería y Tecnología Orientada al Ser Humano, Universitat Politècnica de València,
Camino de Vera s/n,
46022 Valencia, Spain

Keywords Computer vision · Citrus fruit · Decay · Non-destructive inspection · Hyperspectral imaging · ROC curve · Feature selection

Introduction

Decay caused by fungi is among the main defects affecting the post-harvest and marketing processes of citrus fruit. Infected fruit can be neither stored for a long time nor long-term transported during exportation since a small number of decayed fruit can infect a whole consignment. Thus, fungal infections generate great economic losses to the citrus industry if damaged fruit are not early detected, being *Penicillium* sp. as the fungi that lead to the most post-harvest loses in citrus packinghouses (Eckert and Eaks 1989). In current packing lines, the detection of decayed fruit is made visually by trained operators examining the fruit as it passes under ultraviolet (UV) light. Nevertheless, this method is subjective and potentially dangerous for human skin. The use of automatic machine vision systems is a possible solution for preventing these drawbacks.

Technology based on colour cameras has spread rapidly for the detection of skin damage of fruit and vegetables (Zude 2008; Cubero et al. 2011), being a common technique for the inspection of citrus fruit. For instance, Kondo et al. (2000) studied the possibility of detecting sugar content and acid content of oranges 'Iyokan' using a machine vision system and neural networks. Slaughter et al. (2008) developed a non-contact method of detecting freeze-damaged oranges based on UV fluorescence, and López-García et al. (2010) used multivariate image analysis to detect peel diseases in citrus fruit. Nevertheless, decay lesions are difficult to detect using standard artificial vision systems since they are hardly visible to the human eye and, therefore, by

standard colour cameras (Fig. 1). Blasco et al. (2007) used visible computer vision to detect different types of damages in citrus fruit including decay by green mould. While the success in other defects was high, the detection of decay was lower than 60 % because the damages caused for this disease in the citrus skin are not clearly visible before sporulation. On the other hand, following the fluorescence technique used in the industry to detect decay by humans, Kurita et al. (2009) tried to detect decay in citrus using two lighting systems (visible and UV) changing between them while the fruit is under the view of the camera.

Hyperspectral sensors have been used successfully as an alternative to detect non-visible damages on fruit (Lorente et al. 2012). In the particular case of citrus fruit, different works have been carried out to detect decay lesions (Qin et al. 2009, 2012; Gómez-Sanchis et al. 2012). A hyperspectral image consists of a large number of consecutive monochromatic images of the same scene in each wavelength becoming very important to select only those bands with the most relevant information, while discarding those that do not contribute in any significant way to improve the results, containing redundant information or exhibiting a high degree of correlation. There are numerous feature selection methods to reduce dimensionality that retain most of the original information in fewer bands.

For example, Gómez-Sanchis et al. (2008) evaluated four feature selection methods with the aim of selecting an optimal set of wavelengths in the range 460–1,020 nm for detecting decay in citrus fruit. Xing et al. (2005) used principal component analysis (PCA) to reduce data from a hyperspectral imaging system (400–1,000 nm) for detecting bruises on 'Golden Delicious' apples. PCA was also used by Liu et al. (2005) to obtain spectral features for the detection of chilling injury in cucumbers imaged using a hyperspectral system (447–951 nm). More recently, Li et al. (2011) have used PCA to select most discriminant wavelengths in the range 400–1,000 nm for detecting various common skin defects on oranges. Partial least squares (PLS) or artificial neural networks (ANN) are another techniques commonly used for feature selection purposes. ElMasry et al. (2008) determined some important wavelengths for detecting bruises in 'McIntosh' apples using PLS on hyperspectral images in the range 400–1,000 nm and ElMasry et al. (2009) used ANN to classify apples into injured and normal classes and to detect changes in

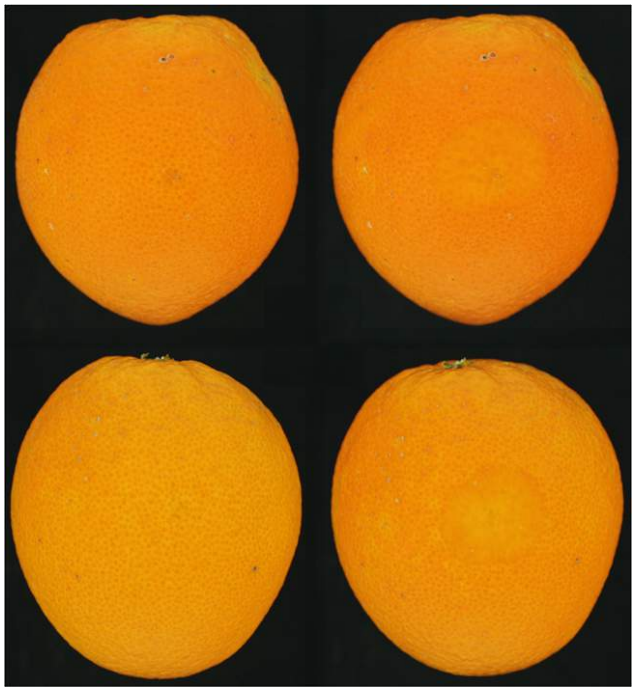

Fig. 1 Sound orange (*left*) and the same fruit showing decay caused by *P. digitatum* (*right*)

firmness due to chilling injury by selecting optimal wavelengths.

Objective

The method used by Lorente et al. (2011) to select most spectral relevant features for detecting decay in citrus fruit was based on the area under the receiver operating characteristic (ROC) curve, which is a promising method to measure the quality of a binary classifier. A novel approach was presented to extend its use to multiclass problems, as is the automatic discrimination of decay lesions in citrus fruits, which is a problem still under research and very important from the agricultural point of view since the damages caused by fungi are hardly visible to the naked human eye and standard vision systems and can be quickly spread to other sound fruits during storage. This work aims to compare our novel approach of the ROC feature selection method with other common feature selection techniques for agricultural multiclass classification problems. We use the detection of decay in citrus fruits using hyperspectral imaging as a benchmark problem by selecting an optimal set of wavelengths effective in the discrimination between common defects and decay lesions in citrus fruit. The comparison of different feature selection techniques is aimed at knowing if the ROC method is a promising technique in multiclass classification problems relative to other commonly used methods in terms of classification accuracy.

Material and Methods

Image Acquisition

The hyperspectral imaging system used was based on liquid crystal tunable filters (LCTF; e.g. Lorente et al. 2011). The system consists of a monochrome camera (CoolSNAP ES, Photometrics, Tucson, USA), a lens providing a uniform focus in the working range (Xenoplan 1.4/17MM, Jos. Schneider Optische Werke GmbH, Bad Kreuznach, Germany), and two LCTF (CRI Varispec VIS07 and NIR07, UK) sensitive to the visible (400–720 nm) and NIR (650–1,100 nm), respectively. The scene was illuminated by halogen lamps placed inside an aluminium hemispherical domo.

For hyperspectral images, a total of 240 'Clemenules' mandarins (*Citrus clementina* Hort. ex Tanaka) collected from a local producer company were used, including 60 without visible damages, 60 presenting external scars, 60 inoculated with spores of *Penicillium digitatum* and 60 inoculated with spores of *Pitalicum italicum*. The inoculation was performed using a suspension of spores with a concentration of 10^6 spores/ml for both fungi, which is sufficient to cause infestation in laboratory conditions (Palou et al. 2001). The images were acquired by presenting manually the damage on the fruit to the camera. A total of 240 hyperspectral images were taken in the range of 460–1,020 nm, with a 10-nm spectral resolution. Each sample pattern in the labelled set consisted of 74 spectral features associated to each pixel (reflectance level for each acquired band—grey level in each monochromatic image—and several spectral indexes) and a class label assigned manually by a human expert. Five different classes were considered in this work: green sound skin (GS), orange sound skin (OS), defective skin by scars (SC), decay caused by *P. digitatum* (PD) and decay caused by *P. italicum* (PI).

Feature Selection Methods

The performance of the method based on the area under the ROC curve is compared with other common feature selection methods. The methods included in this comparative study are: correlation analysis (Rodgers and Nicewander 1988), mutual information (Bonnlander and Weigend 1994), Fisher's discriminant analysis (Venables and Ripley 2002), *t* test (Li et al. 2006), Wilks' lambda (Ouardighi et al. 2007), Bhattacharyya distance (Choi and Lee 2003), minimum redundancy maximum relevance difference criterion (MRMRd) (Ponsa and López 2007), minimum redundancy maximum relevance quotient criterion (MRMRq) (Peng et al. 2005) and Kullback–Leibler divergence (Kullback 1987; Abe et al. 2000). These feature selection techniques have been chosen because they are commonly applied to the analysis of hyperspectral imaging in the fields of pattern recognition and remote sensing, although they have not been used before for automatic fruit or vegetable inspection using computer vision. Therefore it will also be studied if they are suitable and accurate methods for this kind of problems.

In order to get a feature selection for each method, two steps were followed: (1) to obtain a ranking of features ordered according to the discriminant relevance of the features and (2) the selection of an optimal number of features from the feature ranking. The feature selection methods and the classification procedure used in this work were implemented using Matlab 7.9 (The Mathworks, Inc., Natick, USA).

Step I Obtainment of a feature ranking

The obtainment of a feature ranking for each class is the initial step to follow. The feature selection techniques studied are intended for binary classification problems but this work deals with problems with more than two classes. Therefore, the *one vs. all* approach (Rifkin and Klautau 2004) is employed to obtain a feature ranking for each class,

which maximises the separation between that class and the others. The second step consists in obtaining a single global feature ranking for each method that is achieved from the relevance values corresponding to the partial rankings for each class. These relevance values are weighted in proportion to the relative importance of the class in the problem and combined using Eq. 1.

$$\overline{r}_j = \frac{\sum_{k=1}^{N} r_{jk} \cdot w_k}{\sum_{k=1}^{N} w_k} \quad (1)$$

where $\overline{r}_j$ is the global relevance of feature x_j, N is the number of different classes, r_{jk} is the relevance value of feature x_j from the partial ranking for the kth class, and w_k is the weight for the kth class.

After obtaining the global relevance of each feature, each input feature is ranked.

Step II Selection of an optimal number of features

Once the global feature ranking has been obtained, a minimum number of features leading to a saturation trend in the success rate of classification is chosen for each method. The success rate is calculated using the first features in the ranking, then successive features are added in an iterative process until the increment of the success rate is lower than a certain threshold (1 %). The n features that satisfy this condition are then selected.

Area Under ROC Curve

The ROC curve is a graphical plot of the true-positive rate vs. false-positive rate for a binary classifier, as its discrimination threshold is varied; this value being defined as that from which a positive class prediction is made (Fawcett 2006). The area under a ROC curve (AUC) is used as a global measure of classifier performance that is invariant to the classifier discrimination threshold and the class distribution (Bradley 1997). Maximum classification accuracy corresponds to an AUC value of 1, while a random guess separation involves an AUC value of 0.5. Basically, the ROC feature selection method for binary classification problems consists in calculating a z statistic from the discriminant relevance of each feature x_j, defined as the difference between the AUC of a classifier using all the features (AUC_0) and the AUC of a classifier without taking into account the effect of feature x_j (AUC_j) (Serrano et al. 2010).

Classifier

The classifier used in this comparative study is a multilayer perceptron (MLP) with a single hidden layer, being a type of ANN (Plaza et al. 2009). MLP can use a wide range of learning techniques for determining the network parameters, the most commonly used being backpropagation. In these classical learning methods, the parameters of the ANN are usually tuned iteratively, thus entailing several disadvantages, such a high computational complexity and convergence to local minima (Shih 2010). To avoid this, the MLP used in this work avoids these problems by being trained using extreme learning machine (Huang et al. 2006), in the same way as that used in Lorente et al. (2011), which is a new learning algorithm that determines the MLP parameters analytically in a faster way instead of tuning them iteratively providing a good generalisation performance at an extremely fast learning speed.

Approaches to the Problem of Decay Detection

In this work, three different approaches to the problem of the decay detection in mandarins are considered, depending on the number of classes implicated and the importance of each class (Lorente et al. 2011). The approach I involves the five classes described in the labelled set, all of them having equal importance or weight. Therefore, the weights of all the classes were considered to be equal when obtaining the global relevance.

It is, however, realistic to assume that the classes belonging to decaying skin should be more important for decay detection. Hence, approach II gives more importance to decay classes (w_{PD}=w_{PI}=15), medium to the scar class (w_{SC}=5) and less to sound classes (w_{GS}=w_{OS}=1). Furthermore, since the actual objective of a potential inspection system would be to detect decay, it is also important to study the detection of just infected fruit, leading to a binary problem: the separation between infected or not infected fruit (approach III).

Methodology of Comparison

Two different tests were carried out in order to compare the different selection techniques with the ROC feature selection method. The comparison, in both tests, is based on the performance evaluation of the classifier using the different sets of features provided by the methods. The first test (test I) consists in selecting an optimum number of features for each method and for each approach. Therefore, for each method, a different number of features that maximises the classification will be obtained. A different way to make the comparison is using a fixed number of features for all methods (test II). For this test, we have chosen the number of features obtained for the ROC method for each approach.

Table 1 Results of the classifier performance evaluation using the features selected by the different methods for each approach, but being possible a different number of features for each case (test I)

Selection method	Approach I		Approach II		Approach III	
	Success rate (%)	Selected features	Success rate (%)	Selected features	Success rate (%)	Selected features
CA	85.94	5	82.44	3	95.02	2
MI	85.53	5	84.87	4	93.08	4
FDA	86.65	5	82.21	3	95.02	2
TT	85.67	5	79.43	2	95.00	2
WL	85.96	5	82.43	3	95.03	2
BD	83.61	3	81.59	4	94.34	3
MRMRd	85.69	5	85.58	5	96.06	2
MRMRq	85.39	4	88.30	7	95.86	3
KLD	85.55	5	87.48	7	95.43	4
ROC	87.46	6	89.07	7	95.52	4

Results and Discussion

The classification obtained using the ROC method is in general better than those obtained for the other methods in all cases, but MRMRd and MRMRq using the third approach. These results could be expected since the MRMR criterion is recognised as one of the most powerful techniques for feature selection (Peng et al. 2005; Ponsa and López 2007). The success of ROC approach is similar to that obtained using the rest of the methods tested. The differences are not significant and therefore we cannot say that our approach is better than the others in terms of decay detection accuracy. It is, however, important to highlight that the best results are achieved using the ROC method for all tests and all approaches. This result should to be taken into account because it is probably due to the fact that this method not only evaluates the features selection but also optimises the performance of the classifier. Therefore, having similar results, ROC method can achieve slightly better scores.

Table 1 shows the results of the classifier performance evaluation using the different sets of features provided by the feature selection methods, described above, corresponding to the test I. The accuracy, achieved with the ROC method, is higher than that obtained with the other methods, except for MRMR in approach III. However, on one hand, minimal redundancy methods try to extract the features with a high degree of relevance, avoiding those features with redundant information. On the other hand, ROC is a method that provides those bands that were used in a classification problem which fit a classifier in a much robust way in terms of accuracy and significance of the model.

In general, the rest of the methods saturate the criterion of success with fewer bands than those selected by the ROC. This, in theory, means that to reach more approximate results than ROC, the number of bands needed by these methods should be higher. Therefore, the test II was used in order to check the performance of the ROC method using the same number of bands, being six for the first approach, seven for the second approach and four for the third one. As shown in Table 2, the ROC feature method provides higher scores than most of the feature selection methods used in this study. As it happens in test I, the only two methods surpassing the ROC are MRMRd and MRMRq for the third approach. This fact shows that, in the most pessimistic scenario for ROC method (permitting an increase of the number of features for the rest of the methods), it obtains better results than the others except in the case of MRMR methods in approach III. Even though the differences with the other methods are small since all of them are good feature selection methods, in the case of the approach II, which is probably the most realistic scenario

Table 2 Results of the classifier performance evaluation using the features selected by the different methods for each approach, but always employing the same number of features for each method (test II)

Selection method	Approach I (%) (6 features)	Approach II (%) (7 features)	Approach III (%) (4 features)
CA	86.48	83.39	95.09
MI	85.88	87.50	93.08
FDA	86.78	84.12	95.10
TT	85.72	82.92	95.10
WL	86.56	83.39	95.11
BD	85.18	83.59	94.93
MRMRd	86.72	86.37	97.18
MRMRq	86.53	88.30	96.42
KLD	85.77	87.48	95.43
ROC	87.46	89.07	95.52

in the real world, the ROC method is clearly the one that obtains better accuracy.

Conclusions

In the first test, the classification average success rate obtained using the ROC method is greater than that obtained for the other methods in almost every case, except for MRMRd and MRMRq using the third approach. When we use the same number of features for all the methods, the ROC feature method provides generally better results than most of the feature selection methods used in this comparative study, being the average success rate for ROC almost always greater than that obtained for the other methods, only being surpassed by the MRMR methods for the third approach.

Therefore, the ROC feature selection method is a suitable feature selection technique that can be applied with success to multiclass classification problems with a huge amount of features such as the segmentation of hyperspectral images to detect decay in citrus fruit, having at least similar results than other recognised feature selection methods but with the advantage of to optimise, by its nature, the performance of the classifier.

Acknowledgments This work has been partially funded by the Universitat de València through project UV-INV-AE11-41271, by the Instituto Nacional de Investigación y Tecnología Agraria y Alimentaria de España (INIA) through research project RTA2009-00118-C02-01 and by the Ministerio de Ciencia e Innovación de España (MICINN) through research project DPI2010-19457, both projects with the support of European FEDER funds.

References

Abe, N., Kudo, M., Toyama, J., & Shimbo, M. (2000). A divergence criterion for classifier independent feature selection. Lecture notes in computer science. *Advances in Pattern Recognition, 1876*, 668–676.

Blasco, J., Aleixos, N., Gómez, J., & Moltó, E. (2007). Citrus sorting by identification of the most common defects using multispectral computer vision. *Journal of Food Engineering, 83*(3), 384–393.

Bonnlander, B.V., & Weigend, A.S. (1994). Selecting input variables using mutual information and nonparametric density estimation. In: *Proceedings of the 1994 International Symposium on Artificial Neural Networks (ISANN'94)*, Tainan, Taiwan, pp. 42–50.

Bradley, A. P. (1997). The use of the area under the ROC curve in the evaluation of machine learning algorithms. *Pattern Recognition, 30*(7), 1145–1159.

Choi, E., & Lee, C. (2003). Feature extraction based on the Bhattacharyya distance. *Pattern Recognition, 36*(8), 1703–1709.

Cubero, S., Aleixos, N., Moltó, E., Gómez-Sanchis, J., & Blasco, J. (2011). Advances in machine vision applications for automatic inspection and quality evaluation of fruits and vegetables. *Food and Bioprocess Technology, 4*(4), 487–504.

Eckert, J., & Eaks, I. (1989). Postharvest disorders and diseases of citrus. In W. Reuther, E. C. Calavan, & G. E. Carman (Eds.), *The citrus industry*. Berkeley: University California Press.

ElMasry, G., Wang, N., Vigneault, C., Qiao, J., & ElSayed, A. (2008). Early detection of apple bruises on different background colors using hyperspectral imaging. *LWT, 41*, 337–345.

ElMasry, G., Wang, N., & Vigneault, C. (2009). Detecting chilling injury in Red Delicious apple using hyperspectral imaging and neural networks. *Postharvest Biology and Technology, 52*, 1–8.

Fawcett, T. (2006). An introduction to ROC analysis. *Pattern Recognition Letters, 27*(8), 861–874.

Gómez-Sanchis, J., Gómez-Chova, L., Aleixos, N., Camps-Valls, G., Montesinos-Herrero, C., Moltó, E., et al. (2008). Hyperspectral system for early detection of rottenness caused by *Penicillium digitatum* in mandarins. *Journal of Food Engineering, 89*(1), 80–86.

Gómez-Sanchis, J., Martín-Guerrero, J. D., Soria-Olivas, E., Martínez-Sober, M., Magdalena-Benedito, R., & Blasco, J. (2012). Detecting rottenness caused by *Penicillium* in citrus fruits using machine learning techniques. *Expert Systems with Applications, 39*(1), 780–785.

Huang, G. B., Zhu, Q. Y., & Siew, C. K. (2006). Extreme learning machine: theory and applications. *Neurocomputing, 70*, 489–501.

Kondo, N., Ahmad, U., Monta, M., & Murase, H. (2000). Machine vision based quality evaluation of Iyokan orange fruit using neural networks. *Computers and Electronics in Agriculture, 29*, 135–147.

Kullback, S. (1987). The Kullback–Leibler distance. *The American Statistician, 41*, 340–341.

Kurita, M., Kondo, N., Shimizu, H., Ling, P., Falzea, P. D., Shiigi, T., et al. (2009). A double image acquisition system with visible and UV LEDs for citrus fruit. *Journal of Robotics and Mechatronics, 21*(4), 533–540.

Li, S., Liao, C., & Kwok, J. (2006). Gene feature extraction using T-test statistics and Kernel partial least squares. Lecture notes in computer science. *Neural Information and Processing, 4234*, 11–20.

Li, J., Rao, X., & Ying, Y. (2011). Detection of common defects on oranges using hyperspectral reflectance imaging. *Computers and Electronics in Agriculture, 78*(1), 38–48.

Liu, Y., Chen, Y. R., Wang, C. Y., Chan, D. E., & Kim, M. S. (2005). Development of a simple algorithm for the detection of chilling injury in cucumbers from visible/near-infrared hyperspectral imaging. *Applied Spectroscopy, 59*(1), 78–85.

López-García, F., Andreu-García, A., Blasco, J., Aleixos, N., & Valiente, J. M. (2010). Automatic detection of skin defects in citrus fruits using a multivariate image analysis approach. *Computers and Electronics in Agriculture, 71*, 189–197.

Lorente, D., Aleixos, N., Gómez-Sanchis, J., Cubero, S., & Blasco, J. (2011). Selection of optimal wavelength features for decay detection in citrus fruit using the ROC curve and neural networks. *Food and Bioprocess Technology*. doi:10.1007/s11947-011-0737-x.

Lorente, D., Aleixos, N., Gómez-Sanchis, J., Cubero, S., García-Navarrete, O. L., & Blasco, J. (2012). Recent advances and applications of hyperspectral imaging for fruit and vegetable quality assessment. *Food and Bioprocess Technology, 5*(4), 1121–1142.

Ouardighi, A., Akadi, A., Aboutajdine, D. (2007). Feature selection on supervised classification using Wilks lambda statistic. In: *International Symposium on Computational Intelligence and Intelligent Informatics ISCIII07*, 1, pp. 51–55.

Palou, L., Smilanik, J., Usall, J., & Viñas, I. (2001). Control postharvest blue and green molds of oranges by hot water, sodium carbonate, and sodium bicarbonate. *Plant Disease, 85*, 371–376.

Peng, H., Long, F., & Ding, C. (2005). Feature selection based on mutual information: criteria of max-dependency, max-relevance, and min-redundancy. *IEEE Transactions on Pattern Analysis and Machine Intelligence, 27*(8), 1226–1238.

Plaza, A., Benediktsson, J. A., Boardman, J. W., Brazile, J., Bruzzone, L., Camps-Valls, G., et al. (2009). Recent advances in techniques for hyperspectral image processing. *Remote Sensing of Environment, 113*(1), S110–S122.

Ponsa, D., & López, A. (2007). Feature selection based on a new formulation of the minimal-redundancy-maximal-relevance criterion. Lecture notes in computer science. *Pattern Recognition and Image Analysis, 4477*, 47–54.

Qin, J., Burks, T. F., Ritenour, M. A., & Bonn, W. G. (2009). Detection of citrus canker using hyperspectral reflectance imaging with spectral information divergence. *Journal of Food Engineering, 93*, 183–191.

Qin, J., Burks, T. F., Zhao, X., Niphadkar, N., & Ritenour, M. A. (2012). Development of a two-band spectral imaging system for real-time citrus canker detection. *Journal of Food Engineering, 108*(1), 87–93.

Rifkin, R., & Klautau, A. (2004). In defense of one-vs-all classification. *Journal of Machine Learning Research, 5*, 101–141.

Rodgers, J. L., & Nicewander, A. W. (1988). Thirteen ways to look at the correlation coefficient. *The American Statistician, 42*(1), 59–66.

Serrano, A.J., Soria, E., Martín, J.D., Magdalena, R. Gómez, J. (2010). Feature selection using ROC curves on classification problems. In: *International Joint Conference on Neural Networks, IJCNN 2010*. 28th–30th July 2010. Barcelona, Spain. Proceedings, pp. 1980–1985.

Shih, F. Y. (2010). *Image processing and pattern recognition: fundamentals and techniques*. New York: Wiley-IEEE.

Slaughter, D. C., Obenland, D. M., Thompson, J. F., Arpaia, M. L., & Margosan, D. A. (2008). Non-destructive freeze damage detection in oranges using machine vision and ultraviolet fluorescence. *Postharvest Biology and Technology, 48*, 341–346.

Venables, W. N., & Ripley, B. D. (2002). *Modern applied statistics with S* (4th ed.). New York: Springer.

Xing, J., Bravo, C., Jancsók, P. T., Ramon, H., & De Baerdemaeker, J. (2005). Detecting bruises on 'Golden Delicious' apples using hyperspectral imaging with multiple wavebands. *Biosystems Engineering, 90*(1), 27–36.

Zude, M. (Ed.). (2008). *Optical monitoring of fresh and processed agricultural crops*. Boca Raton: CRC.

Postharvest Biology and Technology 86 (2013) 424–430

Contents lists available at ScienceDirect

Postharvest Biology and Technology

journal homepage: www.elsevier.com/locate/postharvbio

Early decay detection in citrus fruit using laser-light backscattering imaging

D. Lorente[a], M. Zude[b], C. Regen[b], L. Palou[c], J. Gómez-Sanchis[d], J. Blasco[a,*]

[a] Centro de Agroingenieria, Instituto Valenciano de Investigaciones Agrarias (IVIA), Cra. Moncada-Náquera km 5, Moncada, 46113 Valencia, Spain
[b] Leibniz-Institute for Agricultural Engineering Potsdam-Bornim (ATB), Max-Eyth-Allee 100, 14469 Potsdam-Bornim, Germany
[c] Centro de Tecnología Poscosecha (CTP), Instituto Valenciano de Investigaciones Agrarias (IVIA), Cra. Moncada-Náquera km 5, Moncada, 46113 Valencia, Spain
[d] Intelligent Data Analysis Laboratory (IDAL), Electronic Engineering Department, Universitat de València, Avda. Universitat s/n, Burjassot, 46100 Valencia, Spain

ARTICLE INFO

Article history:
Received 12 April 2013
Accepted 8 July 2013

Keywords:
Fruit inspection
Citrus fruit
Decay
Laser-light backscattering imaging
LDA classifier
Gaussian–Lorentzian cross product function

ABSTRACT

Early detection of fungal infections in citrus fruit still remains one of the major problems in postharvest technology. The potential of laser-light backscattering imaging was evaluated for detecting decay in citrus fruit after infection with the pathogen *Penicillium digitatum*, before the appearance of fruiting structures (green mould). Backscattering images of oranges cv. Navelate with and without decay were obtained using diode lasers emitting at five different wavelengths in the visible and near infrared range for addressing the absorption of fruit carotenoids, chlorophylls and water/carbohydrates. The apparent region of backscattered photons captured by a camera had radial symmetry with respect to the incident point of the light, being reduced to a one-dimensional profile after radial averaging. The Gaussian–Lorentzian cross product (GL) distribution function with five independent parameters described radial profiles accurately with average R^2 values higher or equal to 0.998, pointing to differences in the parameters at the five wavelengths between sound and decaying oranges. The GL parameters at each wavelength were used as input vectors for classifying samples into sound and decaying oranges using a supervised classifier based on linear discriminant analysis. Ranking and combination of the laser wavelengths in terms of their contribution to the detection of decay resulted in the minimum detection average success rate of 80.4%, which was obtained using laser light at 532 nm that addresses differences in scattering properties of the infected tissue and carotenoid contents. However, the best results were achieved using the five laser wavelengths, increasing the classifier average success rate up to 96.1%. The results highlight the potential of laser-light backscattering imaging for advanced citrus grading.

© 2013 Elsevier B.V. All rights reserved.

1. Introduction

Decay caused by *Penicillium* spp. is among the main problems affecting postharvest and marketing processes of citrus fruit (Palou et al., 2011). Early detection of fungal infections still remains one of the major issues in packinghouses because a small number of decayed fruit can cause the infection of a whole consignment during storage and distribution. Currently, the detection of decayed fruit in packing lines is carried out visually by trained workers inspecting each fruit individually as it passes under ultraviolet (UV) light along a conveyor belt. However, this procedure has a high risk of human error and is potentially harmful for operators (Lopes et al., 2010). Machine vision systems potentially provide a means to detect decayed fruit automatically, thus preventing the drawbacks related to human inspection.

Although the use of technology based on colour cameras has spread rapidly for detecting skin damage of fruit and vegetables (cf. Zude, 2009; Cubero et al., 2011), its application to the external inspection of citrus fruit is only currently under research. For example, Kim et al. (2009) detected peel diseases in grapefruit using colour texture features based on HSI (Hue, Saturation, Intensity) and the colour co-occurrence method. Nevertheless, some defects, such as decay at very early stages, are virtually identical to the sound skin, thus very difficult to detect by the human eye, and consequently, by standard artificial vision systems, which are limited to the visible region of the electromagnetic spectrum (Blasco et al., 2009).

Various machine vision technologies have been incorporated for automatically detecting decay in citrus fruit imitating the fluorescence technique used in the industry by humans. Kurita et al. (2009) developed an inspection system based on two lighting systems

* Corresponding author. Tel.: +34 963424000; fax: +34 963424001.
E-mail address: blasco.josiva@gva.es (J. Blasco).

0925-5214/$ – see front matter © 2013 Elsevier B.V. All rights reserved.
http://dx.doi.org/10.1016/j.postharvbio.2013.07.021

Fig. 1. RGB images of a sound orange used for a control (*left*) and an orange showing early decay symptoms caused by *P. digitatum* (*right*).

(visible and UV) that should be powered alternatively using a stroboscopic mode since the fluorescence effect produced by UV light would be undetectable with a simultaneous use of both systems due to the high intensity of white light. However, the use of UV light has some limitations because not all decay lesions, and not all the citrus cultivars, present the same level of sensitivity to the fluorescence phenomena, and on the contrary, other defects like chilling injury can result in some fluorescence (Slaughter et al., 2008), thus reducing the performance of these systems. In this sense, the recent introduction of hyperspectral sensors for food inspection is a successful alternative to detect non-visible damages on fruit (Lorente et al., 2012b). In the particular case of citrus fruit, different research has been conducted to detect decay lesions. For instance, Gómez-Sanchis et al. (2012, 2013) and Lorente et al. (2012a, 2013) studied the feasibility of a hyperspectral vision system based on liquid crystal tuneable filters (LCTF; 460–1020 nm) for detecting decay in citrus fruit in early stages of infection using halogen lighting instead of the traditional inspection using UV lighting.

Recently, light backscattering imaging (LBI) has been studied as an alternative machine vision technique for assessing fruit quality. When a light beam interacts with a fruit, reflectance, absorption and transmittance occur (Birth, 1976). Particularly, light reflectance (scattering) appears with two different geometries: Fresnel reflectance, which happens when photons are reflected on the surface of the sample; and diffuse reflectance (Meinke and Friebel, 2009). In the latter case, light enters the sample and interacts with the internal components of the fruit, and then it is scattered backward to the exterior tissue surface, thus carrying information related to the morphology and structures of the tissue additional to the absorption properties (Lu, 2004). In recent years, much work has focused on using LBI systems to assess quality of apples and other fresh fruit; however, no research has been reported to detect decay in citrus fruit using this technique. For example, Lu (2004) analyzed backscattering images from apples at multiple wavelengths in the visible and the near-infrared (NIR) region for predicting firmness and soluble solids content. In another study, the variation of moisture content of banana slices subjected to different drying conditions was evaluated by taking backscattering images at 670 nm (Romano et al., 2008). From experiments on bruised apples, Lu et al. (2010) suggested that the scattering analysis would provide good results.

Decay process in citrus fruit implies changes in enzymatic activity, resulting in an enhanced water-soluble pectin fraction, and consequently, weakening of the cell wall (Barmore and Brown, 1979). The subsequent water soaking of the tissue is an early visible symptom of infection in citrus (Barmore and Brown, 1981). Hence, since later changes in the pigment contents, and therefore in the optical properties of fruit tissue, can be expected, the LBI technique could be a promising tool for detecting decay in citrus fruit. The main objective of this research work was to evaluate the potential of laser-light backscattering imaging as a tool for the automatic detection of green mould caused by *P. digitatum* on citrus fruit. For this purpose, diode lasers emitting in the visible and NIR range were used to obtain backscattering images of citrus fruit aiming for the classification of fruit into two classes (sound and decaying oranges). The ultimate aim of this work was to evaluate and compare laser wavelengths in terms of their contribution to the detection of decay.

2. Materials and methods

2.1. Fruit and fungal inoculation

The experiments were carried out using sweet oranges (*Citrus sinensis* L. Osbeck) cv. Navelate collected during the 2012 harvest season from the field collection of the Citrus Germplasm Bank at the IVIA (Spain) (Navarro et al., 2002). A total of 100 fruit were used for the experiments: 50 oranges were superficially injured on the rind and inoculated with spores of *P. digitatum* and the other 50 were injured in the same way but treated with sterilized water for control purposes. *P. digitatum* isolate NAV-7, from the fungal culture collection of the IVIA CTP, was cultured on potato dextrose agar (PDA, Sigma–Aldrich Chemical Co., St. Louis, MA, USA) plates at 25 °C. Conidia from 7 to 14 day old cultures were taken from the agar surface with a sterile glass rod and transferred to a sterile aqueous solution of 0.05% Tween® 80 (Panreac, S.A.U., Spain). The conidial suspension was filtered through two layers of cheesecloth to separate hyphal fragments and adjusted to a concentration of 10^6 spores/mL using a haemocytometer. For inoculation, 20 μL of the conidial suspension was placed on the equator of each fruit by immersing the tip of a stainless steel rod, 1 mm wide and 2 mm in length, in the suspension and inserting it in the fruit rind. A concentration of 10^6 spores/mL of *P. digitatum* is the most appropriate to effectively infect citrus fruit in laboratory conditions (Palou et al., 2001). The fruit were stored for four days in a controlled environment at 20 °C and 65% RH. After this period, all the inoculated fruit presented lesions due to decay of an average diameter of 30 mm. Fig. 1 shows the images of a sound control orange and an infected orange.

2.2. Imaging system

In this work, a laser light backscattering imaging system was employed. This system mainly consisted of a CCD (charge-coupled device) based camera (JAI CV-A50 IR) with a zoom lens (F2.5 and

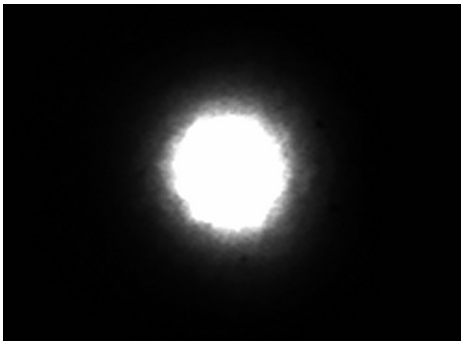

Fig. 2. Example of a raw backscattering image.

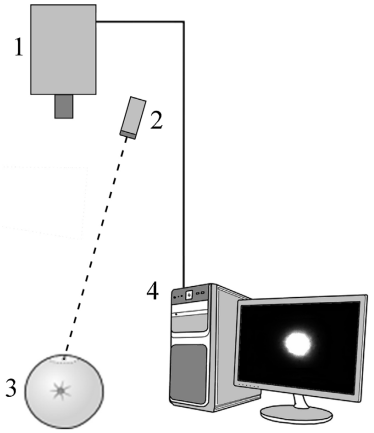

Fig. 3. Scheme of the laser light backscattering system. 1: CCD camera with lens; 2: laser source; 3: fruit sample; and 4: computer.

focal lengths of 18–108 mm), five solid-state laser diode modules emitting at different wavelengths (532, 660, 785, 830 and 1060 nm) used alternately as light sources and a computer for controlling the camera. After penetrating into the fruit tissue, the fraction of the light backscattered to the fruit surface was recorded by the camera and transferred to the computer. A typical raw backscattering image is shown in Fig. 2.

The imaging system was set up in a dark room in order to prevent the influence of ambient light. It was configured to acquire 720 × 576 pixel images with a resolution of 0.073 mm/pixel. Parameters of laser sources are shown in Table 1. The incident angle of the light beam was set to 7° with respect to the vertical axis for all the laser sources and the distance from the laser sources to the fruit sample was chosen according to the focus of each laser (Qing et al., 2007). This setting allowed for the assumption that the light beam was almost perpendicular to the fruit surfaces, thus obtaining images symmetric with respect to the incident point (Mollazade et al., 2012). The arrangement of the image acquisition system is pictured in Fig. 3. The backscattering images were acquired by placing the fruit manually in the imaging system presenting the damage to the camera. A total of five images were acquired for each of the 100 orange samples at the five laser wavelengths which gave a total number of 500 backscattering images.

2.3. Function for describing backscattering profiles

Backscattering images had radial symmetry with respect to the light incident point and their intensity decreases with increasing distance from the incident point (Fig. 2). The images were reduced to one-dimensional profiles after radial averaging (Lu, 2004). For this purpose, the centre of beam incident point was identified for each backscattering image using the weighted centre of gravity method (Weeks, 1996), which considers that the centre is a point in which the maximum light intensity occurs. The radial intensity of the backscattering profiles was then calculated by obtaining the average value of all pixels within each circular ring with one pixel size (0.073 mm).

Backscattering profiles thus obtained could be used directly as a feature vector to predict the presence of damage on the skin of the fruit by a multivariate calibration model. In order to get more robust and fast predictions, data reduction was targeted. One method for this is to find the parameters of symmetric distribution functions describing the backscattering profiles.

Moreover, it is advisable to perform some pre-processing on the profiles to fit the backscattering profiles more accurately, such as removing the data points within and adjacent to the light incident area since these points are saturated, or shifting the profiles towards the profile centre by a distance equal to the number of removed data points in the saturation area (Peng and Lu, 2005). In this work, all the data points with a greyscale level (0–255) higher than 253 were removed.

Subsequently to pretests using various distribution functions (data not shown), the Gaussian–Lorentzian cross product (GL) function was applied. This distribution function is a Voigt approximation that combines a Gaussian and a Lorentzian in a multiplicative form. GL is commonly used in spectroscopy; also for describing laser profiles (Penache et al., 2002; Limandri et al., 2008; Stace et al., 2012). The GL function is mathematically expressed by Eq. (1):

$$I(x) = a + \frac{b}{[1 + e((x-c)/d)^2] \exp[((1-e)/2)((x-c)/d)^2]} \quad (1)$$

where I is the light intensity of each circular band after radial averaging; x is the scattering distance expressed as number of data points (pixels); a is the asymptotic value of light intensity when x approaches infinity; b is the peak value of estimated light intensity at the centre; c is the centre parameter; d is the full scattering width that produces the half maximum peak value; e is related to the shape. The shape parameter e varies from 0 to 1; a value of 0 results in the pure Gaussian function, whereas the pure Lorentzian occurs with a value of 1. Fig. 4 shows a backscattering profile described by this GL distribution function with five parameters.

The GL function was used to fit the backscattering profiles at the five laser wavelengths for each fruit sample. A programme based on nonlinear least squares regression analysis (Gelman and Hill, 2006)

Table 1
Parameters of laser sources.

Wavelength (nm)	Output (mW)	Beam size (mm)
532	10	2.5 × 2.5
660	2	4.0 × 4.0
785	45	1.0 × 1.0
830	30	1.0 × 1.0
1060	85	1.5 × 5.25

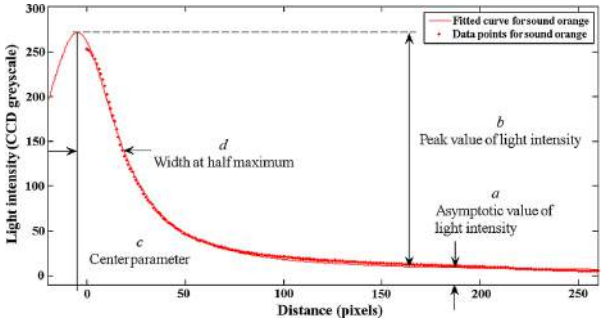

Fig. 4. Gaussian–Lorentzian cross product distribution model for backscattering profiles.

was written using Curve Fitting Toolbox of Matlab 7.9 (Mathworks, Inc.) in order to fit the backscattering profiles to the GL function and to estimate the five GL parameters for each sample at each laser wavelength. The remaining algorithms in this work, such as classification methods, were also implemented using Matlab environment.

2.4. Classifier

Linear discriminant analysis (LDA), also known as Fisher discriminant analysis (Fisher, 1936), is a supervised method of dimensionality reduction and classification used in statistics, pattern recognition and machine learning (Sierra, 2002; Wang et al., 2011). LDA aims to find a linear projection of high-dimensional data onto a lower dimensional space ($c-1$ dimensions in a problem with c classes) where the class separation is maximized. This is achieved by maximizing the ratio of the variance between the classes and variance within the classes (Duda et al., 2001). LDA has no free parameters to be adjusted and the extracted features are potentially interpretable under linearity assumptions. Furthermore, LDA is closely related to principal component analysis (PCA). The main difference between both linear projection techniques is that LDA explicitly attempts to model the difference between the classes of data, while PCA does not take into account any difference in class due to its unsupervised nature. LDA method therefore performs better for classification purposes (Martínez and Kak, 2004).

2.5. Labelled set

In supervised classification, there is a set of n labelled samples, $\{\mathbf{x}_i, t_i\}_{i=1..n}$, where x_i represents the m-dimensional feature vector for the i-th sample with label t_i In this work, the supervised nature of the LDA classifier required the construction of a labelled data set, consisting of $m=25$ features associated to each orange sample, specifically the five GL parameters at each of the five laser wavelengths obtained from fitting the profiles.

In order to build this labelled set, the $n=100$ oranges were assigned to one of the two classes considered in this work: sound oranges and oranges presenting decay. Each sample pattern was therefore composed by 25 features and a class label. The labelled set was divided into a calibration set of 50 samples (50% of the total) and a validation set of 50 samples (50% of the total). The first set was used to build the proposed classification method and the second one to evaluate its performance. In the validation set, the same number of samples as in the calibration set was chosen in order to check the generalization capability of the classifier.

2.6. Development and validation of the classification models

LDA classification method and parameters obtained with GL at five laser wavelengths were used to classify fruit samples. Laser wavelengths were ranked in terms of their contribution to decay detection. In order to rank wavelengths, the LDA classifier was first build and evaluated using the five GL parameters corresponding to each individual wavelength as feature vector. Laser wavelengths were then ranked in ascending order of classification average success rate values. The best single wavelength that had the highest success rate was selected. The next step is to obtain the best two wavelengths. Each of the remaining wavelengths was individually added to the best single wavelength, and the corresponding success rate values were computed for all two-wavelength combinations. The best two wavelengths were chosen when they had the highest success rate among all two-wavelength combinations. This procedure was then repeated for obtaining the best three wavelengths and so on, until all wavelengths were ranked.

The calibration set of labelled data was used to build the classification models and the validation set to evaluate classifier performance. Apart from calculating the classification average success rates to assess the performance of classification, Cohen's kappa statistic values were computed to evaluate the classification bias (Fleiss, 1981). Classification average success rate provided a measure for classification accuracy with a range from 0% to 100%, this parameter being calculated as the number of correctly classified samples divided by the total number of samples. Cohen's kappa statistic gave information about if classifier was biased towards one of the two classes, varying from 0 to 1, with a value of 1 representing a completely unbiased classifier.

3. Results and discussion

3.1. Description of backscattering profiles

For the five laser wavelengths, the GL function described backscattering profiles with average R^2 values higher or equal to 0.998 and average RMSE lower or equal to 2.54 (CCD greyscale) (Table 2). These values were calculated by averaging the coefficients of determination and the RMSEs corresponding to the 100 orange samples at each laser wavelength.

The average GL parameters and the resulting average fitted curves obtained for the backscattering profiles of sound oranges and oranges with decay at the five laser wavelengths are shown in Fig. 5. A significance test (p-value < 0.05, one-tailed paired t-test) was applied to the data in order to determine if the differences between average parameters of sound oranges and decaying

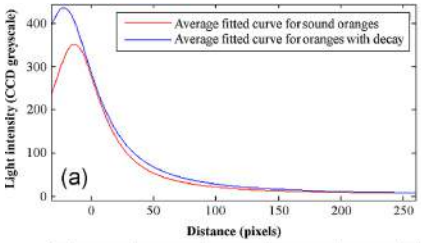

	Sound	Decaying
a (greyscale)*	3.72	2.99
b (greyscale)*	348.80	433.64
c (pixels)*	-13.30	-21.84
d (pixels *	25.97	30.27
e (unitless)	1.000	0.999

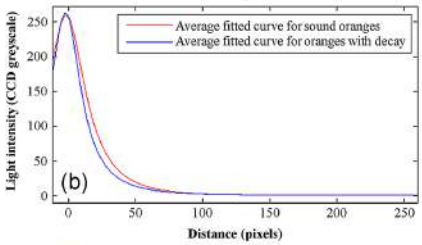

	Sound	Decaying
a (greyscale)*	0.97	0.98
b (greyscale)	257.75	261.57
c (pixels)	-1.65	-2.13
d (pixels)*	16.97	13.67
e (unitless)*	0.921	0.960

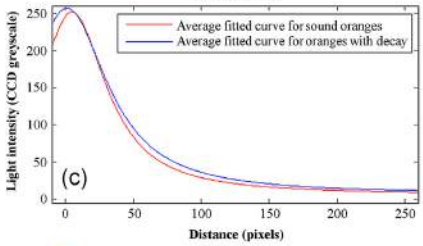

	Sound	Decaying
a (greyscale)*	6.22	7.60
b (greyscale)*	245.53	249.10
c (pixels)*	4.90	1.26
d (pixels)*	30.75	36.14
e (unitless)	0.998	0. 993

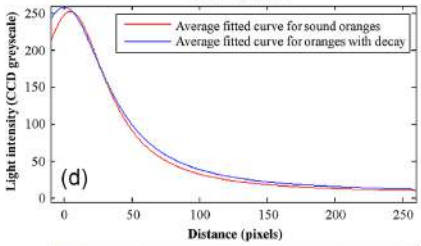

	Sound	Decaying
a (greyscale)*	6.83	7.38
b (greyscale)*	245.23	250.57
c (pixels)*	4.73	0.29
d (pixels)*	33.09	38.08
e (unitless)	0. 998	0. 999

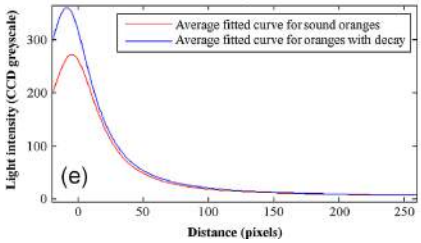

	Sound	Decaying
a (greyscale)	5.23	5.14
b (greyscale)*	266.93	355.48
c (pixels)*	-4.50	-8.40
d (pixels)*	24.16	23.42
e (unitless)	1.000	0.99

Fig. 5. Average Gaussian–Lorentzian cross product (GL) parameters and average GL distribution curves for the backscattering profiles of sound oranges and oranges with decay at: (a) 532 nm, (b) 660 nm, (c) 785 nm, (d) 830 nm, and (e) 1060 nm. Parameters marked with * presented statistically significant differences between sound and decaying oranges.

Table 2
Average determination coefficients (R^2) and average root mean squared errors (RMSE) from fitting backscattering profiles by the GL function for all samples at the five laser wavelengths.

Wavelength (nm)	R^2 (unitless)	RMSE (CCD greyscale)
532	0.998	2.14
660	0.999	0.61
785	0.998	2.48
830	0.998	2.54
1060	0.998	2.32

oranges were statistically significant. Some GL parameters presented a general trend at all the laser wavelengths (parameters *b*, *c* and *e*). The sound oranges had lower peak values (parameter *b*) than the oranges with decay at all wavelengths. By contrast, an opposite trend for centre values (parameter *c*) was observed, these being consistently higher for the sound oranges. However, the differences between both kinds of fruit for these two parameters were not significant enough at 660 nm. Furthermore, for both backscattering profiles, shape parameter (parameter *e*) generally had an almost constant value close to 1, even though this was slightly higher for the oranges with decay at 660 nm.

On the other hand, the asymptotic values (parameter *a*) and scattering widths (parameter *d*) showed a different trend between both backscattering profiles according to the laser wavelength. The sound oranges presented lower asymptotic values than the decaying oranges at almost every wavelength, except at 532 nm (parameter *a* was higher for the sound oranges) and at 1060 nm (parameter *a* did not present significant differences between both kinds of oranges). With regard to scattering widths, for the sound oranges, these values were lower than for the decaying oranges at 532, 785 and 830 nm and, conversely, higher at 660 and 1060 nm. From these results, it can be said that backscattering profiles, and consequently GL parameters, were dependent on the orange state: sound or decaying, since GL parameters differed between both states at the five laser wavelengths.

3.2. Classifier performance evaluation

Table 3 shows the classification results for the ranked wavelength combinations, obtained from the validation set of labelled data. Values of classification average success rate and Cohen's kappa statistic, as well as the corresponding confusion matrixes, are shown for all wavelength combinations. According to the scale proposed by Landis and Kock (1977), Cohen's kappa values were interpreted as follows: 0.00–0.20 regarded as slight, 0.21–0.40 as fair, 0.41–0.60 as moderate, 0.61–0.80 as good and 0.81–1.00 as very good.

When comparing the classification results, it can be noticed that the minimum average success rate of 80.39% and the lowest Cohen's kappa value of 0.610 were obtained for the single wavelength. In contrast, the best classification results were achieved using the five laser wavelengths with an average success rate of 96.08% and a value of Cohen's kappa of 0.921. As shown in the confusion matrix for this classification model using all the wavelengths, the percentage of well-classified fruit samples exceeded 95% for both classes despite the evident similarity between sound oranges and oranges with decay.

Moreover, the increase in the average success rate of around 10% from the single wavelength (80.39%) to the two-wavelength combination (90.20%) should be highlighted. Both wavelengths are in the visible wavelength range. Therefore, we assume that the visible wavelength range may provide more robust information on the differences in the scattering properties of the tissue, due to (i) higher scattering coefficients and resulting increased signal to noise ratio and (ii) increased perturbation in the NIR range due to highly variable water and carbohydrates contents that absorb in the NIR. From the corresponding confusion matrixes, it can be also observed that, while the number of well-classified sound oranges remained the same (87.50%) for both cases, the classification of oranges with decay was greatly improved for the two-wavelength combination, increasing from 74.07% to 92.59%. In practice, this reduction of the number of badly classified oranges with decay is of major importance for a potential inspection system since only a reduced number of infected and sporulated fruit can be the source for important spread of fungal infections to healthy fruit handled or stored in the packinghouse, thus causing great economic losses.

On the other hand, for all the other cases, from one wavelength combination to another, the increase in the average success rate was only approximately 2% by including one wavelength more in the model.

Effective control of green mould and other citrus postharvest diseases has relied for many years on the application of conventional synthetic chemical fungicides such as imazalil or thiabendazole. However, there is currently a clear need to find and implement alternative control methods because of increasing concerns about environmental contamination and human health risks associated with fungicide residues (Palou et al., 2008). Findings from this research are a significant step for the adoption by the citrus industry of nonpolluting alternative control methods, because early decay detection is an effective tool to reduce

Table 3
Classification results for the ranked wavelength combinations.

Number of wavelengths	Wavelength combination (nm)	Average success rate (%)	Cohen's kappa	Confusion matrix	
1	532	80.39	0.610	Sound (%)	Decay (%)
			Sound	87.50	25.93
			Decay	12.50	74.07
2	532, 660	90.20	0.803	Sound (%)	Decay (%)
			Sound	87.50	7.41
			Decay	12.50	92.59
3	532, 660, 1060	92.16	0.843	Sound (%)	Decay (%)
			Sound	91.67	7.41
			Decay	8.33	92.59
4	532, 660, 1060, 830	94.12	0.882	Sound (%)	Decay (%)
			Sound	95.83	7.41
			Decay	4.17	92.59
5	532, 660, 1060, 830, 785	96.08	0.921	Sound (%)	Decay (%)
			Sound	95.83	3.70
			Decay	4.17	96.30

fungicide usage in the context of integrated disease management (IDM) programmes.

4. Conclusions

The feasibility of laser-light backscattering imaging was proved for detecting superficial decay in citrus fruit caused by *P. digitatum*. Backscattering images of oranges at five laser wavelengths in the visible and NIR range were used for non-destructive detection. The GL distribution function with five independent parameters described backscattering profiles accurately, with average R^2 values higher or equal to 0.998. GL parameters were dependent on the orange state (sound or decaying), observing differences between both states at all wavelengths.

In the classification of sound and decaying oranges, all wavelengths contributed to the highest average success rate of 96.1%. The increase in the average success rate of around 10% from the single wavelength (80.4%) to the two-wavelength combination (90.2%), both in the visible range, should be highlighted.

Therefore, the early detection of decaying fruit by means of backscattering imaging analysis has a high potential for its integration in a commercial system. Nevertheless, for future setting up on a sorting line, perhaps a line laser should be applied on rotating fruit, instead of point lasers.

Acknowledgements

This work has been partially funded by the Instituto Nacional de Investigación y Tecnología Agraria y Alimentaria de España (INIA) through research project RTA2012-00062-C04-01 with the support of European FEDER funds. Delia Lorente thanks INIA for the support trough grant FPI-INIA number 42.

References

Barmore, C.R., Brown, G.E., 1981. Polygalacturonase from citrus fruit infected with *Penicillium italicum*. Phytopathology 71, 328–331.
Barmore, C.R., Brown, G.E., 1979. Role of pectolytic enzymes and galacturonic acid in citrus fruit decay caused by *Penicillium digitatum*. Phytopathology 69, 675–678.
Birth, G.S., 1976. How light interacts with foods. In: Gafney J.Jr. (Ed.), Quality Detection in Foods. ASAE, St. Joseph, USA, pp. 6–11.
Blasco, J., Aleixos, N., Gómez-Sanchis, J., Moltó, E., 2009. Recognition and classification of external skin damage in citrus fruits using multispectral data and morphological features. Biosystems Engineering 103, 137–145.
Cubero, S., Aleixos, N., Moltó, E., Gómez-Sanchis, J., Blasco, J., 2011. Advances in machine vision applications for automatic inspection and quality evaluation of fruits and vegetables. Food and Bioprocess Technology 4, 487–504.
Duda, R.O., Hart, P.E., Stork, D.G., 2001. Pattern Classification, second ed. Wiley-Interscience, New York.
Fisher, R., 1936. The use of multiple measurements in taxonomic problems. Annals of Eugenics 7, 179–188.
Fleiss, J.L., 1981. Statistical methods for rates and proportions, second ed. Wiley-Interscience, New York.
Gelman, A., Hill, J., 2006. Data Analysis Using Regression and Multilevel/Hierarchical Models. Cambridge University Press, New York.
Gómez-Sanchis, J., Martín-Guerrero, J.D., Soria-Olivas, E., Martínez-Sober, M., Magdalena-Benedito, R., Blasco, J., 2012. Detecting rottenness caused by *Penicillium* in citrus fruits using machine learning techniques. Expert Systems with Applications 39, 780–785.
Gómez-Sanchis, J., Blasco, J., Soria-Olivas, E., Lorente, D., Escandell-Montero, P., Martínez-Martínez, J.M., Martínez-Sober, M., Aleixos, N., 2013. Hyperspectral LCTF-based system for classification of decay in mandarins caused by *Penicillium digitatum* and *Penicillium italicum* using the most relevant bands and non-linears classifiers. Postharvest Biology and Technology 82, 76–86.
Kim, D.G., Burks, T.F., Qin, J., Bulanon, D.M., 2009. Classification of grapefruit peel diseases using color texture feature analysis. International Journal of Agricultural and Biological Engineering 2, 41–50.
Kurita, M., Kondo, N., Shimizu, H., Ling, P., Falzea, P.D., Shiigi, T., Ninomiya, K., Nishizu, T., Yamamoto, K., 2009. A double image acquisition system with visible and UV LEDs for citrus fruit. Journal of Robotics and Mechatronics 21, 533–540.
Landis, J.R., Kock, G.G., 1977. The measurement of observer agreement for categorical data. Biometrics 33, 159–174.
Limandri, S.P., Bonetto, R.D., Di Rocco, H.O., Trincavelli, J.C., 2008. Fast and accurate expression for the Voigt function. Application to the determination of uranium M linewidths. Spectrochimica Acta Part B 63, 962–967.
Lopes, L.B., VanDeWall, H., Li, H.T., Venugopal, V., Li, H.K., Naydin, S., Hosmer, J., Levendusky, M., Zheng, H., Bentley, M.V., Levin, R., Hass, M.A., 2010. Topical delivery of lycopene using microemulsions: enhanced skin penetration and tissue antioxidant activity. Journal of Pharmaceutical Sciences 99, 1346–1357.
Lorente, D., Blasco, J., Serrano, A.J., Soria-Olivas, E., Aleixos, N., Gómez-Sanchis, J., 2012a. Comparison of ROC feature selection method for the detection of decay in citrus fruit using hyperspectral images. Food and Bioprocess Technology, http://dx.doi.org/10.1007/s11947-012-0951-1.
Lorente, D., Aleixos, N., Gómez-Sanchis, J., Cubero, S., García-Navarrete, O.L., Blasco, J., 2012b. Recent advances and applications of hyperspectral imaging for fruit and vegetable quality assessment. Food and Bioprocess Technology 5, 1121–1142.
Lorente, D., Aleixos, N., Gómez-Sanchis, J., Cubero, S., Blasco, J., 2013. Selection of optimal wavelength features for decay detection in citrus fruit using the ROC curve and neural networks. Food and Bioprocess Technology 6, 530–541.
Lu, R., 2004. Multispectral imaging for predicting firmness and soluble solids content of apple fruit. Postharvest Biology and Technology 31, 147–157.
Lu, R., Cen, H., Huang, M., Ariana, D.P., 2010. Spectral absorption and scattering properties of normal and bruised apple tissue. Transactions of the ASABE 53, 263–269.
Martínez, A.M., Kak, A.C., 2004. PCA versus LDA. IEEE Transactions on Pattern Analysis and Machine Intelligence 23, 228–233.
Meinke, M., Friebel, M., 2009. Determination of optical properties of turbid media: continuous wave approach. In: Zude, M. (Ed.), Optical Monitoring of Fresh and Processed Agricultural Crops. CRC Press, Boca Raton, USA, pp. 44–55.
Mollazade, K., Omid, M., Tab, F.A., Mohtasebi, S.S., 2012. Principles and applications of light backscattering imaging in quality evaluation of agro-food products: a review. Food and Bioprocess Technology 5, 1465–1485.
Navarro, L., Pina, J.A., Juarez, J., Ballester-Olmos, J.F., Arregui, J.M., Ortega, C., Navarro, A., Duran-Vila, N., Guerri, J., Moreno, P., Cambra, M., Zaragoza, S., 2002. The citrus variety improvement program in Spain in the period 1975–2001. In: Proceedings of the 15th Conference of the International Organization of Citrus Virologists, IOCV, Riverside, pp. 306–316.
Palou, L., Smilanick, J., Usall, J., Viñas, I., 2001. Control postharvest blue and green molds of oranges by hot water, sodium carbonate, and sodium bicarbonate. Plant Disease 85, 371–376.
Palou, L., Smilanick, J.L., Droby, S., 2008. Alternatives to conventional fungicides for the control of citrus postharvest green and blue molds. Stewart Postharvest Review 2, 1–16.
Palou, L., Smilanick, J.L., Montesinos-Herrero, C., Valencia-Chamorro, S., Pérez-Gago, M.B., 2011. Novel approaches for postharvest preservation of fresh citrus fruits. In: Slaker, D.A. (Ed.), Citrus Fruits: Properties, Consumption and Nutrition. Nova Science Publishers, Inc., NY, USA, pp. 1–45.
Penache, C., Miclea, M., Bräuning-Demian, A., Hohn, O., Schössler, S., Jahnke, T., Niemax, K., Schmidt-Böcking, H., 2002. Characterization of a high-pressure microdischarge using diode laser atomic absorption spectroscopy. Plasma Sources Science and Technology 11, 476–483.
Peng, Y., Lu, R., 2005. Modeling multispectral scattering profiles for prediction of apple fruit firmness. Transactions of the ASAE 48, 235–242.
Qing, Z., Ji, B., Zude, M., 2007. Predicting soluble solid content and firmness in apple fruit by means of laser light backscattering image analysis. Journal of Food Engineering 82, 58–67.
Romano, G., Baranyai, L., Gottschalk, K., Zude, M., 2008. An approach for monitoring the moisture content changes of drying banana slices with laser light backscattering imaging. Food and Bioprocess Technology 1, 410–414.
Sierra, A., 2002. High-order Fisher's discriminant analysis. Pattern Recognition 35, 1291–1302.
Slaughter, D.C., Obenland, D.M., Thompson, J.F., Arpaia, M.L., Margosan, D.A., 2008. Non-destructive freeze damage detection in oranges using machine vision and ultraviolet fluorescence. Postharvest Biology and Technology 48, 341–346.
Stace, T.M., Truong, G.W., Anstie, J., May, E.F., Luiten, A.N., 2012. Power dependent lineshape corrections for quantitative spectroscopy. Physical Review A: Atomic, Molecular and Optical Physics 86, 012506-1–012506-5.
Wang, S., Li, D., Song, X., Wei, Y., Li, H., 2011. A feature selection method based on improved Fisher's discriminant ratio for text sentiment classification. Expert Systems with Applications 38, 8696–8702.
Weeks, A.R., 1996. Fundamentals of Electronic Image Processing. Wiley-IEEE Press.
Zude, M. (Ed.), 2009. Optical monitoring of fresh and processed agricultural crops. CRC, Press, Boca Raton, USA.

Automatic early detection of decay in citrus fruit using optical technologies and machine learning techniques

Delia Lorente Garrido, December 2014